



UNIVERSIDADE DE BRASÍLIA
INSTITUTO DE GEOCIÊNCIAS

**PETROLOGIA E METALOGENIA DO DEPÓSITO
PRIMÁRIO DE NIÓBIO DO COMPLEXO
CARBONATÍTICO-FOSCORÍTICO DE CATALÃO I,
GO**

DISSERTAÇÃO DE MESTRADO Nº 253

PEDRO FILIPE DE OLIVEIRA CORDEIRO

**Área de Concentração: Geologia Econômica e Prospecção
Orientador: José Affonso Brod – IG/UnB**

Membros da Banca:
Claudinei Gouveia de Oliveira – UnB
Evandro Fernandes de Lima - UFRGS
José Affonso Brod – UnB

**24/04/2009
BRASÍLIA/DF**

Agradecimentos

Ao Affonso e à Elisa

Obrigado pela amizade e pelas horas de conversa, debruçados sobre laptops e copos de café

À minha família

Obrigado pelo suporte e pelo amor

Ao meu Coven

Pelos anos de suporte emocional e espiritual

À Naelyan

*"Meu coração está feliz
Por causa de você
Minha vida mudou de vez
Depois que você chegou
Sou outra pessoa
Uma pessoa bem melhor
Se o amor tivesse uma cor
Seria a sua"*

Ana Carolina – Melhor de mim

Aos Deuses Antigos

*Our elders have seen us grow strong
A wish of the past
Has proven to be
Us, vital,
We keep them alive
As we remain loyal
To our destiny
Dream Theater – Vital Star*

"Quanto maiores a agudeza e severidade com que formulamos uma tese, tanto mais irresistivelmente ela clamará por sua antítese."

Hermann Hesse (1877-1962) - O Jogo das Contas de Vidro

Resumo

O Complexo Carbonatítico-Foscorítico de Catalão I é parte da Província Ígnea do Alto Paranaíba (PIAP) e consiste de um corpo intrusivo formado por rochas da série-bebedourítica (piroxenitos) na borda, e das séries carbonatíticas e foscoríticas no centro. As rochas da série-foscorítica apresentam apatita, magnetita e silicatos magnesianos (flogopita e/ou olivina) e se subdividem em foscoritos (P1), e nelsonitos ricos em apatita (P2) e magnetita (P3). P2 e P3 hospedam a mineralização de Nb+P+Fe do Complexo de Catalão I. Dolomita carbonatito (DC) ocorre associado com P2 e P3 formando associações de carbonatito-foscorito. A composição da mica muda de flogopita em P1 para núcleos de flogopita com bordas de tetra-ferriflogopita em P2 até tetra-ferriflogopita em P3 e DC, similar ao decréscimo de Al observado em micas de foscoritos de outros complexos. Apesar de todas as unidades apresentarem apatitas enriquecidas em ETR, as de P1 são ricas em Si enquanto as de P2, P3 e DC são enriquecidas em Sr. Núcleos de apatita e flogopita mostram uma tendência composicional consistente com a evolução de P1 para DC, corroborando com as variações observadas nos elementos maiores. Relações núcleo-borda de cristais, por sua vez, são mais complexas e evidenciam que a extração de DC em P2 foi menos expressiva quando comparada com a ocorrida em P3. Dolomita primária em DC contém alto-Sr e apresenta-se límpida e coesa, enquanto a secundária ocorre como cristais turvos e friáveis com baixo-Sr. Em termos de isótopos de carbono e oxigênio, enquanto os carbonatos primários apresentam assinatura ígnea, os carbonatos secundários têm $\delta^{18}\text{O}_{\text{SMOW}}$ mais alto e não apresentam variações significativas em $\delta^{13}\text{C}_{\text{PDB}}$. Além disso, os carbonatos preservam também indicativos de desgasificação, alteração por fluidos de baixa temperatura e hidrotermais. Pirocloro ocorre em P2, P3 e DC, e origina um trend composicional ígneo de pirocloros enriquecidos em Ca para enriquecidos em Na. Observa-se também um trend de alteração, marcado pela substituição de Ca-Na por Ba, culminando com a formação de bariopirocloro. ETR normalizados à composição do magma primitivo (flogopita-picrito) mostram padrões tetrad tipo-M em rochas foscoríticas e o padrão complementar, tipo-W, nos bebedouritos, sugerindo que os dois grupos estão relacionados entre si por imiscibilidade de líquidos a partir de um magma parental silico-carbonatado. Padrões normalizados de ETR entre rochas da série-foscorítica e DC são paralelos e sugerem que a associação em pares carbonatito-foscorito é gerada por *filter pressing*. A dissolução dos bolsões de DC e a consequente geração de porosidade secundária permitiram o enriquecimento residual do depósito primário de nióbio associado aos nelsonitos, em função da formação de solos profundos e ricos em minerais resistentes ao intemperismo, dentre eles o bariopirocloro. A ocorrência de rochas ferro-fosfáticas de origem ígnea em Catalão I demonstra a existência de magmas de composição semelhante e sugere que rochas com apatita e óxidos de ferro em outros ambientes geológicos podem ter sido geradas por cristalização de magmas ferro-fosfáticos.

Abstract

The Catalão I carbonatite-phoscorite complex is part of the Alto Paranaíba Igneous Province (APIP) and consists of a multi-intrusion body zoned from bebedourite-(piroxenite)-series rocks in the border to carbonatite- and phoscorite-series rocks in the core. The phoscorite-series rocks consist of apatite, magnetite and a Mg-silicate (phlogopite or olivine) and were subdivided into early-stage, olivine-bearing (P1) and more evolved, olivine-lacking rocks, dominated either by apatite (P2) or magnetite (P3). P1 rocks are typical phoscorites, whereas P2 and P3 are petrographically classified as nelsonites. These latter two units host the Nb+P+Fe mineralization of the Catalão I Complex. Dolomite carbonatite (DC) occurs in association with both P2 and P3, forming paired phoscorite-carbonatite sets, and may also be mineralized in niobium, though at lower grade and volume. Mica composition changes from phlogopite in P1 through phlogopite cores with tetra-ferriphlogopite rims in P2 to tetra-ferriphlogopite in P3 and DC, which is similar to the Al-depletion seen in micas in phoscorites from the Kovdor and Sokli complexes, in the Kola Peninsula. Apatite from P1 is enriched in Si, whereas those from P2, P3, and DC are Sr-rich. Core compositions from both apatite and phlogopite crystals show a composition trend which is consistent with evolution from P1 to DC, further supported by composition variations in whole-rock major oxides. Core-to-rim relationships, on the other hand, are more complex and show that the DC extraction from P2 is less expressive compared to that of P3. Primary carbonate in DC has high-Sr and is clear and cohesive, whilst secondary carbonate occurs as turbid brittle crystals with low-Sr. The C-O isotopes show that whereas the primary carbonate is igneous, secondary carbonate has higher $\delta^{18}\text{O}_{\text{SMOW}}$ and no variation in the $\delta^{13}\text{C}_{\text{PDB}}$. Furthermore, DC carbonates also indicates degassing, hydrothermal and meteoric alteration events. P2, P3 and DC pyrochlore points to an igneous trend from Ca-rich toward Na-rich pyrochlore. The substitution of Ca-Na by Ba defines the alteration trend toward the bariopyrochlore composition. REE normalized to the primitive magma composition (phlogopite-picrite) show M-type tetrad patterns in phoscoritic-rocks and the mirrored W-type in bebedourites, suggesting that the two groups are related by liquid immiscibility from a common, parental carbonated-silicate magma. Normalized parallel REE patterns between phoscorites and DC suggest that the carbonatite-phoscorite sets are generated by filter pressing. The dissolution of the DC pockets and the generation of secondary porosity allowed the residual enrichment of niobium over the primary niobium deposit related to nelsonites. The weathering originated thick soils with resistant minerals enrichment, as bariopyrochlore, thus forming the residual higher-niobium grade deposit. The occurrence of igneous iron-phosphate rocks supports the existence of magmas of similar composition in Catalão I and suggests that iron-oxideapatite rocks from other geological settings can be generated by crystallization of iron-phosphate magmas.

Sumário

CAPÍTULO 1	9
INTRODUÇÃO	9
CONTEXTO GEOLÓGICO REGIONAL	10
COMPLEXO ALCALINO CARBONATÍTICO-FOSCORÍTICO DE CATALÃO I	13
CAPÍTULO 2	15
<i>Immiscibility between silicate- and phoscorite-series in the origin of the Primary Niobium-Ore from the Catalão I Carbonatite Complex, Brazil</i>	15
INTRODUCTION	16
REGIONAL GEOLOGICAL SETTING	17
CATALÃO I COMPLEX	18
METHODS AND SAMPLES	23
MINERAL CHEMISTRY	23
Apatite	23
Phlogopite	29
Carbonate	36
Magnetite	37
Ilmenite	43
Olivine/Ti-Clinohumite	47
WHOLE-ROCK CHEMISTRY	49
Sr AND Nd ISOTOPIC DATA	59
DISCUSSION AND CONCLUSIONS	62
ACKNOWLEDGEMENTS	65
REFERENCES	66
CAPÍTULO 3	69

<i>Pyrochlore Chemistry from the Primary Niobium Deposit of the Catalão I Carbonatite-Phoscorite complex, Brazil</i>	69
INTRODUCTION	70
METHODS AND SAMPLING	71
THE ALTO PARANAÍBA IGNEOUS PROVINCE (APIP)	71
CATALÃO I CARBONATITE COMPLEX	73
PHOSCORITE-SERIES ROCKS AND THE NIOBIUM DEPOSIT	74
PYROCHLORE COMPOSITION	80
CHEMICAL EVOLUTION OF PYROCHLORE	84
SUBSTITUTIONS IN THE A-SITE	86
“A” Trend	86
“B” Trend	87
POSITIVE CORRELATIONS IN THE B-SITE	88
COMPARISON WITH THE CATALÃO I RESIDUAL DEPOSIT	90
THE NIOBIUM MINERALIZATION	93
CONCLUSIONS	95
Acknowledgements	96
REFERENCES	97
CAPÍTULO 4	100
<i>Stable O and C isotopes, and carbonate chemistry in phoscorites and Nb-rich nelsonites from the Catalão I carbonatite complex, central Brazil: implications for phosphate-iron-oxide magmas*</i>	100
Introduction	101
Geological Context	102
The Catalão I Complex	104
Method and Samples	105
Rock nomenclature and petrography	106
Early-stage phoscorites – P1	107

Late-stage phlogopite nelsonites – P2 and P3.....	108
Carbonate pockets and dolomite carbonatite (beforsite) dykes – DC	109
Carbonate chemistry.....	110
C-O isotope in the carbonatite and phoscorite-carbonatite association	113
Textural and carbonate chemistry evidence of post-magmatic alteration.....	119
Phosphate-iron-oxide magmas in other environments	120
Discussion and conclusions	122
Acknowledgements	124
References	124
CAPÍTULO 5	127
CONCLUSÕES	127
REFERÊNCIAS BIBLIOGRÁFICAS.....	132

Índice de Figuras

Fig. 1.1. Diagrama de classificação mineralógica da série foscorítica. Os círculos representam as rochas estudadas neste trabalho. Mapa de localização da cidade de Catalão. A distância aproximada entre Catalão e Brasília são 300 km.	132
Fig. 1.2. Mapa de localização da cidade de Catalão. A distância aproximada entre Catalão e Brasília são 300 km.	13
Fig. 2.1. Geological map of the Alto Paranaíba Igneous Province (APIP). Adapted from Oliveira et al. (2004), with the location of the plutonic alkaline-carbonatite complexes. Small open circles represent minor known alkaline (kamafugite and kimberlite).	17
Fig. 2.2. Geological sketch of the Catalão I carbonatite complex. Modified from Brod et al. (2004) and Ribeiro (2008). There is no drill core or outcrop information for the blank areas.	18
Fig.2.3. Comparative modal composition of Catalão I phoscorite-series rocks and associated carbonatites. The main features of P1 are the occurrence of olivine and the coarse-grained texture. P2 and P3 are olivine-free rocks (nelsonites, magnetitites and apatitites) where the main silicate phases are phlogopite and/or tetra-ferriphlogopite. For a discussion on rock nomenclature see Cordeiro (2009 – Capítulo 4).	19
Fig.2.4. Photograph of drill-core samples from the Catalão I Nb deposit. A. P1 (phoscorite) with altered phlogopite and carbonate. Hydrothermal carbonate veinlets are responsible for the alteration. B. P2 (apatite-nelsonite) with DC pockets. The pinkish tone is due to the presence of pyrochlore and small amounts of tetra-ferriphlogopite. C. P3 (magnetite-nelsonite) with DC pockets, cut by a carbonatite dike. D. P3 dyke containing DC pockets, hosted in altered P1 (note the subhedral crystals of ilmenite and phlogopite elongated toward the center of the pockets).	21
Fig.2.5. Photomicrographs of the phoscorite series rocks from the Catalão I carbonatite complex. A) P1 = coarse- to medium- grained phoscorite with clinohumite pseudomorphs after olivine. B) P2 = apatite-nelsonite showing zoned mica, with phlogopite cores and tetra-ferriphlogopite rims. C) P3 = Magnetite-nelsonite with tetra-ferriphlogopite, apatite and pyrochlore. D) DC = Dolomite carbonatite pocket in P2 with tetra-ferriphlogopite, magnetite and apatite crystallizing at the walls, the same texture shown in hand-sample in Fig. 2.4D. (Chum = clinohumite, Phl = phlogopite, TFP = tetra-ferriphlogopite, Dol = dolomite, Pcl = pyrochlore, Apat = Apatite, and Mag = Magnetite).	22
Fig.2.6. Apatite substitution schemes. Note the variation between different rock types within the phoscorite series. The analyses are compared with the composition fields of apatites in phoscorites and carbonatites from the Kola Province. (Purple = Kovdor Complex, Krasnova et al. 2004b. Grey = Vuoriyarvi, Karchevsky & Moutte, 2004. Orange = Sokli, Lee et al. 2004). P1 = Blue circles, P2 = green circles; P3= red circles; DC = white circles. All variables are cations per formula unit.	27
Fig.2.7. $Ca^{2+}=Sr^{2+}$ substitution in rims and cores of selected euhedral apatite crystals. Note that the apatite rims from P2 are richer in Sr than the corresponding cores, whereas P3 apatites show the opposite. Ca and Sr values are cations per formula unit. Symbols as in Figure 2.6.	28
Fig.2.8. Chemical composition of phlogopites in Catalão I phoscorites, nelsonites and dolomite carbonatites. (A) Al vs Fe^{3+} (a.p.f.u.) showing the spreading of the analyses along the phlogopite – tetra-ferriphlogopite 1:1 substitution line, with indication of the composition corresponding to the reversal in pleochroism. (B) Mg^{2+} vs Fe^{2+} (a.p.f.u.) diagram showing that the phlogopite-annite substitution also occurs, but is subordinate (total span of ca. 0.5 a.p.f.u.). (C) triangular classification plot showing the composition of the analysed micas in the phlogopite – tetra-ferriphlogopite series. Symbols as in Fig. 2.6.	31
Fig.2.9. Chemical composition of cores and rims of phlogopites from Catalão I. The areas near the base of the triangular plot are further detailed in the Mg vs Total Fe diagram. Symbols as in Fig. 2.6.	34

<i>Fig.2.10. Phlogopite-annite substitution in cores and rims of micas from the Catalão I phoscorites, nelsonites, and carbonatites. Note that, as also observed for apatite (Fig. 2.7), there is a reversal in the core to rim trend between P2 and P3 micas. Symbols as in Figure 2.6.</i>	35
<i>Fig.2.11. Variation of selected elements (cations per formula unit) in magnetite from the Catalão I phoscorites and nelsonites. Symbols as in Figure 2.6. Fields for magnetite from Kola phoscorites and carbonatites (Kovdor = purple, Krasnova et al., 2004b; Sokli = orange, Lee et al., 2005; Vuorijarvi = grey Karchevsky & Moutte, 2004), as well as Jacupiranga (black, Gaspar & Wyllie, 1983) and Turiy (yellow, Dunworth & Bell, 2003) carbonatites are shown for comparison. The red field in the left-hand side diagram represents magnetite from primitive silicate rocks (phlogopite picrites) in the Tapira complex in the extreme south of APIP (Brod et al., 2005).</i>	38
<i>Fig.2.12. Compositional variation and classification of ilmenite from the Catalão I phoscorites, nelsonites and carbonatites (symbols as in Fig. 2.6). Also plot for comparison are the fields of ilmenite from the Jacupiranga carbonatites (dashed line, Gaspar & Wyllie, 1983), Kola carbonatites and phoscorites (yellow, Lee et al., 2005, and references therein), kimberlites (red outline, Mitchell, 1978), and other rocks (green outline – lamprophyres, granites, basalts, carbonatites, Mitchell, 1978). Phoscorites from the Sokli massif, Finland (Lee et al., 2005), are individualized as grey fields, with lighter shades indicating more evolved rocks. The red solid fields represent the compositions of ilmenite from monazite-rich apatites and nelsonites in the Catalão I rare-earth deposit (Ribeiro et al., 2005).</i>	45
<i>Fig.2.13. Microprobe profiles for selected ilmenite crystals. Horizontal scales are proportional to the distance between analytical points. All concentration data is in wt. %.</i>	46
<i>Fig.2.14. Nb and Ti (a.p.f.u.) variation in Catalão I ilmenites. The composition of P1 and P3 ilmenites suggest niobium increase and titanium decrease with evolution, but P2 and DC ilmenites overlap the entire composition range.</i>	47
<i>Fig.2.15. Variation diagrams of selected major element oxides for the Catalão I samples. Arrows indicate the differentiation in the sequence P1-P2-P3.</i>	50
<i>Fig.2.16. SiO₂ and MgO variations in phoscorite-series rocks and carbonatites from Catalão I. Colored fields are from silicate rocks, phoscorites and carbonatites from the Kovdor Complex (Krasnova et al., 2004b; http://www.emse.fr/~moutte). Also plotted are silicate rocks from the Catalão I complex (star symbols, 1: phlogopitite – Araújo, 1996; 2: glimmerite – this work; 3: kamafugite – Gomes & Comin-Chiaromonti, 2005; 4: pyroxenite – Araújo, 1996).</i>	53
<i>Fig.2.17. REE patterns for the studied rocks. Above: samples normalized to chondrite. Below: samples normalized to an average phlogopite picrite (FLP, primitive magma for the APIP complexes, our unpublished data). Also plotted is an analysis of a Catalão I pyroxenite (bebedourite, light blue symbols) from Araújo (1996). Note the M-type tetrad pattern in all rocks of the phoscorite-series and related carbonatites, and the inverse W-type pattern in the bebedourite.</i>	56
<i>Fig.2.18. W-type tetrad patterns in Catalão I (light blue, Araujo, 1996) and Araxá (dark blue, Traversa et al., 2001).</i>	57
<i>Fig.2.19. REE and trace-element patterns for paired phoscorite-carbonatite, normalized to the average APIP phlogopite-picrite.</i>	59
<i>Fig.2.20. Sr and Nd isotopic composition of Catalão I dolomite carbonatites. Compositional fields from Phalaborwa (Eriksson, 1989; Yuhara et al., 2005), Kovdor (Zaitsev & Bell, 1995), Turiy (Dunworth & Bell, 2001), Catalão I and II (Comin-Chiaromonti et al., 2005 and references therein), MORB and APIP (Gibson et al., 1995) are shown for comparison. The inset shows a detailed diagram for different rocks from Turiy and Kovdor.</i>	60
<i>Fig.3.1. Geological map of the Alto Paranaíba Igneous Province showing the location of alkaline-carbonatite complexes. Dots represent kamafugite, kimberlite and lamproite from the province. Adapted from Oliveira et al. (2004).</i>	72
<i>Fig.3.2. Geological sketch of the Catalão I Complex. The studied samples were obtained from the niobium-rich phlogopite nelsonite and from the phoscorite with subordinated phlogopitite and calcite carbonatite units. Modified from Brod et al. (2004) and Ribeiro (2008). Blank areas represent lacking of outcrops or drill core informations.</i>	74

Fig.3.3. Schematic model of occurrence of phoscorites in Catalão I. P1, P2, P3, and DC crosscut all the former rock types. The DC pockets and dikes are usually accompanied by a magnetite rim and by crystals pointing toward the center of the pocket. (P1 = phoscorite; P2 = apatite nelsonite; P3 = magnetite nelsonite; DC = dolomite carbonatite) 75

Fig.3.4. Ultramafic rocks, phoscorites and nelsonites from the Catalão I niobium deposit. A. Metasomatic phlogopite with green relicts of the original ultramafic rock. At the upper portion of the drill core, a magnetite nelsonite dike (P3) with DC pockets cuts the metasomatic phlogopitite. B. Altered, coarse-grained P1, crosscut by P3 dikes with DC pockets. C. Equigranular P2 with DC pockets. (P1 = phoscorite; P2 = apatite nelsonite; P3 = magnetite nelsonite; DC = dolomite carbonatite) 77

Fig.3.5. Structures and textures related to pyrochlore-rich nelsonites. A. Mineralized P2 with DC pockets. Note the mingling texture between the carbonatite and the apatite nelsonite, the thin rim of magnetite between them and the phenocrysts of phlogopite (brown-red subhedral) that nucleated at the magnetite rim, pointing toward DC. B. Magnetite-rich nelsonite (P3) and DC pocket with nelsonite spheres or droplets. C. Mingling between two different carbonatites. Pyrochlore, magnetite and phlogopite crystallize at the mingling interface. (P1 = phoscorite; P2 = apatite nelsonite; P3 = magnetite nelsonite; DC = dolomite carbonatite) 78

Fig.3.6. Photomicrographs of pyrochlore-bearing phoscorites. A. P2 nelsonite with subhedral, brown to orange pyrochlore. B. P3 nelsonite with anhedral to subhedral brown to orange pyrochlore. C. Sector zoning in pyrochlore from dolomite carbonatite pocket (DC). D. Mingling-like texture of P2 spheres in DC, crossed polars. (Mag = magnetite; Apt = apatite; TFP = tetra-ferriphlogopite; Carb = carbonate; Pcl = piroclore) 80

Fig.3.7. Triangular Nb-Ti-Ta classification scheme (Hogarth, 1977 and 1989) for the studied pyrochlores (black circles). Outlines for pyrochlore compositions from the Catalão I residual deposit (square pattern, Fava, 2001), Oka (gray, Gold, 1986; Zurevinski and Mitchell, 2004), Sokli (solid black outline; Lee et al., 2004; Lee et al., 2006) and Salitre (dotted black outline, Barbosa et al., in preparation). BET = betafite, PCL = piroclore, MCL = microlite. 81

Fig.3.8. Triangular plots of Ca, Na and A-site vacancy. Compositional fields of pyrochlore of other deposits are shown for comparison. White dots = bariopyrochlore; Light gray dots = High-Ba pyrochlore; Dark gray dots = Low-Ba pyrochlore; Black dots = pyrochlore inclusions in ilmenite from DC. Data sources as in Figure 3.7, plus Bingo field from Williams et al. (1997). 85

Fig.3.9. A. Substitution scheme in fresh pyrochlore of the Catalão I phoscorite, according to the “A” Trend. This trend represents the crystallization of early Ca-rich pyrochlore and its shift toward Na-rich composition with magma evolution. The fields for Salitre and Oka represent Ca-rich pyrochlore crystallized from more primitive liquids than Catalão I. B. Sr enrichment in the “A” Trend toward Na-rich pyrochlore, and in the “B” Trend toward Na-poor pyrochlore. Note that pyrochlore from the Catalão I residual deposit is Na-Sr-poor. Symbols and data sources as in Figure 3.8. 86

Fig.3.10. A. Chemical variation of pyrochlore from the Catalão I phoscoritic rocks in terms of Ba, Ca and Na. The “B” Trend is defined by the high-Ba pyrochlore and bariopyrochlore toward the field of Catalão I residual deposit. While pyrochlore from Oka and Salitre are virtually Ba-free, pyrochlore from Sokli phoscorites is comparatively Ba-richer but bears no relation to the substitution scheme. B. Pyrochlore from Sokli phoscorites (Lee et al. 2004, 2006). C2-P2, C3-P3 are paired phoscorite-carbonatite, while D4 and D5 are dolomite carbonatite. The phoscorites show a trend going from C2-P2 primitive, high-U and -Ta pyrochlore toward more evolved Ca-Na pyrochlore (low-U and -Ta) in C3-P3, D4 and D5. Note that this trend is very similar to that of high-Ba pyrochlore from Catalão I. Outlines of pyrochlore compositions of other complexes as in Figures 3.7 and 3.8. 88

Fig.3.11. Correlations involving the B-site elements. A. Si and Ba 2:1 positive correlation is related to high-Ba pyrochlore and bariopyrochlore. The Bingo composition is more enriched in Si respectively to Ba than Catalão I. B. U and Ta show a 2:1 positive correlation in primary pyrochlore probably according a coupled substitution. Salitre, Oka and Sokli pyrochlores also show a positive correlation, though the compositional fields of Oka and Sokli are wider and cannot be represented in the adopted scale. Symbols and compositional fields as in Figure 3.8. 89

<i>Fig.3.12. A. Binary plot of Sr and Ca showing the positive correlation in pyrochlore from fresh rock and crystal cores from the Catalão I residual deposit (Fava, 2001). A negative correlation occurs in the bariopyrochlore of fresh rock and the residual deposit. B. Plot of Si and U, showing two groups of samples from the “B” trend, bariopyrochlore with high-Si and the high-Ba pyrochlore with high-U.</i>	91
<i>Fig.3.13. Relationship between zoning and weathering. Note that the pyrochlore rims from samples 093 and 056 have systematically higher A-site vacancies than the corresponding cores. In the case of sample 056, the mineralogy changes from pyrochlore to bariopyrochlore without an intermediate composition. Samples 192B and 178 have restricted compositional fields. The C-O stable isotopes (Cordeiro, 2009 – Capítulo 4) show that samples with bariopyrochlore rims have wider variations in the $\delta^{18}\text{O}_{\text{SMOW}}$ content while samples with a more restricted alteration preserve the original composition.</i>	92
<i>Fig.4.1 Location of the Alto Paranaíba Igneous Province on the border of the Paraná Basin (modified from Gibson et al. 1995). Black dots represent cretaceous alkaline rocks from different provinces.</i>	102
<i>Fig.364.2 Geological sketch of the Catalão I Complex. The studied samples were obtained from the niobium-rich phlogopite nelsonite and from the phoscorite with subordinated phlogopitite and calcite carbonatite units (modified from Ribeiro 2008).</i>	104
<i>Fig.4.3 Metassomatised P1 phoscorite. Olivine from this sample was substituted by clino-humite, but the original shapes of olivine grains are still recognizable.</i>	107
<i>Fig.4.4 P3 dyke (magnetite-rich nelsonite) hosted in slightly metassomatised P2 (apatite-rich nelsonite) with metassomatic phlogopitite (MP) xenoliths. Note the thin (5 cm) reaction rim in the contact, and the dolomite-carbonatite pockets within the P3 dyke</i>	108
<i>Fig.4.5 P3 nelsonite with dolomite carbonatite pockets. Note the growth of tetra-ferriphlogopite in the boundary between P3 and the DC pocket, where ilmenite and apatite are also common.</i>	109
<i>Fig.4.6 Dolomite carbonatite pocket in a P3 dyke. Cloudy dolomite is often related to fractures and is common along the boundary between the dolomite carbonatite and the magnetite wall. (Apat=apatite, TFP=tetra-ferriphlogopite)</i>	110
<i>Fig.4.7 Location of dolomite electron probe microanalyses from a DC pocket in sample NRD-178. Note the different textures between cloudy and clear dolomite, which are attributed to subsolidus alteration. Dots 1 and 2 are represented by arrows in figure 4.8 (Mag = magnetite, Pcl = pyrochlore, Dol = dolomite, Apat = apatite)</i>	112
<i>Fig.4.8 Dolomite compositions from Catalão I phoscorites, nelsonites and dolomite carbonatites. There is a relationship between SrO content and texture, whereby “cloudy” dolomites are SrO poorer than grains with clear aspect. The arrows indicate the composition of both carbonate types from NRD-178 (figure 4.7)</i>	113
<i>Fig.4.9 Carbon and oxygen stable isotope data for carbonatites in this study. The isotopic composition of samples dominated by clear- and cloudy-dolomite is indicated, as well as the expected isotopic composition of primary carbonatite (gray box). Key: black dots = dolomite-carbonatite (DC) pockets in P3; gray dots = DC pockets in P2; squares = carbonatites; crosses = carbonate veins</i>	115
<i>Fig.4.10 Oxygen and carbon isotopes of different carbonates from the Catalão I complex. Samples were grouped according the isotopic behavior. Key: black = dolomite-carbonatite (DC) pockets in P3; gray = DC pockets in P2; squares = carbonatites; crosses = veins</i>	116
<i>Fig.4.11 Diagram showing the isotopic composition of calcite in equilibrium with apatite and magnetite at temperatures ranging between 500 and 800°C. The number near the curves indicate the proportion of calcite:apatite:magnetite. The gray area shows the approximate isotopic composition of the carbonates generated by immiscibility. Isotopic fractionations were based on Clayton and Kieffer (1991) and Zhao and Zheng (2003)</i>	117

Fig.4.12 Comparison between the hand-sample aspect of cloudy and clear carbonates in P2 (sample 178). Cloudy dolomite is more white and brittle compared to clear dolomite, and represents the recrystallisation product of primary (high-SrO) carbonates..... 119

Fig.4.13 Textural and chemical classification of primary and secondary dolomites from Catalão I..... 120

Índice de Tabelas

Tab.2.1 Representative apatite compositions from the Catalão I phoscorite-series rocks and carbonatites	25
Tab. 2.2 Representative phlogopite compositions from the Catalão I phoscorite-series rocks and carbonatites.....	32
Tab. 2.3 Representative analyses of magnetite from Catalão I phoscorites, nelsonites and dolomite carbonatites. Cations calculated on the basis of 32 O.	41
Tab. 2.4 Representative analyses of ilmenite from the Catalão I phoscorites, nelsonites, and associated carbonatites. Formulae recalculated on the basis of 6 O.	44
Tab.2. 5 Analyses of Ti-clinohumite from the Catalão I early-stage (P1) phoscorites.....	48
Tab. 2.6 Whole-rock chemistry of the Catalão I glimmerite, phoscorites, nelsonites and carbonatites	51
Tab. 2.7 Sm-Nd-Sr isotopes of dolomite carbonatite DC related to nelsonites. $87\text{Sr}/86\text{Sr}$ and $143\text{Nd}/144\text{Nd}$ isotopic ratios are presented as measured (m) and initial values (i) corrected to 85 Ma.	61
Tab.3.1. Pyrochlore, betafite and Fe-columbite composition from the Catalão I nelsonites. Bario = bariopyrochlore, Ca-Na = Ca-Na pyrochlore, H-Ba = High-Ba pyrochlore, Incl = pyrochlore inclusions in ilmenite from DC.	82
Tab.3.2. Geological information of the main niobium mines (adapted from Tither, 2001).....	93
Tab. 4.1 Modal composition of the Catalão I phoscorites and nelsonites. The values are expressed as volume percentages.	107
Tab.4.2 Representative analyses of dolomites from Catalão I phoscorites, nelsonites, and carbonatites. n.d. = not determined; b.d. = below detection	111
Tab.4.3 Chemical compositions of norsethite and magnesite from Catalão I phoscorites and carbonatites. n.d. = not determined; b.d. = below detection	111
Tab.4.4 Carbon and oxygen isotopic composition of carbonates from carbonatites, veins, DC dykes, and DC pockets in the Catalão I carbonatite complex.....	114

CAPÍTULO 1

INTRODUÇÃO

Foscoritos são rochas ígneas raras com apatita, magnetita e um silicato magnesiano (olivina, diopsídio e/ou flogopita) como minerais-base. Essas rochas foram descritas em apenas 21 localidades (Krasnova et al. 2004), e estão quase sempre associadas com carbonatitos. Apesar de terem sido bem descritas em termos de relações de contato e aspectos mineralógicos e texturais, a petrogênese dos foscoritos é pouco compreendida e permanece inconclusiva. Evidências de relações de contato e de química mineral apontam para a possibilidade de geração a partir de um magma ferro-fosfático bem como cumulados de um magma carbonatítico ou silicático. Além de possuir petrologia complexa, envolvendo múltiplos estágios de evolução, essas rochas apresentam grande interesse econômico, uma vez que portam mineralizações de fosfato, nióbio, terras raras e mais raramente, cobre.

Estudos anteriores argumentam que a petrogênese dos magmas foscoríticos envolve AFC como uma forma de modificar a composição do magma ao longo da evolução (Krasnova et al. 2004a). Esses estudos incluíram também interpretações sobre se a série foscorítica é derivada de um magma parental carbonatítico-silicático ou se foi gerada como um magma primário independente. Concluiu-se que a série foscorítica representa magmas derivados do manto que ocorrem em próxima associação temporal e espacial com complexos carbonatíticos.

Nos complexos de Araxá e Catalão I e II, parte da Província Ígnea do Alto Paranaíba (PIAP, Cretáceo Superior), rochas da série foscorítica são particularmente abundantes (Brod et al. 2004; Ribeiro et al. 2005). No caso do Complexo Carbonatítico de Catalão I, foscoritos e dolomita carbonatitos associados, ocorrem como pequenas intrusões e enxames de diques em *stockwork* que são observados em afloramentos das minas de nióbio e fosfato e em testemunhos de sondagem. Nesses casos, apesar das grandes espessuras de solo, é possível encontrar rochas alcalinas bem preservadas que mostram associações múltiplas de foscorito-carbonatito e permitem uma boa descrição das relações de contato das rochas entre si e com as demais rochas do complexo. Além disso, foscoritos de Catalão I contém um importante depósito de nióbio, cuja versão intemperizada vem sendo explorada por mais de trinta anos.

Estudos anteriores atribuem a mineralização de nióbio como consequência do intemperismo de carbonatitos e concentração residual de pirocloro, (Carvalho and Bressan, 1981; Gierth and Baecker, 1986) sem detalhar o grande enriquecimento que havia na rocha. No entanto, relações texturais de

campo e em testemunhos de sondagem permitem afirmar que a mineralização primária de nióbio está diretamente associada com a ocorrência de rochas da série foscorítica, particularmente as rochas foscoríticas cuja fase silicática é flogopita e tetra-ferriflogopita em vez de olivina. Yegorov (1993) classifica rochas com essa composição mineralógica como nelsonitos.

Nesse contexto, apesar de os demais complexos carbonatíticos da PIAP apresentarem a mesma filiação geoquímica, apenas os complexos de Araxá e Catalão I e II apresentaram até o momento ocorrências de nelsonitos mineralizados em nióbio. Portanto, esperam-se outros processos geológicos que controlem a formação de depósitos econômicos de nióbio em carbonatitos além de apenas concentração residual por intemperismo.

CONTEXTO GEOLÓGICO REGIONAL

A Província Ígnea do Alto Paranaíba, Cretáceo Superior (PIAP), abarca rochas alcalinas que ocorrem nos estados de Minas Gerais e Goiás, no Brasil central (Gibson et al. 1995). A província ocupa uma área orientada NW entre o Cráton do São Francisco e a borda nordeste da Bacia do Paraná. A PIAP consiste de uma variedade de magmas ultrapotássicos encaixados em rochas metasedimentares da Faixa Brasília (Proterozóico) e é principalmente constituída por kamafugitos, com kimberlitos, lamproítos e complexos alcalinos plutônicos de associação carbonatito-foscorito. A gênese da província tem sido relacionada com o impacto da pluma de Trindade sob a litosfera brasileira durante o Cretáceo Superior, originando a fusão de porções ricas em potássio do manto litosférico subcontinental (Gibson et al. 1995; Thompson et al. 1998; Brod et al. 2004).

Os complexos plutônicos carbonatíticos-foscoríticos da PIAP incluem intrusões de noroeste para sudeste: Catalão II e Catalão I em Goiás; e Serra Negra, Salitre I, Salitre II, Salitre III, Araxá e Tapira em Minas Gerais. As intrusões desses magmas alcalinos originaram estruturas dômicas nas rochas encaixantes da Faixa Brasília. Os padrões radiais de drenagem, resultado da diferença de alteração entre rochas alcalinas e encaixantes, aliado ao intenso intemperismo tropical produziram profundos perfis lateríticos sobre os complexos. O intemperismo é também responsável por reconcentrar nióbio, titânio, terras raras e fosfato no solo desses complexos, sobre rochas já extremamente enriquecidas nesses elementos. Atualmente, Tapira, Araxá e Catalão I são explorados para fosfato, enquanto Araxá, Catalão I e Catalão II são os únicos depósitos economicamente viáveis de nióbio da PIAP e responsáveis por mais de 90% da demanda mundial de nióbio no mundo.

Com exceção de raras ocorrências de sienitos tardios, as rochas alcalinas carbonatíticas da PIAP não apresentam nefelina e portanto, não pertencem a associação comum nefelinito (ijolito) –

carbonatito de Le Bas (1985). Brod et al (2000) sugere que a PIAP é uma província ultrapotássica com associação kamafugito-carbonatito, similar à proposta por Stoppa e Cundarini (1995) e por Stoppa et al. (1997) na Itália.

Três séries magmáticas de diferenciação podem ser reconhecidas nos complexos alcalino-carbonatíticos da PIAP: as séries bebedourítica, carbonatítica e foscorítica, geradas a partir de um magma primitivo de natureza silicática ultrapotássica. Diques de flogopita-picrítico, que cortam os complexos da PIAP são interpretados como representantes desse líquido primitivo.

Bebedouritos são produtos da cristalização fracionada a partir do magma primitivo e são caracterizados por quantidades variáveis de olivina, diopsídio, apatita, perovskita, magnetita e flogopita. Granadas de titânio (melanita) e titanita podem também ocorrer em menor proporção. Essas rochas representam o equivalente à série ijolítica nos complexos de filiação potássica, em vez da filiação sódica mais comum que origina os ijolitos (Brod 1999; Brod et al. 2000; Brod et al. 2004). Na PIAP, bebedouritos bem preservados ocorrem em Tapira e Salitre enquanto em Catalão I e Araxá, essas rochas foram extensivamente transformadas em flogopititos por metassomatismo carbonatítico.

Segundo Yegorov (1993) foscoritos são rochas definidas por variações modais de apatita, magnetita e olivina (Figura 1.1). Krasnova et al. (2004) recomendou que o nome foscorito fosse aplicado a rochas plutônicas ultramáficas contendo apatita, magnetita e um dos silicatos flogopita, diopsídio e forsterita. Acessórios comuns incluem pirocloro, badeleita, anfibólios sódicos e dolomita. Rochas da série foscorítica ocorrem em todos os complexos da PIAP e são particularmente comuns em Araxá e Catalão I e II. Os depósitos de nióbio estão associados a rochas da série-foscorítica mais empobrecida em silicatos (nelsonitos). A gênese dessa série pode estar relacionada tanto com magmas ferro-fosfáticos quanto com acumulação mecânica de cristais a partir de magmas carbonatíticos.

Carbonatitos incluem rochas com mais de 50% de carbonatos e sua nomenclatura é baseada no tipo de carbonato dominante. Dolomita, calcita, Fe-dolomita e ankerita são comuns nessas rochas (Woolley e Kempe 1989).

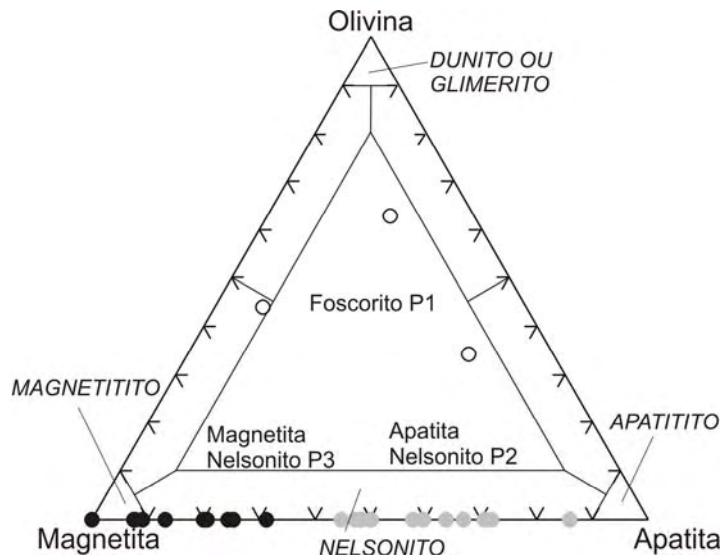


Fig. 1.1. Diagrama de classificação mineralógica da série foscorítica. Os círculos representam as rochas estudadas neste trabalho.

Essas três séries de diferenciação que ocorrem na PIAP estão relacionadas entre si por intrincadas combinações de cristalização fracionada e imiscibilidade de líquidos a partir de um magma primitivo (flogopita picrito) que possui filiação kamafugítica (Brod 1999; Brod et al. 2000; Brod et al. 2004).

Assim como em Catalão I, a mineralização primária de nióbio de Araxá também está associada a rochas da série foscorítica (nelsonitos), como diques centimétricos a métricos. Minerais acessórios comuns incluem dolomita, barita, norsetita e sulfetos de Fe-Cu (Issa Filho et al. 1984; Silva 1986). Além disso, tanto Catalão I quanto Araxá apresentam ampla ocorrência de flogopititos metassomáticos, interpretados como bebedouritos, piroxenitos e dunitos posteriormente alterados por fluidos derivados de carbonatitos. Esse amplo evento de metassomatismo pode estar relacionado com a natureza dos magmas primitivos desses complexos, uma vez que líquidos primitivos apresentam capacidade de alteração da encaixante muito maior uma vez que são mais enriquecidos em álcalis e CO₂, enquanto magmas mais evoluídos podem já ter passado por desgaseificação e fracionamento de carbonato e minerais hidratados. É importante também ressaltar a associação desse amplo metassomatismo representado por flogopititos metassomáticos com a ocorrência das mineralizações de nióbio em rochas foscoríticas tardias. Por outro lado, essa associação não é direta, i.e. magmas foscoríticos sendo os responsáveis por metassomatizar as rochas encaixantes, uma vez que as rochas adjacentes aos nelsonitos e foscoritos mostram pouca capacidade de alteração metassomática.

COMPLEXO ALCALINO CARBONATÍCO-FOSCORÍTICO DE CATALÃO I

O complexo de Catalão I está localizado perto da cidade de Catalão, no estado de Goiás (Figura 1.2), e intrude quartzitos e xistos da Faixa Brasília, originando uma estrutura quase circular em formato de domo que ocupa uma área de 27 km^2 (Figura 2.1). Datação K-Ar em flogopita indica idade para intrusão de $85 \pm 6.9 \text{ Ma}$ (Sonoki e Garda 1988). A ocorrência próxima de Catalão II, localizado 15 km a norte de Catalão I, indica uma provável origem comum para os dois complexos e Machado Júnior (1992) obteve idade Rb-Sr de $83.4 \pm 0.9 \text{ Ma}$ para Catalão II, muito similar à descrita por Sonoki e Garda (1988) para Catalão I. Taxas de erosão baseadas em traços de fissão em apatita (Amaral et al. 1997), junto com evidência da presença de atividades explosivas na câmara magmática, foram utilizadas por Ribeiro et al. (2005) para estimar uma profundidade de intrusão mais rasa que 2.5 km para os complexos de Catalão I e II.

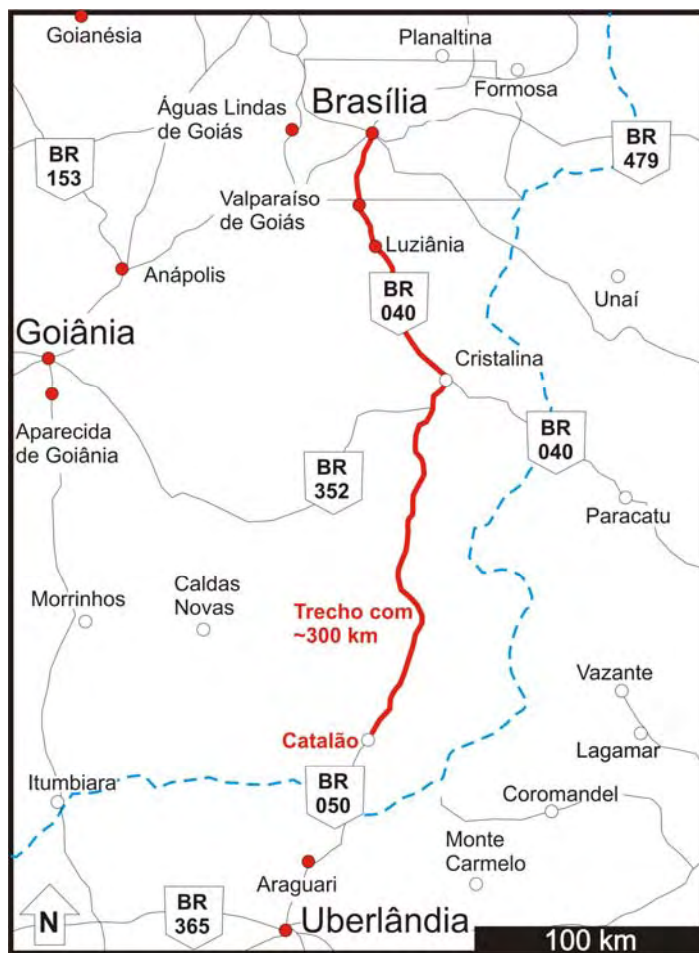


Fig. 2.2. Mapa de localização da cidade de Catalão. A distância aproximada entre Catalão e Brasília são 300 km.

Em Catalão I, a zonação concêntrica comum em complexos ultramáfico-carbonatíticos é definida por um núcleo de carbonatito-foscorito-nelsonito e porções externas de rochas ultramáficas alcalinas metassomatizadas (flogopítito metassomático). Rochas comuns incluem dunitos, clinopiroxenitos, bebedouritos, carbonatitos, foscoritos, nelsonitos, apatítitos e magnetítitos (Brod et al. 2004; Ribeiro et al. 2005).

A predominância de flogopítito metassomático sobre rochas silicáticas primárias atesta a importância e intensidade dos eventos metassomáticos que afetaram as rochas ultramáficas. Apesar de serem comuns em outros complexos da PIAP como Tapira e Salitre, flogopítitos metassomáticos são extremamente abundantes em Catalão I e Araxá. Isso sugere que a fonte de voláteis desses complexos era particularmente rica em álcalis comparativamente a outros complexos da província. A predominância de dolomita carbonatito sobre calcita carbonatito pode estar relacionada com esse evento extensivo de metassomatismo.

Processos comuns de diferenciação em carbonatitos incluem cristalização fracionada, imiscibilidade de líquidos, perda de álcalis por desgasificação e contaminação com encaixantes (Le Bas 1989). Vários modelos que incluem processos metassomáticos, magmáticos, hidrotermais e intempéricos foram propostos para a evolução do Complexo de Catalão I (Baecker 1983, Araújo 1996, Ribeiro et al. 2005, Brod et al. 2001). No entanto, em função da evolução em múltiplos estágios com recorrente magmatismo e metassomatismo, um modelo único ligando as três séries petrogenéticas ainda precisa ser desenvolvido.

CAPÍTULO 2

Immiscibility between silicate- and phoscorite-series in the origin of the Primary Niobium-Ore from the Catalão I Carbonatite Complex, Brazil

PEDRO F O CORDEIRO^{1,2}, JOSÉ A. BROD², ELTON L. DANTAS² AND ELISA S. R. BARBOSA²

¹ANGLO AMERICAN EXPLORATION BRAZIL, AV. INTERLÂNDIA 502, SETOR SANTA GENOVEVA, GOIÂNIA-GO, BRAZIL

²INSTITUTO DE GEOCIÊNCIAS, UNIVERSIDADE DE BRASÍLIA, BRASÍLIA-DF, BRAZIL

The Catalão I carbonatite complex is part of the Late-Cretaceous Alto Paranaíba Igneous Province (APIP), and consists of a multi-intrusion body zoned from bebedourite-(piroxenite)-series rocks in the border to carbonatite- and phoscorite-series rocks in the core. The phoscorite-series rocks consist of apatite, magnetite, and a Mg-silicate (phlogopite or olivine) and were subdivided into early-stage, olivine-bearing (P1) and more evolved, olivine-lacking rocks, dominated either by apatite (P2) or magnetite (P3). P1 rocks are typical phoscorites, whereas P2 and P3 are petrographically classified as nelsonites. These latter two units host the Nb+P+Fe mineralization of the Catalão I complex. Dolomite carbonatite (DC) occurs in association with both P2 and P3, forming paired phoscorite-carbonatite sets. Mica composition changes from phlogopite in P1 through phlogopite cores with tetra-ferriphlogopite rims in P2 to tetra-ferriphlogopite in P3 and DC, which is similar to the Al-depletion seen in micas in phoscorites from the Kovdor and Sokli complexes. P1 apatite is enriched in Si, whereas those from P2, P3, and DC are Sr-rich. Core compositions from both apatite and phlogopite crystals show a composition trend which is consistent with evolution from P1 to DC, further supported by composition variations in whole-rock major oxides. Core-to-rim and textural relationships, are more complex and suggest the smaller amounts of DC in P2 that allowed Sr-enrichment from core to rim and Mg-depletion in the micas. In P3, large amounts of DC were extracted only in the later stages of the crystallization, originating Sr-depletion in apatite and Mg-enrichment in micas. Ilmenites from P1 are Mg-rich whilst those from P2, P3 and DC tend to nearly pure FeTiO₃. Catalão I phoscoritic-rocks and the related dolomite carbonatites (DC) show negative spikes in Gd and Er that correspond to M-type tetrad patterns whilst bebedourites from the complex show a W-type tetrad pattern which mirrors that of phoscorites. This strongly suggests that the two rock-types are related to each other by a liquid immiscibility event from a common, parental carbonated-silicate magma. On the other hand, parallel REE patterns and multielemental diagrams between phoscorite-series rocks and DC suggest that the paired carbonatite-phoscorite associations are generated by fractionation (probably aided by late-stage filter pressing).

KEYWORDS: Phoscorite; Nelsonites; Carbonatite; Catalão I; tetrad patterns

INTRODUCTION

The phoscorite series is an association of rare igneous rocks, including alkaline dunite, phoscorite, nelsonite, apatite, and magnetite. Phoscorites have been described from few localities worldwide, but are of great petrological importance, since they may derive from unusual phosphate-oxide magmas, or be produced as cumulates from carbonatitic or alkaline silicate magma. They are also of economic interest, as phoscorite-series rocks may bear phosphate, niobium, rare-earth and, more rarely, copper mineralization.

Yegorov (1993) defined phoscorite as an igneous rock essentially composed of apatite, magnetite and olivine. Krasnova *et al.* (2004a) suggest that similar rocks containing other magnesian silicates such as diopside and phlogopite instead of olivine should also be termed phoscorite. Cordeiro (2009 – *Capítulo 4*) argued that the essential silicate phase is of paramount importance to establish the evolution stage of phoscorite-series rocks, favouring the Yegorov classification for the phoscoritic rocks of the Catalão I complex. The reader is referred to Cordeiro (2009 - *Capítulo 4*) for a more detailed discussion on this topic.

Phoscorites are often associated with carbonatites, forming multiphase phoscorite-carbonatite associations in alkaline-carbonatite complexes. The magmas may evolve rather complexly, through a combination of crystal fractionation and liquid immiscibility.

Phoscorite-series rocks are being increasingly recognized in the Alto Paranaíba Igneous Province (APIP), Central Brazil, particularly in the Catalão I and Araxá carbonatite-bearing complexes (Brod *et al.*, 2004; Ribeiro *et al.*, 2005; Cordeiro, 2009 - *Capítulos 3 and 4*), where they host major primary phosphate and niobium mineralization. However, because of the thick lateritic cover developed on the alkaline complexes in the studied region, outcrops are very rare or non-existent. In this context, fresh drill-core samples made available by Mineração Catalão (Anglo American Brazil) from the Catalão I Nb deposit provide an excellent opportunity for describing the petrographic features of phoscorite-series rocks, their contact relationships, and their whole-rock and mineral chemistry.

Recent studies regarding phoscorite-series rocks have focused on the description of petrographic and geochemical features, and on the genesis and evolution processes that control magma differentiation (Krasnova *et al.*, 2004a). This paper focuses on textural features, mineral chemistry, and whole-rock chemistry of phoscorites, nelsonites, and associated dolomite carbonatites. We use variations in the mineral chemistry of phlogopite, apatite, magnetite, carbonate, and olivine to define an evolution trend for the phoscorite-series rocks from Catalão I.

REGIONAL GEOLOGICAL SETTING

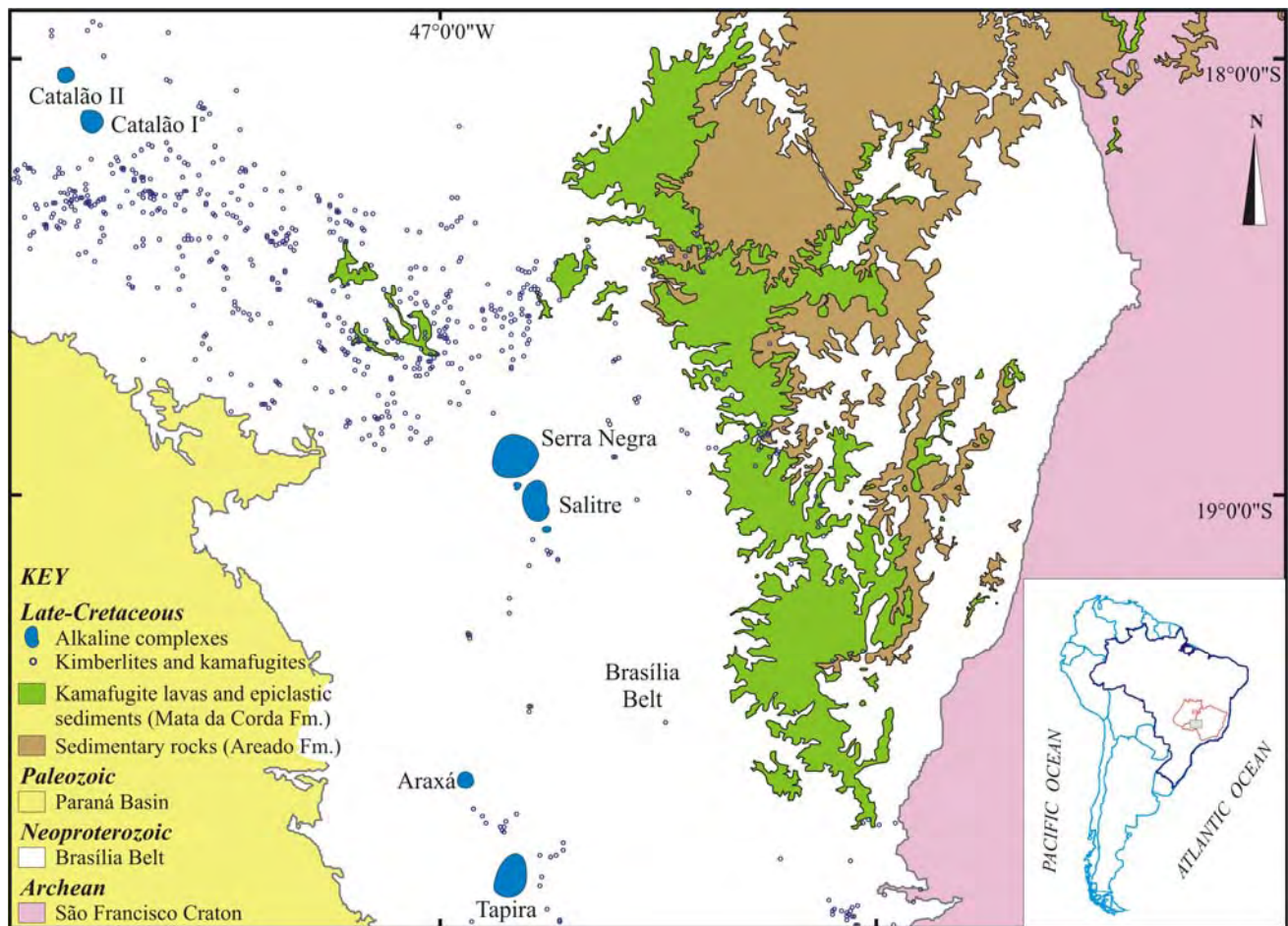


Fig. 3.1. Geological map of the Alto Paranaíba Igneous Province (APIP). Adapted from Oliveira et al. (2004), with the location of the plutonic alkaline-carbonatite complexes. Small open circles represent minor known alkaline (kamafugite and kimberlite).

The Catalão I complex belongs to the Alto Paranaíba Igneous Province (APIP, Fig. 2.1), a NW-trending Late-Cretaceous association of alkaline ultrapotassic rocks intruding Neoproterozoic rocks of the Brasília Mobile Belt. The APIP is located between the Southwest margin of the Archaean São Francisco Craton and the Northeast border of the Palaeozoic Paraná Basin, in Central Brazil (Gibson *et al.*, 1995). The province consists mainly of kamafugites, with subordinate amounts of kimberlites, and minor lamproites, besides the large plutonic alkaline-carbonatite complexes of Catalão I and II, Serra Negra, Salitre I, II and III, Araxá (Barreiro) and Tapira. Both Gibson *et al.* (1995) and Thompson *et al.* (1998) argued for a subcontinental lithospheric mantle source for the Cretaceous alkaline magmatism of central and southeastern Brazil, where a thinspot in the lithosphere allowed the heat of the Trindade mantle plume to penetrate by conduction and advection and, eventually,

cause the melting of readily fusible, K-rich parts of the lithospheric mantle. Brod *et al.* (2000) presented field and whole-rock chemistry evidence for a common origin of the APIP kamafugites and carbonatites, from the same ultrapotassic parental magma, establishing a kamafugitic–carbonatitic association similar to that described in Italy by Stoppa & Cundari (1995) and Stoppa *et al.* (1997), implying in the absence of the ijolitic-series.

CATALÃO I COMPLEX

The Catalão I carbonatite-phoscorite complex (Fig. 2.2) is located in Central Brazil at coordinates $18^{\circ}08'S$, $47^{\circ}48'W$, near the city of Catalão. It intrudes quartzites, schists, and phyllites of the Late-Proterozoic Brasília Belt, forming a vertical, multi-intrusion body with ~ 6 km diameter at the present surface. Sonoki & Garda (1988) report a K-Ar age of 85 ± 6.9 Ma in phlogopite from the complex.

Catalão I contains a variety of mineralizations, including apatite, pyrochlore, monazite, anatase, and vermiculite (Carvalho & Bressan, 1981; Gierth & Baecker, 1986; Ribeiro, 2008). The weathering cover of the complex is currently mined for phosphate and niobium, both deposits associated with the alteration of phoscorite-series rocks.

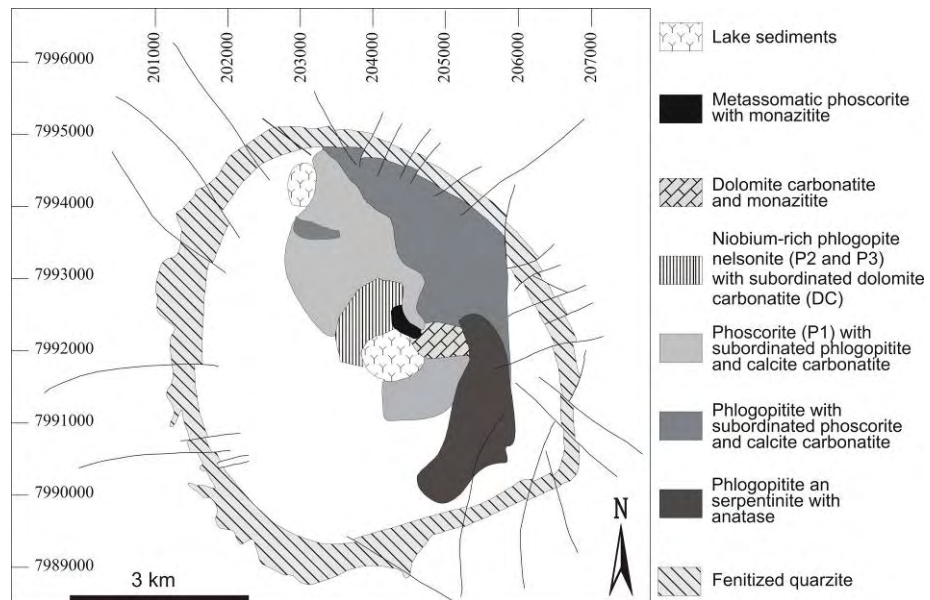


Fig. 2.2. Geological sketch of the Catalão I carbonatite complex. Modified from Brod *et al.* (2004) and Ribeiro (2008). Blank areas represent absence of information from drill core or outcrop.

Metasomatic phlogopite, formed by the interaction of the primary ultramafic alkaline rocks with intrusive carbonatites (Brod *et al.*, 2001), is the dominant petrographic type in the complex, with rare

preserved remnants of the primary dunites and bebedourites. This testifies to the particularly intense self-metasomatism that affected Catalão I, only rivaled in the province by the Araxá complex, further to the south. Phoscorite and carbonatite occur as dykes swarms, rather than massive intrusions, and become increasingly common towards the centre of the complex.

The Catalão I phoscorite-series rocks are divided in four stages (Cordeiro, 2009 – *Capítulo 4*) according to their modal mineralogy and magma evolution (Fig. 2.3). The P1 stage consists mainly of phoscorites, P2 and P3 are represented by nelsonitic rocks, and DC by dolomite carbonatites (Fig. 2.4 and 2.5). The primary pyrochlore mineralization is mostly contained in P2 and P3 rocks. In the late-stage nelsonites P2 and P3, there are no evidences of the wide metasomatic alteration that affected the ultramafics and the P1 phoscorites.

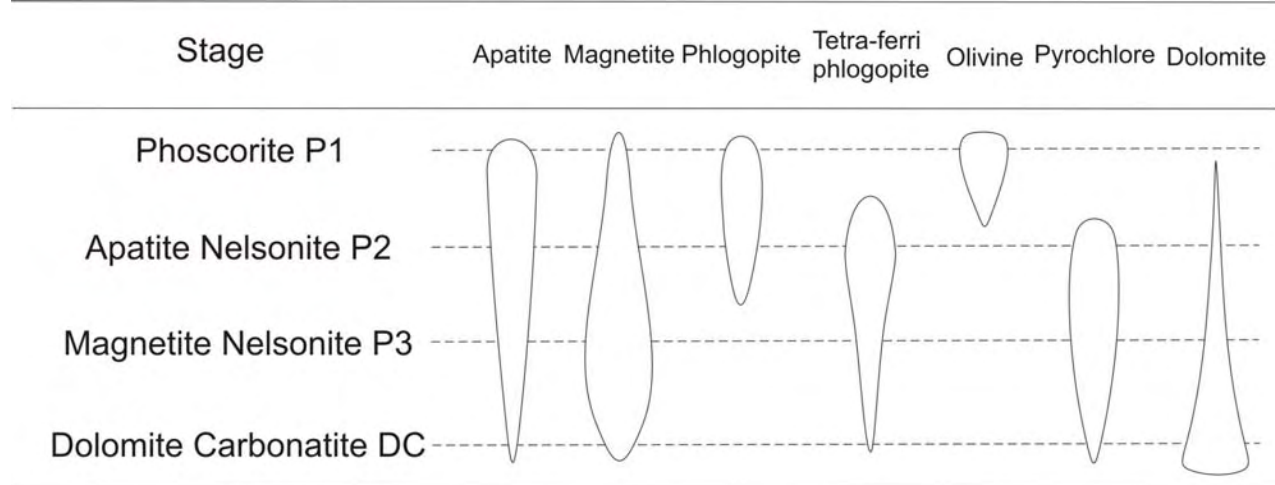


Fig. 2.3. Comparative modal composition of Catalão I phoscorite-series rocks and associated carbonatites. The main features of P1 are the occurrence of olivine and the coarse-grained texture. P2 and P3 are olivine-free rocks (nelsonites, magnetites and apatites) where the main silicate phases are phlogopite and/or tetra-ferriphlogopite. For a discussion on rock nomenclature see Cordeiro (2009 – *Capítulo 4*).

The wall rock of the early-stage phoscorites P1 (Fig. 2.4A and 2.5A) are usually carbonatite, bebedourite or metasomatic phlogopite, occurring as coarse- to medium-grained small plugs or dikes near the core of the Catalão I complex. They are composed of olivine, apatite, phlogopite, and magnetite, with accessory baddeleyite, ilmenite, clinohumite, rutile, dolomite, and magnesite. Compared to late-stage nelsonites, P1 phoscorites were more affected by metasomatism, which induced the transformation of olivine into minute tetra-ferriphlogopite crystals and clinohumite.

Late-stage, phlogopite nelsonites P2 (Fig. 2.4B and 2.5B) and P3 (Fig. 2.4C and 2.5C) typically lack olivine and have tetra-ferriphlogopite and subordinate phlogopite as the essential silicate phases.

Pyrochlore varies in abundance from an accessory phase to up to 16 vol. %. Other accessories include dolomite, barite, norsethite, pyrite, sphalerite, and chalcopyrite. P2 rocks are apatite-rich (apatite/magnetite > 0.8) and often contain mica with phlogopite cores surrounded by tetra-ferriphlogopite rims. P3 are magnetite-rich (apatite/magnetite < 0.8%) and the only silicate present is tetra-ferriphlogopite.

The nelsonitic rocks often contain pockets of dolomite carbonatite grouped here under the DC designation (white pockets in figures 2.4B, 2.4C, and 2.4D), which may locally represent up to 20 vol. % in P2 rocks and up to 40 vol. % in P3. The intimately-related carbonatites and phoscorites in several worldwide complexes are interpreted by Krasnova *et al.* (2004b) and Lee *et al.* (2004) as pairs of carbonatite and phoscorite which share the same mineralogy and evolve from one differentiation stage to the other. Lee *et al.* (2004) described mineral chemistry variations between the paired carbonatites and phoscorites of the Sokli complex (Finland), consistent with magma evolution. In this work we could not find mineral or whole-rock chemistry criteria to unequivocally discriminate between dolomite carbonatites associated with P2 and with P3. Therefore, the DC term is used indiscriminately in this paper to designate dolomite carbonatite pockets and dikes related to both P2 and P3.

The DC pockets are rounded to irregularly-shaped, sometimes globular or amoeboid, resembling mingling textures (Fig. 2.4B and 2.4C). They are often composed of a central zone of dolomite with subordinate barite, norsethite, pyrite and chalcopyrite, and a rim at the contact with the host nelsonite, composed of magnetite aggregates, subhedral pyrochlore, radial prismatic apatite, tetra-ferriphlogopite, and ilmenite. Crystals in the rim zone are often elongated toward the center of the pocket (Fig. 2.5D), resembling a comb-layering texture. In some pockets the rim zone may be absent, or restricted to a magnetite aggregate. This texture was called a “bunch of grapes” texture by Hirano *et al.* (1990).

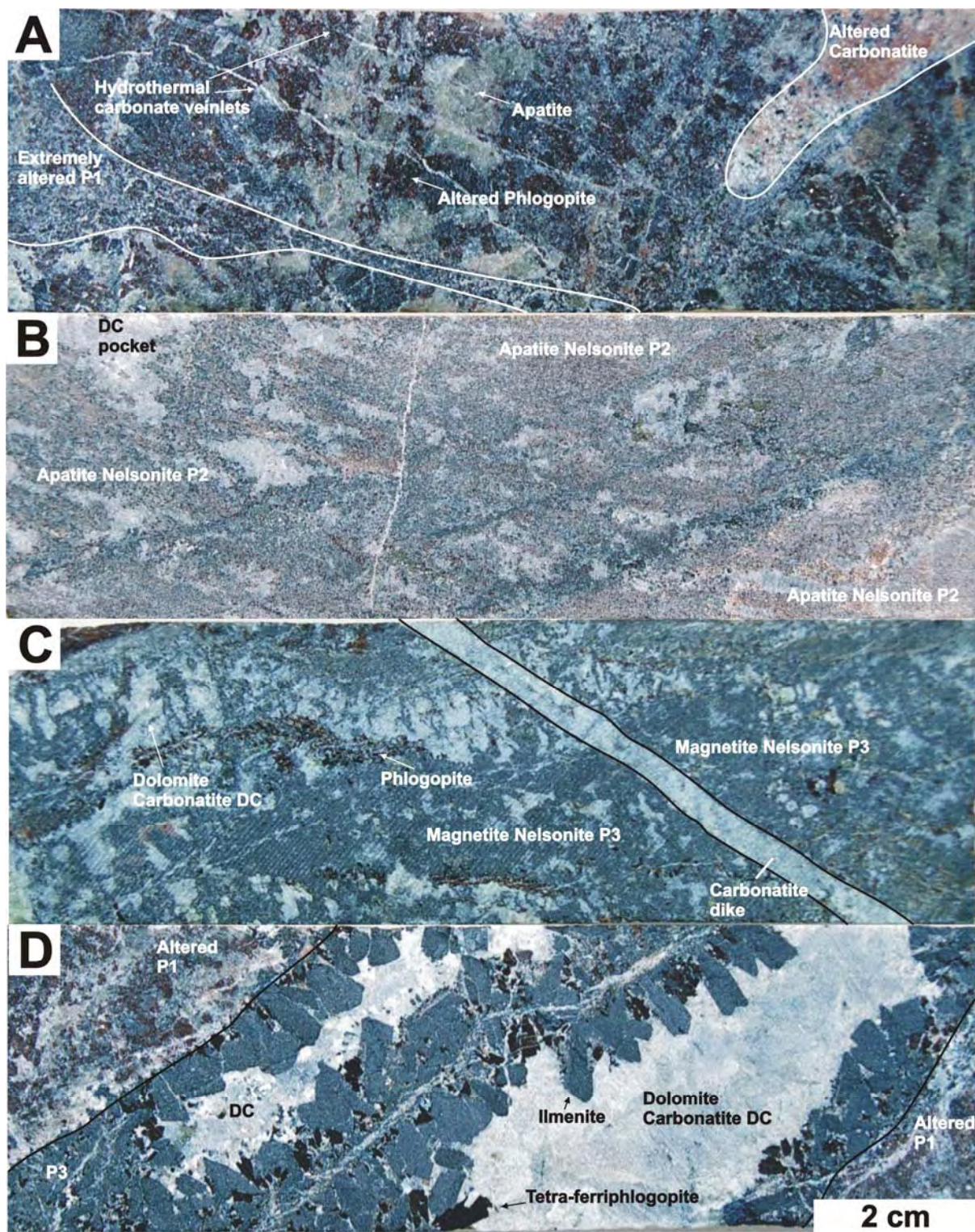


Fig. 2.4. Photograph of drill-core samples from the Catalão I Nb deposit. A. P1 (phoscorite) with altered phlogopite and carbonate. Hydrothermal carbonate veinlets are responsible for the alteration. B. P2 (apatite-nelsonite) with DC pockets. The pinkish tone is due to the presence of pyrochlore and small amounts of tetra-ferriphlogopite. C. P3 (magnetite-nelsonite) with DC pockets, cut by a carbonatite dike. D. P3 dyke containing DC pockets, hosted in altered P1 (note the subhedral crystals of ilmenite and phlogopite elongated toward the center of the pockets).

The DC dikes crosscutting both the phoscorite-series rocks and their hosts are up to 20 cm-thick, with texture and mineralogy similar to the dolomite carbonatite pockets in the nelsonites. They are composed of dolomite, ilmenite, tetra-ferriphlogopite, apatite, norsethite, barite, pyrochlore, and magnetite, and interpreted as carbonatite melts extracted either from a phoscorite or nelsonite magma or cumulate pile.

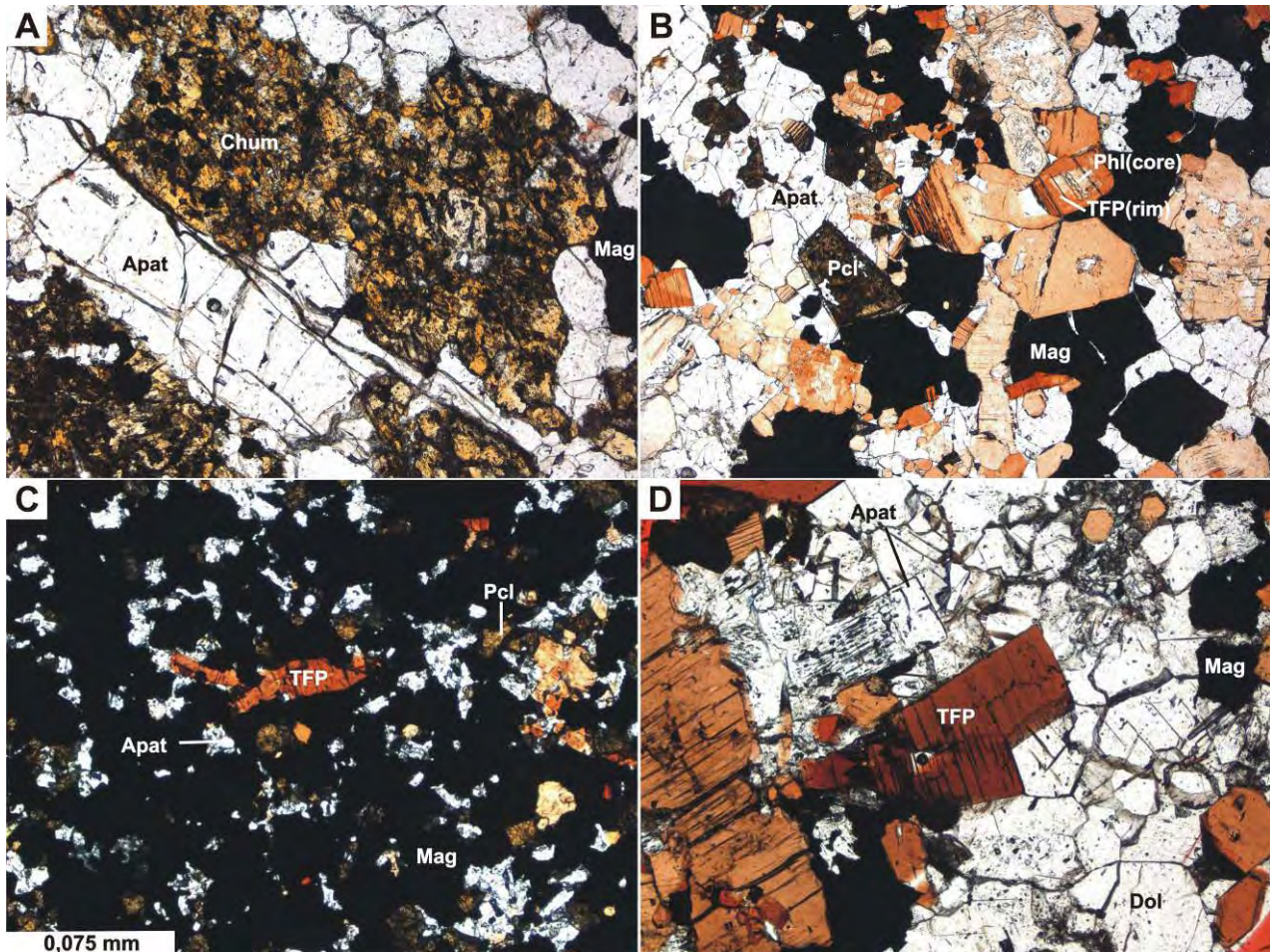


Fig. 2.5. Photomicrographs of the phoscorite series rocks from the Catalão I carbonatite complex. A) P1 = coarse- to medium- grained phoscorite with clinohumite pseudomorphs after olivine. B) P2 = apatite-nelsonite showing zoned mica, with phlogopite cores and tetra-ferriphlogopite rims. C) P3 = Magnetite-nelsonite with tetra-ferriphlogopite, apatite and pyrochlore. D) DC = Dolomite carbonatite pocket in P2 with tetra-ferriphlogopite, magnetite and apatite crystallizing at the walls, the same texture shown in hand-sample in Fig. 2.4D. (Chum = clinohumite, Phl = phlogopite, TFP = tetra-ferriphlogopite, Dol = dolomite, Pcl = pyrochlore, Apat = Apatite, and Mag = Magnetite).

METHODS AND SAMPLES

Samples were collected from drill cores of the Catalão I primary niobium deposit, made available by Mineração Catalão (Anglo American Brazil). Sampling was aimed at rocks as fresh as possible and free from metasomatic alteration. Polished thin sections of each sample were studied by transmitted and reflected light microscopy in order to determine their composition and textural properties.

Chemical composition of selected mineral phases was determined by WDS using a CAMECA SX-50 electron microprobe at the University of Brasília. The analytical conditions were set at 20 kV and 20 nA.

Samples destined to whole-rock geochemistry were ground in an agate mill. Where necessary, small-volume samples from carbonate pockets and dykes were extracted using a manual tungsten-carbide drill and ground manually in an agate mortar. Major and trace element compositions were determined by a combination of ICP-AES and ICP-MS at the Acme Laboratories, Canada.

Sample preparation for Sm-Nd analyses was carried out according to Gioia & Pimentel (2000). For Nd isotope analyses, 50 to 100 mg of whole-rock powder were mixed with a ^{149}Sm - ^{150}Nd spike and dissolved in a HF-HNO₃ mixture in closed savilex vials. Sm and Nd were extracted in ion exchange columns with LN-Spec resin, evaporated, deposited on Re filaments and analysed in a Finnigan MAT-262 mass spectrometer with 7 Faraday-cup type collectors at the Geochronology Laboratory, University of Brasília. $^{143}\text{Nd}/^{144}\text{Nd}$ was normalized to $^{146}\text{Nd}/^{144}\text{Nd}=0.7219$, and the decay constant used was $6.54 \times 10^{-12}/\text{y}$ (Lugmair & Marti, 1978).

Samples for Sr isotope analyses were dissolved in the same way as those for Sm-Nd. Sr was separated in an ion exchange column using Bio-Rad AG 50W-X8 200-400 *mesh* resin. Samples were deposited in Re filaments and analysed in a Finnigan MAT-262 multicollector mass spectrometer, in static mode, at the Geochronology Laboratory, University of Brasília. Typical 2σ errors for $^{87}\text{Sr}/^{86}\text{Sr}$ were $< 0.017\%$.

MINERAL CHEMISTRY

Apatite

Apatite is one of the most abundant non-silicate minerals in the crust and it is also the source of phosphate for the agricultural and food industries. In Brazil, phosphate is mainly mined from carbonatite complexes, rather than from sedimentary phosphorites as in most other countries (Toledo & Pereira, 2001). In the APIP carbonatite complexes, apatite occurs in all rock types and, therefore,

can be used to compare rocks at different evolution stages. Zoned crystals are common and may provide a valuable contribution to the understanding of the evolution of carbonatite-related magmas.

The ideal apatite composition may be expressed by the formula $\text{Ca}_{10}(\text{PO}_4)_6\text{F}_2$. Substitutions can occur in all Ca-, P-, and F-sites.

Since carbonatite and phoscorite magmas are Sr- and REE-rich, apatite crystallized from them is expected to reflect this enrichment. REE substitution is usually coupled with Na or Si in the apatite structure and the LREE may be strongly fractionated from the HREE (Toledo & Pereira, 2001). Torres (1996) described Sr-rich apatite from the Araxá Complex, in the southern portion of the APIP, with average SrO content between 0.8 and 1.2 wt.%, but highly variable between rock types.

The occurrence of Si in the P-site of carbonatite-related apatite is highly variable. The coupled substitution $\text{Ca}^{2+} + \text{P}^{5+} = \text{Si}^{4+} + \text{REE}^{3+}$ (britholite substitution) is one of the most commonly evoked schemes for Si in apatite (Hogarth, 1989; Toledo & Pereira, 2001).

The textural features of apatites from the Catalão I phoscorites and nelsonites vary greatly between rocks of different evolution stages. In P1 phoscorites, apatite tends to be light-green, typically forming coarse to medium-grained aggregates of anhedral to subhedral crystals. In P2 nelsonites, apatite occurs as prismatic fine-grained euhedral to subhedral crystals, commonly displaying flow texture. In this stage, the apatite rims usually contain tiny opaque-mineral and fluid inclusions which give a turbid aspect to the grains in thin section whilst its cores are free from inclusions. P3 apatite occurs as subhedral to anhedral, fine-grained crystals within homogenous magnetite aggregates. Apatite from this stage tends to form monomineralic aggregates with poorly defined outlines. Similar textures have been reported from the Vuoriyarvi late-stage phoscorites (P3 from Karchevsky & Moutte, 2004), and described as meshes of interlocked apatite needles.

In DC pockets and dikes, apatite occurs as typical subhedral crystals varying from fine to coarse grained and commonly also as radial aggregates. The crystals are often perpendicular to the walls, growing toward the center of the pocket or dike (Fig. 2.5D).

Apatite microprobe analyses were recalculated on the basis of 25 oxygens in order to avoid any effects of P-site vacancy or substitution by elements that were not analysed such as S and C. There is a wide composition range in Ca, P, ETR (La+Ce), Si, and Sr in apatite from the Catalão I phoscorites, nelsonites, and dolomite carbonatites (Table 2.1), although the fields for apatite from different rock-types overlap.

Tab.2.1 Representative apatite compositions from the Catalão I phoscorite-series rocks and carbonatites.

Sample	110-46		056		093		099a		099b		183r	
Rock type	P1	P1	DC	DC	P2	P2	P3	P3	P2	P2	P3	P3
Position	core	rim	-	-	rim	core	rim	core	rim	core	rim	core
Oxides (wt%)												
P ₂ O ₅	41.13	40.89	40.40	39.82	40.56	41.95	42.09	41.86	41.07	42.05	43.06	42.19
SiO ₂	1.01	0.89	0.00	0.00	0.00	0.03	0.00	0.00	0.00	0.04	0.05	0.00
La ₂ O ₃	0.47	0.64	0.65	0.28	1.17	0.24	0.37	0.37	0.55	0.08	0.12	0.42
Ce ₂ O ₃	1.00	0.88	0.90	0.82	1.79	0.60	0.85	0.81	1.27	0.31	0.36	0.83
Al ₂ O ₃	0.04	0.00	0.01	0.00	0.01	0.00	0.00	0.02	0.00	0.00	0.02	0.01
CaO	51.81	52.29	50.76	50.70	48.18	53.66	50.64	50.08	50.32	53.17	52.85	51.53
SrO	1.04	0.69	3.09	4.00	3.34	0.90	3.45	3.59	3.40	1.30	2.25	3.67
MgO	0.07	0.05	0.12	0.17	0.03	0.00	0.00	0.09	0.04	0.09	0.04	0.03
Fe ₂ O _{3T}	0.04	0.08	1.09	0.09	0.04	0.00	0.47	0.02	0.65	0.03	0.26	0.10
BaO	0.00	0.00	0.03	0.19	0.22	0.00	0.11	0.06	0.00	0.00	0.16	0.00
Na ₂ O	0.00	0.00	0.00	0.51	0.48	0.00	0.00	0.00	0.00	0.00	0.00	0.00
K ₂ O	0.00	0.00	0.04	0.06	0.01	0.00	0.02	0.02	0.02	0.00	0.02	0.00
Total	96.61	96.41	97.08	96.62	95.83	97.38	97.99	96.91	97.31	97.07	99.18	98.77
Cations (p.f.u.)												
P	5.935	5.921	5.933	5.899	6.021	6.015	6.065	6.084	5.993	6.041	6.076	6.038
Si	0.171	0.153	0.000	0.000	0.000	0.004	0.000	0.000	0.000	0.006	0.009	0.000
La	0.029	0.040	0.042	0.018	0.075	0.015	0.023	0.023	0.035	0.005	0.007	0.026
Ce	0.119	0.105	0.109	0.100	0.219	0.071	0.101	0.098	0.153	0.036	0.042	0.098
Al	0.007	0.000	0.001	0.000	0.002	0.000	0.000	0.004	0.000	0.000	0.005	0.002
Ca	9.461	9.582	9.433	9.506	9.052	9.737	9.234	9.213	9.291	9.667	9.437	9.333
Sr	0.103	0.068	0.311	0.406	0.339	0.089	0.341	0.357	0.339	0.128	0.217	0.360
Mg	0.017	0.014	0.030	0.044	0.007	0.000	0.000	0.023	0.010	0.023	0.009	0.009
Fe _T	0.011	0.022	0.316	0.025	0.013	0.000	0.133	0.005	0.188	0.009	0.071	0.028
Ba	0.000	0.000	0.002	0.013	0.015	0.000	0.008	0.004	0.000	0.000	0.010	0.000
Na	0.000	0.000	0.000	0.173	0.163	0.000	0.000	0.000	0.000	0.000	0.000	0.000
K	0.001	0.000	0.010	0.013	0.003	0.000	0.005	0.005	0.004	0.000	0.005	0.000
Sum	15.854	15.905	16.187	16.197	15.910	15.931	15.909	15.816	16.012	15.916	15.888	15.894

Table 2.1 (continued)

Sample	206		207		230a		244		304a		319	
Rock type	P3	P3	DC	DC	P2	P2	P1	P1	P2	P2	P1	P1
Position	rim	core	rim	-	rim	core	rim	core	rim	core	rim	core
Oxides (wt%)												
P ₂ O ₅	40.90	42.33	41.98	42.76	41.91	42.80	42.67	42.75	41.61	41.38	42.41	42.75
SiO ₂	0.06	0.03	0.00	0.00	0.00	0.01	0.04	0.18	0.00	0.03	0.04	0.22
La ₂ O ₃	0.28	0.22	0.10	0.26	0.37	0.28	0.65	0.11	0.53	0.28	0.09	0.49
Ce ₂ O ₃	0.74	0.61	0.26	0.62	0.85	0.71	0.80	0.93	1.25	0.50	0.37	0.65
Al ₂ O ₃	0.01	0.01	0.00	0.00	0.00	0.00	0.00	0.04	0.02	0.02	0.00	0.01
CaO	51.18	51.25	51.85	51.23	51.21	52.58	52.97	53.42	49.76	52.21	53.03	51.65
SrO	1.94	2.95	2.33	3.36	3.18	1.54	1.02	0.98	4.21	1.55	1.35	1.15
MgO	0.11	0.05	0.00	0.08	0.01	0.00	0.00	0.07	0.01	0.10	0.06	0.06
Fe ₂ O _{3T}	0.21	0.22	0.28	0.06	0.04	0.11	0.04	0.00	0.14	0.07	0.01	0.04
BaO	0.00	0.07	0.00	0.00	0.20	0.00	0.09	0.00	0.03	0.00	0.00	0.00
Na ₂ O	0.00	0.00	0.00	0.00	0.00	0.00	0.07	0.00	0.09	0.00	0.00	0.00
K ₂ O	0.01	0.02	0.01	0.00	0.01	0.01	0.00	0.01	0.00	0.02	0.00	0.00
Total	95.42	97.75	96.81	98.36	97.78	98.04	98.35	98.49	97.65	96.15	97.36	97.02
Cations (p.f.u.)												
P	6.014	6.081	6.072	6.103	6.049	6.087	6.059	6.038	6.045	6.023	6.066	6.113
Si	0.010	0.005	0.000	0.000	0.000	0.002	0.006	0.031	0.000	0.005	0.007	0.036
La	0.018	0.014	0.006	0.016	0.023	0.017	0.040	0.007	0.034	0.018	0.006	0.031
Ce	0.090	0.073	0.031	0.072	0.101	0.083	0.094	0.108	0.150	0.060	0.043	0.077
Al	0.002	0.001	0.000	0.000	0.000	0.000	0.000	0.008	0.004	0.005	0.000	0.003
Ca	9.524	9.317	9.492	9.253	9.354	9.461	9.518	9.548	9.149	9.617	9.600	9.347
Sr	0.195	0.291	0.231	0.328	0.314	0.150	0.099	0.095	0.419	0.154	0.133	0.113
Mg	0.029	0.013	0.000	0.021	0.002	0.001	0.000	0.017	0.002	0.024	0.014	0.015
Fe _T	0.060	0.063	0.079	0.018	0.012	0.032	0.011	0.000	0.040	0.019	0.004	0.010
Ba	0.000	0.004	0.000	0.000	0.013	0.000	0.006	0.000	0.002	0.000	0.000	0.000
Na	0.000	0.000	0.000	0.000	0.000	0.000	0.022	0.000	0.030	0.000	0.000	0.000
K	0.002	0.004	0.003	0.000	0.002	0.002	0.000	0.003	0.000	0.003	0.000	0.001
Sum	15.944	15.864	15.914	15.811	15.871	15.834	15.855	15.853	15.874	15.930	15.872	15.745

Figure 2.6 shows substitution schemes for the apatites from the phoscorite-series rocks of the Catalão I complex, compared with those from Kovdor in Russia (Krasnova *et al.*, 2004b), Vuoriyarvi in Russia (Karchevsky & Moutte, 2004) and Sokli in Finland (Lee *et al.*, 2004). In the Sr vs. Ca diagram, apatites from the P1 early phoscorites vary along a 1Sr:4Ca substitution line, and are characterized by low strontium content. The trend of late-stage P2 and P3 nelsonites is parallel to Sr/Ca 1:2 ratio, indicating that $\text{Ca}^{2+}=\text{Sr}^{2+}$ substitution plays a more important role in the evolution of these apatites. Analyses of DC apatites are scattered in the Ca-Sr diagram and can be interpreted as partly following the 1:2 substitution along with P2 and P3, but partly evolving along a 1:4 trend parallel with that of the early phoscorites. Kovdor apatites are Sr-poor when compared with Catalão I, and do not show significant $\text{Ca}^{2+}=\text{Sr}^{2+}$ substitution. On the other hand, apatites from Sokli and Vuoriyarvi have a similar trend to that of apatite from Catalão I early phoscorites. Regardless of the Sr:Ca ratio governing the substitution, it is clear that Ca decreases and Sr increases in Catalão I apatite with magma evolution. This is also true of apatites in phoscorites from the Kola Province Complexes (Krasnova *et al.* 2004b; Karchevsky & Moutte, 2004; Lee *et al.*, 2004), suggesting that Sr content in apatite is a reliable index of magma evolution in apatites and carbonatites related to the phoscorite-series.

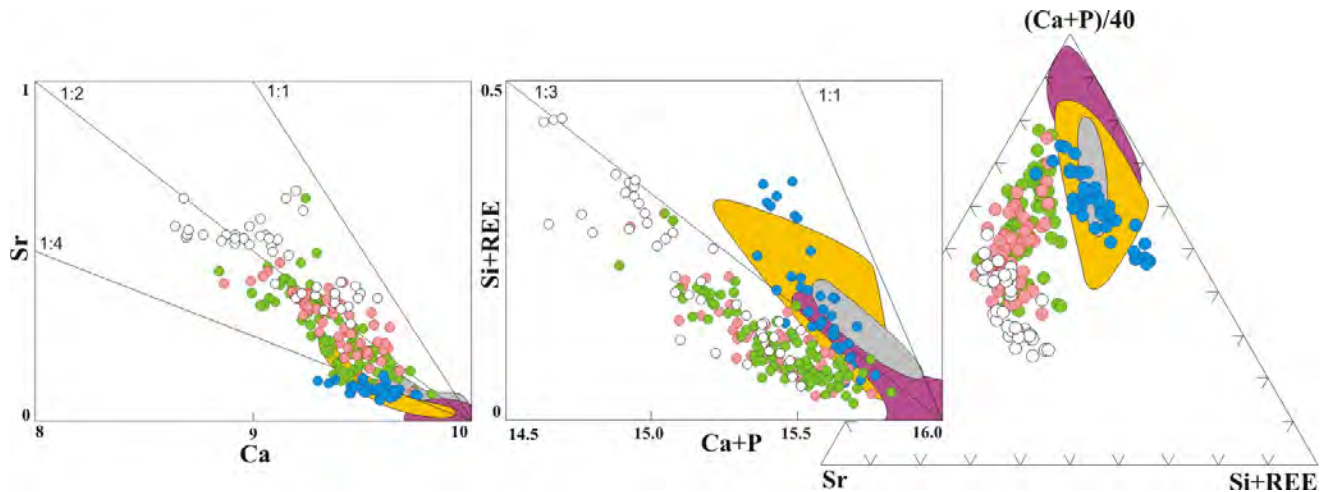


Fig. 2.6. Apatite substitution schemes showing the Sr-enrichment from P1 towards DC. Note that in the case of the occurrence of Si+REE in the apatite structure, the substitution scheme varies from 1:1 in P1 to 1:3 in P2/P3/DC. The analyses are compared with the composition fields of apatites in phoscorites and carbonatites from the Kola Province. (Purple = Kovdor Complex, Krasnova *et al.* 2004b. Grey = Vuoriyarvi, Karchevsky & Moutte, 2004. Orange = Sokli, Lee *et al.* 2004). P1 = Blue circles, P2 = green circles; P3= pink circles; DC = white circles. All variables are cations per formula unit.

The britholite-type substitution is defined by the equation $\text{Ca}^{2+}+\text{P}^{5+}=\text{Si}^{4+}+\text{REE}^{3+}$ (Hogarth, 1989) and occurs in P1 apatites, which plot parallel to a 1:1 substitution line. Apatites from P2, P3 and DC are virtually Si-free (less than 0.03 a.p.f.u.) therefore not related to the britholite substitution.

Apatite in phoscorites from Kovdor and Vuoriyarvi, and phoscorite-related carbonatites from Sokli are plotted for comparison and seem to parallel a 1:2 line.

The ternary Sr-(Ca+P)-(REE+Si) diagram summarizes the identified substitutions in the Catalão I phoscorites and related carbonatites (Fig. 2.6). In the early phoscorites (P1) apatite evolution is controlled by the britholite substitution, leading to enrichment in Si and REE, whereas Sr substitution for Ca is less significant. The more evolved nelsonites, on the other hand, have a wider range of Sr variation, indicating that these apatites evolved by Sr enrichment. Apatite analyses from DC seem to realign with the early phoscorite P1 trend. Kovdor, Vuoriyarvi and Sokli apatites show an evolution path dominated by the britholite-type substitution.

Chemical variations can also be recognized between rim and core of individual crystals. The results of the profiling of selected euhedral grains are represented in Figure 2.7 which shows that the cores of apatite crystals become progressively more enriched in Sr in the sequence P1-P2-P3-DC. This is consistent with the expected Sr enrichment in apatite with magma evolution as discussed above. The zoning patterns, however, are more complex.

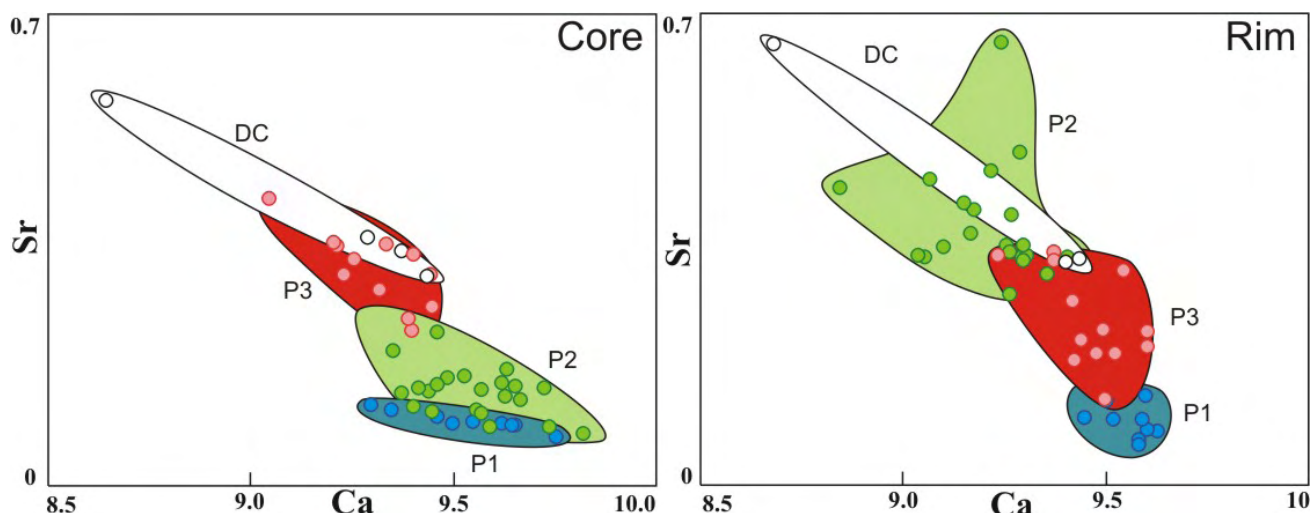


Fig. 2.7. Ca^{2+} - Sr^{2+} substitution in rims and cores of selected euhedral apatite crystals. Note that the apatite rims from P2 are richer in Sr than the corresponding cores, whereas P3 apatites show the opposite. Ca and Sr values are cations per formula unit. Symbols as in Figure 2.6.

There is little Sr variation between cores and rims of P1 apatites, which is in good agreement with the dominance of the britholite-type substitution at this evolution stage. P2 apatite cores are slightly more Sr-rich than P1 apatite, and evolve by Sr enrichment toward the rims, as expected. Finally, the cores of apatite crystals from P3 nelsonites and from DC have the highest Sr contents, but a consistent decrease in Sr content is observed from core to rim. This may be related with the

onset and continued crystallization of large amounts of carbonates from the magma, with Sr preferably partitioning to the carbonate rather than to apatite or, with an increasing carbonate content in the residual magma.

Overall, apatite from the Catalão I rocks shows compositional variations consistent with a general progression in the sense P1-P2-P3-DC with magma evolution. However, the opposite zoning patterns observed between P2 and P3 apatites are noteworthy and probably controlled by other magmatic parameters.

Phlogopite

Phlogopite is the most common silicate mineral in the APIP phoscorite-series rocks and carbonatites. Both the phlogopite-annite and the tetra-ferriphlogopite – tetra-ferriannite series occur in the alkaline-carbonatite complexes of the province, but the former is mainly associated with alkaline silicate rocks such as dunites, bebedourites and syenites, whereas the latter is typical of carbonatites and metasomatic phlogopitites (Araújo, 1996; Brod *et al.*, 2001).

A wide range of solid-solutions occurs between the ideal end-members of micas described by Rieder *et al.* (1998). The most common cations in the interlayer site are Na and K although Ba, Cs, NH₄, Rb and Ca are also possible alternatives. Lee *et al.* (2003) report that micas from carbonatites are distinctively rich in Na₂O reaching up to 2.1 wt%. Gaspar & Wyllie (1982) describe Ba-rich micas (up to 10.3% of BaO) from the Jacupiranga complex in SE Brazil.

The phlogopite-annite series is defined by the substitution of Fe²⁺ for Mg²⁺ in the octahedral site. Brod *et al.* (2001) and Barbosa *et al.* (in preparation) demonstrated that the Mg-depletion is an excellent marker of magma differentiation in silicate alkaline rocks of the Tapira and Salitre complexes in the APIP. Brod *et al.* (2001) also argued that in carbonatites this relationship is not straightforward, because of the concomitant precipitation of substantial magnetite from the liquid. This may also be the case in other magnetite-rich rocks such as phoscorites and nelsonites. Ti is also a common element in phlogopite of carbonatite-related rocks (up to 13.8 wt.% TiO₂, Lee *et al.*, 2003). Although some authors argued for the occurrence of Ti in the tetrahedral site (Farmer & Boetcher, 1981), this was not supported for the APIP carbonatites (Brod *et al.* 2001).

The main tetrahedral cations are Si⁴⁺ and Al³⁺, although Fe³⁺ commonly substitutes for tetrahedral Al³⁺ in alkaline rocks, generating the tetra-ferriphlogopite/tetra-ferriannite series K(Mg,Fe²⁺)₃(Al,Fe³⁺)Si₃O₁₀(OH)₂. Mitchell and Bergman (1991) and Mitchell (1995) interpreted Al-deficiency in micas as a direct consequence of the peralkalinity of the magma which explains the

frequent occurrence of tetra-ferriphlogopite in carbonatites and rocks of the phoscorite series. The $\text{Al}^{3+}=\text{Fe}^{3+}$ tetrahedral substitution in the Catalão I micas was confirmed by Araújo (1996) through Mössbauer spectroscopy. Reverse pleochroism ($\alpha > \beta = \gamma$), induced by the presence of ${}^{\text{IV}}\text{Fe}^{3+}$, is a characteristic feature of tetra-ferriphlogopite.

Tetra-ferriphlogopite occurs as both igneous and metasomatic varieties in the APIP carbonatitic complexes. Although their chemistry can be very similar, textural evidence can be used to determine their origin. Aggregates of minute, anhedral tetra-ferriphlogopite flakes occurring at the contact between carbonatite intrusions and ultramafic rocks result from the metasomatic replacement of olivine, pyroxene, and/or primary aluminous phlogopite (Brod *et al.* 2001). Metasomatic tetra-ferriphlogopite also occurs in rocks of the phoscorite series, characterized by replacement of the original phlogopite or olivine by rims and patches of tetra-ferriphlogopite. On the other hand, tetra-ferriphlogopite of igneous origin, occurring in carbonatites, phoscorites and nelsonites is often euhedral, with sharp contours, and may show concentric optical zoning.

In the early phoscorites P1, phlogopite occurs as centimetric- to milimetric euhedral to anhedral flakes. It commonly shows cores with normal absorption directions, but rims of reversely-pleochroic tetra-ferriphlogopite can occur.

In the P2 nelsonites, there is a clear predominance of tetra-ferriphlogopite over phlogopite. Tetra-ferriphlogopite occurs as euhedral to subhedral, medium to fine grained flakes. More rarely, phlogopite crystals contain a core of aluminous, phlogopite, with normal pleochroism.

In the P3 nelsonites, mica consists almost entirely of tetra-ferriphlogopite, with extremely rare occurrences of more aluminous cores. Tetra-ferriphlogopite occurs as euhedral to subhedral, fine grained flakes in these rocks.

Mica from the DC pockets and dikes is fine to coarse grained, subhedral tetra-ferriphlogopite. Similarly to apatite, it may occur as large crystals growing inward, perpendicularly to the contact of carbonatite pockets or dikes with the host nelsonites.

Table 2.2 shows representative analysis of Catalão I phlogopite. Structural formulae were recalculated according to Brod *et al.* (2001). The analyses were initially recalculated on the basis of 22 oxygen and part of the Fe was recast as ${}^{\text{IV}}\text{Fe}^{3+}$ in order to fulfill the equation:



This calculations assume that initial vacancies in the tetrahedral site in Al-deficient phlogopites are entirely filled by $^{(IV)}\text{Fe}^{3+}$. After completion of the tetrahedral position, the remaining Fe is assumed as octahedral Fe^{2+} . FeO and Fe_2O_3 are back-calculated into oxide proportions and a new structural formula is calculated on the basis of 24 O (OH,F,Cl). If this still produces tetrahedral deficiency the procedure can be repeated until fulfillment of the tetrahedral site (Brod *et al.*, 2001).

All micas from the Catalão I phoscorites, nelsonites and dolomite carbonatites plot as members of the tetra-ferriphlogopite/tetra-ferri-annite series (Fig. 2.8A and 2.8C), although subordinate octahedral $\text{Fe}^{2+}=\text{Mg}^{2+}$ substitution is also present (Fig. 2.9B).

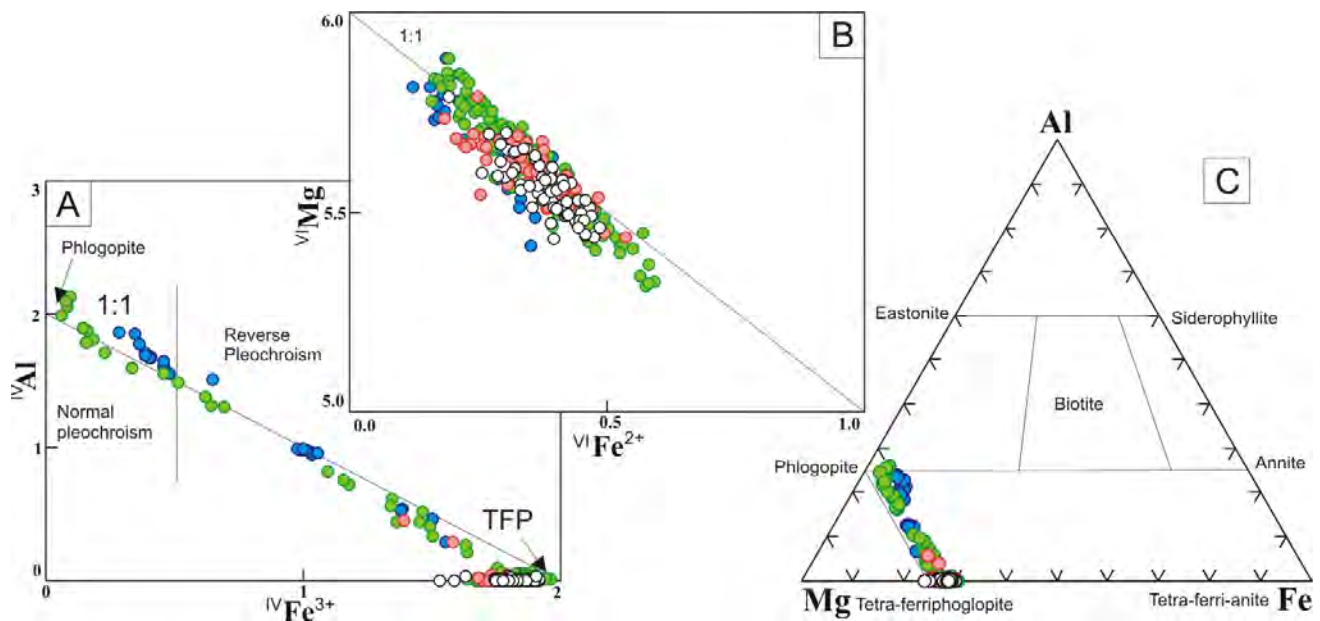


Fig. 2.8. Chemical composition of phlogopites in Catalão I phoscorites, nelsonites and dolomite carbonatites. (A) Al vs Fe^{3+} (a.p.f.u.) showing the spreading of the analyses along the phlogopite – tetra-ferriphlogopite 1:1 substitution line, with indication of the composition corresponding to the reversal in pleochroism. (B) Mg^{2+} vs Fe^{2+} (a.p.f.u.) diagram showing that the phlogopite-annite substitution also occurs, but is subordinate (total span of ca. 0.5 a.p.f.u.). (C) triangular classification plot showing the composition of the analysed micas in the phlogopite – tetra-ferriphlogopite series. Symbols as in Fig. 2.6.

The $^{(VI)}\text{Fe}^{3+}=\text{Al}^{3+}$ substitution in the 1:1 ratio defines the solid-solution between phlogopite and tetra-ferriphlogopite (Fig. 2.8). Phlogopites from P1 phoscorites and P2 phlogopite nelsonites plot along the solid-solution line, though most P2 micas have tetra-ferriphlogopite composition. All phlogopites from P3 and DC plot at or very near the tetra-ferriphlogopite end-member. This indicates that the magma from which they crystallized was extremely depleted in Al, since phlogopite is the only Al-bearing mineral in these rocks.

Tab. 2.2 Representative phlogopite compositions from the Catalão I phoscorite-series rocks and carbonatites.

Sample	206		230B		157B		178		93		192B	
Rock type	P3	P3	P3	P3	P3	P3	P2	P2	P2	P2	P2	P2
Position	rim	core										
Oxides (wt%)												
SiO ₂	40.94	40.43	40.57	40.91	41.88	40.32	40.24	41.76	41.00	41.39	39.94	39.56
TiO ₂	0.06	0.07	0.15	0.09	0.12	0.11	0.06	0.02	0.10	0.11	0.11	0.10
Al ₂ O ₃	0.04	0.09	0.00	0.04	0.02	0.01	0.12	7.68	0.07	0.03	0.12	0.00
Fe ₂ O ₃	15.97	15.61	16.38	16.35	16.81	16.01	15.86	6.39	16.43	15.27	16.34	16.07
FeO	1.91	2.40	2.73	2.52	2.64	3.43	3.73	1.45	3.30	4.51	2.30	2.52
MnO	0.05	0.07	0.01	0.00	0.10	0.08	0.12	0.03	0.08	0.11	0.05	0.02
MgO	25.31	24.42	24.73	25.18	25.91	24.07	24.15	27.20	24.73	23.71	24.89	24.27
Na ₂ O	0.00	0.27	0.06	0.06	0.00	0.00	0.00	0.00	0.57	0.13	0.00	0.00
K ₂ O	10.65	10.49	10.79	10.59	10.28	10.69	10.03	10.96	10.17	10.16	10.54	10.56
BaO	0.01	0.00	0.06	0.00	0.16	0.00	0.09	0.09	0.01	0.00	0.12	0.14
CaO	0.02	0.10	0.00	0.04	0.06	0.03	0.04	0.01	0.04	0.03	0.03	0.04
H ₂ O	3.82	3.77	3.81	3.83	3.93	3.77	3.77	4.11	3.85	3.82	3.77	3.72
Cl	0.02	0.01	0.00	0.02	0.02	0.01	0.02	0.01	0.01	0.01	0.00	0.01
Total	98.80	97.73	99.29	99.64	101.93	98.53	98.21	99.68	100.37	99.28	98.21	96.99
Cations (p.f.u.)												
Si	6.180	6.186	6.135	6.145	6.142	6.158	6.153	6.007	6.132	6.254	6.099	6.127
^{IV} Al	0.006	0.016	0.001	0.007	0.003	0.002	0.022	1.301	0.012	0.006	0.022	0.000
Fe ³⁺	1.814	1.798	1.864	1.848	1.855	1.840	1.825	0.692	1.855	1.741	1.878	1.873
T site	8.000	8.000	8.000	8.000	8.000	8.000	8.000	8.000	8.000	8.000	7.999	8.000
Ti	0.007	0.008	0.017	0.011	0.013	0.012	0.007	0.002	0.011	0.012	0.012	0.012
Fe ²⁺	0.241	0.307	0.345	0.316	0.324	0.438	0.477	0.174	0.407	0.565	0.293	0.327
Mn	0.006	0.009	0.001	0.000	0.013	0.011	0.016	0.003	0.010	0.014	0.006	0.002
Mg	5.696	5.569	5.576	5.638	5.664	5.478	5.504	5.833	5.515	5.341	5.666	5.604
O site	5.950	5.893	5.939	5.965	6.014	5.939	6.004	6.012	5.942	5.932	5.977	5.945
Ba	0.001	0.000	0.004	0.000	0.009	0.000	0.005	0.005	0.001	0.000	0.007	0.008
Ca	0.004	0.016	0.000	0.007	0.010	0.004	0.006	0.001	0.007	0.006	0.005	0.006
Na	0.000	0.081	0.018	0.018	0.000	0.000	0.000	0.000	0.166	0.038	0.000	0.000
K	2.050	2.047	2.082	2.028	1.923	2.082	1.956	2.012	1.940	1.958	2.053	2.086
A site	2.055	2.144	2.104	2.053	1.942	2.086	1.967	2.018	2.114	2.001	2.065	2.100
Sum	16.005	16.037	16.043	16.018	15.956	16.025	15.971	16.030	16.056	15.933	16.041	16.045

Table 2.2 (continued)

Sample	110-46		244		116		149		183		56	
Rock type	P1	P1	P1	P1	DC							
Position	core	rim	rim	core	core	Rim	core	rim	rim	core	core	rim
Oxides (wt%)												
SiO ₂	41.07	40.90	40.66	41.53	41.29	40.82	41.15	41.39	40.25	40.75	41.306	40.354
TiO ₂	0.87	0.23	0.05	0.46	0.13	0.06	0.06	0.07	0.04	0.08	0.056	0.101
Al ₂ O ₃	9.94	3.03	0.34	5.66	0.02	0.06	0.05	0.04	0.07	0.02	0.002	0.021
Fe ₂ O ₃	3.55	12.31	16.30	9.45	15.43	16.56	15.55	15.94	16.27	15.61	15.55	16.46
FeO	2.72	0.99	1.70	1.82	3.09	3.15	3.36	2.57	2.51	2.60	3.51	3.09
MnO	0.10	0.05	0.05	0.07	0.04	0.11	0.12	0.08	0.05	0.08	0.07	0.074
MgO	25.63	26.19	25.84	26.35	24.28	24.73	24.38	25.13	24.91	24.54	24.381	24.681
Na ₂ O	0.00	0.07	0.00	0.25	0.21	0.46	0.00	0.00	0.18	0.00	0.064	0.192
K ₂ O	10.75	10.54	10.33	10.64	10.65	10.46	10.51	10.66	10.35	10.57	10.515	10.363
BaO	0.41	0.00	0.03	0.11	0.00	0.00	0.00	0.04	0.00	0.05	0	0
CaO	0.00	0.08	0.17	0.06	0.00	0.00	0.00	0.00	0.00	0.07	0.005	0.037
H ₂ O	4.12	3.91	3.84	4.06	3.82	3.84	3.82	3.85	3.79	3.79	3.83	3.799
Cl	0.00	0.01	0.01	0.01	0.00	0.01	0.01	0.02	0.00	0.01	0	0.018
Total	99.16	98.30	99.30	100.45	98.96	100.25	99.00	99.78	98.43	98.16	99.29	99.19
Cations (p.f.u.)												
Si	5.925	6.089	6.100	6.007	6.241	6.121	6.222	6.197	6.123	6.207	6.229	6.113
^{IV} Al	1.690	0.532	0.060	0.965	0.004	0.011	0.009	0.007	0.013	0.004	0.000	0.004
Fe ³⁺	0.386	1.380	1.840	1.028	1.755	1.868	1.769	1.796	1.863	1.789	1.770	1.883
T site	8.001	8.001	8.000	8.000	8.000	8.000	8.000	8.000	7.999	8.000	8.000	8.000
Ti	0.094	0.025	0.006	0.050	0.014	0.007	0.006	0.008	0.005	0.009	0.006	0.012
Fe ²⁺	0.328	0.122	0.213	0.220	0.390	0.395	0.425	0.321	0.319	0.331	0.437	0.384
Mn	0.012	0.006	0.006	0.009	0.005	0.013	0.015	0.011	0.007	0.010	0.009	0.009
Mg	5.512	5.812	5.779	5.680	5.472	5.528	5.496	5.610	5.650	5.571	5.481	5.574
O site	5.946	5.965	6.004	5.959	5.881	5.943	5.942	5.950	5.981	5.921	5.934	5.978
Ba	0.023	0.000	0.002	0.006	0.000	0.000	0.000	0.002	0.000	0.003	0.000	0.000
Ca	0.000	0.013	0.027	0.009	0.000	0.000	0.000	0.000	0.001	0.011	0.001	0.006
Na	0.000	0.019	0.000	0.069	0.062	0.133	0.000	0.000	0.053	0.000	0.019	0.056
K	1.979	2.002	1.977	1.962	2.053	2.001	2.028	2.036	2.009	2.053	2.023	2.003
A site	2.002	2.034	2.006	2.046	2.115	2.134	2.028	2.038	2.063	2.067	2.043	2.065
Sum	15.949	16.000	16.010	16.005	15.996	16.077	15.970	15.988	16.043	15.988	15.976	16.043

All micas with $(^{IV})\text{Fe}^{3+} < 0.5$ p.f.u. and $\text{Al}^{3+} > 1.5$ p.f.u. display normal pleochroism, whereas all others are reversely-pleochroic. This correlation was first observed by Araújo (1996) for Catalão I metasomatic phlogopites and confirmed by Brod *et al.* (2001) for phlogopite and tetra-ferriphlogopite in the Tapira complex. Our results show that the same limits can be applied also to igneous phlogopites from phoscoritic rocks of Catalão I.

Figure 2.8C shows that the octahedral site $\text{Fe}^{2+}=\text{Mg}^{2+}$ substitution is in place for all the studied phlogopites, although it is much subordinate if compared with the phlogopite – tetra-ferriphlogopite substitution. The Fe^{2+}/Mg ratio has been successfully used an indication of magma evolution in silicate rocks from the Tapira, Salitre, and Jacupiranga carbonatitic complexes (Brod *et al.*, 2001; Barbosa *et al.*, in preparation). However, in the case of Catalão I phoscorites, nelsonites, and carbonatites, the mica compositions overlap widely (Fig. 2.8B).

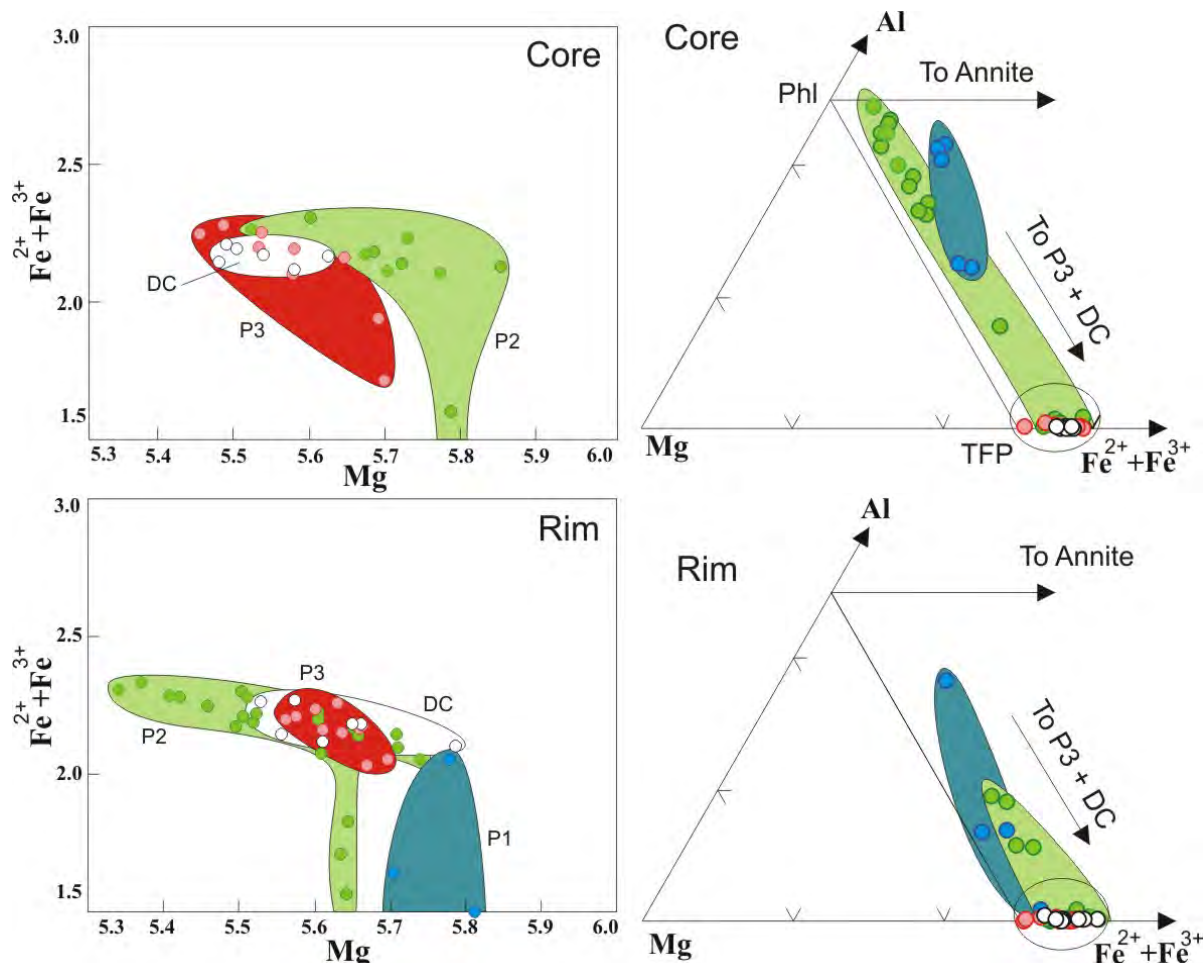


Fig. 2.9. Chemical composition of cores and rims of phlogopites from Catalão I. The areas near the base of the triangular plot are further detailed in the Mg vs Total Fe diagram. Symbols as in Fig. 2.6.

A detailed study of phlogopite microprobe profiles led to more accurate considerations in terms of chemical evolution (Fig. 2.9). The comparison between phlogopite cores and rims shows a general decrease in the Al content toward the rims. The compositions of P1 phlogopites plot along the solid solutions between phlogopite and tetra-ferriphlogopite. Figure 2.9 shows that the rims of phlogopites in this group are richer in Mg than those in more evolved rocks.

Half of the analysed phlogopite crystals in P2 have aluminous cores with tetra-ferriphlogopite rims, but the other half consist entirely of tetra-ferriphlogopite.

The octahedral $\text{Fe}^{2+}=\text{Mg}^{2+}$ substitution (Fig. 2.10) also indicates distinct zoning patterns in micas from different rocks. Micas from P1 phoscorites, P3 nelsonites, and dolomite carbonatites show enrichment in Mg toward the rims. P2 nelsonites, on the other hand, show an opposite behavior, with Fe^{2+} enrichment in the mica from core to rim. Compositional zoning of phlogopite towards Mg depletion and Fe enrichment is expected and has been reported as a reliable indicator of magma differentiation for silicate rocks in other complexes, such as Jacupiranga and Tapira (Gaspar & Wyllie, 1987; Brod *et al.*, 2001). However, those authors also point out that phlogopite in carbonatites from the same complexes shows reverse zoning patterns, with the rims enriched in Mg relatively to the cores. This is also the case for phlogopites in Catalão I carbonatites, phoscorites and nelsonites, except for the P2 rocks.

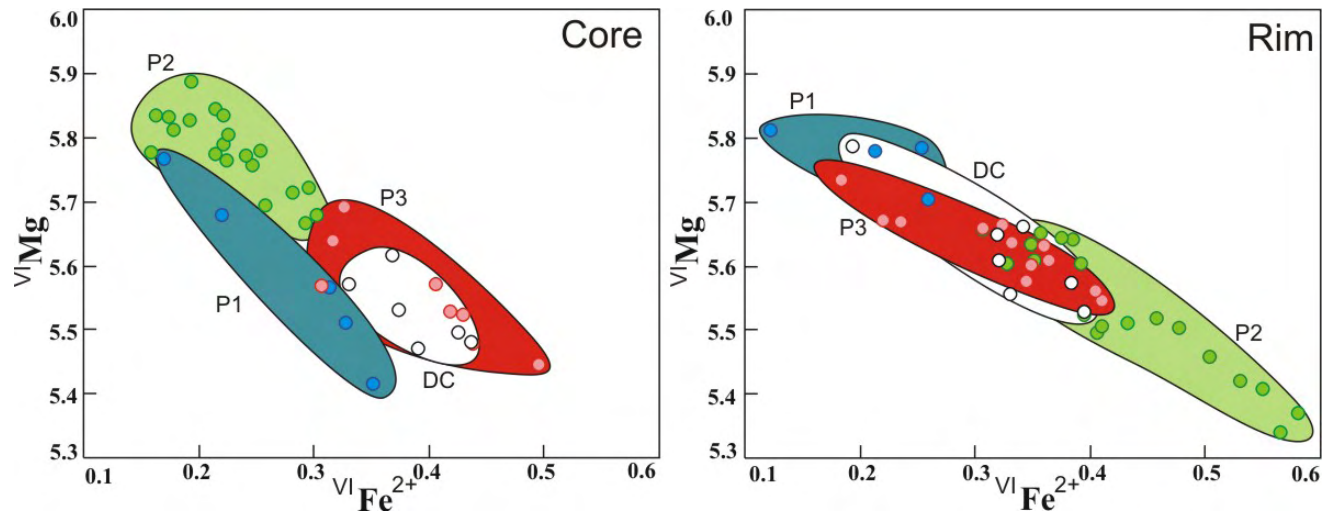


Fig. 2.10. Phlogopite-annite substitution in cores and rims of micas from the Catalão I phoscorites, nelsonites, and carbonatites. Note that, as also observed for apatite (Fig. 2.7), there is a reversal in the core to rim trend between P2 and P3 micas. Symbols as in Figure 2.6.

When compared to Jacupiranga and Tapira carbonatites from Brod *et al.* (2001), the role of octahedral Ti^{4+} is subordinate in the studied rocks. P1 phoscorites are the only group with significant

TiO₂ content in phlogopite (usually < 1.5 wt.%, exceptionally reaching 2.5 wt.%). On the other hand, TiO₂ is virtually absent (<0.5 wt.%, averaging 0.08 wt.%) in the nelsonites and dolomite carbonatites. Low-Ti micas are characteristic in late stage phoscorites from Sokli (P3 and C3), Kovdor (evolved rock types with dolomite) and Vuoriyarvi (P3 and C3), in comparison with micas from more primitive phoscorites in the same complexes (Lee *et al.*, 2003; Lee *et al.*, 2004; Krasnova *et al.*, 2004b; Karchevsky & Moutte, 2004).

Carbonate

Dolomite is the most common carbonate mineral in the phoscorite-series of Catalão I. Several cations may substitute in the ideal CaMg(CO₃)₂ formula, such as Sr, Ba, Fe and Mn (Deer *et al.*, 1992). Besides these cations, REE are also known to occur in dolomites from carbonatites.

Other carbonate species found in Catalão I phoscorites, nelsonites, and dolomite carbonatites are calcite, norsethite BaMg(CO₃)₂ and magnesite. Traversa *et al.* (2001) describe norsethite in the Araxá (Barreiro) Carbonatite complex, in the southern portion of the APIP, also in association with dolomite carbonatites. In the Jacupiranga Complex, norsethite inclusions were found in apatite crystals from calcite carbonatite (Constanzo *et al.*, 2006).

Carbonates in P1 phoscorites comprise dolomite occurring as an interstitial phase or magnesite occurring as inclusions in altered olivine. Both phases are believed to represent a product of secondary alteration, probably related to carbonatitic metasomatism, and therefore do not represent the igneous paragenesis. Secondary magnesite was also described in phoscorites from the Catalão I phosphate deposit (Ribeiro, 2008), equivalent to the P1 unit in this work.

In P2 and P3 nelsonites, carbonates occur as variably-sized pockets (1 cm to 20 cm) within the rock. Since these pockets are mainly composed of carbonates, they might represent carbonatitic segregations from the cooling nelsonite liquid, either by filter pressing or by liquid immiscibility. Primary carbonates are coarse to medium grained with a clear aspect in thin section, whereas secondary carbonates are anhedral and develop a turbid aspect. Carbonates from the DC dikes are very similar to those from the DC pockets within P2 and P3. Cordeiro (2009 - *Capítulo 4*) described the carbonate chemistry and carbon and oxygen stable isotope composition of carbonates from the Catalão I phoscorites, nelsonites and carbonatites, and the reader is referred to that work for the analytical data. The author's results have shown the existence of two varieties of dolomite with distinct Sr content. Primary dolomites are clear in thin section, cohesive in hand sample, and contain over 1.78 wt. % SrO. Secondary dolomites are turbid, often with recrystallized aspect in thin section

and brittle in hand specimens. Their SrO content is less than 1.4%, probably due to exsolution of Sr-bearing minerals during subsolidus recrystallization. Calcite analyses from the Tapira complex (Brod, 1999) exhibit similar characteristics. FeOT and MnO are low in the Catalão I dolomites, <1.5% and 1% respectively, and the BaO content is up to 0.8%.

Magnetite

Magnetite is one of the most abundant oxides in alkaline silicate rocks and carbonatites, and an essential constituent of phoscorites and nelsonites. Commonly observed substitutions are Ti⁴⁺ for Fe³⁺, towards ulvöspinel, Mg²⁺ for Fe²⁺, towards magnesioferrite, and Mn²⁺ for Fe²⁺, towards jacobsite (Deer *et al.*, 1992). Cr³⁺ substitution for Fe³⁺ is common in carbonatite-bearing complexes, although it is restricted to magnetites from primitive silicate rocks (e.g. Brod *et al.*, 2005).

Magnetite from the Catalão I phoscorites and nelsonites have variable textures. In P1, magnetite is an intercumulus phase, usually anhedral, and containing exsolved ilmenite lamellae. In these rocks, magnetite is the latest crystallizing essential mineral, forming after the onset of olivine, apatite, and phlogopite crystallization.

P2 magnetites occur as subhedral to anhedral fine grained crystals often with intercumulus texture. Unlike P1, magnetite in P2 nelsonites is abundant (up to 45 vol. %) and the crystals tend to form aggregates. P3 magnetite tends to develop a massive homogenous aspect and can reach up to 70 vol. %. Magnetite in P2 and P3 is mostly free from exsolutions, though very thin (< 0.05 mm) exsolved ilmenite lamellae can occur.

In the dolomite carbonatite (DC) pockets and dikes, magnetite shows textural features similar to those in P3. Additionally it is a common mineral at the contact between the carbonatite and its host nelsonite, occurring as a crust of anhedral magnetite together with apatite, tetra-ferriphlogopite and ilmenite.

Representative magnetite analyses are given in table 2.3, and the variations of selected elements are depicted in Figure 2.11. There is a wide overlap in the chemical composition between magnetite from different rock units or between magnetite from the nelsonites and the associated carbonatite pockets.

TiO₂ content in the phoscorite-series Catalão I magnetite is up to 15 wt.% with average between 1 and 3 wt.%. The common presence of ilmenite exsolution lamellae in magnetite from the studied rocks suggests that their TiO₂ content was originally higher. Relatively high Ti⁴⁺ contents in spinel seem to be typical of phoscoritic rocks from the APIP, but apparently are not a reliable indicator of

magma evolution stage within this petrogenetic series. Ribeiro *et al.* (2001, 2005) describe trellis ilmenite aggregates in altered, very late-stage monazite-rich nelsonites in the Catalão I rare-earth deposit, suggesting that Ti-rich magnetite crystallized up to the very latest stages of phoscoritic activity in the complex. Palmieri *et al.* (2008) reported up to 5.7 wt. % TiO_2 in magnetite from a late-stage orbicular magnetitite in Catalão I, and Barbosa *et al.* (in preparation) found up to 3 wt. % TiO_2 in more primitive phoscorites from the Salitre Complex, further south in the APIP.

Magnetite from other phoscorite-carbonatite world associations also show widely overlapping TiO_2 contents, although in phoscorites from the Sokli and Vuorijarvi complexes there is a consistent TiO_2 decrease with the evolution stage of the host phoscorite (Lee *et al.*, 2005; Karchevsky & Moutte, 2004). On the other hand, magnetites in carbonatites paired to phoscorites in Sokli overlap the entire composition range of the phoscorite magnetites and do not seem to vary systematically. Magnetites from the Jacupiranga carbonatites, Brazil, show a consistent TiO_2 decrease with the magma evolution (C1 to C5, Gaspar & Wyllie, 1982). The very strong Ti^{+4} - Fe^{3+} negative correlation in Fig. 2.11A indicates that most of the titanium variation in the Catalão I magnetites (as well as those from Sokli, Vuorijarvi and Kovdor phoscorites and carbonatites, and those in the Jacupiranga carbonatites) is in the range of the magnetite-ulvöspinel solid solution series. The composition of magnetite in the primitive silicate rocks from the Tapira Complex, in the APIP, vary mostly along the chromite-ulvöspinel series (Brod *et al.*, 2005) and is plotted for comparison in Fig. 2.11A.

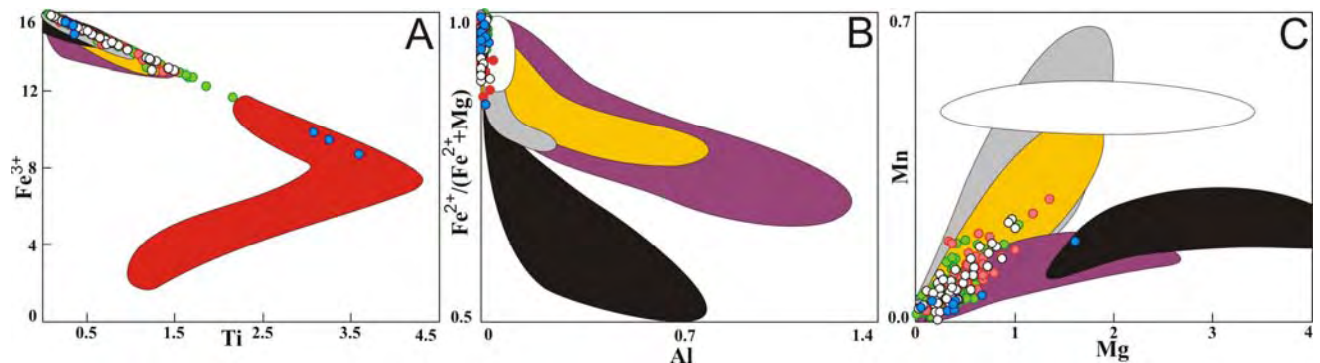


Fig. 2.11. Variation of selected elements (cations per formula unit) in magnetite from the Catalão I phoscorites and nelsonites. Symbols as in Figure 2.6. Fields for magnetite from Kola phoscorites and carbonatites (Kovdor = purple, Krasnova *et al.*, 2004b; Sokli = orange, Lee *et al.*, 2005; Vuorijarvi = grey Karchevsky & Moutte, 2004), as well as Jacupiranga (black, Gaspar & Wyllie, 1983) and Tury (yellow, Dunworth & Bell, 2003) carbonatites are shown for comparison. The red field in the left-hand side diagram represents magnetite from primitive silicate rocks (phlogopite picrites) in the extreme south of APIP (Brod *et al.*, 2005).

Cr_2O_3 is usually a very useful indicator of magmatic evolution and is virtually absent in the magnetites studied in this work, as well as in magnetites related to other phoscorites and carbonatites worldwide. In general, magnetite from these rocks contains below 0.1 wt. % Cr_2O_3 (e.g. Gaspar & Wyllie, 1983; Karchevsky & Moutte, 2004; Krasnova *et al.*, 2004b; Lee *et al.*, 2005; Brod *et al.*, 2005). Two analyses of magnetite from P2 yielded 0.22 and 0.38 wt. % Cr_2O_3 respectively. Similarly, Karchevsky & Moutte (2004) report only two analyses with significant chromium in magnetite from Vuorijarvi P2 and P3 phoscorites (0.32 and 0.24 wt.% Cr_2O_3 , respectively). Data available in the literature thus suggest that very low chromium content is a characteristic of both phoscorite and carbonatite magnetites.

Al_2O_3 is very low (mostly below 0.1 wt. %, with one analysis at 0.12 wt. %) in magnetite from the Catalão I phoscorites, nelsonites and carbonatites (Fig. 2.11B). In other occurrences of phoscoritic and carbonatitic rocks, however, magnetite may be more aluminum-rich. Magnetite from the least evolved phoscorites at Kovdor reach up to 4 wt. % Al_2O_3 (Krasnova *et al.*, 2004b), those from the least evolved phoscorites and carbonatites from Sokli contain up to 1.5 wt. % Al_2O_3 (Lee *et al.*, 2005), and those from Vuorijarvi phoscorites have up to 0.64 wt. % Al_2O_3 (Karchevsky & Moutte, 2004). In all three complexes, aluminum in magnetite decreases with magma evolution. In this context, the extremely low aluminum content of the Catalão I magnetites suggest that their host nelsonites are a late stage in phoscorite magma evolution, comparable in composition to the late-stage D4 and D5 (dolomite-carbonatites) of the phoscoritic-series from Sokli (Lee *et al.*, 2004).

MgO content in the studied magnetites reaches up to 3.5 wt. %, averaging 1 wt.%, but MgO contents as high as 8.2 wt. % (Palmieri *et al.*, 2008) and 9.2 wt. % (Barbosa *et al.*, in preparation) have been reported from other APIP nelsonites and phoscorites. MnO reaches up to 1.1 wt. % in the Catalão I magnetites. Palmieri *et al.* (2008) reported similar (up to 1.2 wt.%) MnO contents in magnetites from a Catalão I orbicular magnetitite, and Barbosa *et al.* (in preparation) reported up to 1.5 wt.% MnO in magnetites from phoscorites in the Salitre Complex, further south in the APIP. Together with Al_2O_3 and MnO , the MgO decrease in magnetite is considered a good indication of magma evolution in the phoscorite series (e.g. Lee *et al.*, 2005). Figure 2.11C shows that the composition of the Catalão I magnetites studied here is similar to that in the most evolved part of the Vuorijarvi, Sokli, and Kovdor trends, which is consistent with the interpretation of the Catalão rocks, especially P2 and P3 as evolved members of the phoscorite series. The composition of magnetite in the different rock units described here have largely overlapping MnO and MgO contents, which is

probably a result of a limited composition range of the host rocks, when compared with the whole phoscorite series.

Nb_2O_5 is significant, up to 1.16 wt.%, in the Catalão I magnetites. This is substantially higher than the published analyses of magnetite in other phoscorite localities, but similar to the Catalão I orbicular magnetitite (up 0.97 wt.% Nb_2O_5 Palmieri *et al.*, 2008). However, niobium content in magnetite from different rock units is widely overlapping and cannot be used as a marker for magma evolution.

Tab. 2.3 Representative analyses of magnetite from Catalão I phoscorites, nelsonites and dolomite carbonatites.
Cations calculated on the basis of 32 O.

Sample	038-2	056-1	056-2	93	099a-5	099a-3	099a-6	099b-5	099b-9	103-4	156-11	157b-5
Rock Type	P2	DC	DC	P2	P3	P3	P3	P2	P2	P3	P2	P3
Nb ₂ O ₅	0.00	0.18	0.00	0.13	0.74	0.05	0.03	0.22	1.06	0.01	0.01	0.04
SiO ₂	0.02	0.07	0.00	0.03	0.07	0.00	0.00	0.03	0.07	0.00	0.04	0.00
TiO ₂	6.33	1.62	1.88	8.11	5.93	2.78	3.01	4.42	5.07	1.88	0.58	2.37
Al ₂ O ₃	0.00	0.06	0.00	0.00	0.01	0.02	0.00	0.00	0.00	0.03	0.06	0.00
Cr ₂ O ₃	0.04	0.00	0.00	0.03	0.04	0.00	0.04	0.04	0.00	0.02	0.01	0.01
Fe ₂ O ₃	57.53	65.43	65.65	54.01	56.48	63.93	63.45	60.41	57.59	66.04	68.30	64.77
FeO	32.77	32.34	31.18	34.98	35.15	32.18	32.19	33.09	34.05	30.87	30.00	31.64
MnO	0.81	0.15	0.35	0.69	0.69	0.35	0.36	0.68	0.67	0.32	0.23	0.25
MgO	2.17	0.16	0.58	1.97	0.79	0.69	0.78	0.89	1.35	0.80	0.14	0.83
CaO	0.02	0.03	0.17	0.00	0.07	0.00	0.09	0.10	0.03	0.04	0.57	0.02
Total	99.69	100.02	99.81	99.95	99.97	100.00	99.95	99.88	99.89	100.01	99.94	99.93
Cations (p.f.u.)												
Nb	0.000	0.024	0.000	0.018	0.102	0.007	0.004	0.030	0.147	0.001	0.002	0.006
Si	0.006	0.021	0.000	0.009	0.022	0.000	0.000	0.008	0.021	0.000	0.013	0.001
Ti	1.480	0.370	0.458	1.845	1.362	0.639	0.699	1.028	1.173	0.426	0.135	0.553
Al	0.000	0.020	0.000	0.000	0.003	0.005	0.000	0.000	0.000	0.012	0.023	0.001
Cr	0.010	0.000	0.000	0.006	0.009	0.000	0.011	0.011	0.000	0.005	0.002	0.003
Fe ³⁺	13.026	15.130	15.107	12.240	12.948	14.707	14.581	13.847	13.181	15.174	15.748	14.885
Fe ²⁺	8.245	8.311	7.974	8.809	8.957	8.227	8.221	8.430	8.662	7.883	7.687	8.081
Mn	0.214	0.039	0.095	0.177	0.178	0.090	0.094	0.179	0.175	0.083	0.061	0.065
Mg	1.007	0.071	0.282	0.890	0.362	0.316	0.358	0.412	0.620	0.359	0.065	0.384
Ca	0.005	0.009	0.059	0.000	0.024	0.000	0.029	0.033	0.011	0.013	0.189	0.007
Sum	23.992	23.996	23.976	23.993	23.965	23.990	23.997	23.978	23.989	23.955	23.926	23.986

Table 2.3 (continued)

Sample	192b-3	200-3	200-8	207-5	207-5	244-2	244-3	304a-4	304a-8	339-5	339-1	F4-1-5
Rock Type	P2	P3	P3	P3	P1	P1	P2	P2	P2	P2	P2	P1
Nb ₂ O ₅	0.09	0.12	0.01	0.04	0.12	0.00	0.03	0.05	1.15	0.00	0.00	0.00
SiO ₂	0.08	0.01	0.00	0.02	0.03	0.00	0.30	0.00	0.13	0.01	0.05	0.04
TiO ₂	1.76	4.85	2.41	0.94	5.96	13.38	14.89	0.46	5.28	0.76	0.24	1.48
Al ₂ O ₃	0.02	0.00	0.00	0.00	0.00	0.04	0.00	0.00	0.00	0.00	0.03	0.03
Cr ₂ O ₃	0.00	0.00	0.00	0.00	0.00	0.07	0.03	0.02	0.01	0.00	0.00	0.00
Fe ₂ O ₃	65.51	60.00	64.73	67.36	57.60	44.16	38.14	68.70	57.27	67.84	68.53	66.35
FeO	31.85	33.20	31.74	30.78	33.61	37.53	44.64	29.37	32.95	30.75	30.98	31.52
MnO	0.19	0.56	0.34	0.22	0.73	0.71	0.15	0.26	0.86	0.10	0.07	0.19
MgO	0.45	1.22	0.74	0.63	1.59	3.54	0.80	1.07	2.03	0.35	0.02	0.36
CaO	0.06	0.02	0.01	0.00	0.04	0.00	0.01	0.06	0.08	0.16	0.07	0.03
Total	100.01	99.98	99.98	99.99	99.68	99.43	98.98	99.99	99.76	99.97	99.99	100.01
Cations (p.f.u.)												
Nb	0.012	0.017	0.001	0.006	0.017	0.000	0.004	0.007	0.161	0.000	0.000	0.000
Si	0.023	0.002	0.000	0.007	0.008	0.001	0.097	0.000	0.040	0.002	0.016	0.013
Ti	0.406	1.112	0.557	0.217	1.410	3.071	3.581	0.105	1.228	0.177	0.057	0.339
Al	0.006	0.000	0.000	0.000	0.000	0.015	0.000	0.000	0.000	0.000	0.011	0.010
Cr	0.001	0.000	0.000	0.000	0.000	0.016	0.007	0.005	0.003	0.000	0.000	0.000
Fe ³⁺	15.107	13.722	14.889	15.535	13.113	9.825	8.638	15.787	13.019	15.664	15.868	15.308
Fe ²⁺	8.162	8.440	8.114	7.890	8.503	9.279	11.235	7.500	8.323	7.891	7.972	8.083
Mn	0.048	0.145	0.088	0.057	0.194	0.184	0.040	0.068	0.225	0.027	0.018	0.048
Mg	0.207	0.554	0.340	0.288	0.743	1.609	0.380	0.485	0.934	0.163	0.011	0.164
Ca	0.019	0.006	0.003	0.000	0.012	0.000	0.004	0.020	0.026	0.052	0.022	0.010
Sum	23.991	23.998	23.994	24.000	24.000	24.000	23.987	23.977	23.959	23.977	23.975	23.976

Ilmenite

Ilmenite is an accessory phase in the phoscorite-series rocks of the Catalão I complex, except in some DC dikes and pockets where it can represent 10 vol% of the rock. In P1, ilmenite occurs as blebs and as exsolved trellis lamellae in anhedral magnetite. In P2 and P3, ilmenite is very rare, occurring as blebs or small inclusions in magnetite. In DC, ilmenite occurs at the rims of dikes and pockets as euhedral crystals, up to 2 cm, usually with small inclusions of pyrochlore (Cordeiro 2009 – *Capítulo 3*).

Table 2.4 shows representative analyses of Catalão I ilmenites. These are typically enriched in MgO, with lesser but significant contents of MnO and Nb₂O₅, and poor in Fe₂O₃. These characteristics have been described in ilmenite from other carbonatites and phoscorites (e.g. Gaspar & Wyllie, 1983; Lee *et al.*, 2005 and references therein).

Figure 2.12 shows the composition of the ilmenites studied in this work in comparison with those of Kola phoscorites and carbonatites (Lee *et al.*, 2005 and references therein), Jacupiranga carbonatites (Gaspar & Wyllie, 1983) and previously published analyses of ilmenite from nelsonites and apatites/monazitites in the Catalão I rare-earth deposit (Ribeiro *et al.*, 2005; Ribeiro, 2008).

The ilmenites analysed here plot in two distinct fields: ilmenite from P1, occurring as blebs within magnetite crystals have a strong MgO enrichment (12 to 16 wt. %), plotting near the 50 mol% limit between ilmenite and geikielite. Ilmenite from the more evolved P2 and P3 nelsonites and the associated dolomite carbonatites have lower MgO (0.6 to 5 wt. %), similar MnO (2.3 to 4.5 wt.% in P1 ilmenites, 1.4 to 5 wt. % in P2, P3, and DC), and slightly higher Fe₂O₃ (up to 1 wt.% in P1, up to 3% in P2, P3, and DC). Analyses of ilmenite in monazite-rich apatites and nelsonites from the Catalão I rare-earth deposit (Ribeiro *et al.*, 2005) show the same behavior, plotting in two separate (high-Mg and low-Mg) fields. In addition, ilmenite from Catalão I primitive silicate-rock dykes (phlogopite picrites, our unpublished data) cover the whole compositional span of Catalão I phoscorite and nelsonite ilmenites and show the same trend. Overall, the composition range of the Catalão I ilmenites is consistent with other phoscorites and carbonatites worldwide. It is distinguished from that of kimberlitic ilmenite by the higher MnO and lower Fe₂O₃ content, and from ilmenites in other rocks (lamprophyres, granites, basalts) by the generally higher MgO content.

Tab. 2.4 Representative analyses of ilmenite from the Catalão I phoscorites, nelsonites, and associated carbonatites. Formulae recalculated on the basis of 6 O.

Sample	244-2	319-1	319-3	319-5	178-3	230A-2	230A-3	230A-4	116-1	116-5	116-17	149-3	149-4	149-11	183-1
Rock Type	P1	P1	P1	P1	P2	P2	P2	P2	P2	P2	P3	P3	P3	P3	P3
SiO ₂	0.00	0.00	0.00	0.01	0.02	0.00	0.03	0.00	0.00	0.00	0.01	0.00	0.00	0.02	0.06
TiO ₂	57.02	55.21	57.38	57.43	52.83	49.99	50.53	50.53	50.55	53.30	51.71	53.80	53.22	54.84	49.59
Al ₂ O ₃	0.02	0.00	0.00	0.00	0.01	0.01	0.02	0.03	0.01	0.01	0.01	0.04	0.02	0.00	0.02
Cr ₂ O ₃	0.01	0.03	0.00	0.08	0.00	0.03	0.00	0.02	0.00	0.00	0.00	0.02	0.01	0.00	0.00
FeO	24.56	21.73	21.00	20.70	36.21	40.29	40.25	40.50	40.60	41.49	41.89	39.86	39.77	36.46	39.74
Fe ₂ O ₃	1.10	0.00	0.00	0.00	0.69	1.63	1.57	1.11	2.51	0.00	1.32	0.00	0.00	0.00	0.52
MnO	4.31	2.46	2.45	2.47	4.60	4.73	4.82	4.81	2.28	2.79	2.77	2.09	3.74	1.89	4.90
MgO	12.63	15.52	15.45	16.38	4.01	0.99	1.28	1.01	2.40	1.87	1.20	3.35	1.37	5.00	1.36
CaO	0.05	0.13	0.02	0.10	0.01	0.06	0.03	0.00	0.01	0.10	0.07	0.00	0.01	0.01	0.02
Nb ₂ O ₅	0.20	2.29	1.00	1.25	0.47	1.83	1.83	1.61	1.60	0.39	0.39	0.68	0.10	0.32	2.31
Total	99.90	97.37	97.31	98.41	98.84	99.56	100.36	99.62	99.95	99.95	99.38	99.83	98.24	98.54	98.52
Cations (p.f.u.)															
Si	0.000	0.000	0.000	0.000	0.001	0.000	0.002	0.000	0.000	0.000	0.001	0.000	0.000	0.001	0.003
Ti	1.974	1.928	1.990	1.966	1.970	1.905	1.906	1.923	1.899	1.995	1.961	1.992	2.023	2.021	1.906
Al	0.001	0.000	0.000	0.000	0.000	0.001	0.001	0.002	0.001	0.000	0.000	0.002	0.001	0.000	0.001
Cr	0.000	0.001	0.000	0.003	0.000	0.001	0.000	0.001	0.000	0.000	0.000	0.001	0.000	0.000	0.000
Fe ²⁺	0.945	0.844	0.809	0.788	1.502	1.707	1.688	1.713	1.695	1.726	1.766	1.641	1.681	1.494	1.699
Fe ³⁺	0.038	0.000	0.000	0.000	0.026	0.062	0.059	0.042	0.094	0.000	0.050	0.000	0.000	0.000	0.020
Mn	0.168	0.097	0.096	0.095	0.193	0.203	0.205	0.206	0.096	0.118	0.118	0.087	0.160	0.078	0.212
Mg	0.866	1.074	1.062	1.111	0.297	0.075	0.096	0.076	0.179	0.139	0.091	0.246	0.103	0.365	0.104
Ca	0.003	0.007	0.001	0.005	0.000	0.003	0.001	0.000	0.000	0.005	0.004	0.000	0.000	0.000	0.001
Nb	0.004	0.048	0.021	0.026	0.011	0.042	0.041	0.037	0.036	0.009	0.009	0.015	0.002	0.007	0.053
Sum	4.000	3.999	3.979	3.994	4.000	4.000	4.000	4.000	4.000	3.992	4.000	3.980	3.970	3.970	4.000

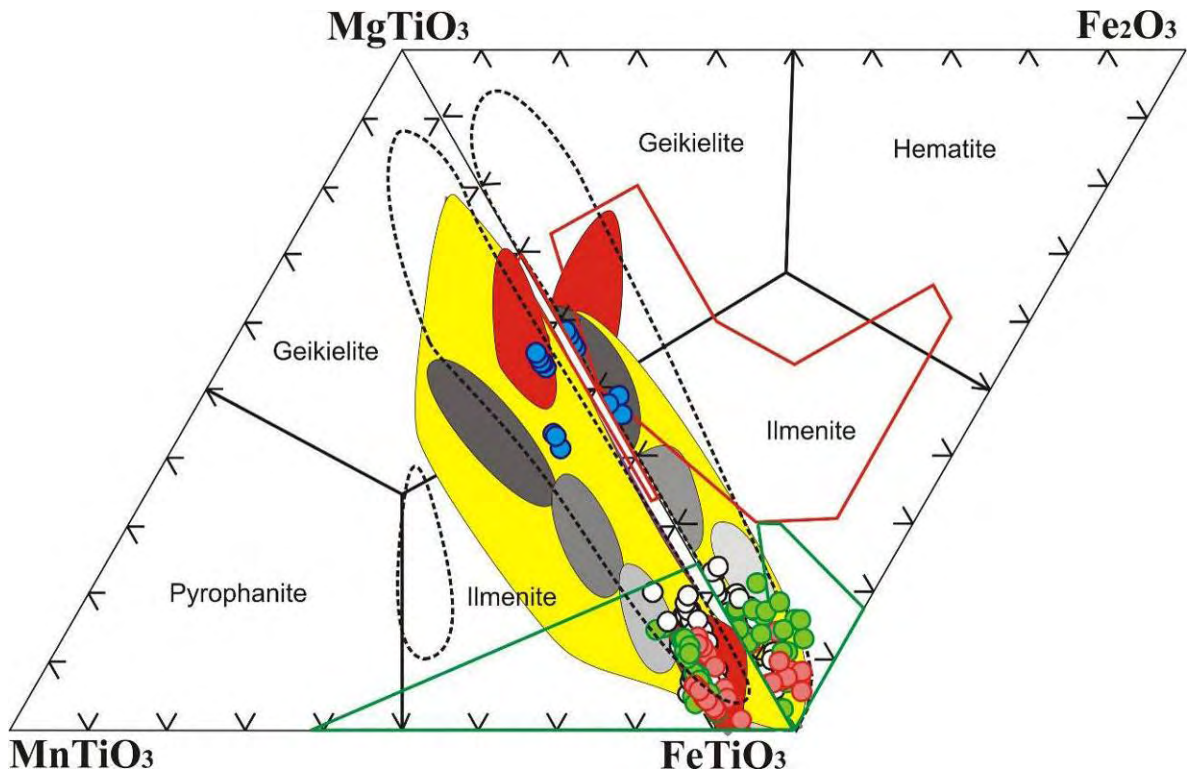


Fig. 2.12. Compositional variation and classification of ilmenite from the Catalão I phoscorites, nelsonites and carbonatites (symbols as in Fig. 2.6). Also plot for comparison are the fields of ilmenite from the Jacupiranga carbonatites (dashed line, Gaspar & Wyllie, 1983), Kola carbonatites and phoscorites (yellow, Lee *et al.*, 2005, and references therein), kimberlites (red outline, Mitchell, 1978), and other rocks (green outline – lamprophyres, granites, basalts, carbonatites, Mitchell, 1978). Phoscorites from the Sokli massif, Finland (Lee *et al.*, 2005), are individualized as grey fields, with lighter shades indicating more evolved rocks. The red solid fields represent the compositions of ilmenite from monazite-rich apatites and nelsonites in the Catalão I rare-earth deposit (Ribeiro *et al.*, 2005).

Figure 2.12 also shows the individualized fields for phoscorites from the Sokli massif in which the ilmenite composition evolves continuously by substantial decrease in MgO, accompanied by a slight decrease in MnO and nearly constant Fe₂O₃ from P1 through P2 to the most evolved P3 phoscorites (Lee *et al.*, 2005), as indicated by progressively lighter shaded *grey* fields in the diagrams. This is consistent with the behavior of the Catalão I ilmenites studied here, which vary from geikielite in P1 towards nearly pure FeTiO₃ in P2, P3, and DC, whilst MnO and Fe₂O₃ remain approximately constant. It is also in good agreement with Ribeiro *et al.* (2005) for ilmenites in the Catalão I rare-earth deposit, which point to a substantial decrease in MgO with evolution. The general evolution trend of Catalão I ilmenite is confirmed by microprobe profiles of individual crystals (Fig. 2.13), except for the analyzed grain in the dolomite-carbonatite associated with P3. The FeO and MgO profiles for this grain suggest that it started crystallizing with a trend similar to the others, but the zoning was reversed at an intermediate stage during the crystallization.

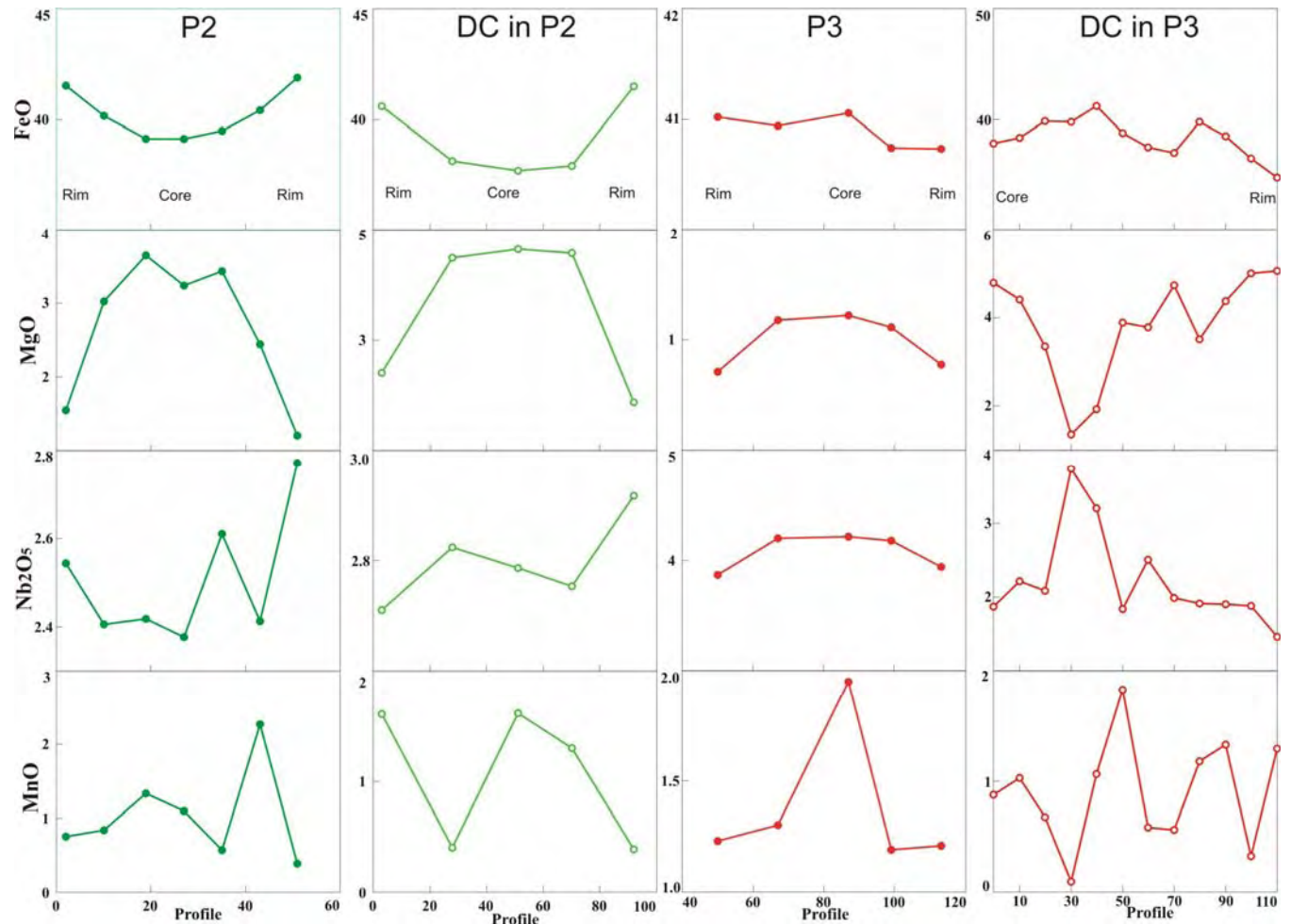


Fig. 2.13. Microprobe profiles for selected ilmenite crystals. Horizontal scales are proportional to the distance between analytical points. All concentration data is in wt. %.

The Nb₂O₅ content varies from 0.1 to 2.5 wt.%. Ilmenites from P1 tend to concentrate in the lower range of niobium and higher range of titanium content and those from P3 are concentrated towards higher Nb, but ilmenites from P2 and from DC span the whole range. Cr₂O₃ and Al₂O₃ contents are negligible (<0.1 wt.%) in the analyzed ilmenites. Niobium distribution within single grains appears to be mostly irregular (Fig. 2.14).

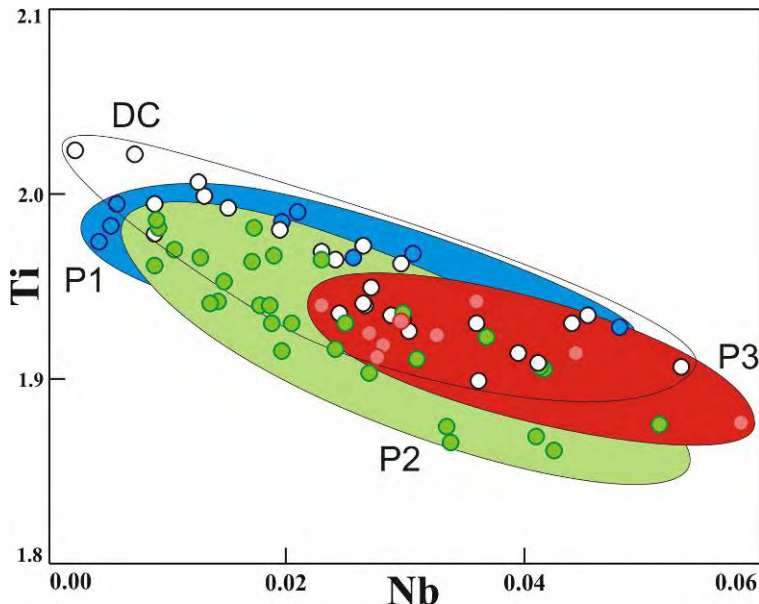


Fig. 2.14. Nb and Ti (a.p.f.u.) variation in Catalão I ilmenites. The composition of P1 and P3 ilmenites suggest niobium increase and titanium decrease with evolution, but P2 and DC ilmenites overlap the entire composition range.

Olivine/Ti-Clinohumite

Although phoscoritic magmatism as a whole is a relatively late-stage magmatic event in the complex, the earliest phoscorites (P1) were still variably affected by carbonatitic metasomatism (e.g. Ribeiro, 2008), whereas the later stage nelsonites (P2 and P3) were less or not affected at all. Metasomatic alteration resulted in the replacement of olivine in phoscorites and earlier silicate rocks by clinohumite, magnesite and tetra-ferriphlogopite. Pseudomorphs of the original olivine are often found in these rocks, indicating that primary olivine was euhedral to subhedral, coarse- to medium-grained.

We did not analyse olivine in this work, but Araújo (1996) reports olivine compositions from Catalão I phoscorites ranging from Fo 84 to 94 mol.%, with MnO varying from 0.34 to 0.63 wt. %, NiO up to 0.15 wt. % and CaO up to 0.44 wt. %. These ranges are consistent with olivine composition from other phoscorite and carbonatite occurrences (e.g. Verhulst *et al.*, 2000, Gaspar *et al.*, 1998, Barbosa *et al.*, in preparation).

Ti-clinohumite is described in association with olivine in phoscorites from Vuoriyarvi (Karchevsky & Moutte, 2004) and Kovdor (Verhulst *et al.*, 2000), in phoscorites and carbonatites from Sokli (Lee *et al.*, 2003) and in carbonatites and metasomatic rocks from Jacupiranga (Gaspar,

1992). Reported TiO_2 contents in Ti-Clinohumite are up to 2 wt.% from Vuorijarvi, and up to 3.78 wt.% from Jacupiranga.

In table 2.5 we present analysis of a possible member of the humite group occurring as an alteration product of olivine in a P1 phoscorite. The analysis were conducted on the cores of very slightly olivine grains (as opposed to the intense clinohumite alterarion shown in Fig. 2.5A) and originally intended to determine the composition of P1 relict olivine. However, the TiO_2 contents (up to 2.09 wt. %) are far too high to be accommodated in the olivine structure. Furthermore, the analyzed phase is enriched in MgO , yielding $\text{MgO}/(\text{MgO}+\text{FeO}+\text{MnO})$ between 0.90 and 0.95, which is substantially higher than the $\text{MgO}/(\text{MgO}+\text{FeO}+\text{MnO})$ range reported by Araujo (1996) for olivine in Catalão 1 phoscorites (0.75 – 0.85). A similar feature was noted by Gaspar (1982) in the Jacupiranga complex, where Ti-clinohumite is enriched in magnesium and titanium, and depleted in iron, relatively to coexisting olivine. Gaspar (1992) pointed out that the Fe-Mg ratio of the Jacupiranga clinohumite is not a function of the initial Fe-Mg ratio of olivine, but is controlled mostly by external variables such as temperature, pressure, and chemical composition of the reacting fluids.

We were not able to analyze fluorine, but the high analytical totals in table 2.5 suggest that both F^- and OH^- are much lower than expected for clinohumite. Gaspar (1992) argued that the composition of Ti-bearing humite-group minerals can vary substantially away from the general formula $n[\text{M}_2\text{SiO}_4][\text{M}_{1-x}\text{Ti}_x(\text{OH},\text{F})_{2-2x}\text{O}_{2x}]$, where n varies from 1 in stoichiometric norbergite to 4 in clinohumite. In these cases, interlayered, disordered structures would result in higher n values (the upper limit being olivine, at $n = \infty$). At the present stage we interpret these analyses as representing an intermediate step in the transformation of the original olivine to clinohumite, but the subject merits further detailed studies in the future.

Tab.2. 5 Analyses of Ti-clinohumite from the Catalão I early-stage (P1) phoscorites.

Sample	319-3	319-4	319-5	319-6	319-7	319-8	319-9	319-10	319-11
SiO_2	41.97	38.67	38.76	39.97	38.75	38.74	39.15	38.62	39.41
TiO_2	0.20	1.44	2.09	1.30	1.15	1.09	1.30	1.20	1.25
FeO	5.20	4.88	4.53	4.73	3.31	3.24	3.39	3.28	2.89
MnO	0.37	0.32	0.39	0.49	0.23	0.33	0.27	0.27	0.25
MgO	53.17	54.58	54.00	54.61	55.76	55.34	55.98	56.39	56.21
CaO	0.02	0.03	0.01	0.04	0.01	0.01	0.00	0.00	0.08
NiO	0.02	0.00	0.01	0.00	0.01	0.06	0.04	0.00	0.00
Cr_2O_3	0.00	0.00	0.00	0.01	0.00	0.02	0.00	0.04	0.01
Total	100.93	99.92	99.79	101.14	99.21	98.83	100.13	99.79	100.09

WHOLE-ROCK CHEMISTRY

The chemical composition of the phoscorite-series rocks reflects a different magmatic evolution, compared to carbonatites and silicate rocks. In this work we analysed 24 samples from the Catalão I primary rocks, including phoscorites, nelsonites, carbonatites and one sample of a mica-rich rock (glimmerite). All samples were chosen from fresh drill cores and the analytical results are given in Table 2.6. A previous carbon and oxygen stable isotope study on carbonates of the same rocks (Cordeiro 2009 - *Capítulo 4*) confirmed that they are of primary (magmatic) origin, but some may have been partially affected by low-temperature H₂O fluids that affected restrictly the carbonate composition.

The studied rocks are very silica-poor, with the glimmerite reaching the highest SiO₂ content (33 wt. %), P1 phoscorites varying from 12 to 25 wt. % SiO₂, and all the P2 and P3 nelsonite samples below 13 wt. % SiO₂. P₂O₅ may reach up to 23 wt. % in a P2 nelsonite, whereas the maximum Fe₂O_{3T} (total iron expressed as Fe₂O₃) occurs in a P3 magnetitite (ca. 70 wt. %). Al₂O₃ is very low (up to 0.35 wt.%) which is consistent with the large dominance of tetra-ferriphlogopite over phlogopite in these rocks. The glimmerite sample, at ca. 9.5 wt. % Al₂O₃, is an exception, containing normal, aluminous phlogopite, and is probably related to the bebedourite series. Na₂O is always below 0.8 wt. %, and K₂O reaches up to 3.4 wt. % in a P2 nelsonite (9 wt. % in the glimmerite).

The general magmatic progression of the Catalão I phoscoritic rocks is marked by the succession of olivine (and phlogopite), then apatite, and finally magnetite as the dominant mineral. This sequence is also seen as the crystallization sequence, with olivine and phlogopite as euhedral phenocrysts and magnetite as anhedral intercumulus mineral. The succession of dominant minerals is well marked by the variations in major element oxides shown in figures 2.15 and 2.16. In the sequence P1-P2-P3 there is a decrease in MgO and P₂O₅, whereas Fe₂O_{3T} increases with magma differentiation. K₂O increases at first in P1, where the main silicate is olivine, but then decreases signaling the onset of primary phlogopite crystallization in P2 and P3 instead of olivine. Na₂O increases from P1 to P2/P3, probably controlled by the occurrence of Ca-Na pyrochlore.

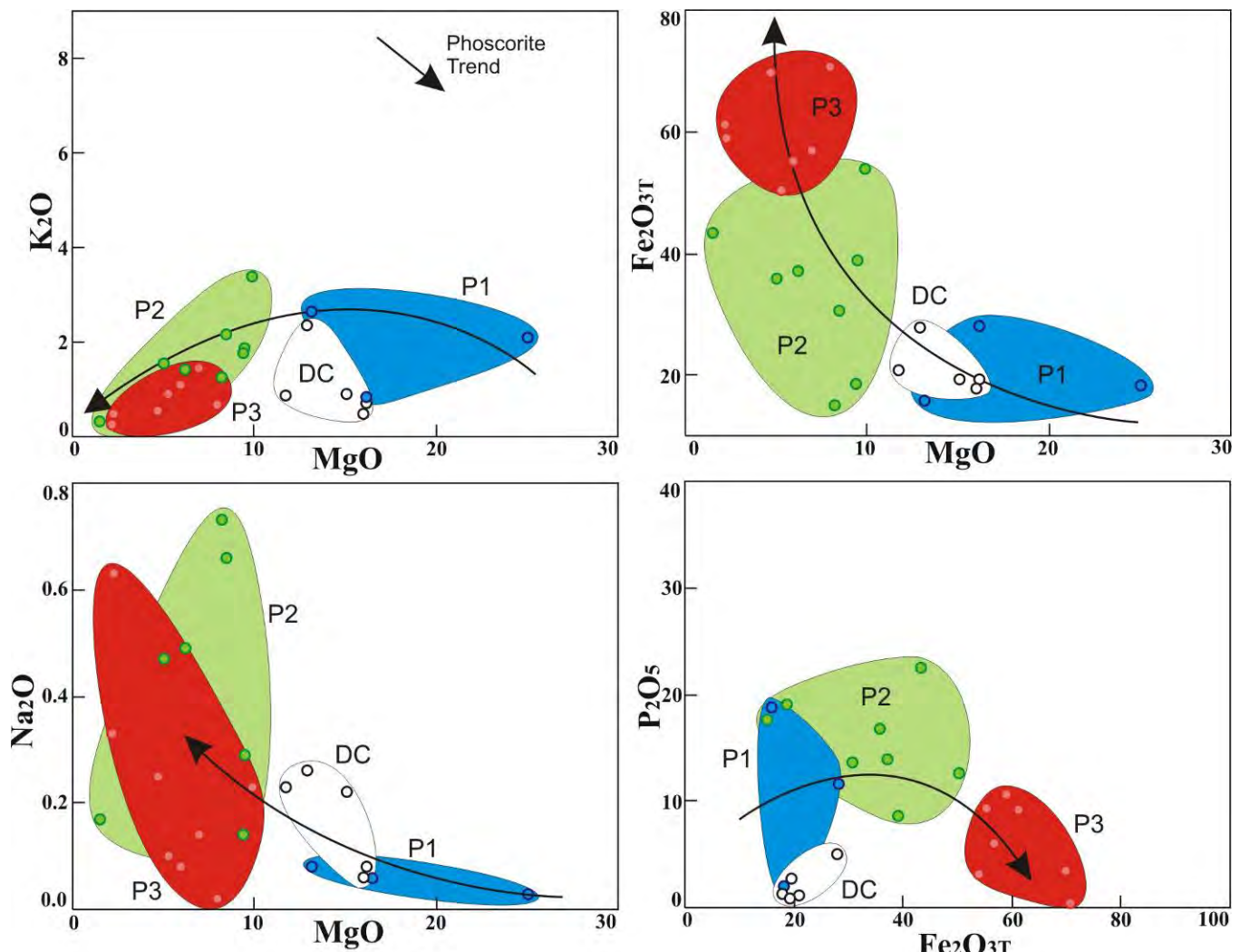


Fig. 2.15. Variation diagrams of selected major element oxides for the Catalão I samples. Arrows indicate the differentiation in the sequence P1-P2-P3.

Tab. 2.6 Whole-rock chemistry of the Catalão I glimmerite, phoscorites, nelsonites and carbonatites

Sample	225	244	319	F4	116	156	178	192B	230A	304 A	339	157B
Rock Type	Glim	P1	P1	P1	P2	P3						
<i>Wt %</i>												
SiO ₂	32.75	12.22	12.75	23.80	9.69	1.26	8.44	4.87	5.84	5.62	6.89	1.79
TiO ₂	1.69	1.75	3.36	2.35	7.16	0.58	0.90	0.69	1.69	1.41	0.34	2.51
Al ₂ O ₃	9.46	0.35	0.26	0.20	0.08	0.10	0.20	0.06	b.d.	0.07	0.03	b.d.
Fe ₂ O _{3T}	12.61	15.83	28.12	18.25	38.96	43.31	30.62	15.05	35.79	37.05	18.56	58.85
MnO	0.14	0.26	0.37	0.31	0.45	0.14	0.18	0.14	0.21	0.21	0.14	0.26
MgO	20.46	13.16	16.15	25.03	9.42	1.50	8.43	8.22	4.99	6.18	9.37	2.27
CaO	5.88	26.61	18.51	12.36	13.85	27.56	18.92	33.39	22.50	21.61	31.01	14.93
Na ₂ O	0.03	0.08	0.06	0.03	0.29	0.17	0.66	0.73	0.47	0.49	0.14	0.63
K ₂ O	8.89	2.66	0.84	2.09	1.88	0.34	2.17	1.25	1.55	1.41	1.78	0.48
P ₂ O ₅	4.16	18.80	11.68	2.03	8.61	22.58	13.70	17.71	16.80	13.87	19.12	10.62
BaO	0.24	0.04	0.13	0.08	0.19	0.09	2.66	0.40	0.77	0.78	0.67	0.52
SrO	0.17	0.46	0.46	0.37	0.93	0.96	1.76	1.48	1.47	1.18	0.94	1.12
Nb ₂ O ₅	0.06	0.06	0.11	0.06	1.82	0.58	2.45	1.98	2.52	3.35	0.22	3.16
REE ₂ O ₃	0.19	0.67	0.41	0.12	0.63	0.51	1.44	0.99	0.96	0.74	0.45	0.77
ZrO ₂	0.21	0.19	0.21	0.06	0.03	0.02	0.03	0.72	0.73	0.37	0.46	0.33
LOI	2.50	6.80	6.30	12.50	5.50	0.10	6.80	11.10	3.10	5.00	9.70	1.40
Total	99.43	99.94	99.71	99.63	99.50	99.79	99.36	98.78	99.39	99.34	99.82	99.64
CO ₂	0.95	5.72	5.31	10.11	4.73	0.81	5.17	10.00	2.38	5.20	10.33	1.87
S	0.02	0.04	0.19	0.24	0.04	0.02	1.54	0.49	0.02	0.02	0.03	0.14
<i>ppm</i>												
Ba	2120	320	1120	733	1739	776	23788	3567	6893	7013	6013	4668
Rb	439.2	121.6	46.1	99.2	114.6	22.1	135.3	80.7	88.1	88.9	101.5	29.1
Sr	1407	3907	3884	3089	7890	8084	14902	12494	12405	9949	7924	9448
Cs	4.00	0.90	0.80	1.10	0.80	0.10	0.60	0.60	0.60	0.60	0.50	0.30
Li	15.5	36.1	16.2	14.3	207.9	155.4	665.0	84.2	83.0	789.1	16.2	271.4
Ta	18.5	15.9	27.3	18.0	134.8	77.5	113.0	15.4	21.7	153.7	18.6	54.5
Nb	413	454	794	432	12697	4021	17144	13842	17617	23434	1528	22101
Hf	35.7	35.2	38.5	11.1	10.1	5.1	11.4	89.7	110.4	75.4	63.4	70.9
Zr	1568	1425	1539	416	221	182	222	5345	5440	2719	3427	2420
Y	25.1	124.0	82.6	24.4	60.0	52.4	86.6	101.9	85.7	53.8	65.5	51.1
Th	21.8	162.1	155.0	64.7	322.9	250.6	746.3	2854.0	1761.0	2041.0	49.9	1198.0
U	109.0	192.0	354.0	213.0	407.0	504.0	322.0	146.0	466.0	447.0	183.0	571.0
Cr	13.7	27.4	61.6	253.2	20.5	102.6	41.1	27.4	27.4	47.9	13.7	13.7
Ni	26.9	63.5	28.4	598.6	9.0	19.8	14.6	4.6	4.8	9.8	6.4	5.8
Co	59.8	47.8	48.1	99.4	102.3	28.4	73.2	103.4	111.6	40.4	41.1	104.2
Sc	50.0	37.0	46.0	28.0	12.0	5.0	11.0	34.0	23.0	25.0	16.0	17.0
Cu	7.30	167.80	33.10	46.50	88.40	1.30	109.10	14.80	41.40	0.70	8.30	16.00
Pb	0.50	14.10	2.30	1.80	1.90	1.30	28.90	3.30	2.00	2.30	2.20	1.60
Zn	69.0	117.0	102.0	111.0	155.0	87.0	218.0	58.0	160.0	128.0	69.0	170.0
La	374.1	1202.0	663.6	196.3	1273.0	883.3	2820.0	1394.0	1812.0	1246.0	774.9	1347.0
Ce	751.8	2477.0	1543.0	461.3	2424.0	2083.0	5933.0	4329.0	3752.0	3226.0	1751.0	3359.0
Pr	90.29	341.20	205.90	59.89	337.30	258.10	735.60	528.40	523.20	378.70	227.30	384.20
Nd	300.7	1235.0	775.5	217.0	1102.0	892.8	2305.0	1729.0	1681.0	1210.0	837.9	1228.0
Sm	34.12	150.60	99.25	28.24	119.60	100.20	223.10	200.30	183.00	129.80	100.30	125.80
Eu	8.19	38.15	25.58	7.27	30.11	23.90	52.28	46.99	45.53	29.04	25.81	28.84
Gd	12.04	66.28	46.54	11.76	41.14	39.31	56.81	49.29	55.10	29.11	45.59	33.01
Tb	1.940	9.650	6.540	1.890	6.180	5.270	9.670	10.120	9.060	6.200	6.150	5.860
Dy	6.960	37.150	25.570	7.320	20.680	17.690	31.500	34.260	30.280	20.030	22.600	20.300
Ho	0.800	4.740	3.240	1.030	2.140	2.040	2.880	3.890	3.210	2.000	2.500	2.000
Er	1.420	8.820	6.050	1.930	2.880	2.870	3.870	6.070	5.050	3.020	4.220	2.520
Tm	0.180	1.030	0.690	0.270	0.380	0.360	0.540	0.760	0.580	0.380	0.510	0.320
Yb	0.950	5.410	3.460	1.300	1.930	1.630	2.870	3.730	3.140	2.040	2.450	1.730
Lu	0.090	0.640	0.380	0.150	0.180	0.150	0.260	0.360	0.320	0.210	0.290	0.160

Table 2.6 (continued)

Sample	183R	206	207	099a	230B	304 BR	091	149	170	183G1	304BG	056B
Unit	P3	P3	P3	P3	P3	P3	P3	DC	DC	DC	DC	DC
<i>Wt %</i>												
SiO ₂	13.12	4.21	3.91	1.39	2.64	5.92	2.72	9.07	3.98	2.04	2.74	3.29
TiO ₂	1.42	0.97	0.86	2.31	2.23	1.78	1.76	2.62	16.00	1.73	0.51	1.02
Al ₂ O ₃	0.07	0.03	0.05	0.03	b.d.	b.d.	0.16	0.01	b.d.	0.03	b.d.	b.d.
Fe ₂ O _{3T}	53.92	55.17	50.38	61.24	69.80	56.82	70.60	27.82	20.88	17.90	19.27	19.38
MnO	0.22	0.23	0.21	0.28	0.32	0.30	0.40	0.28	0.86	0.39	0.30	0.37
MgO	9.91	5.95	5.27	2.18	4.65	6.95	7.98	12.86	11.70	16.01	16.17	15.07
CaO	5.86	14.31	18.59	13.69	7.21	11.59	5.42	11.74	11.90	15.90	19.43	22.24
Na ₂ O	0.23	0.08	0.10	0.33	0.25	0.14	0.02	0.26	0.23	0.06	0.08	0.22
K ₂ O	3.40	1.10	0.90	0.27	0.54	1.46	0.68	2.36	0.87	0.48	0.71	0.92
P ₂ O ₅	3.22	9.34	12.60	9.25	3.53	6.07	0.41	5.07	1.23	1.27	0.91	2.82
BaO	0.30	1.19	0.10	1.10	2.21	1.20	0.30	9.17	8.20	11.13	3.43	1.39
SrO	0.48	0.69	0.74	1.04	0.53	0.85	0.25	1.62	3.56	1.76	2.71	1.46
Nb ₂ O ₅	1.98	0.47	0.29	3.33	1.50	1.10	0.23	1.82	1.58	0.40	0.60	1.22
REE ₂ O ₃	0.35	0.27	0.30	0.64	0.35	0.31	0.05	0.59	0.28	0.16	0.19	0.44
ZrO ₂	1.43	0.79	0.77	0.89	0.54	0.51	0.22	0.03	0.02	0.18	0.10	0.34
LOI	3.60	4.70	4.88	1.60	2.80	4.30	8.50	15.40	17.40	30.60	32.60	29.40
Total	99.51	99.49	99.95	99.56	99.10	99.30	99.70	100.71	98.69	100.04	99.74	99.57
CO ₂	2.38	5.61	4.95	2.68	5.28	5.72	9.67	14.36	17.41	33.42	34.54	30.93
S	0.12	0.47	0.02	0.15	3.78	0.20	0.08	0.38	2.17	0.85	0.10	0.98
<i>ppm</i>												
Ba	2678	10664	931	9844	19772	10707	2673	82136	73462	99722	30705	12457
Rb	199.8	63.4	49.4	17.1	30.8	80.7	41.9	143.5	45.4	28.9	40.6	55.6
Sr	4026	5846	6249	8791	4448	7202	2145	13707	30109	14891	22926	12359
Cs	1.20	0.50	0.28	0.10	0.20	0.70	0.20	0.80	0.20	0.10	0.35	0.40
Li	651.9	890.1	41.4	533.6	36.3	522.8	55.7	333.7	62.2	75.1	193.1	252.4
Ta	186.3	110.1	27.0	131.9	11.7	91.8	162.3	83.4	146.1	30.4	55.6	82.2
Nb	13849	3253	2033	23272	10508	7694	1610	12724	11026	2789	4167	8508
Hf	202.9	133.0	115.4	135.3	78.4	89.1	42.9	11.0	8.6	23.2	19.5	61.7
Zr	10592	5853	5726	6578	4019	3791	1606	215	149	1296	739	2534
Y	23.9	39.3	42.4	46.3	20.0	26.9	5.1	43.7	21.9	15.6	11.1	137.0
Th	928.9	418.0	116.5	738.8	844.8	1135.0	167.1	284.8	80.5	100.6	368.2	576.1
U	584.0	784.0	512.5	638.0	779.0	651.0	750.0	267.0	96.0	163.0	195.5	209.0
Cr	54.7	13.7	12.8	27.4	13.7	20.5	13.7	20.5	13.7	27.4	17.1	20.5
Ni	5.8	9.5	4.8	7.3	62.6	18.4	10.5	12.9	33.3	7.7	6.0	13.8
Co	93.3	256.1	92.3	136.7	866.2	93.2	106.3	69.1	44.9	77.0	26.6	59.2
Sc	45.0	39.0	30.0	25.0	26.0	32.0	41.0	12.0	21.0	17.0	20.0	20.0
Cu	2.50	974.90	0.56	2.85	2735.00	40.30	1.90	22.30	6.70	64.90	4.40	95.30
Pb	1.60	4.30	1.13	1.50	4.00	3.30	0.70	4.70	6.00	3.50	2.20	20.50
Zn	170.0	140.0	138.9	240.0	307.0	263.0	209.0	101.0	145.0	125.0	88.0	103.0
La	580.5	448.5	505.0	1084.0	637.7	499.5	79.0	1193.0	586.2	333.8	408.0	707.6
Ce	1565.0	1079.0	1184.5	2689.0	1543.0	1350.0	232.6	2412.0	1147.0	654.5	832.8	1738.0
Pr	179.00	133.40	147.18	313.90	173.10	155.50	24.11	288.90	127.70	70.60	88.79	208.00
Nd	558.0	454.8	537.0	1076.0	535.8	519.7	75.1	913.0	420.4	236.5	272.1	686.1
Sm	59.52	56.42	65.69	116.00	55.03	58.20	9.15	92.27	45.94	25.33	27.21	96.70
Eu	14.04	13.79	16.45	25.88	11.94	14.43	2.13	22.02	9.91	5.84	5.79	28.90
Gd	11.65	24.87	30.90	50.10	13.01	19.82	2.47	24.06	14.77	10.81	3.75	57.63
Tb	2.800	3.540	3.999	5.380	2.470	3.100	0.520	4.380	2.230	1.410	1.125	9.760
Dy	8.990	12.920	14.980	17.830	8.190	10.860	2.130	14.610	8.000	5.740	3.830	40.650
Ho	0.980	1.760	1.793	1.610	0.800	1.020	0.220	1.460	0.780	0.510	0.360	5.510
Er	1.490	2.600	2.459	2.810	0.810	1.710	0.370	2.140	1.020	0.890	0.540	8.870
Tm	0.210	0.360	0.338	0.330	0.140	0.230	0.050	0.280	0.140	0.110	0.085	0.850
Yb	1.300	1.810	1.708	2.080	0.940	1.100	0.280	1.600	0.630	0.600	0.445	3.530
Lu	0.170	0.200	0.160	0.200	0.100	0.130	0.040	0.160	0.070	0.070	0.045	0.340

Figure 2.16 compares the evolution trends of the Catalão I rocks and phoscorites and carbonatites from the Kovdor Complex (Krasnova *et al.*, 2004b; <http://www.emse.fr/~moutte>) in terms of MgO and SiO₂. The positive Si-Mg correlation is a common feature of the phoscorite series (e.g. Downes *et al.*, 2005), where the early fractionation of olivine drives the magma towards SiO₂ decrease with evolution. This is well marked for the phoscorite series described here, whereby both MgO and SiO₂ decrease from P1 to P3. The same general evolution is observed for the Kovdor phoscorites, with P1+P2 plotting in a higher SiO₂ and MgO field than P3+P4. Also plotted in the diagram are the composition of silicate rocks (pyroxenites, melilitolites, ijolites) from Kovdor, and various Catalão I silicate rocks (glimmerite, this work; kamafugite, Gomes & Comin-Chiaromonti, 2005; phlogopitite and pyroxenite, Araújo, 1996). In both complexes the silicate rocks evolve along a path of negative correlation between SiO₂ and MgO. Kovdor olivinite analyses plot in a field that is intermediate between the two trends, and it is possible that some of these rocks represent phoscorite-related olivinites whereas others are actually dunites derived from a silicate magma. The divergent trends between silicate rocks and phoscorites + carbonatites in the diagram, could not be originated by AFC, which suggests that an event of liquid immiscibility might have been involved in the generation of the phoscorite series. This event would also be responsible by the silicate trend, marked by silicate rocks of Catalão I and Kovdor.

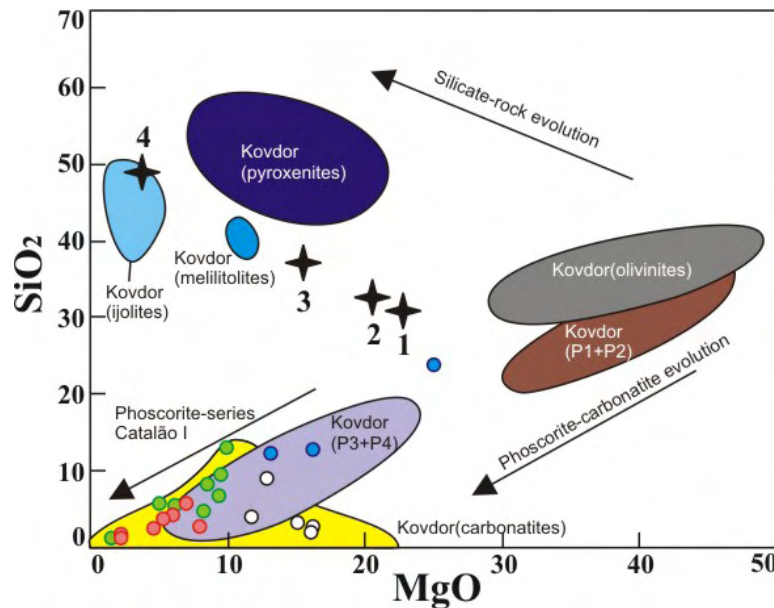


Fig. 2.16. SiO₂ and MgO variations in phoscorite-series rocks and carbonatites from Catalão I. Colored fields are from silicate rocks, phoscorites and carbonatites from the Kovdor Complex (Krasnova *et al.*, 2004b; <http://www.emse.fr/~moutte>). Also plotted are silicate rocks from the Catalão I complex (star symbols, 1: phlogopitite – Araújo, 1996; 2: glimmerite – this work; 3: kamafugite – Gomes & Comin-Chiaromonti, 2005; 4: pyroxenite – Araújo, 1996).

The Catalão I phoscorite-series rocks are variably enriched in incompatible trace elements, particularly Ba, Sr, REE, Nb, and Zr, all of which may have contents in the range of a few wt. % as oxides, but U (up to 800 ppm), Th (up to 2800 ppm), Hf (up to 200 ppm), and Ta (up to 180 ppm) also show extreme enrichment. In some cases, there is a systematic variation with magma evolution: U, Zr, Hf, and S increase, whereas Cr, Ni, and Rb decrease in the sequence P1-P2-P3. This is consistent with the magmatic evolution of the Catalão I rocks deduced from the mineral chemistry and whole-rock major element data. In other cases, such as Nb, Ta, and Th, incompatible elements are substantially enriched in the nelsonites (P2+P3), relatively to the phoscorites (P1). It should be stressed that the P2 and P3 nelsonites are the hosts for the bulk of the primary Nb mineralization in the complex. The associated dolomite carbonatites DC are even further enriched in BaO (1.4 – 11 wt.%) and SrO (1.4 to 3.5 wt.%), but are relatively less enriched in U, Th, Zr, and Hf than the coexisting nelsonites.

Figure 2.17 shows the rare-earth element patterns for the different rock groups. The field for the primitive magmas of the APIP complexes (phlogopite-picrites, Brod *et al.*, 2000) is shown for comparison. All rocks studied here show highly fractionated REE patterns with the LREE enriched 2 to 3 orders of magnitude relatively to the HREE. The P1 phoscorites show a pattern that is similar or only slightly more fractionated than that of the primitive phlogopite picrites. The P2 and P3 nelsonites, and the coexisting DC, on the other hand, have patterns that are substantially more fractionated than the primitive magmas. The REE patterns within each rock unit are consistently similar, suggesting that the rocks in each group are cogenetic. One P1 phoscorite (sample F4) and one P3 magnetitite (sample 091) have overall REE lower than the other rocks in their respective units, which suggests that these rocks are cumulates of REE-poor minerals such as olivine and magnetite, respectively. This is consistent with the very high MgO content (25.03 wt. %) in sample F4 and the very high $\text{Fe}_2\text{O}_{3(\text{T})}$ content (70.6 wt. %) in sample 091. One dolomite-carbonatite (sample 056B), representing a dike hosted by an altered carbonatite shows a distinctive HREE enrichment relatively to the other DC samples.

Most chondrite-normalized REE patterns (left-hand side diagrams in Fig. 2.17) show unexpected slight negative spikes in Gd and Er. When the samples are normalized to the average composition of phlogopite-picrite in the APIP (right-hand side diagrams, Fig. 2.17), it becomes clear that the negative spikes conform to an M-type tetrad REE pattern, i.e. the normalized pattern is split into four sections (La-Nd, Sm-Gd, Gd-Ho, and Er-Lu). This type of REE distribution has been increasingly recognized in connection with various processes, such as hydrothermal fluid-rock interactions (Jahn

et al., 2001; Kempe & Götze, 2002), weathering (Takahashi *et al.*, 2002), and bacterial activity (Takahashi *et al.*, 2005). In igneous-related systems, it has been often described in highly differentiated granites and their residual melts (Irber, 1999), interaction of residual melts with hydrothermal fluids (Jahn *et al.*, 2001), late-stage granite-related mineralization, such as pegmatites and greisens (Jahn *et al.* 2001; Kempe & Götze, 2002), fluorine complexation (Irber, 1999) and silicate-fluorine liquid immiscibility (Veksler *et al.*, 2005). Examples of tetrad REE patterns resulting from fluid-rock interaction in carbonatite systems were reported by Bühn *et al.* (2003a). The association of tetrad patterns with fluorite mineralization (Kempe & Götze, 2002; Bühn *et al.*, 2003a), the correlation of tetrad intensity with whole-rock fluorine contents (Irber, 1999), and recent experimental results (Veksler *et al.*, 2005) all point to the importance of the fluorine in generating the REE tetrad patterns. Late-stage activity in both granitic and carbonatitic systems is consistent with the fluorine complexation of the REE. The results by Veksler *et al.* (2005) indicate that REE tetrad patterns may be linked to aluminofluoride complexes, rather than fluorine-only.

Although it is generally recognized that there is an association between tetrad patterns and late-stage, diluted, volatile (F, H₂O)-rich, residual melts or fluids, the question whether this is still related to magma evolution (Irber, 1999; Veksler *et al.*, 2005) or already a hydrothermal phenomenon (Jahn *et al.*, 2001; Kempe & Götze, 2002; Bühn *et al.*, 2003a), or both, is not yet resolved. In the case of Catalão I, Cordeiro (2009 – *Capítulo 4*) analysed some of the same samples studied here for carbon and oxygen stable isotopes. The results of $\delta^{13}\text{C}$ in the range -5.5 to -6.5 ‰ and $\delta^{18}\text{O}$ in the range of 10.5 to 13 ‰, suggest that these samples bear primary (igneous) carbonates which did not undergo extensive interaction with hydrothermal fluids. We therefore favor a magmatic origin for the observed tetrad patterns.

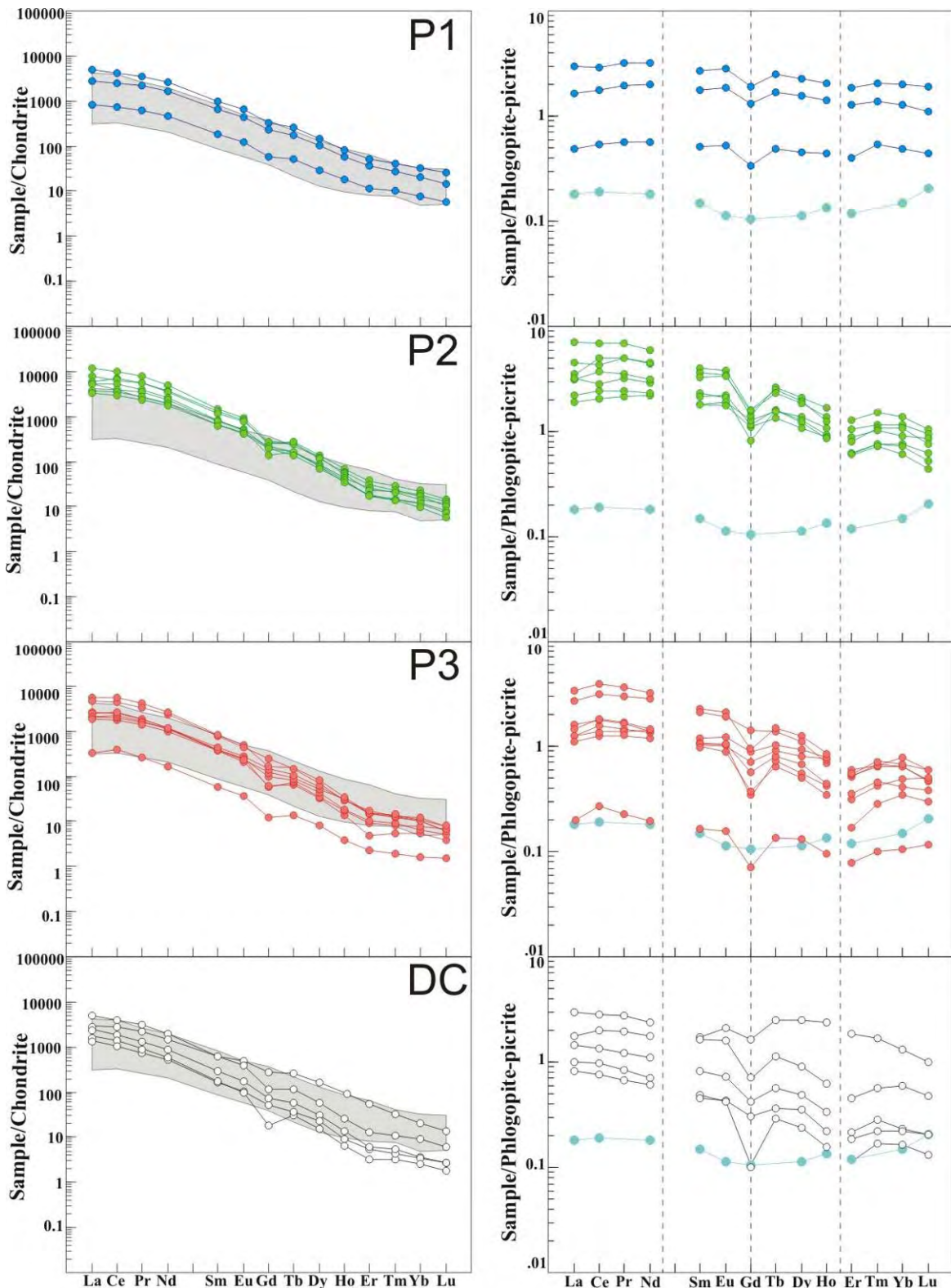


Fig. 2.17. REE patterns for the studied rocks. Above: samples normalized to chondrite. Below: samples normalized to an average phlogopite picrite (FLP, primitive magma for the APIP complexes, our unpublished data). Also plotted is an analysis of a Catalão I pyroxenite (bebedourite, light blue symbols) from Araújo (1996). Note the M-type tetrad pattern in all rocks of the phoscorite-series and related carbonatites, and the inverse W-type pattern in the bebedourite.

Tetrad-type fractionation requires the production of a pair of mirrored tetrad patterns, i.e. removal of a fluid or immiscible melt with a W-type tetrad pattern would leave an M-type pattern in its counterpart (Irber, 1999; Veksler *et al.*, 2005; Takahashi *et al.*, 2002). An analysis of a Catalão I pyroxenite (bebedourite) from Araujo (1996) is plotted in Figure 2.17 for comparison. Although Pr, Tb and Tm are missing in this analysis, a W-type tetrad pattern, complementary to those of the phoscorite-series rocks, is still clearly visible in the diagrams. Figure 2.18 shows the same bebedourite compared with analyses of similar rocks from the Araxá complex (Traversa *et al.*, 2001), in the south of the APIP, on a more suitable scale. When normalized to the average phlogopite-picrite, the Araxá bebedourites show the same W-type pattern as the Catalão sample, although this feature is not clearly visible in chondrite-normalized rare-earth diagrams. The mirrored tetrad patterns suggest that the silicate magma that produced the Catalão I bebedourite and the phosphate- and carbonate-rich magma that produced the phoscorites, nelsonites and carbonatites studied here may have a common origin, as immiscible liquids from a primitive, carbonated silicate magma such as the phlogopite picrites.

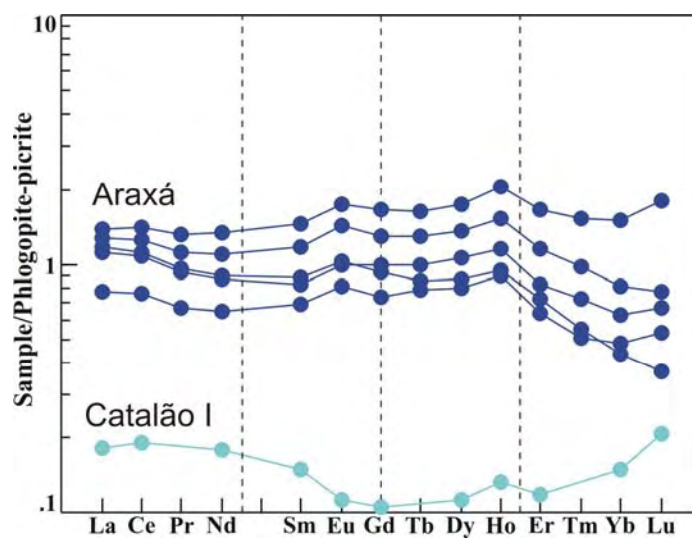


Fig. 2.18. W-type tetrad patterns in Catalão I (light blue, Araujo, 1996) and Araxá (dark blue, Traversa *et al.*, 2001).

Interestingly, after it is produced the tetrad pattern persists up to the most differentiated dolomite carbonatites, which is in good agreement with the suggestion by Irber (1999) that the fractionation of specific minerals is unlikely to produce tetrad REE patterns. Different ways of quantifying the tetrad effect have been put forward by Irber (1999) and Monecke *et al.* (2002). Although the method proposed by Monecke *et al.* (2002) is statistically more rigorous, it does not allow the distinction

between the M and W types of patterns. Thus, we opted by the quantification method of Irber (1999), according to which the absence of tetrad is indicated by a TE value of 1.0, whereas M-type tetrads yield $TE > 1$, and W type yield TE values < 1 . The different Catalão I rock-types have a total tetrad magnitude (computed from the combined contributions of the first, third and fourth branches) varying from 1.06 to 1.4. Except for the P1 phoscorites, which are characterized by the lowest TE values, averaging 1.09, all other rocks have extensively overlapping TE ranges and virtually equal TE averages (1.21 for P2, 1.23 for P3, and 1.21 for the dolomite carbonatites). At the present stage, it is not possible to determine whether the relatively lower TE average on P1 is an artifact of petrological features or a consequence of the smaller number of analysed samples. In any case, the remarkably similar results for the three last differentiation stages suggest that the tetrad effect is not sensitive to fractional crystallization and once imprinted in a magma, it is retained as a permanent geochemical signature.

Two sets of paired nelsonite-carbonatite samples from P2 and P3 are plotted in Figure 2.19. The slope of the REE patterns of the nelsonite and associated DC (normalized to the average phlogopite picrite) are very similar, suggesting that these rocks are related through fractionation rather than liquid immiscibility.

Bühn & Trumbull (2003b) described the occurrence of several complementary (mirrored) anomalies in normalized trace-element diagrams as a characteristic of immiscible carbonatite and nefoidite or ne-syenite from Namibia. In our case, the trace-element patterns in the normalized diagrams (Fig. 2.19) show similar signatures for the paired nelsonites and carbonatites, with the exception of small opposite spikes in Ba and Sr, which may be readily explained by variations in carbonate concentration. This adds further support to a fractionation process linking the nelsonites and carbonatites.

Furthermore, we could find no significant discrepancies in the zoning pattern of crystallizing minerals between the host nelsonite and in the coexisting DC pocket, which suggests that the two domains crystallized in equilibrium. Therefore, we propose that the studied dolomite-carbonatites are the result of filter-pressing of a residual (rather than immiscible) carbonatite liquid into locally developed vugs within a nelsonitic crystal mush, thus forming the DC pockets shown in Figure 2.4. Such carbonatite pockets could eventually coalesce into larger bodies, which could, in turn, supply suitable volumes of carbonatite magma to form the DC dikes.

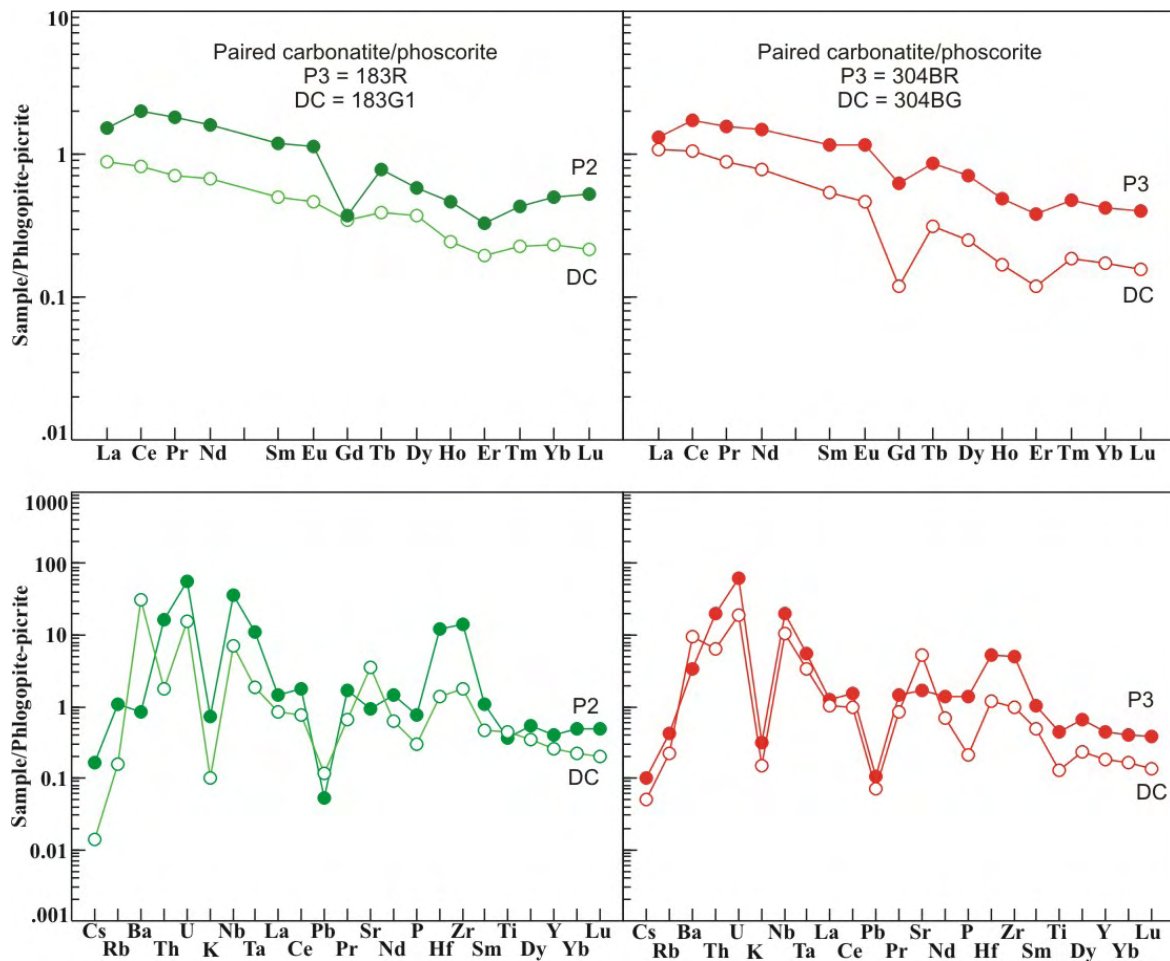


Fig. 2.19. REE and trace-element patterns for paired phosphorite-carbonatite, normalized to the average APIP phlogopite-picrite.

Sr AND Nd ISOTOPIC DATA

Isotopic data from 3 dolomite carbonatites (DC) is reported in table 2.7. Isotopic ratios are corrected for the 85 Ma age of the intrusion (Sonoki & Garda, 1988).

Figure 2.20 compares the isotopic composition of Catalão I phosphorites and carbonatites with that of the APIP (Gibson *et al.*, 1995), and of other complexes where a clear carbonatite and phosphorite association occurs, such as Kovdor (Zaitsev & Bell, 1995; Lee *et al.*, 2006) and Turiy (Dunworth & Bell, 2001), in Russia, and Phalaborwa (Eriksson, 1989; Yuhara *et al.* 2005), in South Africa.

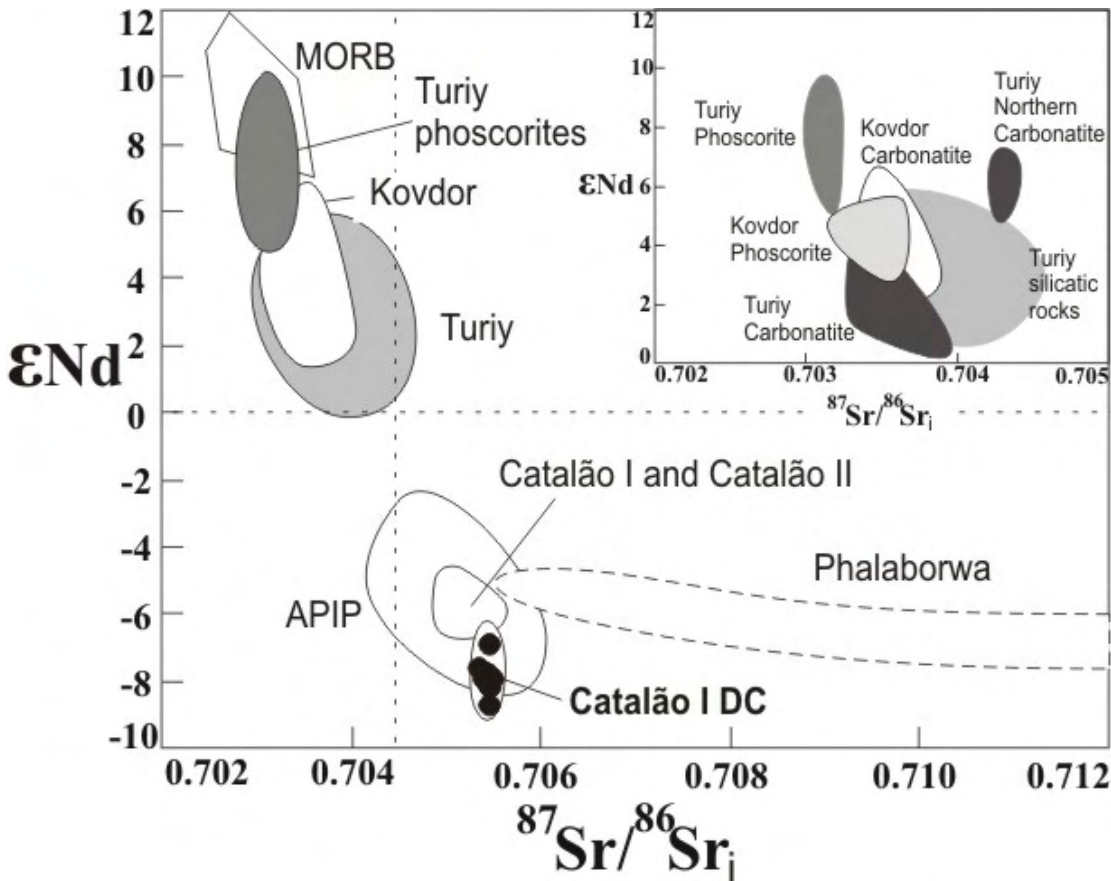


Fig. 2.20. Sr and Nd isotopic composition of Catalão I dolomite carbonatites. Compositional fields from Phalaborwa (Eriksson, 1989; Yuhara et al., 2005), Kovdor (Zaitsev & Bell, 1995), Turiy (Dunworth & Bell, 2001), Catalão I and II (Comin-Chiaromonti et al., 2005 and references therein), MORB and APIP (Gibson et al., 1995) are shown for comparison. The inset shows a detailed diagram for different rocks from Turiy and Kovdor.

Sr and Nd isotopic composition of phoscorites and carbonatites from Kovdor and Turiy plot in the depleted-mantle quadrant, indicating a depleted source for these magmas. In the case of Turiy, the phoscorites have distinctively higher ϵ_{Nd} than the associated carbonatites and alkaline silicate rocks, whereas in Kovdor the fields for different rock-types overlap. On the other hand, piroxenites, phoscorites, and carbonatites samples from the Phalaborwa carbonatite-phoscorite complex plot within the enriched quadrant with a wide range in the initial Sr isotopic ratio (Eriksson, 1989; Yuhara et al. 2005).

Dunworth & Bell (2001) argued in favor of a multi-source magma mixing for the formation of the Turiy Complex that could have involved plume contribution, two different kimberlite sources and an unknown crustal component. Moreover, they considered the most depleted isotopic signatures of Sr-Nd for the phoscorites as unrelated to any other rock they studied. Dunworth & Bell (2003) added evidences from mineral chemistry and whole rock analysis and pointed out that the differences between phoscorite, carbonatite and piroxenite-melilitolite indicate that the parental magmas from

the carbonatite-phoscorite association of Turiy cannot be the same as the magmas that originated the silicate rocks.

Tab. 2.7 Sm-Nd-Sr isotopes of dolomite carbonatite DC related to nelsonites. $87\text{Sr}/86\text{Sr}$ and $143\text{Nd}/144\text{Nd}$ isotopic ratios are presented as measured (*m*) and initial values (*i*) corrected to 85 Ma.

Sample	149	170	304BG	206	230 A	339	304BR	319
Sr	13707	30109	22926	5846	12405	7924	7202	3884
Sm	97.55	51.8	42.182	54510.0	215.4	102898.0	52175.0	94671.0
Nd	911.24	453.989	575.627	414885.0	1385104.0	793013.0	431584.0	657168.0
($^{147}\text{Sm}/^{144}\text{Nd}$)m	0.065	0.069	0.044	0.079	0.094	0.078	0.073	0.087
($^{143}\text{Nd}/^{144}\text{Nd}$)m	0.5121	0.5122	0.5121	0.5122	0.5122	0.5122	0.5122	0.5123
($^{143}\text{Nd}/^{144}\text{Nd}$)i	0.5121	0.5121	0.5121	0.5121	0.5122	0.5122	0.5122	0.5122
$\epsilon\text{Nd m}$	-9.59	-9.32	-9.44	-8.70	-7.939	-7.627	-7.959	-6.925
$\epsilon\text{Nd i}$	-8.16	-7.94	-7.79	-7.43	-6.83	-6.35	-6.62	-5.74
($^{87}\text{Sr}/^{86}\text{Sr}$)m	0.70549	0.70549	0.70544	0.7055	0.7054	0.7054	0.7054	0.7055
($^{87}\text{Sr}/^{86}\text{Sr}$)i	0.70545	0.70548	0.70543	0.7054	0.7054	0.7053	0.7054	0.7054
TDMNd0	0.92	0.93	0.81	0.97	1.04	0.90	0.89	0.92

Isotopic variations in the Kovdor complex were interpreted by Zaitsev & Bell (1995) as a function of at least three different mantle components. Lee *et al.* (2006) interpreted that the Kovdor rocks were formed from the interaction between a mantle plume and a previously metasomatized mantle.

Eriksson (1989) and Yuhara *et al.* (2005) point out that the wide Sr-isotope variation in the Phalaborwa rocks cannot be explained by magmatic differentiation, and invoke the mixing of two unknown isotopically heterogeneous sources in the formation of the parental magma.

Sr-Nd data from Catalão I rocks also plot within the enriched quadrant, with a Nd isotopic composition similar to that of Phalaborwa but a much more restricted range in Sr isotopic ratios. Both the previously published data for Catalão I (Comin-Chiaromonti *et al.*, 2005) and our results plot within the overall isotopic range of the APIP (Gibson *et al.*, 1995), although the samples analyzed here are near the lowest ϵNd limit of the APIP field. The isotopic composition of the Catalão I complex and other APIP rocks is consistent with the origin of the alkaline magmas from a metasomatized subcontinental lithospheric mantle. The Nd model ages obtained in this work are similar to other APIP data (Gibson *et al.*, 1995) and suggest that the mantle source was metasomatized during the Neoproterozoic.

DISCUSSION AND CONCLUSIONS

Several lines of evidence indicate a magmatic origin for the Catalão I phoscorite-series rocks, such as the emplacement of phoscorites and nelsonites as widespread dikes crosscutting metasomatic phlogopite and the continuous variations in modal proportions and mineral chemistry from early-stage phoscorites (P1), through apatite nelsonites (P2) to late-stage magnetite nelsonites and magnetitites (P3). The occurrence of dolomite carbonatites pockets with C-O stable isotope igneous signature (Cordeiro, 2009 - *Capítulo 4*) adds further support to a magmatic origin for these rocks.

The evolution of the silicate phase from olivine (altered to Ti-clinohumite) in P1, through tetraferriphlogopite with phlogopite cores in P2, to nearly pure tetra-ferriphlogopite in P3 and DC is consistent with observations in other phoscorite-bearing complexes, such as Kovdor and Sokli, where Al-bearing phlogopite is more abundant in early phoscorites, shifting to tetra-ferriphlogopite in the late-stage phoscorites (Krasnova *et al.* 2004b; Lee *et al.* 2003, Lee *et al.* 2004) and in carbonatites (Heathcote and McCormick, 1989). The transition from olivine to phlogopite is consistent with the expected Si-depletion in magmatic evolution, and the progression from phlogopite to tetraferriphlogopite signals the Al-depletion with magma evolution. If only analyses from crystal cores are considered, phlogopite evolution is also accompanied by a slight increase in the Fe/Mg ratio from P1 to DC. On the other hand, zoning of individual crystals often results in Mg-enrichment towards the rims, which appears to be a common feature in primary tetra-ferriphlogopite from carbonatite and carbonate-rich alkaline magmas (e.g. Brod *et al.*, 2001). In this sense, the core-to-rim Mg enrichment in P3 and DC phlogopites could be related to increasing carbonate activity in the more differentiated magma, in comparison with P2, whose micas show a normal Mg-decreasing zoning pattern. Some P1 micas also show slightly Mg-enriched, Al-depleted rims, which probably result from minor interaction with carbonate-rich intercumulus material.

Chemical variations in apatite are also consistent with magma evolution in the sequence P1-P2-P3-DC, whereby the cores of apatite crystals become progressively more Sr-rich. Nevertheless, as observed for phlogopite, the core-to-rim variation in individual crystals is often in the opposite sense (Sr-depletion), particularly in P3 and DC. This is possibly due to the increasing competition for Sr between apatite and crystallizing carbonates or between apatite and a progressively more carbonate-rich residual magma. Dawson & Hinton (2003) pointed out that Sr partitioned to only slightly greater extent into calcite than into coexisting apatite in a Phalaborwa carbonatite ($Sr_{\text{calcite}}/Sr_{\text{apatite}} = 1.22$), and Klemme & Dalpé (2003) reported experimentally determined apatite/carbonatite melt partition coefficient in the range 0.28-0.42. These relationships suggest that the presence of a carbonate-rich

residual melt would be a more efficient means of preventing Sr from being incorporated into apatite than competition from crystallizing carbonate.

The described zoning patterns of both apatite and phlogopite are consistent with a more evolved magma with increased carbonate activity in P3 and DC. P3 nelsonites typically contain well-developed carbonatite pockets, but relatively little amounts of interstitial carbonate, suggesting that the carbonate-rich residual liquid was segregated into the pockets and then crystallized as a carbonatite. Because the phlogopite and apatite zoning patterns are coincident in P3 and DC, such segregation would have to take place at a very late-stage in the P3 crystallization, probably when most of the nelsonite was already crystallized, which suggests a filter-pressing process for the formation of the DC pockets. An origin of the DC pockets by liquid immiscibility is unlikely, as it would tend to produce contrasting mineral and whole-rock chemistry features.

Ilmenites are also a good marker for magma evolution in the Catalão I phoscorites and nelsonites. They vary mostly along the geikielite-ilmenite solid solution series, becoming progressively less magnesian from P1 to P3. Similar features have been reported from phoscoritic rocks from Sokli (Lee *et al.* 2005). Magnetite composition, on the other hand, is a relatively poor index for magma evolution in the Catalão I phoscorites, nelsonites, and dolomite carbonatites. Although some Ti and Mg substitution occurs, the composition of magnetites from different rock types overlaps widely.

Whole-rock major element chemistry is also consistent with magma evolution from P1 to P3. As in other worldwide phoscorite-carbonatite-alkaline complexes, the phoscorite magmas at Catalão I are very SiO₂-poor, and evolve toward decreasing contents of both Si and Mg, through fractionation of olivine and phlogopite. The associated silicate rocks follow a divergent path of Si increase with decreasing Mg. Such divergent trends in MgO-SiO₂ diagrams seem to be typical of phoscorite-bearing alkaline complexes (e.g. Downes *et al.*, 2005).

The field, textural, and mineral chemistry evidence suggests that, if the entire composition range of Catalão I magmas is considered, the rocks studied in this work may be collectively regarded as a late stage in the evolution of the complex. This conclusion is further supported by the presence of conspicuous M-type tetrad REE patterns in all studied rock units. The tetrad effect is relatively rare type of REE distribution present in hydrothermal (e.g. Jahn *et al.*, 2001; Kempe & Götze, 2002, Bühn *et al.* 2003a) and weathering processes (Takahashi *et al.*, 2002), but is also recognized as a feature of very late-stage activity in granitic magmas (Irber, 1999) and related mineralization (Jahn *et al.* 2001; Kempe & Götze, 2002). Furthermore, recent experimental results indicate that it may be produced by immiscibility processes (Veksler *et al.*, 2005).

Our results show that REE tetrad distribution may also develop during magmatic evolution of phoscorite-carbonatite-alkaline complexes, but may have been often overlooked in chondrite-normalized REE diagrams. The normalization of the REE data to a more similar set of reference values (e.g. a primitive magma in the complex) will enhance this feature and allow its identification more easily. This approach led to the recognition of W-type tetrad patterns in published analyses of ultramafic silicate rocks (bebedourites) from the APIP complexes of Catalão I (Araujo, 1996) and Araxá (Traversa et al., 2001). Such features mirror the M-type patterns of phoscorites, carbonatites and nelsonites described here, suggesting that the phoscoritic magma (and carbonatites which possibly evolved from them) in these complexes was produced by a liquid immiscibility event from a parental silicate magma, during the early evolution stages of the complex. Furthermore, it indicates that, once established, the tetrad signature is not affected by further fractional crystallization.

There appears to be a marked Sr- and Nd-isotope difference between phoscorite-carbonatite-alkaline rock complexes of potassic (e.g. APIP, Brod et al., 2000; Phalabora, Eriksson, 1989; Yuhara et al., 2005) and sodic (i.e. ijolite-bearing, Kola, Zaitsev & Bell, 1995, Dunworth & Bell, 2001) affiliation. In a Sr-Nd isotope diagram, the potassic complexes plot in the enriched mantle quadrant whereas the ijolite-bearing complexes plot in the depleted-mantle quadrant. This may indicate that the former are mainly generated from a metasomatized lithospheric mantle, whilst the latter are more strongly influenced by asthenospheric sources or mixed lithospheric-asthenospheric contributions.

The petrogenetic links between phoscorites and the coexisting carbonatites and silicate rocks are still a matter of debate. The Sr- and Nd-isotope differences between phoscorites and other rocks of the Turiy complex, in the Kola Province, led Dunworth & Bell (2001, 2003) to argue a multi-source origin for the complex, and that the carbonatites, phoscorites and alkaline silicate rocks in the complex could not have been generated by the same parental magmas.

On the other hand, there is compelling field, textural, geochemical and mineral chemistry evidence suggesting a strong petrogenetic link between phoscorites and the associated rocks. Phoscorites occur exclusively in carbonatite-related environments, which also supports a genetic relation between these two rock-types, regardless of the radiogenic signature of the source. The occurrence of paired carbonatite-phoscorite sets in several complexes (e.g. Krasnova *et al.* 2004a, Lee *et al.* 2004, and this work) where phoscorite and carbonatites share the same mineralogy and similar mineral chemistry also argue in favor of a common parental magma.

The mirrored REE tetrad patterns described here suggest that, although the phoscorites, nelsonites, and dolomite carbonatites in the Catalão Nb deposit are related to each other through

crystal fractionation, the initial, carbonate-rich phoscorite magma derived by liquid immiscibility from a primitive (phlogopite-picrite) carbonated silicate magma. The silicate branch derived from this immiscibility event followed a divergent crystallization path, generating the Catalão I bebedourites.

ACKNOWLEDGEMENTS

This paper is part of a MSc thesis granted by CNPq—Brazilian Council for Research and Technological Development to the first author and had the support of Mineração Catalão and Anglo American Brazil Exploration Division. The work was further supported by research grants from CNPq to JAB, ELD and ESRB. University of Brasília is gratefully acknowledged for fieldwork support and access to laboratory facilities.

REFERENCES

- Araújo, D. P. (1996). Metasomatism no complexo carbonatítico Catalão-I: implicações para a composição do magma carbonatítico e para o metasomatismo carbonatítico no manto superior. Unpublished M.Sc. Thesis, University of Brasília, Brasília, DF, 188 pp.
- Brod J. A., Gibson S. A., Thompson R. N., Junqueira-Brod T. C., Seer H. J., Moraes L. C., Boaventura G. R. (2000). Kamafugite affinity of the Tapira alkaline-carbonatite complex (Minas Gerais, Brazil). *Revista Brasileira de Geociências* **30**, 404-408.
- Brod, J. A., Gaspar, J. C., Araújo, D. P., Gibson, S. A., Thompson, R. N., Junqueira-Brod, T. C. (2001). Phlogopite and tetra-ferriphlogopite from Brazilian carbonatite complexes: petrogenetic constraints and implications for mineral-chemistry systematic. *Journal of Southeast Asian Earth Sciences* **19**, 265-296.
- Brod, J. A., Ribeiro, C. C., Gaspar, J. C.; Junqueira-Brod, T. C.; Barbosa, E. S. R., Riffel, B. F., Silva, J. F., Chaban, N. & Ferrarri, A. J. D. (2004). In: 42 Congresso Brasileiro de Geociências, Geologia e Mineralizações dos Complexos Alcalino-Carbonatíticos da Província Ígnea do Alto Paranaíba. Field Trip Guide, 29 pp.
- Brod, J. A., Gaspar, J. C., Diniz-Pinto, H. S., Junqueira-Brod, T. C. (2005). Spinel chemistry and petrogenetic processes in the Tapira alkaline-carbonatite complex, Minas Gerais, Brazil. *Revista Brasileira de Geociências* **35**, 23-32.
- Bühn, B. M., Schneider, J., Dulski, P., Rankin, A. H. (2003a). Fluid–rock interaction during progressive migration of carbonatitic fluids, derived from small-scale trace element and Sr, Pb isotope distribution in hydrothermal fluorite. *Geochimica et Cosmochimica Acta* **67**, 4577–4595.
- Bühn, B. M., Trumbull, R.B. (2003b). Comparison of petrogenetic signatures between mantle-derived alkali silicate intrusives with and without associated carbonatite, Namibia. *Lithos* **66**, 201-221
- Carvalho, W. T. & Bressan, S. R. (1981). *Depósitos minerais associados ao Complexo ultramáfico-alcalino de Catalão I – Goiás*. In: Schmaltz, W. H. (ed.) *Os principais depósitos minerais da Região Centro Oeste*. Brasília: DNPM, 139-183.
- Comin-Chiaromonti, P., Gomes, C. B., Censi, P., Speziale S. (2005). *Carbonatites from southeastern Brazil: a model for the carbon and oxygen isotope variations*. In: Comin-Chiaromonti, P. & Gomes, C. B. (eds.) *Mesozoic to Cenozoic alkaline magmatism in the Brazilian Platform*, São Paulo, Edusp/Fapesp, 629-650 pp.
- Constanzo A., Moore, K. R., Wall, F., Feely, M. (2006). Fluid inclusions in apatite from Jacupiranga calcite carbonatites: Evidence for a fluid-stratified carbonatite magma chamber. *Lithos* **91**, 208-228.
- Cordeiro, P. F. O. (2009). Petrologia e metalogenia do depósito primário de nióbio do Complexo Carbonatítico-Foscórritico de Catalão I, GO. Unpublished M.Sc. Thesis, University of Brasília, Brasília, DF, 140 pp.
- Dawson, J. B., Hinton, R. W. (2003). Trace-element content and partitioning in calcite, dolomite and apatite in carbonatite, Phalaborwa, South Africa. *Mineralogical Magazine* **67**, 921-930.
- Deer, W. A., Howie, R. A., & Zussman, J. (1992). *Minerais constituintes das rochas uma introdução*. Lisboa: Fundação Calouste Gulbenkian, p. 358.
- Downes, H., Balaganskaya E., Beard, A., Liferovich, R. & Demaiffe, D. (2005). Petrogenetic processes in the ultramafic, alkaline and carbonatite magmatism in the Kola Province: A review. *Lithos* **85**, 48-75.
- Dunworth, E. & Bell, K. (2001). The Turiy Massif, Kola Peninsula, Russia: Isotopic and geochemical evidence for multi-source evolution. *Journal of Petrology* **42**, 377-405.
- Dunworth, E. & Bell, K. (2003). The Turiy Massif, Kola Peninsula, Russia. Mineral chemistry of an ultramafic-alkaline-carbonatite intrusion. *Mineralogical Magazine* **67**, 423-451.
- Eriksson, S.C. (1989). *Phalaborwa: a saga of magmatism, metasomatism and miscibility*. In: Bell, K. (ed.) *Carbonatites: genesis and evolution*. London: Unwin Hyman, 221-254 pp.
- Farmer, G. L., Boetcher, A. L. (1981). Petrologic and crystal-chemical significance of some deep-seated phlogopites. *American Mineralogist* **66**, 1154-1163.
- French J. E., Heaman, L. M. and Chacko, T. 2002. Feasibility of chemical U-Th total Pb baddeleyite dating by electron microprobe. *Chemical Geology* **188**, 85-104.
- Gaspar, J.C., Araújo, D.P. and Melo, M.V.L.C. 1998. Olivine in carbonatitic and silicate rocks in carbonatite complexes. Ext. Abstr. 7th Int. Kimb. Conf., pp. 239-241.
- Gaspar, J. C. & Wyllie, P. J. (1982). Barium phlogopite from the Jacupiranga carbonatite, Brazil. *American Mineralogist* **67**, 997-1000.
- Gaspar, J. C. & Wyllie, P. J. (1987). The phlogopites from the Jacupiranga carbonatite intrusions. *Mineralogy and Petrology* **36**, 121-134.
- Gaspar J. C & Wyllie P. J. (1983a). Magnetite in the carbonatites from the Jacupiranga complex, Brazil. *American Mineralogist* **68**, 195-213.
- Gaspar J. C & Wyllie P. J. (1983b). Ilmenite (high Mg,Mn,Nb) in the carbonatites from the Jacupiranga complex, Brazil. *American Mineralogist* **68**, 960-971.

- Gibson, S. A., Thompson, R. N., Leonards, O. H., Dickin, A. P., Mitchell, J. G. (1995). The Late Cretaceous impact of the Trindade mantle plume – evidence from large-volume, mafic, potassic magmatism in SE Brazil. *Journal of Petrology* **36**, 189-229.
- Gierth, E. & Baecker, M. L. (1986). *A mineralização de nióbio e as rochas alcalinas associadas no complexo Catalão I, Goiás*. In Schobbenhaus, C. (ed.) *Principais depósitos minerais do Brasil*. Brasília: MME/DNPM, 455-462.
- Gioia, S. M. & Pimentel, M. M. (2000). A metodologia Sm-Nd no Laboratório de Geocronologia da Universidade de Brasília. *Anais da Academia Brasileira de Ciências* **72**, 219-245.
- Gullbrandsen, R. A. (1966). Chemical composition of phosphorites of the Phosphoria Formation. *Geochimica et Cosmochimica Acta* **30**, 769-778.
- Heathcote, R. C., McCormick, G. R. (1989). Major-cation substitution in phlogopite and evolution of carbonatite in the Potash Sulfur Springs complex, Garland County, Arkansas. *American Mineralogist* **74**, 132-140.
- Hirano, H., Kamitani, M., Sato, T., Sudo, S. (1990). Niobium mineralization of Catalao I carbonatite complex, Goias, Brazil. *Bulletin of the Geological Survey of Japan* **41**, 619-626.
- Hogarth, D. D., Hartree, R., Loop J., Solberg, T. N. (1985). Rare-earth element minerals in four carbonatites near Gatineau, Quebec. *American Mineralogist* **70**, 1135-1142.
- Hoggarth, D. D. (1989). *Pyrochlore, apatite and amphibole: distinctive minerals in carbonatite*. In: Bell, K. (ed.) *Carbonatites – Genesis and evolution*. London: Unwin Hyman, 105-148.
- Karchevsky, P. I. & Moutte, J. (2004). *The phoscorite-carbonatite complex of Vuoriyarvi, northern Karelia*. In: Wall, F. & Zaitsev, A. N. (eds.) *Phoscorites and Carbonatites from Mantle to Mine: the Key Example of the Kola Alkaline Province*. London: Mineralogical Society Series, 163-169.
- Klemme, S., Dalpé, C. (2003). Trace-element partitioning between apatite and carbonatite melt. *American Mineralogist* **88**, 639-646.
- Irber W. (1999) The lanthanide tetrad effect and its correlation with K/Rb, Eu/Eu*, Sr/Eu, Y/Ho, and Zr/Hf of evolving peraluminous granite suites. *Geochimica et Cosmochimica Acta* **63**, 489-508.
- Jahn, B., Wu, F., Capdevila, R., Martineau, F., Zhao, Z. & Wang, Y (2001). Highly evolved juvenile granites with tetrad REE patterns: the Woduhé and Baerzhe granites from the Great Xing'an Mountains in NE China. *Lithos* **59**, 171-198.
- Kempe, U. & Götze, J. (2002). Cathodoluminescence (CL) behaviour and crystal chemistry of apatite from rare-metal deposits. *Mineralogical Magazine* **66**, 135-156.
- Krasnova, N. I., Petrov, T. G., Balaganskaya, E. G., Garcia, D., Moutte, D., Zaitsev, A. N. & Wall, F. (2004a). *Introduction to phoscorites: occurrence, composition, nomenclature and petrogenesis*. In: Wall, F. & Zaitsev, A. N. (eds.) *Phoscorites and Carbonatites from Mantle to Mine: the Key Example of the Kola Alkaline Province*. London: Mineralogical Society Series, 45-79.
- Krasnova, N. I., Balaganskaya, E. G. & Garcia, D. (2004b). *Kovdor – classic phoscorites and carbonatites*. In: Wall, F. & Zaitsev, A. N. (eds.) *Phoscorites and Carbonatites from Mantle to Mine: the Key Example of the Kola Alkaline Province*. London: Mineralogical Society Series, 99-132.
- Lee, M. J., Garcia, D., Moutte, J., Lee, J. I. (2003). Phlogopite and tetraferriphlogopite from phoscorite and carbonatite associations in the Sokli massif, Northern Finland. *Geosciences Journal* **7**, 9-20.
- Lee, M. J., Garcia, D., Moutte, J., Williams, C. T. & Wall, F. (2004) *Carbonatites and phoscorites from the Sokli complex, Finland*. In: Wall, F. & Zaitsev, A. N. (eds.) *Phoscorites and Carbonatites from Mantle to Mine: the Key Example of the Kola Alkaline Province*. London: Mineralogical Society Series, 133-162.
- Lee, M. J., Lee, J. I., Moutte, J. (2005). Compositional variation of Fe-Ti oxides from the Sokli complex, northeastern Finland. *Geosciences Journal* **9**, 1-13.
- Lugmair, G. W. & Marti, K. (1978). Lunar initial $^{143}\text{Nd}/^{144}\text{Nd}$: Differential evolution of the lunar crust and mantle. *Earth and Planetary Science Letters* **39**, 349- 357.
- Mitchell, R. H. (1978). Manganese magnesian ilmenite and titanian clinohumite from the Jacupiranga carbonatite, São Paulo, Brazil. *American Mineralogist* **63**, 544-547.
- Mitchell, R. H. & Bergman, S. C. (1991). Petrology of Lamproites. New York: Plenum Press, p. 440.
- Mitchell, R. H. (1995). Kimberlites, Orangeites and Related Rocks. New York: Plenum Press, p. 410.
- Monecke, T., Kempe, U., Monecke, J., Sala, M. & Wolf, D. (2002). Tetrad effect in rare earth element distribution patterns: a method of quantification with application to rock and mineral samples from granite-related rare metal deposits. *Geochimica et Cosmochimica Acta* **66**, 1185-1196.
- Oliveira I. W. B., Sachs L. L. B., Silva V. A., Batista I. H. 2004. Folha SE.23-Belo Horizonte. In: Schobbenhaus C., Gonçalves J. H., Santos J. O. S., Abram M. B., Leão Neto R., Matos G. M. M., Vidotti R. M., Ramos M. A. B., Jesus J. D. A. (Eds.). *Carta geológica do Brasil ao millionésimo: Sistema de Informações Geográficas – SIG e 46 folhas na escala 1: 1.000.000*. Brasília, Brazil: CPRM 41 CD-ROM Pack.

- Palmieri, M., Pereira, G. S. B., Brod, J. A., Junqueira-Brod, T. C., Petrinovic, I. A. & Ferrari, A. J. D. (2008). Orbicular magnetite from the Catalão I phoscorite-carbonatite complex. In: 9th International Kimberlite Conference, 2008, Frankfurt. Extended Abstracts. p. 9IKC-A-00337.
- Ribeiro, C. C. (2008). Geologia, geometalurgia, controles e gênese dos depósitos de fósforo, terras raras e titânio do Complexo Carbonatítico Catalão I, GO. Unpublished Ph.D. thesis, University of Brasília, Brasília, DF, 473 pp.
- Ribeiro, C. C.; Brod, J. A.; Gaspar, J. C.; Petrinovic, I. A., Junqueira-Brod, T. C. (2001). Pipes de Brecha e Atividade Magmática Explosiva no Complexo Carbonatítico de Catalao I, GO. *Revista Brasileira de Geociências* **31**, 417-426.
- Ribeiro, C. C.; Brod, J. A.; Junqueira-Brod, T. C.; Gaspar, J. C.; Petrinovic, I. A. (2005). Mineralogical and field aspects of magma fragmentation deposits in a carbonate phosphate magma chamber: evidence from the Catalão I complex, Brazil. *Journal of South American Earth Sciences* **18**, 355-369.
- Rieder, M., Cavazzini, G., D'Yakonov, Y. S., Frank-Kamenetskii, V. A., Gottardi, G., Guggenheim, S., Koval, P. V., Müller, G., Neiva, A. M. R., Radoslovich, E. W., Robert, J. L., Sassi, F. P., Takeda, H., Wiss, Z., Wones, D. R. (1998). Nomenclature of the micas. *Canadian Mineralogist* **36**, 905-912.
- Sonoki I. K. & Garda G. M. (1988). Idades K-Ar de rochas alcalinas do Brasil Meridional e Paraguai Oriental: compilação e adaptação as novas constantes de decaimento. *Boletim do Instituto de Geociências Universidade de São Paulo* **19**, 63-85.
- Stoppa, F. & Cundari, A. (1995). A new Italian carbonatite occurrence at Cupaello (Rieti) and its genetic significance. *Contributions to mineralogy and Petrology* **122**, 275-288.
- Stoppa, F., Sharygin, V. V., Cundari, A. (1997). New data from the carbonatite-kamafugite association: The melilitolite from Pian di Celle, Italy. *Mineralogy and Petrology* **61**, 27-45.
- Takahashi, Y., Yoshida, H., Sato, N., Hama, K., Yusa, Y. & Shimizu, H. (2002). W- and M-type tetrad effects in REE patterns for water-rock systems in Tono uranium deposit, central Japan. *Chemical Geology* **184**, 311-335.
- Takahashi, Y., Châtelier, X., Hattori, K. H., Kato, K. & Fortin, D. (2005). Adsorption of rare earth elements onto bacterial cells and its implication for REE sorption onto natural microbial mats. *Chemical Geology* **219**, 53-67.
- Thompson, R. N., Gibson, S. A., Mitchell, J. G., Dickin, P., Leonards, O. H., Brod, J. A., Greenwood, J. C. (1998). Migrating Cretaceous-Eocene magmatism in the Serra do Mar alkaline province, SE Brazil: melts from the deflected Trindade mantle plume?. *Journal of Petrology* **39**, 1439-1526.
- Toledo, M. C. M. & Pereira, V. P. (2001). A variabilidade de composição da apatita associada a carbonatitos. *Revista do Instituto Geológico* **22**, 27-64.
- Torres, M. G. (1996). Caracterização mineralógica do minério fosfático da Arafértil S.A., no Complexo Carbonatítico de Barreiro, Araxá, MG. Unpublished M.Sc. Thesis, University of Brasília, Brasília, DF, 149 pp.
- Traversa, G., Gomes, C. B., Brotzu, P., Buraglini, N., Morbidelli, L., Principato, M. S., Ronca, S., Ruberti, E. (2001). Petrography and mineral chemistry of carbonatites and mica-rich rocks from the Araxá complex (Alto Paranaíba Province, Brazil). *Anais da Academia Brasileira de Ciências* **73**, 71-98.
- Veksler, I. V., Dorfman, A. M., Kamenetsky, M., Dulski, P. & Dingwell, D. B. (2005). Partitioning of lanthanides and Y between immiscible silicate and fluoride melts, fluorite and cryolite and the origin of the lanthanide tetrad effect in igneous rocks. *Geochimica et Cosmochimica Acta* **69**, 2847-2860.
- Verhulst, A., Balaganskaya, E., Kirnarsky, Y., Demaiffe, D. (2000). Petrological and geochemical (trace elements and Sr-Nd isotopes) characteristics of the Paleozoic Kovdor ultramafic, alkaline and carbonatite intrusion (Kola Peninsula, NW Russia). *Lithos* **51**, 1-25.
- Yegorov, L. S. (1993). Phoscorites of the Maymecha-Kotuy ijolite-carbonatite association. *International Geology Review* **35**, 346-358.
- Yuhara, M., Hirahara, Y., Nishi, N., Kagami, H. (2005). Rb-Sr, Sm-Nd of the Phalaborwa Carbonatite Complex, South Africa. *Polar Geosciences* **18**:101-113.
- Zaitsev, A. & Bell, K. (1995). Sr and Nd isotope data of apatite, calcite and dolomite as indicators of source, and the relationships of phoscorites and carbonatites. *Contributions to Mineralogy and Petrology* **121**:324-335.

CAPÍTULO 3

Pyrochlore Chemistry from the Primary Niobium Deposit of the Catalão I Carbonatite-Phoscorite complex, Brazil

PEDRO F. O. CORDEIRO

*Anglo American Exploration Brazil, Av. Interlândia 502, Setor Santa Genoveva, CEP 74672-360,
Goiânia-GO, Brasil*

JOSÉ A. BROD, JOSÉ C. GASPAR, ELISA S. R. BARBOSA, ROBERTO V. SANTOS

*Universidade de Brasília, Campus Darcy Ribeiro, ICC Central, Instituto de Geologia
LUIS C. ASSIS AND MATHEUS PALMIERI*

*Anglo American Exploration Brazil, Av. Interlândia 502, Setor Santa Genoveva, CEP 74672-360,
Goiânia-GO, Brasil*

Abstract

Pyrochlore is the ore-mineral of niobium in the Nb-P-Fe mineralization of the Catalão I phoscorite-carbonatite complex and represents the main current source of this element. In the Catalão I complex, niobium mineralization is related to stockworks of thin dikes of olivine-free phoscorite-series rocks characterized as phlogopite nelsonites either rich in apatite (P2) or magnetite (P3). The dolomite carbonatites (DC) are interpreted as intimately related with P2 and P3 and represent the last stage of crystallization of a phoscoritic magma. Pyrochlore chemistry shows a compositional trend from Ca-rich toward Na-rich composition regarded as a result of magmatic evolution. The Ca-rich end-member is not clear in the Catalão I pyrochlores, but it can be extended further if compared to the early-pyrochlore compositions from Oka and Salitre. The Na-rich end-member occurs as pyrochlore inclusions in ilmenites from DC. Another compositional trend is related to pyrochlore affected by meteoric fluids, showing that weathering can alter the igneous Ca-Na pyrochlore composition into bariopyrochlore through the substitution of Na and Ca by Ba, with an additional enrichment in Si. Important substitutions in the B-site were observed neither in the igneous trend nor in the alteration trend. While the primary niobium mineralization is related to phoscoritic rocks (nelsonites), the dissolution of dolomite carbonatite pockets and of interstitial carbonate generated secondary porosity, thus allowing concentration of weathering-resistant phases such as pyrochlore in the soil. This secondary enrichment characterizes the residual deposit and is responsible for higher niobium grades compared to the primary mineralization.

Keywords: Phoscorite, Nelsonite, Carbonatite, Catalão I, pyrochlore, niobium

INTRODUCTION

The genesis of niobium deposits related to carbonatite complexes in Brazil is often attributed to residual enrichment of Nb in carbonatite-related rocks (Carvalho and Bressan, 1981; Gierth and Baecker, 1986). This is the case of the Catalão I niobium deposit, from the Late-Cretaceous Alto Paranaíba Igneous Province (APIP), Central Brazil, where weathered products of the phoscorite-series rocks (nelsonites) originated an economic deposit that has been mined for more than 30 years. On the other hand, there are carbonatite complexes in the same province in which the occurrence of economic niobium deposits is unknown, although some of their rocks do contain pyrochlore, and despite the fact that all complexes in the province share many similarities and the same geochemical affiliation. It is clear now that there are other geological processes controlling the formation of economic niobium deposit in carbonatites, previously to the residual (weathering) concentration.

In the Catalão I deposit, primary pyrochlore enrichment occurs in phoscorite-series rocks (nelsonites), rather than in carbonatites. The phoscorite series is a group of rocks composed essentially by apatite, magnetite and a magnesian silicate phase such as olivine, phlogopite or clinopyroxene (Yegorov, 1993; Krasnova et al., 2004a). These rocks are spatially, texturally and compositionally related to carbonatites, often forming multiphase phoscorite-carbonatite associations, and represent magmas that evolved by crystal fractionation, crystal accumulation, and/or liquid immiscibility.

The Catalão I deposit provides a rare opportunity for describing and sampling phoscorite-series rocks and to investigate their contact relationships. Moreover, it also allows exploring the petrological implications of the relationships between different types of phoscorite-series rocks for pyrochlore concentration in magmatic systems.

In this paper we compare the mineral chemistry of pyrochlore from fresh and weathered rocks, aiming to establish the main chemical features and substitutions. Furthermore, the comparison of the Catalão I pyrochlore with other carbonatite-related niobium deposits in Lueshe (Nasraoui and Bilal, 2000) and Oka (Gold et al., 1986; Zurevinski and Mitchell, 2004), and with pyrochlore in phoscorite rocks from Sokli (Lee et al., 2006) helps establishing a broader model. We also discuss and provide insights on the importance of magmatic processes for the origin of a niobium deposit.

METHODS AND SAMPLING

Samples were collected between 100-500 m depths from drill cores of the Catalão I primary niobium deposit, made available by Mineração Catalão (Anglo American Brazil). Sampling was aimed at rocks as fresh as possible and free from hydrothermal alteration. In order to avoid weathering effects, sampling followed the criteria established by Cordeiro (2009 – *Capítulo 4*) for identification of primary and secondary carbonates as well as other evidence of rock alteration.

Polished thin sections of each sample were studied under transmitted and reflected light microscopy in order to determine their composition and textural properties. Chemical composition of selected mineral phases was determined by WDS using a CAMECA SX-50 electron microprobe at the University of Brasília. The analytical conditions were set at 20 kV and 20 nA.

THE ALTO PARANAÍBA IGNEOUS PROVINCE (APIP)

The APIP is a NW-trending concentration of Late-Cretaceous alkaline igneous rocks, intruding Neoproterozoic rocks of the Brasilia Belt, between the NE border of the Paleozoic Paraná Basin and the SW border of the Archean São Francisco Craton (Fig. 3.1). Its origin is attributed to the Trindade Mantle Plume that affected the South American Platform ca. 85 Ma (Gibson et al., 1995; Thompson et al., 1998). A thinspot of the lithosphere under the Brasilia Belt allowed the heat of the mantle plume to penetrate by conduction and advection causing melting of readily fusible, K-rich parts of the lithospheric mantle.

The xenoliths of bebedourite and pyroxenite that occur within kamafugite lavas in the APIP are analogous to ultramafic rocks in the carbonatite complexes, thus testifying the intimate association between them (Brod, 1999, Brod et al., 2000, Brod et al., 2001). Those authors argued in favor of a common origin in the subcontinental lithospheric mantle for kamafugites and the parental magma of the APIP complexes (phlogopite-picrite). The temporal and spatial association between these alkaline rocks defines a kamafugitic-carbonatitic association in the APIP, similarly to what happens in Italy (Stoppa and Cundari, 1995; Stoppa et al., 1997), and was more recently reported from China (Yang and Woolley, 2006).

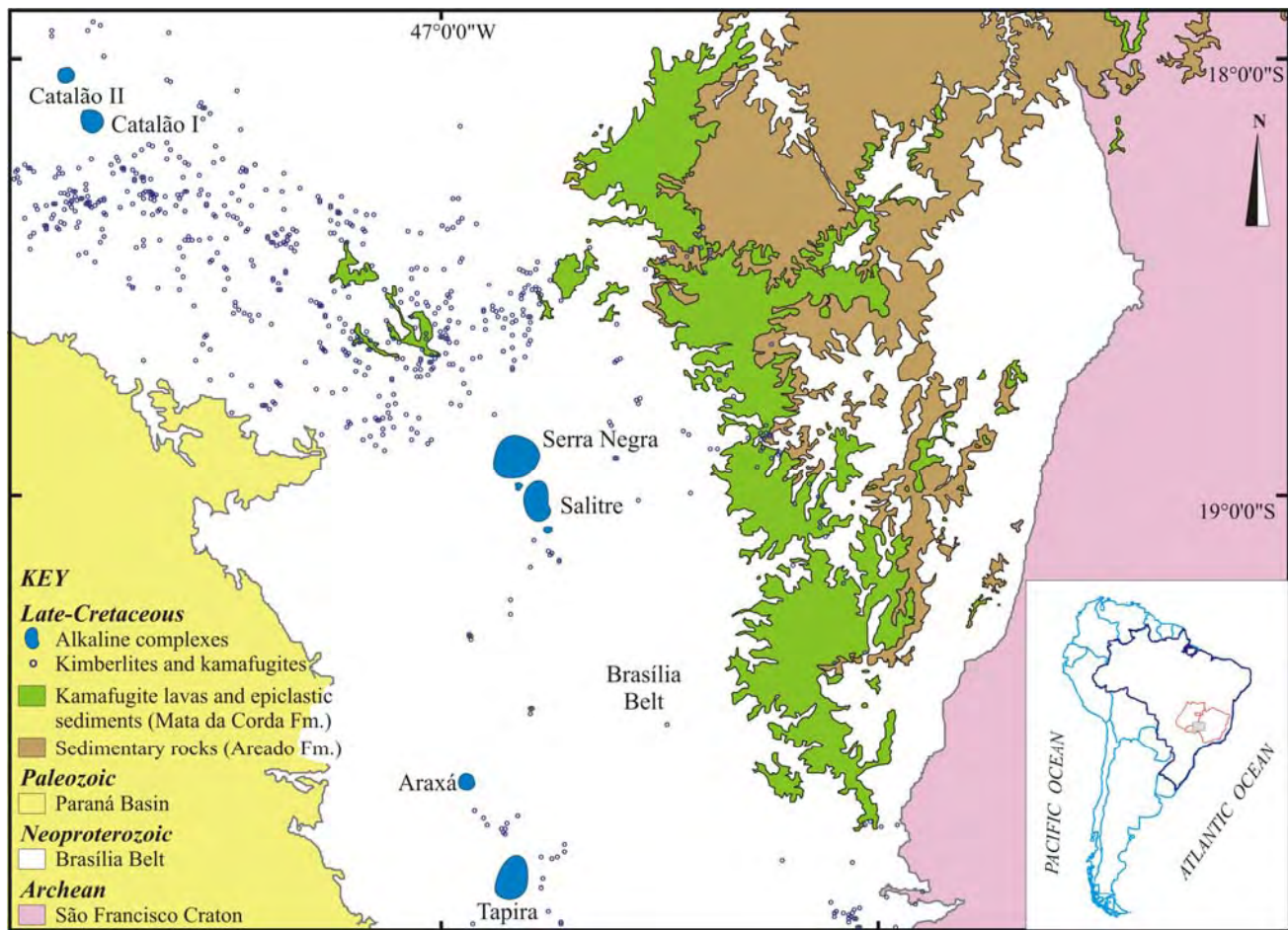


Fig. 3.1. Geological map of the Alto Paranaíba Igneous Province showing the location of alkaline-carbonatite complexes. Dots represent kamaufugite, kimberlite and lamproite from the province. Adapted from Oliveira et al. (2004).

The APIP carbonatite-complexes intruded Late-Proterozoic metamorphic rocks of the internal and external domains of the Brasília Belt, which are conspicuously deformed into dome structures. These occurrences comprise the complexes of Catalão I and Catalão II in the Goiás State, and Serra Negra, Salitre I, Salitre II, Salitre III, Araxá (Barreiro) and Tapira in the Western Minas Gerais State (Brod et al., 2001; Brod et al., 2004).

Araxá, Catalão I and Catalão II contain the only known economic niobium deposits in the APIP and are responsible for supplying more than ninety percent of the niobium demand in the world. These complexes are being mined for niobium and phosphate, and have potential for titanium, rare-earths, copper, and vermiculite deposits. These complexes share similar features that are not found in Tapira, Salitre I, II, and III and Serra Negra (Brod et al. 2004; Barbosa et al. in preparation).

The primary Nb mineralization in the Araxá Complex is related to phoscorites that are cut by thin veins of similar composition plus dolomite, barite, norsethite and Fe-Cu sulfides (Issa Filho et

al., 1984; Silva, 1986). At Catalão I these late-stage veins were characterized as phlogopite nelsonites and magnetites (Cordeiro, 2009 – *Capítulos* 2 and 4). The intrusion style and the mineralogy of the phoscoritic rocks in the Nb deposits of Araxá and Catalão II (Palmieri et al., in preparation) are very similar to those of Catalão I (Hirano et al., 1990; Cordeiro, 2009 – *Capítulos* 2 and 4). Furthermore, both Araxá and Catalão I present widespread occurrence of metassomatic phlogopitites, interpreted as former bebedourites, pyroxenites and dunites, thus indicating more intense metassomatism if compared to other complexes of the province. This high-intensity event of metassomatism appears to be restricted to Araxá and Catalão I, and might be related to the more primitive nature of the carbonate-rich magmas in these complexes, which may have intruded before they lost alkalis and CO₂ by degassing and/or fractioned carbonate and hydrous minerals.

CATALÃO I CARBONATITE COMPLEX

The Catalão I carbonatite complex (Fig. 3.2) is located in Central Brazil at 18°08'S, 47°48'W, near the city of Catalão. It has intruded quartzites and schists of the Late Proterozoic Araxá Group as a vertical pipe with ~6km in diameter at surface, originating a dome-like structure and fenitizing the surrounding rocks. The age of the intrusion is reported by Sonoki and Garda (1988) as 85±6.9 Ma (K-Ar in phlogopite).

Catalão I is currently mined for niobium and phosphate, but there are also important deposits of rare-earth elements, titanium and vermiculite (Carvalho and Bressan, 1981; Gierth and Baecker; 1986; Ribeiro, 2008).

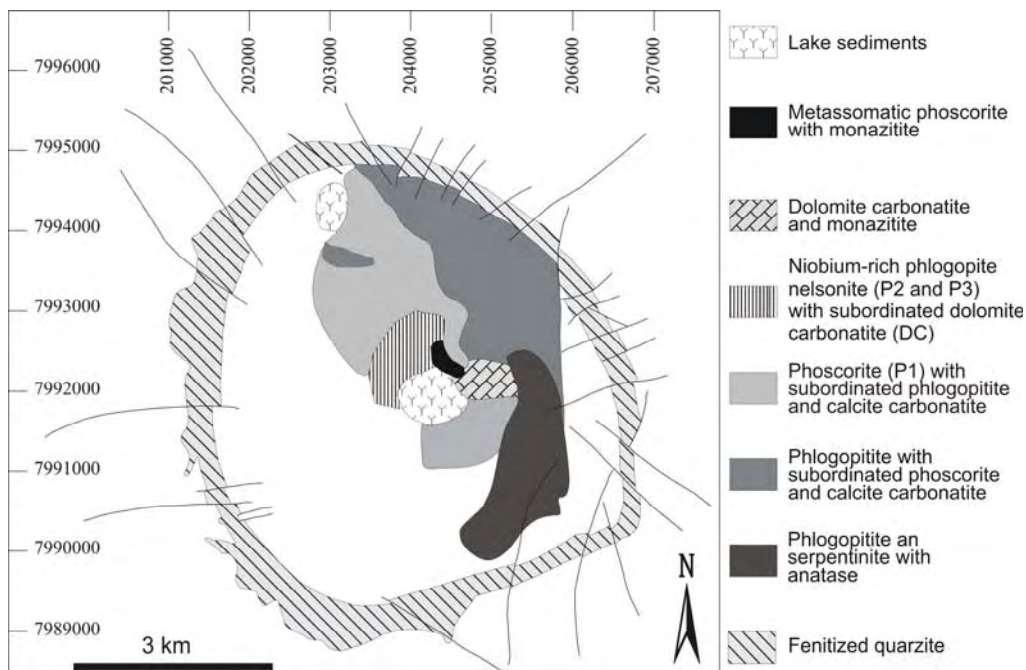


Fig. 3.2. Geological sketch of the Catalão I Complex. The studied samples were obtained from the niobium-rich phlogopite nelsonite and from the phoscorite with subordinated phlogopite and calcite carbonatite units. Modified from Brod et al. (2004) and Ribeiro (2008). Blank areas represent lacking of outcrops or drill core informations.

PHOSCORITE-SERIES ROCKS AND THE NIOBIUM DEPOSIT

There is an intimate association between the occurrence of phoscorite-series rocks and the niobium deposit of Catalão I. Cordeiro (2009 – *Capítulo 4*) divided the phoscorite series into four units according to their modal mineralogy, mineral chemistry and magma evolution stage. The P1 unit consists mainly of phoscorites, while P2 are phlogopite apatite nelsonites and P3 are phlogopite magnetite nelsonites. Dolomite carbonatites occurs both related to P2 and P3 and are grouped here under the designation DC.

The phoscorites and nelsonites crosscut metassomatic phlogopite, carbonatite and ultramafic rocks (Fig. 3.3) and may be cut by late-stage DC dikes. While P1 is often altered by metasomatic fluids or by weathering, P2 and P3 are generally fresh and show no clear imprint of hydrothermal alteration. Interaction with meteoric waters imprints changes in the primary oxygen isotopic composition of the carbonate (Cordeiro, 2009 – *Capítulo 4*). This event also originates patches of low-SrO turbid (inclusion-rich) carbonate that replace the primary, high-SrO carbonates.

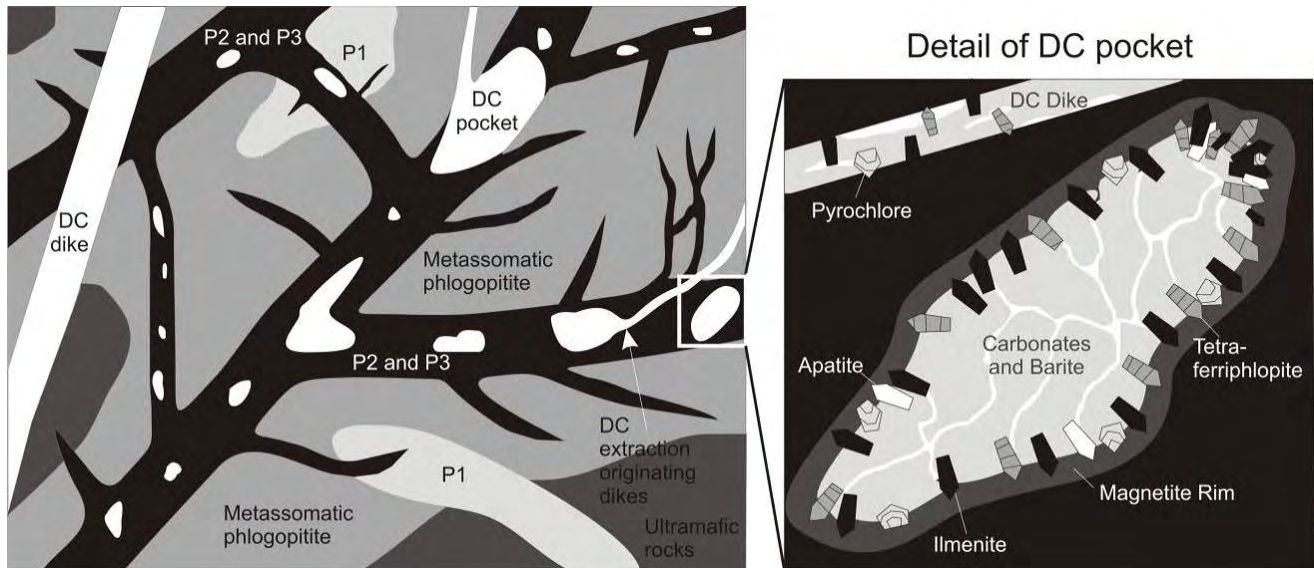


Fig. 3.3. Schematic model of occurrence of phoscorites in Catalão I. P1, P2, P3, and DC crosscut all the former rock types. The DC pockets and dikes are usually accompanied by a magnetite rim and by crystals pointing toward the center of the pocket. (P1 = phoscorite; P2 = apatite nelsonite; P3 = magnetite nelsonite; DC = dolomite carbonatite)

P1, P2 and P3 dikes share similar emplacement style with Catalão I carbonatites , i.e. dominantly stockworks of thin dikes and veins, which indicates similarities in the physical properties of the original magmas. Cordeiro (2009 – *Capítulo 4*) showed that the best preserved phoscorite-series rocks from Catalão I have igneous carbon- and oxygen-isotope signatures, and though there may be a subsequent isotopic variation due to degassing, metassomatism, and weathering, they originally crystallized from phosphate-iron-oxide magmas. Phosphate-iron-oxide rocks are described from Kiruna in Sweden, El Laco in Chile, Gole Gohar, and Hamadan in Iran (Frietsch, 1978; Mücke and Younessi, 1994; Nyström and Henríquez, 1994; Henríquez et al., 2003) and evidence for the occurrence of phosphate-titanium-iron-oxide magmas is reported in subvolcanic andesitic rocks from Peru (Clark and Kontak, 2004).

The main host rock of the phoscorite-series is a metassomatic phlogopite (Fig. 3.4A), which is mainly composed of fine-grained tetra-ferriphlogopite and coarse- to medium-grained magnetite and perovskite. Olivine and pyroxene also occur in these rocks, but in most cases are completely altered to the minute flakes of tetra-ferriphlogopite. Relicts of the original ultramafic rock may be preserved in areas less affected by the late-stage carbonatite veins.

Early-stage phoscorites (P1, Fig. 3.4B) occur as coarse- to medium-grained thin dikes or small plugs in metasomatic phlogopite near the core of the Catalão I complex, and are composed mainly of olivine, apatite, phlogopite, and magnetite. Figure 3.4B shows P1 with typical decimetric light-

green apatite aggregates and brown-red tetra-ferriphlogopite flakes. The replacement of olivine and phlogopite due to metasomatic alteration usually produces aggregates of tetra-ferriphlogopite with clino-humite and magnesite. Texture relations of the subhedral crystals of apatite and phlogopite suggests that they crystallized after olivine, while magnetite is intercumulus. Ilmenite lamellae (< 0.1 mm) and blebs are common features in the P1 magnetites. Baddeleyte, ilmenite, clinohumite, rutile, dolomite, and magnesite are accessories. Though this rock type is pyrochlore-free, it is the primary source for the large apatite deposits formed by residual concentration in the weathering mantle developed on Catalão I complex (Ribeiro, 2008).

The late-stage P2 and P3 phlogopite nelsonites are the most Nb-rich rocks of the complex. They constitute the primary niobium mineralization, whose grade is directly related to the abundance of P2 and P3 dikes. The most abundant niobium mineral is pyrochlore, which may reach up to 13 modal percent. Rare Fe-columbite occurs in DC, but only as inclusions in ilmenites. The P2 and P3 wallrock are the metasomatic phlogopitite, the early P1 phoscorite, and carbonatite, emplaced as stockworks of fine to medium-grained dikes varying in width between one meter and a few millimeters. Contrary to P1, these rocks typically lack olivine.

P2 is apatite rich and the essential silicate phases are tetra-ferriphlogopite with subordinate phlogopite occurring mostly as crystal cores. The contact between phlogopite cores and tetra-ferriphlogopite rims is often sharp, lacking a zone of intermediate composition. Apatite is prismatic and may show flow texture. The crystals are frequently zoned with clear cores surrounded by fluid inclusions-rich rims, which gives the grain a turbid aspect at the edges. Magnetite is intercumulus and may contain very thin (ca. <0.01 mm) ilmenite lamellae.

P3 is magnetite-rich (apatite/magnetite < 0.8 vol. %) and has tetra-ferriphlogopite as the essential silicate phase. More aluminous phlogopite is virtually absent. The mica crystals are euhedral to subhedral and less abundant than in P2. Apatite crystals vary from prismatic to ovoid, but may also occur as aggregates of anhedral grains (Fig. 3.6D), usually associated with massive anhedral magnetite concentrations at the walls of DC pockets. Magnetite is intercumulus and may reach up to 71 modal percent of the rock (Cordeiro 2009 – *Capítulo 4*).

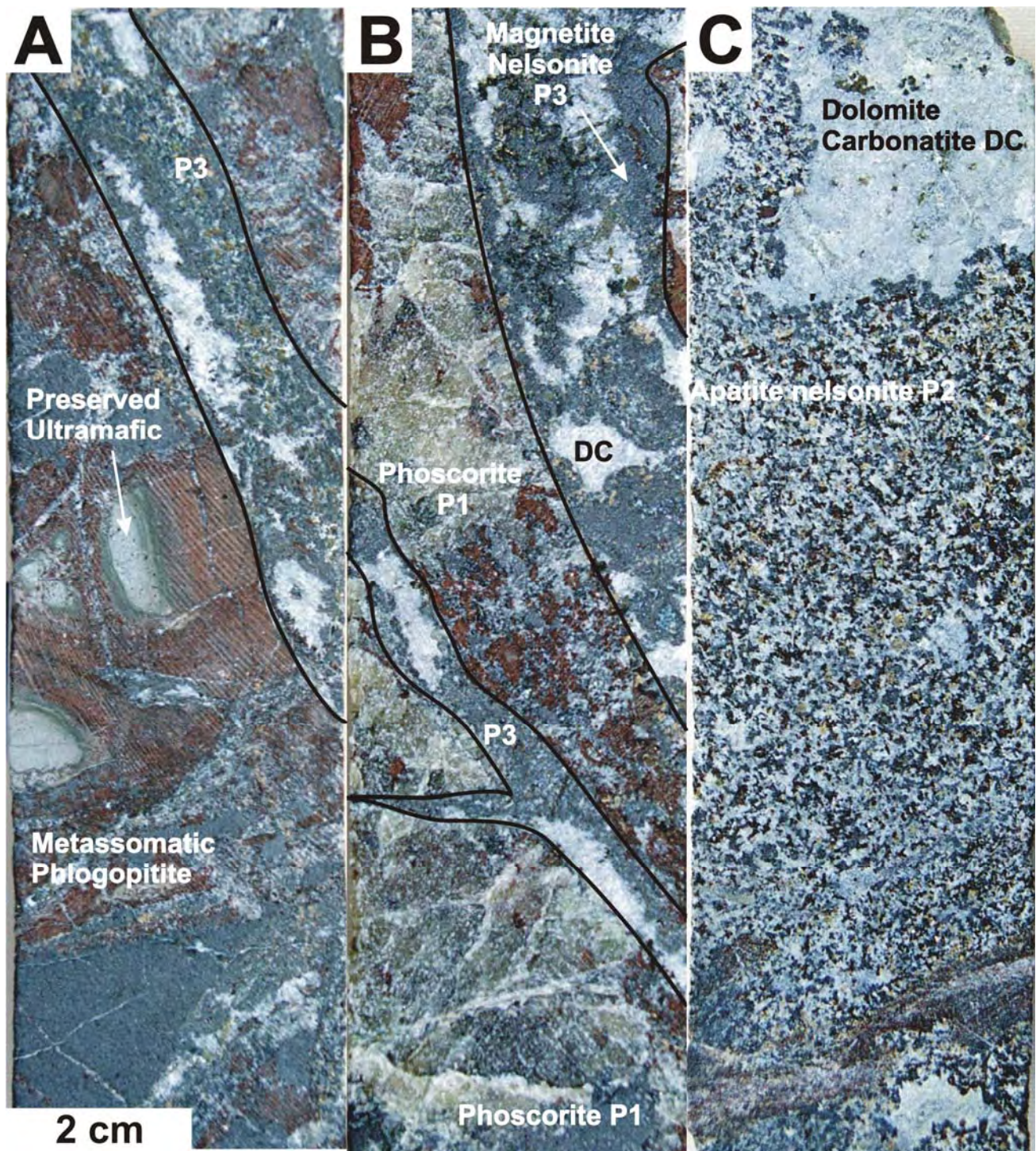


Fig. 3.4. Ultramafic rocks, phoscorites and nelsonites from the Catalão I niobium deposit. A. Metasomatic phlogopite with green relicts of the original ultramafic rock. At the upper portion of the drill core, a magnetite nelsonite dike (P3) with DC pockets cuts the metasomatic phlogopite. B. Altered, coarse-grained P1, crosscut by P3 dikes with DC pockets. C. Equigranular P2 with DC pockets. (P1 = phoscorite; P2 = apatite nelsonite; P3 = magnetite nelsonite; DC = dolomite carbonatite)

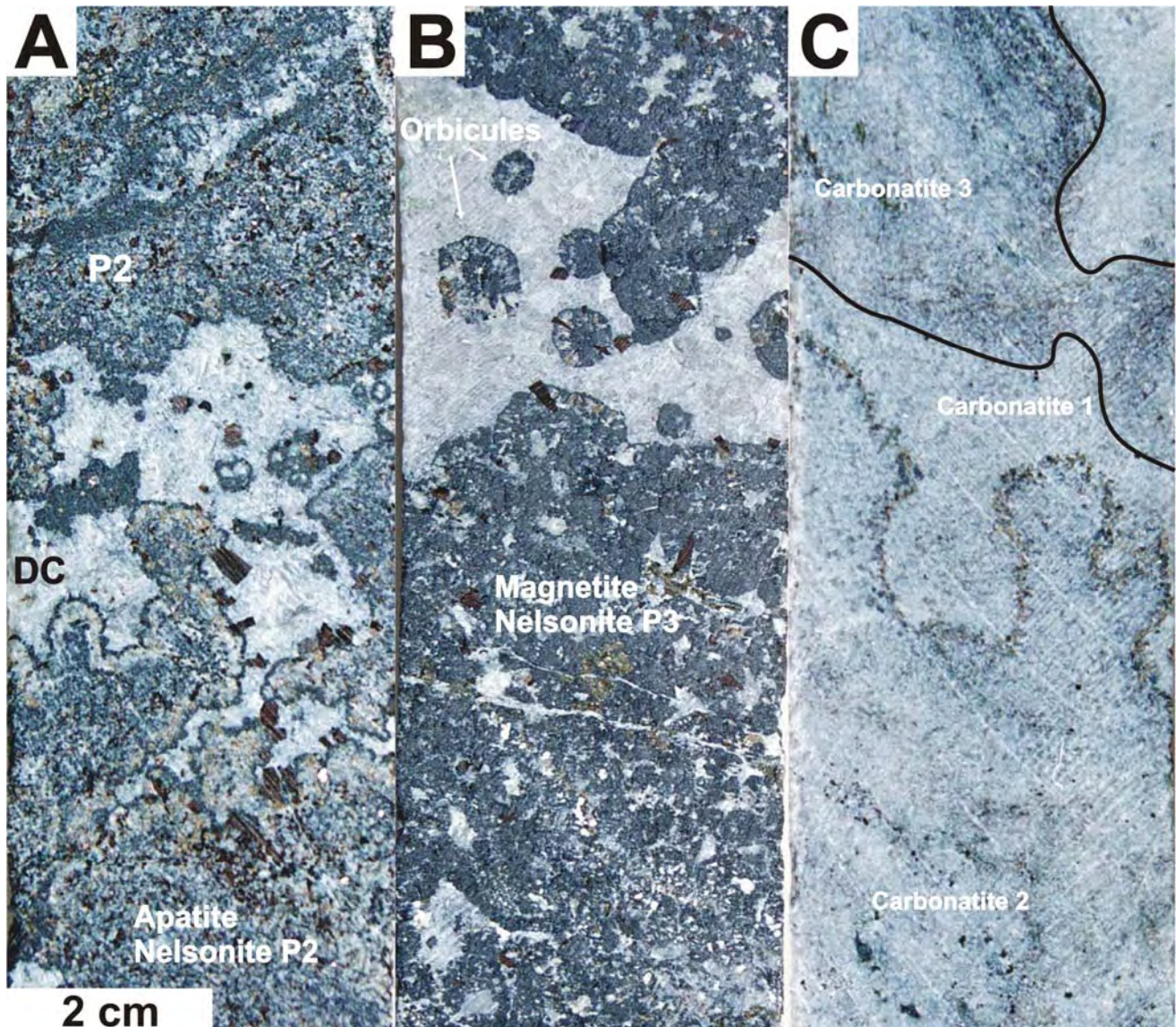


Fig. 3.5. Structures and textures related to pyrochlore-rich nelsonites. A. Mineralized P2 with DC pockets. Note the mingling texture between the carbonatite and the apatite nelsonite, the thin rim of magnetite between them and the phenocrysts of phlogopite (brown-red subhedral) that nucleated at the magnetite rim, pointing toward DC. B. Magnetite-rich nelsonite (P3) and DC pocket with nelsonite spheres or droplets. C. Mingling between two different carbonatites. Pyrochlore, magnetite and phlogopite crystallize at the mingling interface. (P1 = phoscorite; P2 = apatite nelsonite; P3 = magnetite nelsonite; DC = dolomite carbonatite)

Dolomite carbonatite (DC) occurs as pockets within the nelsonites and also as dikes and veins. In both cases, the mineralogy and modal abundances are very similar. DC dikes are hosted in open fractures in metassomatic phlogopitite, carbonatite and even in P1 phoscorite. DC pockets are rounded to irregular, sometimes globular or amoeboid, resembling mingling textures (Fig. 3.5) and can represent up to 20 modal percent in P2 rocks and up to 40 modal percent in P3. DC pockets and,

more rarely, DC dikes show strong modal variations between the central zone and the margin. The central zone is composed of dolomite with subordinated barite, norsethite, pyrite and chalcopyrite. The margin zone, at the contact with the host nelsonite or wall rock, is composed of magnetite aggregates, subhedral pyrochlore, radial prismatic apatite, tetra-ferriphlogopite, and ilmenite. Calcibetafite and Fe-columbite occur exclusively as inclusions in ilmenite from DC, associated with pyrochlore. Crystals in the marginal zone are often oriented, elongated toward the center of the pocket or dike, resembling comb-layering. In some pockets the margin zone may be absent, or restricted to a magnetite aggregate (Fig. 3.5A).

Cordeiro (2009 – *Capítulo 2*) argue that the phosphate-iron-oxide magmas from which the Catalão I phoscorites, nelsonites and dolomite carbonatites crystallized derived from a more primitive, carbonate-rich silicate alkaline magma (phlogopite picrite) by liquid immiscibility. Once formed, this magma would have differentiated by crystal fractionation to progressively generate the P1 phoscorites, and the P2 and P3 nelsonites. Mineral and whole-rock chemistry evidence suggests that the DC pockets formed by extraction (segregation) of the interstitial carbonate-liquid from a largely crystallized nelsonite magma through a filter pressing process, and the DC dikes are interpreted as a continuation of this process, with coalescence of pockets and extraction of larger volumes of carbonatite melts. In this context, the globular structures in figure 3.5 indicate that some degree of mobility still existed during the formation of DC pockets. In particular, the nelsonite spheres/droplets in a DC pocket (Fig. 3.5B and 3.6D) show a rhythmic internal structure with a magnetite-rich core followed by a magnetite+apatite+tetra-ferriphlogopite+pyrochlore intermediate zone and a magnetite rim (Fig. 3.5B) which resembles an orbicular texture. Lapin (1982), Lapin and Vartiainen (1983), and Haggerty and Fung (2006) considered similar orbicular textures from carbonatites and kimberlites as a fundamental criterion for the identification of liquid immiscibility processes. Other orbicular rocks have been identified in the APIP alkaline-carbonatite-phoscorites, such as Salitre (Oliveira et al., 2007) and an orbicular magnetitite from Catalão I is described by Palmieri et al. (2008). In view of the textural evidence, the occurrence of further liquid immiscibility in relatively evolved stages of the phoscoritic magma cannot be ruled out. However, liquid immiscibility between phoscorites and carbonatites in Catalão I is not recorded in the overall whole-rock and mineral chemistry signature of these rocks (Cordeiro, 2009 – *Capítulo 2*). The amoeboid mingling textures between two or more carbonatites in Figure 3.5 indicate that different carbonatites also coexisted as liquids or, at least, as crystal mush and liquids in the Catalão I Nb deposit.

PYROCHLORE COMPOSITION

Pyrochlore is the ore-mineral for niobium and can be found mainly in carbonatite complexes, syenites and in late-stage granites. Its general formula is $A_{2-m}B_2X_{6-w}Y_{1-n} \bullet pH_2O$ (from Lumpkin and Ewing, 1995) where the A site is occupied by large anions such as As, Ba, Bi, Ca, Cs, K, Mg, Mn, Na, Pb, REE, Sb, Sr, Th, U and Y. The B site comprises smaller and highly charged cations as Nb, Ta, Ti, Zr, Fe^{3+} , Al and Si (Zurevinski and Mitchell, 2004) and rarely W^{+5} (Caprilli et al., 2006). The Y and X anions can be O, OH and F. Due to the high susceptibility to alteration and consequent exchange of large ions and H_2O , vacancies commonly occur in the A and the Y sites. In this paper we adopt the classification of pyrochlore group minerals proposed by Hogarth (1977).

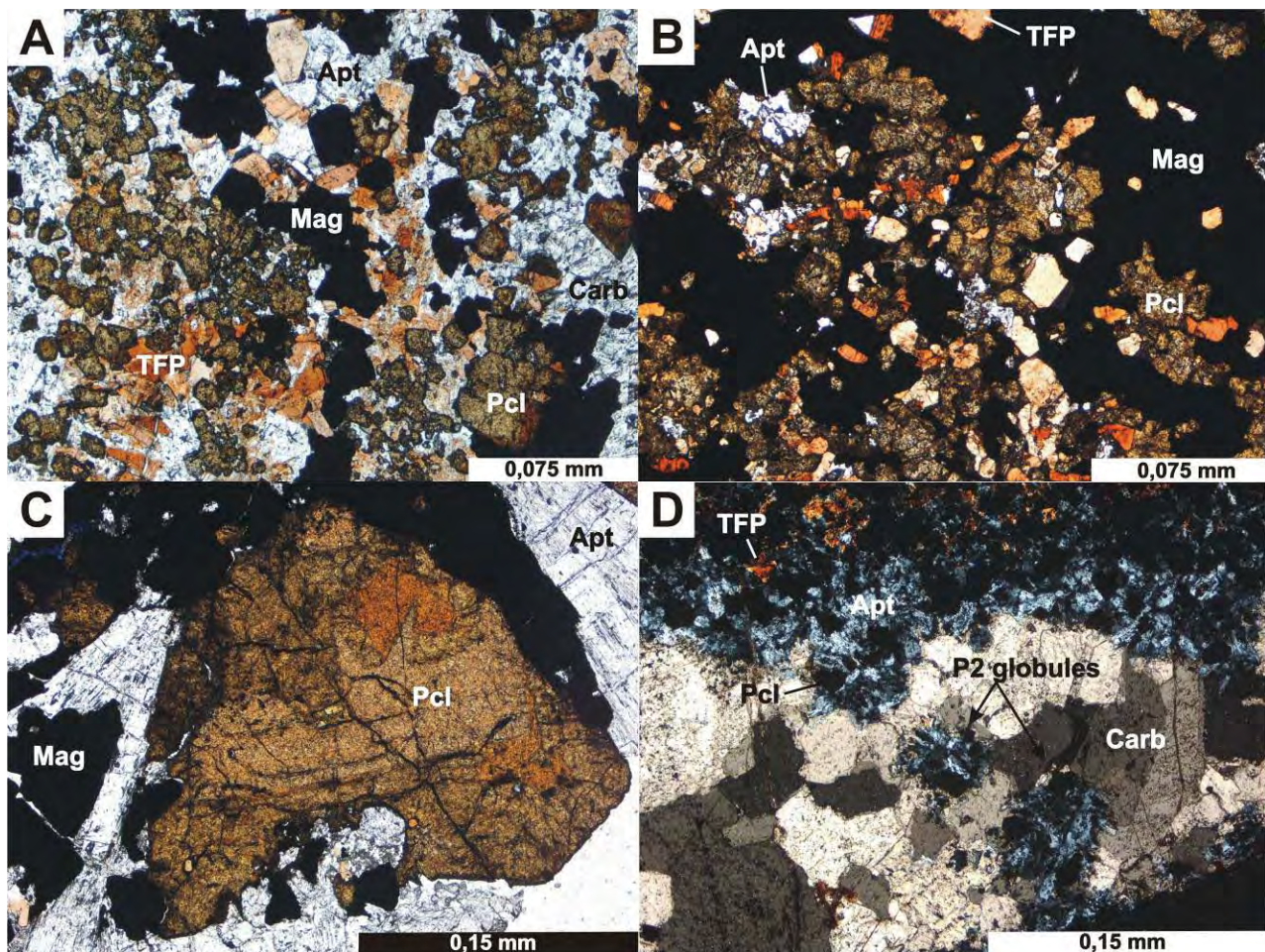


Fig. 3.6. Photomicrographs of pyrochlore-bearing phosphorites. A. P2 nelsonite with subhedral, brown to orange pyrochlore. B. P3 nelsonite with anhedral to subhedral brown to orange pyrochlore. C. Sector zoning in pyrochlore from dolomite carbonatite pocket (DC). D. Mingling-like texture of P2 spheres in DC, crossed polars. (Mag = magnetite; Apt = apatite; TFP = tetra-ferriphlogopite; Carb = carbonate; Pcl = piroclore)

Though pyrochlore crystallizes directly from the carbonatite and phoscorite magmas there is evidence from substitutions in the A-site, that weathering and hydrothermal processes can change its composition widely (Hogarth, 1989; Chackhmouradian and Mitchell, 1998; Geisler et al., 2004).

Pyrochlore grains studied here are from rock samples obtained from drill cores, and considered to be mostly fresh (as opposed to the weathered pyrochlore from the laterite ore, studied by Fava, 2001). We found no optically recognizable evidence of hydrothermal alteration in the analyzed pyrochlore grains but, because we did not carry out a MEV investigation, some degree of hydrothermal alteration cannot be ruled out at this stage. The stable carbon and oxygen isotopic composition of the coexisting carbonates (Cordeiro, 2009 – *Capítulo 4*) suggests that some of the samples used in this study were mildly affected by interaction with H₂O-rich fluids probably of meteoric origin. Therefore, the definition of fresh pyrochlore is used loosely, and may include both primary (magmatic) and slightly hydrothermally/weathered pyrochlore.

Pyrochlores from P2 and P3 nelsonites are texturally similar, occurring as anhedral to subhedral brownish or yellowish crystals (Fig. 3.6A and 3.6B). In some samples pyrochlore color can vary from pale yellow through orange to red. Pyrochlore from DC is often euhedral to subhedral, and optically zoned (Fig. 3.6C).

Pyrochlore representative compositions are shown in table 3.1. The low TiO₂ and Ta₂O₅ content in the fresh pyrochlore-group minerals in the Catalão I niobium deposit allows them be classified as pyrochlore (Nb+Ta>Ti and Nb>Ta; Ca-Na rich) as seen in Figure 3.7.

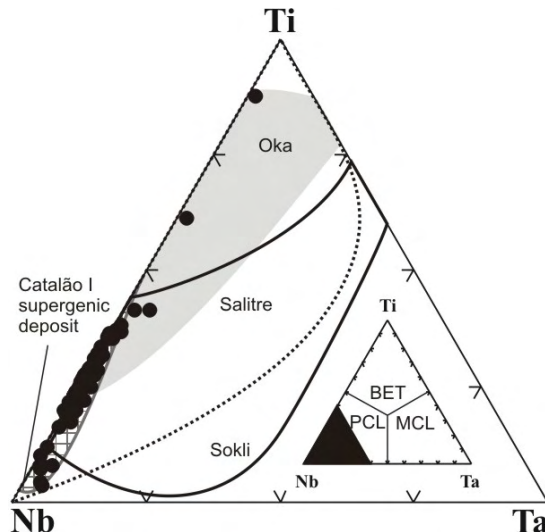


Fig. 3.7. Triangular Nb-Ti-Ta classification scheme (Hogarth, 1977 and 1989) for the studied pyrochlores (black circles). Outlines for pyrochlore compositions from the Catalão I residual deposit (square pattern, Fava, 2001), Oka (gray, Gold, 1986; Zurevinski and Mitchell, 2004), Sokli (solid black outline; Lee et al., 2004; Lee et al., 2006) and Salitre (dotted black outline, Barbosa et al., in preparation). BET = betafite, PCL = piroclore, MCL = microlite.

Tab. 3.1. Pyrochlore, betafite and Fe-columbite composition from the Catalão I nelsonites. Bario = bariopyrochlore, Ca-Na = Ca-Na pyrochlore, H-Ba = High-Ba pyrochlore, Incl = pyrochlore inclusions in ilmenite from DC.

Type	Bario	Bario	Bario	Bario	Bario	Bario	Bario	Bario	Bario	Bario	Bario	Bario	Bario	Bario	Bario	Bario	Bario
Sample	230A-1	304A-1B	339-4	093-3	207-1	304B-2	056-1	170-6	178-2C	192B-2	192B-8	230A-2	339-3C	099A-1C	157B-06	157B-12	056-2
Unit	P2	P2	P2	P3	P3	P3	DC	DC	P2	P2	P2	P2	P2	P3	P3	P3	DC
Nb ₂ O ₅	58.61	52.58	59.55	59.99	53.18	52.26	50.1	63.96	62.66	59.26	55.76	63.76	55.26	45.65	64.26	63.14	59.93
Ta ₂ O ₅	0	0.54	0.36	0.81	0.32	0.8	0.77	0.81	0.15	0	0.07	0.37	0.16	0	0	0.07	0.07
SiO ₂	0.74	0.69	1.89	1.2	3.15	0.61	2.93	1.1	0	0	0.16	0.03	0	0.1	0	0.04	0.12
TiO ₂	5.47	2.9	4.1	3.16	4.45	2.37	5.27	1.26	3.52	4.64	5.59	4.2	3.67	3.16	3.91	4.71	6.15
ZrO ₂	0.32	3.31	0.13	0.06	0.6	3.2	2.44	0.75	0.17	2.05	0.9	0.94	0.26	1.27	1.78	1.65	2.13
UO ₂	0	2.46	0.85	0.77	0.7	3.72	1.01	0.12	0.36	0	0.04	0.82	0.19	0.09	0.14	0.05	1.02
ThO ₂	3.48	4.97	1.2	0.41	2.22	4.94	2.15	0.74	1.08	3.39	2.13	1.72	1.44	1	1.12	1.13	2.04
La ₂ O ₃	0.8	0.49	0.82	1.3	0.56	0.42	0.32	0.92	1.21	0.39	0.75	0.96	0.87	0.38	0.95	0.68	0.62
Ce ₂ O ₃	3.52	3.5	2.74	3.37	2.86	3.04	2.91	3.54	4.2	2.9	2.85	2.68	3.09	1.33	2.47	2	2.37
Y ₂ O ₃	0.31	0.51	0.52	0.26	0.31	0.2	0.4	0.68	0.44	0.57	0.49	0.55	0.34	0.36	0.45	0.46	0.55
FeO	0.98	1.82	0.71	0.69	1.82	1.49	4.47	0.77	0.14	0.5	0.7	0.16	0.31	24.2	0.86	0.46	0.4
MnO	0.26	0.13	0.04	0.11	0.10	0.08	0	0	0	0.05	0.04	0	0	0.011	0	0	
CaO	6.61	2.23	5.31	5.11	1.43	3.34	2.8	0.12	9.02	14.31	14.46	12.05	14.50	9.37	13.11	15.74	16.14
BaO	9.86	14.2	9.66	11.03	17.43	12.24	14.61	15.20	0.35	0	0.24	0	0.13	0.38	0	0	0
SrO	3.26	1.85	2.79	4.64	3.38	3.56	2.23	0.75	2.78	0.69	1.06	2.08	2.41	1.64	2.29	1.59	1.17
Na ₂ O	2.39	0.34	1.41	0.34	0.26	0.38	0.77	1.29	5.59	4.23	3.83	6.46	2.96	4.38	5.94	6.09	4.70
Total	96.62	92.48	92.09	93.25	92.76	92.65	93.18	92.01	91.67	92.97	89.07	96.78	85.59	93.32	97.32	97.81	97.41
Structural formulae calculated based on \sum B-site elements=2																	
Nb	1.682	1.674	1.680	1.753	1.555	1.700	1.464	1.833	1.822	1.713	1.679	1.770	1.790	1.739	1.768	1.733	1.647
Ta	0.000	0.010	0.006	0.014	0.006	0.016	0.014	0.014	0.003	0.000	0.001	0.006	0.003	0.000	0.000	0.001	0.001
Si	0.047	0.048	0.118	0.077	0.204	0.044	0.189	0.070	0.000	0.000	0.011	0.002	0.000	0.008	0.000	0.003	0.007
Ti	0.261	0.154	0.192	0.153	0.217	0.128	0.256	0.060	0.170	0.223	0.280	0.194	0.198	0.200	0.179	0.215	0.281
Zr	0.010	0.114	0.004	0.002	0.019	0.112	0.077	0.023	0.005	0.064	0.029	0.028	0.009	0.052	0.053	0.049	0.063
B-site sum	2.000	2.000	2.000	1.999	2.001	2.000	2.000	2.000	2.000	2.000	2.000	2.000	2.000	1.999	2.000	2.001	1.999
U	0.000	0.039	0.012	0.011	0.010	0.060	0.015	0.002	0.005	0.000	0.001	0.011	0.003	0.002	0.002	0.001	0.014
Th	0.050	0.080	0.017	0.006	0.033	0.081	0.032	0.011	0.016	0.049	0.032	0.024	0.023	0.019	0.016	0.016	0.028
La	0.019	0.013	0.019	0.031	0.013	0.011	0.008	0.022	0.029	0.009	0.018	0.022	0.023	0.012	0.021	0.015	0.014
Ce	0.082	0.090	0.063	0.080	0.068	0.080	0.069	0.082	0.099	0.068	0.070	0.060	0.081	0.041	0.055	0.045	0.053
Y	0.010	0.019	0.017	0.009	0.011	0.008	0.014	0.023	0.015	0.019	0.017	0.018	0.013	0.016	0.014	0.015	0.018
Fe ²⁺	0.052	0.107	0.037	0.037	0.098	0.090	0.241	0.041	0.007	0.027	0.039	0.008	0.019	1.706	0.044	0.023	0.020
Mn	0.014	0.008	0.002	0.006	0.006	0.005	0.000	0.000	0.000	0.003	0.002	0.000	0.000	0.001	0.000	0.000	0.000
Ca	0.450	0.168	0.355	0.354	0.099	0.257	0.194	0.008	0.621	0.980	1.032	0.793	1.113	0.847	0.855	1.024	1.051
Ba	0.246	0.391	0.236	0.280	0.442	0.345	0.370	0.378	0.009	0.000	0.006	0.000	0.004	0.013	0.000	0.000	0.000
Sr	0.120	0.076	0.101	0.174	0.127	0.149	0.084	0.028	0.104	0.025	0.041	0.074	0.100	0.080	0.081	0.056	0.041
Na	0.295	0.047	0.171	0.043	0.032	0.054	0.097	0.158	0.697	0.524	0.495	0.769	0.411	0.717	0.701	0.717	0.555
A-site sum	1.337	1.037	1.031	1.030	0.938	1.139	1.122	0.752	1.602	1.705	1.754	1.780	1.790	3.452	1.790	1.911	1.794

Table 3.1 (continued)

Type	H-Ba P2	H-Ba P2	H-Ba P2	H-Ba P2	H-Ba P3	H-Ba P3	H-Ba P3	H-Ba P3	H-Ba P3	Incl DC	Incl DC	Incl DC	Betafite DC	Fe-Columbite DC	Fe-Columbite DC		
Sample Unit	156-2 P2	178-1 P2	304A-5 P2	304A-7 P2	093-2 P3	183-3 P3	183-5 P3	207-2B P3	304B-1 P3	304B-3 DC	116-1 DC	149-1 DC	170-4 DC	170-7 DC	170-2 DC	170-8 DC	149-2 DC
Nb ₂ O ₅	62.97	61.68	62.67	59.6	65.55	55.58	62.17	62.84	56.93	57.03	66.99	68.71	72.56	70.29	52.85	74.84	84.68
Ta ₂ O ₅	0.36	0.33	0.19	0.1	0.74	0.7	0.57	0.43	0.49	0.26	0.05	0.28	1.61	1.85	0.92	0.94	0.34
SiO ₂	0.39	0.61	0.31	0.33	0.11	0.57	0.02	0.55	0.75	0.43	0	0.05	0	0	0	b.d.	0.03
TiO ₂	3.71	3.15	4.19	1.5	3.39	4.16	4.87	4.55	2.93	2.38	4.12	2.04	0.78	0.63	17.35	5.1	1.37
ZrO ₂	0.46	0.13	0.86	1.77	0.18	3.95	0.32	0.39	3.21	3.26	0.28	0.53	0.02	0	0.09	1.41	0.48
UO ₂	0.89	0.59	0.31	1	1.02	2.35	1.17	0.75	2.06	2.25	0.02	0.02	0.02	0	0	b.d.	b.d.
ThO ₂	2.14	1.09	1.46	2.11	0.53	2.69	4.66	2.21	5.35	6.23	0.53	0.22	0.19	0.03	0.06	b.d.	b.d.
La ₂ O ₃	0.5	1.14	0.83	0.87	1.3	0.62	1.13	0.86	0.53	0.51	0.79	1.63	0.37	0.11	0.35	b.d.	0.05
Ce ₂ O ₃	1.94	3.42	2.24	3.37	3.39	2.92	4.09	3.04	2.78	2.73	2.21	3.26	0.73	0.42	0.24	0.11	0.07
Y ₂ O ₃	0.6	0.32	0.45	0.57	0.4	0.26	0.48	0.46	0.44	0.55	0.47	0.57	0.39	0.41	0.2	0.75	0.94
FeO	3.13	0.94	0.55	1.14	0.16	1.93	0.4	0.81	2.02	2.18	0.13	0.18	0.18	0.64	4.22	10.10	8.9
MnO	0.07	0.07	0.04	0.02	0.02	0.36	0.04	0.053	0.14	0.09	0.00	2.00	0.06	0.08	0.90	1.10	1.53
CaO	7.67	7.46	10.75	9.89	9.88	8.53	8.51	10.05	8.91	7.81	14.00	9.87	11.32	11.75	10.98	1.09	0.01
BaO	1.6	4.89	4.38	2.36	1.60	3.67	2.81	4.1	2.71	4.61	0.00	0.00	0.18	0.10	0.00	b.d.	0.05
SrO	1.12	3.95	1.96	1.60	3.08	3.48	2.03	2.17	2.03	1.66	2.79	2.50	4.61	4.26	3.008	0.58	b.d.
Na ₂ O	2.01	4.09	2.73	3.17	3.38	2.52	1.16	2.74	2.21	1.60	6.75	7.31	7.83	6.84	7.75	0.75	b.d.
Total	89.56	93.87	93.92	89.39	94.74	94.28	94.43	96	93.48	93.59	99.14	97.17	100.84	97.41	98.91	96.77	98.44
Structural formulae calculated based on \sum B-site elements=2																	
Nb	1.781	1.798	1.756	1.839	1.819	1.624	1.752	1.738	1.694	1.738	1.806	1.884	1.939	1.940	1.284		
Ta	0.006	0.006	0.003	0.002	0.012	0.012	0.010	0.007	0.009	0.005	0.001	0.005	0.026	0.031	0.013		
Si	0.024	0.039	0.019	0.023	0.007	0.037	0.001	0.033	0.049	0.029	0.000	0.003	0.000	0.000	0.000		
Ti	0.174	0.153	0.195	0.077	0.156	0.202	0.228	0.210	0.145	0.121	0.185	0.093	0.035	0.029	0.701		
Zr	0.014	0.004	0.026	0.059	0.006	0.125	0.010	0.012	0.103	0.107	0.008	0.016	0.001	0.000	0.002		
B-site sum	1.999	2.000	1.999	2.000	2.000	2.000	2.001	2.000	2.000	2.000	2.000	2.001	2.001	2.000	2.000		
U	0.012	0.009	0.004	0.015	0.014	0.034	0.016	0.010	0.030	0.034	0.000	0.000	0.000	0.000	0.000		
Th	0.031	0.016	0.021	0.033	0.007	0.040	0.066	0.031	0.080	0.096	0.007	0.003	0.003	0.000	0.001		
La	0.012	0.027	0.019	0.022	0.029	0.015	0.026	0.020	0.013	0.013	0.017	0.037	0.008	0.003	0.007		
Ce	0.044	0.081	0.051	0.084	0.076	0.069	0.093	0.068	0.067	0.067	0.048	0.072	0.016	0.009	0.005		
Y	0.020	0.011	0.015	0.021	0.013	0.009	0.016	0.015	0.016	0.020	0.015	0.018	0.012	0.013	0.006		
Fe2	0.164	0.051	0.028	0.065	0.008	0.104	0.021	0.042	0.111	0.123	0.006	0.009	0.009	0.033	0.189		
Mn	0.004	0.004	0.002	0.001	0.001	0.020	0.002	0.003	0.008	0.005	0.000	0.000	0.003	0.004	0.041		
Ca	0.514	0.516	0.714	0.723	0.650	0.591	0.568	0.659	0.628	0.564	0.895	0.641	0.717	0.769	0.632		
Ba	0.039	0.124	0.106	0.063	0.039	0.093	0.069	0.098	0.070	0.122	0.000	0.000	0.004	0.002	0.000		
Sr	0.041	0.148	0.070	0.064	0.110	0.131	0.073	0.077	0.078	0.065	0.097	0.088	0.158	0.151	0.094		
Na	0.244	0.511	0.329	0.419	0.403	0.316	0.140	0.325	0.282	0.210	0.781	0.860	0.897	0.810	0.807		
A-site sum	1.124	1.496	1.360	1.510	1.350	1.420	1.092	1.347	1.382	1.318	1.866	1.728	1.826	1.794	1.781		

Nb_2O_5 content varies from 50 to 70 wt. percent. The average TiO_2 content ranges from 3 to 5 wt. percent, but may reach up to 17 wt. percent in some calciobetafite inclusions in ilmenite from DC. Most analysis show an unusually low Ta_2O_5 , less than 1 wt. percent, up to a maximum of 2 wt. percent in a grain from P2 and pyrochlore inclusions in DC. ZrO_2 and SiO_2 reach up to 5 percent and 3 wt. percent respectively.

The A-site shows a wider variance, probably because the elements related to this site are much more mobile than those of the B-site. Several analyses indicate the occurrence of bariopyrochlore ($\text{Ba} > 20\%$ of A-atoms) along with pyrochlore in the fresh rock. Rare occurrences of strontiumpyrochlore ($\text{Sr} > 20\%$ of A-atoms) and calciobetafite ($2\text{Ti} > \text{Nb} + \text{Ta}$) were found within pyrochlore grains.

Strontiumpyrochlore is restrict to patches in pyrochlore from P3, in a zoning pattern similar to that found by Hogarth et al. (2000) in pyrochlores from the Fen complex. Lumpkin and Ewing (1995) show that the occurrence of altered, Sr-enriched pyrochlore from the Alno complex is controlled by fractures, but we identified Sr-enrichment in pyrochlore from Catalão I fresh rocks, apparently unrelated to any visible fractures. Calciobetafite, along with Fe-columbite and pyrochlore, occurs as individual crystals included in ilmenite from DC.

Ca and Na are the main A site elements, ranging up to 19 and 8 wt. percent oxide, respectively. Ba is one of the most common substitutes for both Na and Ca in this site and can reach 18 wt. percent BaO in the analyzed pyrochlores whereas SrO may reach 7 wt. percent. The sum of the rare earth ($\text{La} + \text{Ce}$) oxides varies from 3 to 6 wt. percent. ThO_2 is up to 6 wt. percent but its average content is less than 2 wt. percent. UO_2 is up to 4 wt. percent averaging less than 1 wt. percent. FeO may reach 3 wt. percent, and MnO is always lower than 1 wt. percent.

CHEMICAL EVOLUTION OF PYROCHLORE

The compositions of pyrochlore from the apatite-rich P2 and magnetite-rich P3 nelsonites overlap widely. We could not find an applicable chemical criterion to discriminate pyrochlores from the two units, which suggests that variation in pyrochlore chemistry with magma evolution in the Catalão I phoscorite series may be less pronounced than that observed for phlogopite and apatite (Cordeiro, 2009 – *Capítulo 2*). Zoning (Hogarth et al., 2000) in individual crystals is probably responsible for the data spread.

Lumpkin and Ewing (1995) argued that large cations such as K, Ba and Sr can be useful chemical indicators of pyrochlore alteration since their occurrence is related to the degree of alteration in the rock. Therefore, we adopted a division based on the Ba concentration and key chemical features to discriminate pyrochlore groups.

Bariopyrochlore (white dots in figure 3.8) is the group with the highest A-site vacancy. From the high-Ba pyrochlore (> 0.02 apfu, light gray dots) to the Ca-Na pyrochlore (< 0.02 apfu, dark gray dots) A-site vacancy is less pronounced though still present. If expressed in terms of oxides, 0.02 apfu of Ba correspond to approximately 1 wt. percent BaO. Pyrochlore and calciobetafite inclusions in ilmenite from DC are grouped (black dots) because of their association with Fe-columbite and their occurrence exclusively as inclusions. Free pyrochlore from DC is accounted in the other groups. Fields for the Lueshe (Nasraoui and Bilal, 2000) and Oka (Gold et al., 1986; Zurevinski and Mitchell, 2004) pyrochlore deposits, Bingo Carbonatite (Williams *et al.*, 1997), Catalão I residual deposit (Fava, 2001) and occurrences related to phoscorites such as Sokli (Lee *et al.*, 2004; Lee *et al.*, 2006) and Salitre (Barbosa *et al.*, in preparation) are depicted for comparison in figure 3.8.

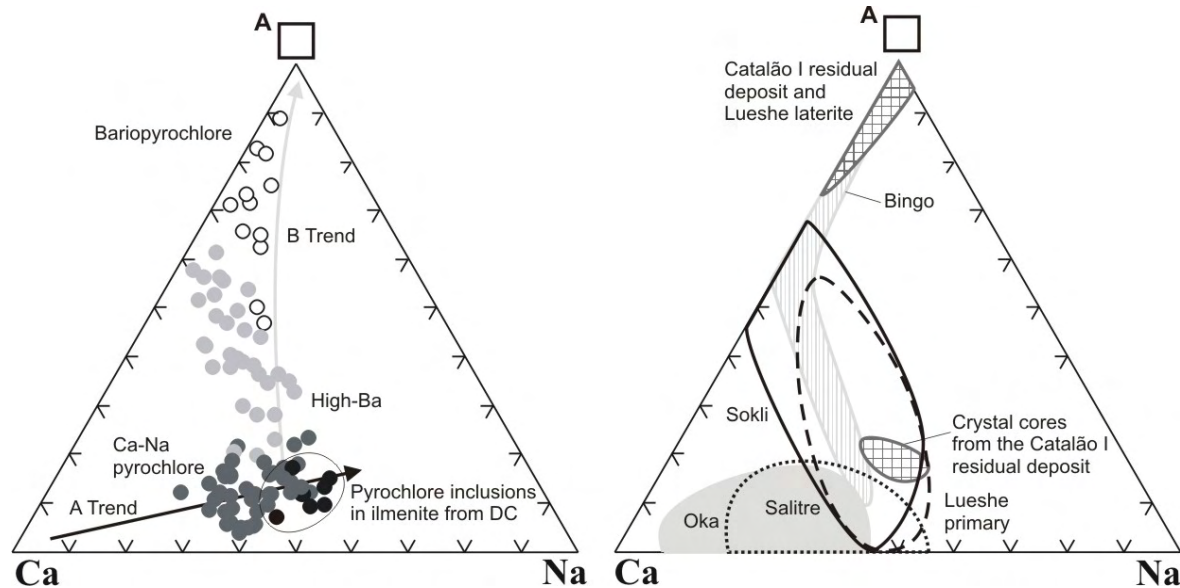


Fig. 3.8. Triangular plots of Ca, Na and A-site vacancy. Compositional fields of pyrochlore of other deposits are shown for comparison. White dots = bariopyrochlore; Light gray dots = High-Ba pyrochlore; Dark gray dots = Low-Ba pyrochlore; Black dots = pyrochlore inclusions in ilmenite from DC. Data sources as in Figure 3.7, plus Bingo field from Williams *et al.* (1997).

Two main trends related to different substitution schemes can be found in the studied pyrochlore. These trends reflect the chemical variance of pyrochlore and may be related to its chemical evolution along the differentiation of the phoscorite series and during post magmatic alteration, respectively.

The “A” trend (Fig. 3.8) can be described as an exchange of Ca for Na in the A-site. The Na-rich end-member would be represented by the pyrochlore inclusions in ilmenite from DC (red dots). The Ca-rich end-member may be represented by pyrochlore from Oka and Salitre and extend this trend even further.

The “B” trend (Fig. 3.8) is related to the exchange of Ba for Ca+Na in the A-site and Si for Nb in the B-site, and is defined by high-Ba pyrochlore and bariopyrochlore. Similar trends can be found in

pyrochlore from Lueshe (Nasraoui and Bilal, 2000) and Bingo (Williams et al., 1997) described as alteration products related to lateritization. Pyrochlores from the residual deposit of Catalão I (Fava, 2001) have higher Ba and are Ca-Na free, when compared with the respective primary compositions. This chemical shifting is attributed to weathering and results in up to 1.7 a.p.f.u. vacancy in the A-site in pyrochlore.

SUBSTITUTIONS IN THE A-SITE

“A” Trend

The A site shows two types of substitutions, each related to a different trend. “A” Trend substitution is more expressive in Ca-Na pyrochlore (dark gray dots) and pyrochlore inclusions in ilmenite from DC (black dots). This trend is depicted in Figure 3.9 for the different types of Catalão I fresh pyrochlores and is represented by Ca-rich and Na-rich pyrochlore end-members.

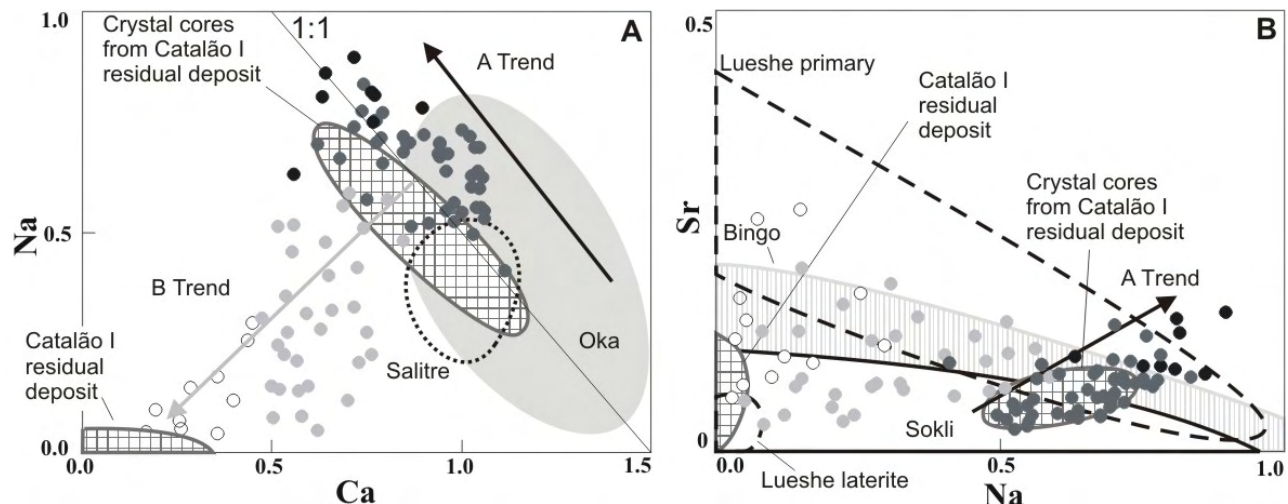


Fig. 3.9. A. Substitution scheme in fresh pyrochlore of the Catalão I phoscorite, according to the “A” Trend. This trend represents the crystallization of early Ca-rich pyrochlore and its shift toward Na-rich composition with magma evolution. The fields for Salitre and Oka represent Ca-rich pyrochlore crystallized from more primitive liquids than Catalão I. B. Sr enrichment in the “A” Trend toward Na-rich pyrochlore, and in the “B” Trend toward Na-poor pyrochlore. Note that pyrochlore from the Catalão I residual deposit is Na-Sr-poor. Symbols and data sources as in Figure 3.8.

Despite the considerable scatter, the Ca-Na pyrochlore, the pyrochlore inclusions in DC ilmenites, and the fields for primary pyrochlore from Oka and Salitre show an overall alignment to the 1:1 line. This trend is even more marked in the crystal cores from the Catalão I weathered pyrochlore deposit (Fava, 2001), which may represent preserved relicts of the primary pyrochlore.

Pyrochlore from the Sokli phoscoritic rocks (Lee et al., 2006) also shows an evolution path toward Na-rich pyrochlore from early paired carbonatite-phoscorite C2-P2 to late-stage dolomite carbonatite D5 (see discussion further in the text).

Pyrochlore inclusions in ilmenite from DC (black dots), are believed to represent the Na-rich end-member of the “A” Trend. Cordeiro (2009 – *Capítulo 4*) show that the dolomite carbonatites (DC) were originated from one of the most evolved magmas in the complex, and ilmenite is one of the last minerals to crystallize in this liquid. Therefore, the composition of these pyrochlore inclusions is directly related to chemical characteristics of the most evolved phoscoritic magma. Fe-columbite was found exclusively as inclusions in DC ilmenite, along with pyrochlore. Its occurrence suggests that extremely evolved magmas in this system tend to shift towards the crystallisation of other Nb-oxides instead of pyrochlore. This is consistent with and end-member character for Na-rich pyrochlore.

The end-member at the other extreme of 1:1 substitution line in Figure 3.9 is the Ca-rich pyrochlore, also enriched in Ta and U. Oka and Salitre pyrochlore compositions plot in the same trend, but nearer to the Ca-rich extreme than Catalão I (see Figure 3.11).

During the early stages of carbonatitic magmatism in a magmatic chamber, Nb and Ta are probably transported as phosphate and fluorine complexes, which might explain the common correlation between the occurrence of apatite and pyrochlore (Knudsen, 1989; Hogarth *et al.*, 2000). Knudsen (1989) argued that during the carbonatitic magmatism Nb is more soluble than Ta, which could explain the occurrence of Ta-rich pyrochlore in primitive magmas and Nb-rich, Ta-poor pyrochlore in later stages. U, Th, and REE would also be preferably incorporated into early-crystallizing pyrochlore, which would tend to Ca-Na rich pyrochlore with evolution. Cordeiro (2009, *Capítulo 2*) described the P2 and P3 nelsonites from Catalão I as petrogenetically more evolved than phoscorites from Oka, Salitre, and the early paired phoscorite-carbonatite P2-C2 and P3-C3 from Sokli, which is consistent with the pyrochlore chemical characteristics reported here.

“B” Trend

The “B” Trend is defined by the substitution of Ca+Na+Nb for Ba+Si, which is accompanied of a vacancy in the A site. High-Ba pyrochlore (light gray dots, figures 3.8 and 3.9) and bariopyrochlore are also enriched in U+Ta compared to Ca-Na pyrochlore. This substitution produces a 1:2 negative correlation of the calculated formula expressed as a.p.f.u. (Fig. 3.10A) and evolves to the composition of bariopyrochlore, which is the typical variety present in the Catalão I residual deposit (Fava, 2001). The chemical tendency for A-site vacancy, sometimes accompanied of Ba-enrichment, was attributed to alteration at Sokli (Lee et al., 2006), to hydrothermal overprint at Oka (Zurevinski

and Mitchell, 2004) and Lueshe (Nasraoui and Bilau, 2000), to both oscillatory zoning and alteration in the Bingo carbonatite (Williams et al., 1997) and to lateritization by Lumpkin and Ewing (1995).

The trend formed by the pyrochlores from Sokli is parallel to that defined by the high-Ba pyrochlore of Catalão I (Fig. 3.9b). Lee et al. (2006) described U and Ta rich pyrochlore from Sokli as typical of early phoscorites, and pointed out that depletion in these elements is a feature connected with phoscorite magma evolution. While the C1-P1 unit of Sokli is pyrochlore-free (as occurs in the P1 unit in Catalão I), the pyrochlore composition becomes systematically richer in Ca-Na-Nb from the U-Ta-rich C2-P2 unit toward the D5 unit. In terms of mineral assemblage and composition, the Sokli D5 unit is very similar to the DC of Catalão I and they might represent the same evolution stage of the phoscorite-series.

Lee et al. (2006) describe abundant internal fractures and patch alteration in pyrochlore from the Sokli P2 and P3 phoscorites where the altered patches are Ba-rich. This enrichment is consistent with the “B” Trend of Catalão I toward pyrochlores from the residual deposit. The correspondence between the two complexes helps to establish a broader model for the evolution of pyrochlore in phoscorites and carbonatites where the evolution occurs toward the Na rich end-member despite the degree of alteration.

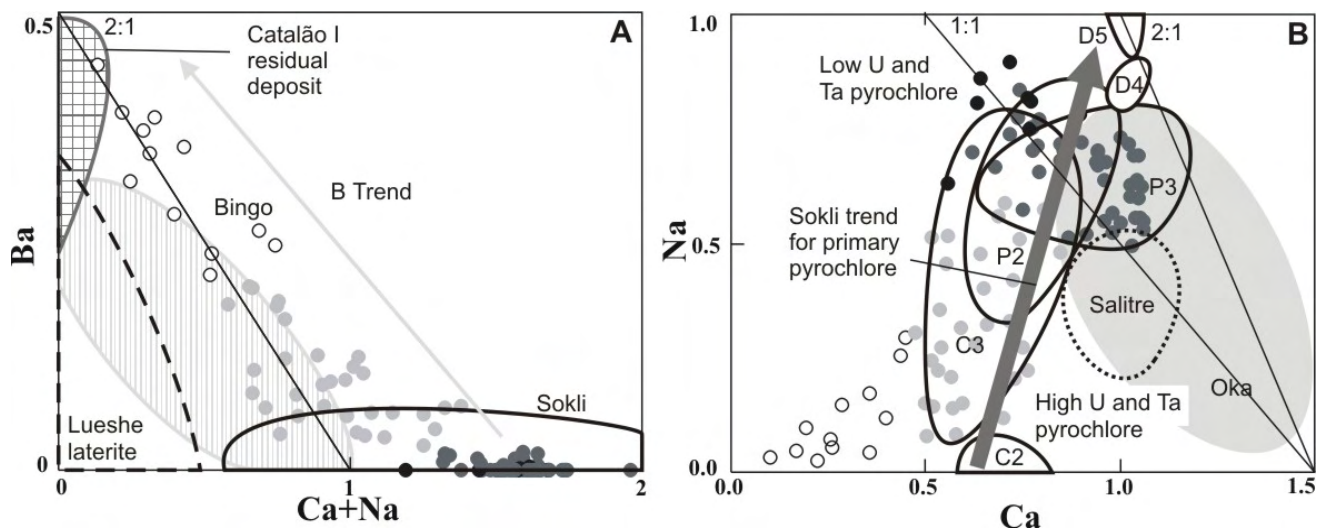


Fig. 3.10. A. Chemical variation of pyrochlore from the Catalão I phoscoritic rocks in terms of Ba, Ca and Na. The “B” Trend is defined by the high-Ba pyrochlore and bariopyrochlore toward the field of Catalão I residual deposit. While pyrochlore from Oka and Salitre are virtually Ba-free, pyrochlore from Sokli phoscorites is comparatively Ba-richer but bears no relation to the substitution scheme. B. Pyrochlore from Sokli phoscorites (Lee et al. 2004, 2006). C2-P2, C3-P3 are paired phoscorite-carbonatite, while D4 and D5 are dolomite carbonatite. The phoscorites show a trend going from C2-P2 primitive, high-U and -Ta pyrochlore toward more evolved Ca-Na pyrochlore (low-U and -Ta) in C3-P3, D4 and D5. Note that this trend is very similar to that of high-Ba pyrochlore from Catalão I. Outlines of pyrochlore compositions of other complexes as in Figures 3.7 and 3.8.

POSITIVE CORRELATIONS IN THE B-SITE

The samples defining the “B” Trend in Figure 3.11 also have unusual Si, Ba, Ta and U enrichment compared to Ca-Na pyrochlore and pyrochlore inclusions in ilmenites from DC. This feature allows unequivocal discrimination between pyrochlores of the “A” Trend and those of the “B” Trend, suggesting that they evolve along different paths.

The positive correlation between Ba and Si and between U and Ta (Fig. 3.11) is due to undefined coupled substitutions. The role of Si in pyrochlore from carbonatites was described by Williams et al. (1997) in high-Si-Ba pyrochlore from the Bingo carbonatite and interpreted as due to partial alteration. On the other hand, pyrochlore with oscillatory zoning from the same carbonatite also resulted in positive correlation between Ba and Si. This indicates that the coupled substitution is not restricted to alteration and may occur at some level along the magmatic evolution.

Lumpkin and Ewing (1995) showed that U and Ta are immobilized by pyrochlore during both hydrothermal and weathering alteration, as also seen in altered pyrochlores from Sokli (Lee et al., 2006). In Catalão I, bariopyrochlore and the high-Ba pyrochlore are also enriched in Ta and U, compared to Ca-Na pyrochlore which suggests that the composition of these pyrochlores is controlled by more complex parameters than simple lateritization, such as pre-existing oscillatory U+Ta zoning, as described by Hogarth et al. (2000) in pyrochlores from Fen, Norway.

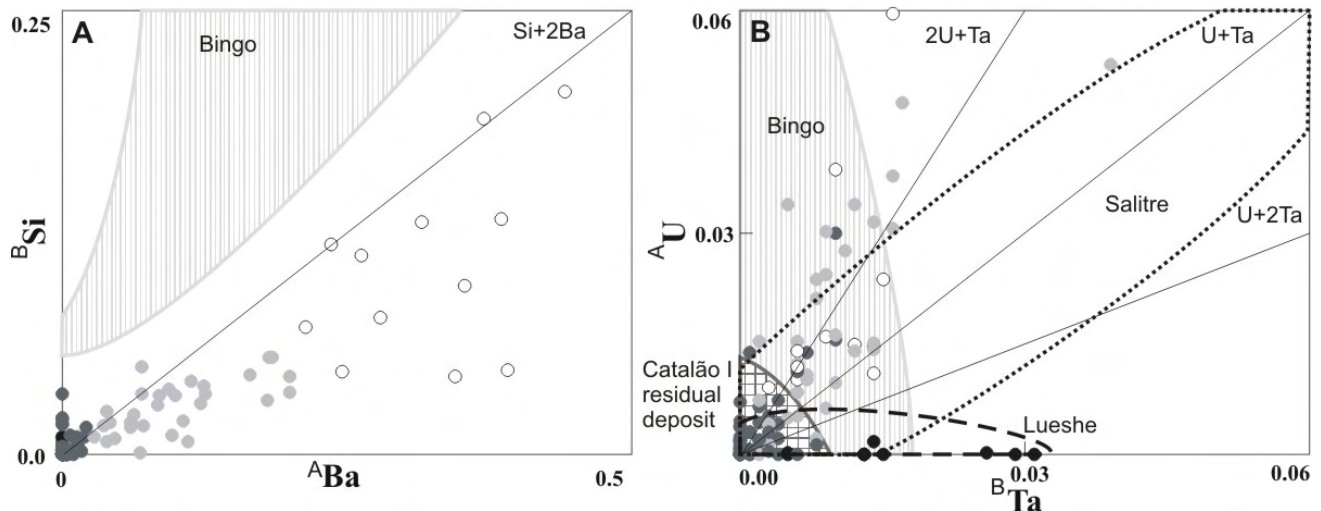


Fig. 3.11. Correlations involving the B-site elements. A. Si and Ba 2:1 positive correlation is related to high-Ba pyrochlore and bariopyrochlore. The Bingo composition is more enriched in Si respectively to Ba than Catalão I. B. U and Ta show a 2:1 positive correlation in primary pyrochlore probably according a coupled substitution. Salitre, Oka and Sokli pyrochlores also show a positive correlation, though the compositional fields of Oka and Sokli are wider and cannot be represented in the adopted scale. Symbols and compositional fields as in Figure 3.8.

Hogarth et al. (2000) showed that U- and Ta- rich layers can occur in pyrochlore during quiescent conditions of crystallization because of supersaturation of these elements in the magma. The positive correlation 2:1 between U and Ta in Catalão I occurs at different ratios in pyrochlore from Salitre, Oka, and Sokli. The latter two have a wider U and Ta composition and their field occupies the whole range shown in Figure 3.11. Lueshe pyrochlore (Nasraoui and Bilal, 2000) is almost U-free, while pyrochlore from the Bingo carbonatite is Ta-poor (Williams et al., 1997). Fava (2001) did not report Si in his analyses, but his data shows that U and Ta are mostly absent in bariopyrochlore from the Catalão I weathered ore, occurring exclusively in preserved cores of primary crystals.

Hogarth et al. (2000) concluded that the normal path of evolution of pyrochlore in carbonatites is one of progressive enrichment in Na, Ca and Nb and depletion in Ta, Th, REE, Ti and U, though narrow growth layers rich in Ta+U occur related to oscillatory zoning.

COMPARISON WITH THE CATALÃO I RESIDUAL DEPOSIT

Fava (2001) describes the mineralogical characteristics of pyrochlore from the residual deposit developed on the Catalão I nelsonites and carbonatites, and conclude that the weathering affected mainly the elements in the A site originating bariopyrochlore. It can also be observed from his data that several crystal cores retain the original Ca-Na composition, whereas the rims were converted into bariopyrochlore. In Catalão I, High-Ba pyrochlore and bariopyrochlore occur both in the weathered ore and in the fresh mineralized rocks.

Ca and Sr (Fig. 3.12A) show a negative correlation in pyrochlore from fresh rock and from crystal cores of the residual deposit, and a diffuse, possible positive, correlation between bariopyrochlore from fresh rock and the residual deposit. Lumpkin and Ewing (1995) argued in favor of major exchanges involving Sr in pyrochlore as a feature of lateritization in carbonatites. Therefore, this shifting toward the Sr-poor bariopyrochlore from the residual deposit might indicate that in Catalão I, the weathering-related Sr-enrichment occurs only in the incipient weathering stages.

With the continuation of the alteration, bariopyrochlore loses completely its correlation with Na and Ca (green dotted field in Fig. 3.10) and is Sr-depleted. With the weathering evolution, even Ba is leached from the structure leaving vacancy up to 1.7 a.p.f.u., which may lead to the total destruction of the mineral structure.

Compared to the pyrochlore from the Catalão I residual deposit (Fava, 2001), pyrochlore from the Bingo Carbonatite (Williams et al., 1997) has a similar evolution in terms of Ca, Sr and Ba, while pyrochlore from the Lueshe laterite (Nasraoui and Bilal, 2000) is Sr-richer. In Bingo, there is a

positive correlation between Ba and Si which is seen both in the unaltered pyrochlore with oscillatory zoning and in the bariopyrochlore of laterite.

Catalão I bariopyrochlore and high-Ba pyrochlore have vacancies > 0.3 a.p.f.u. and show a positive correlation of Si and Ba, which suggests a coupled substitution (Fig. 3.11). On the other hand, the occurrence of different positive correlations of Si and U between bariopyrochlore and high-Ba pyrochlore (Fig. 3.12B) from the fresh rock, suggests that their evolution might be related to a complex alteration process.

The comparison of pyrochlore from fresh rock (this paper) to that of the weathering mantle (Fava, 2001), shows that their compositions in terms of the B-site cations are very similar. The A-site is deeply affected by the weathering process, which leached out Ca and Na, and replaced F by OH. Along with these changes, the B-site becomes gradually more vacant and incorporates Ba and Si. The final A-site vacancy can reach up to 1.7 percent. Other A-elements are apparently not affected by weathering.

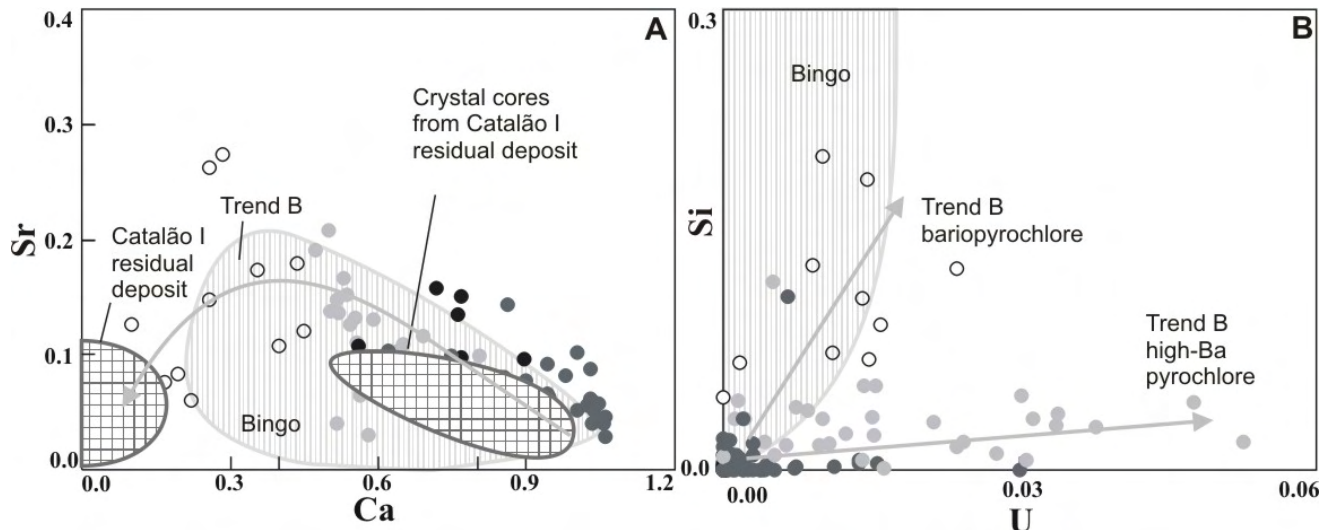


Fig. 3.12. A. Binary plot of Sr and Ca showing the positive correlation in pyrochlore from fresh rock and crystal cores from the Catalão I residual deposit (Fava, 2001). A negative correlation occurs in the bariopyrochlore of fresh rock and the residual deposit. B. Plot of Si and U, showing two groups of samples from the “B” trend, bariopyrochlore with high-Si and the high-Ba pyrochlore with high-U.

There is a correlation between the low-T alteration in carbonate crystals in nelsonites from Catalão I (Cordeiro, 2009 – *Capítulo 4*) and the occurrence of bariopyrochlore rims. Gray, fresh carbonate crystals from the nelsonite sample 093G1 and from the carbonatite sample 056 have mantle-like carbon- and oxygen-isotope signature and were interpreted as of igneous-origin. Brittle, white carbonates collected from the same samples revealed to be enriched in $\delta^{18}\text{O}_{\text{SMOW}}$ compared to the primary isotopic composition (Fig. 3.13). Cordeiro (2009 – *Capítulo 4*) regard these differences

within the same sample as product of interaction with low temperature H₂O rich fluids, probably of meteoric origin. The same alteration could induce the leaching of Ca and Na from the pyrochlore structure, originating vacancies and replacement by Ba in the A site. The pyrochlore rims from the samples 093 and 056 are more altered compared to the respective cores (Fig. 3.13) which is consistent with a patch alteration in the rims and along fractures in the pyrochlore. Pyrochlores in rocks with less interaction with meteoric waters, such as the nelsonites 192B and 178 were more preserved from alteration and show smaller Ba differences between core and rim, though some degree of alteration is still seen in sample 178.

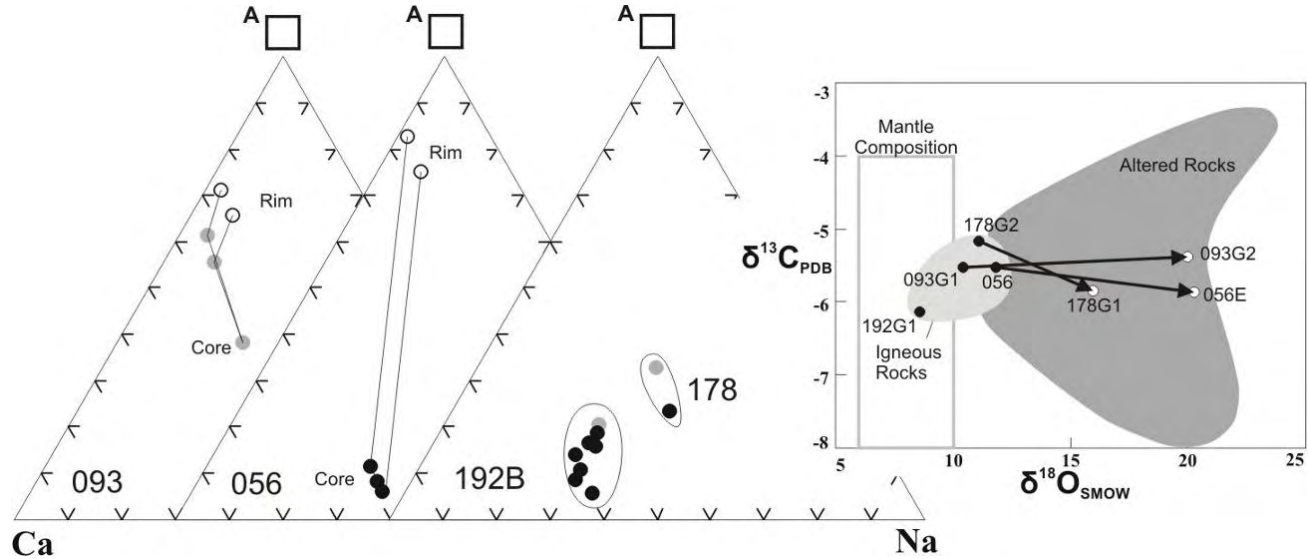


Fig. 3.13. Relationship between zoning and weathering. Note that the pyrochlore rims from samples 093 and 056 have systematically higher A-site vacancies than the corresponding cores. In the case of sample 056, the mineralogy changes from pyrochlore to bariopyrochlore without an intermediate composition. Samples 192B and 178 have restricted compositional fields. The C-O stable isotopes (Cordeiro, 2009 – *Capítulo 4*) show that samples with bariopyrochlore rims have wider variations in the $\delta^{18}\text{O}_{\text{SMOW}}$ content while samples with a more restricted alteration preserve the original composition.

THE NIOBIUM MINERALIZATION

According to Tither (2001), Araxá, Catalão I from the APIP in Brazil and St. Honoré in Canada, are the main niobium producers in the world (Tab. 3.2).

Tab. 3.2. Geological information of the main niobium mines (adapted from Tither, 2001)

Deposit	Araxá		Catalão I and II	St Honoré
Country	Brazil		Brazil	Canadá
Geology	Carbonatite/Nelsonite		Carbonatite/Nelsonite	Carbonatite
Company	CBMM		Anglo American	Niobec
Ore type	Residual	Fresh Rock	Residual	Fresh rock
% Nb ₂ O ₅	3	1.57	1.34	0.67
Reserve (Mt)	456	936	18	22
Mining	Open Pit		Open Pit	Underground

The major factor that contributes for the economicity of the niobium deposits in the APIP is the residual enrichment due to the weathering, which induced a concentration of pyrochlore over previously Nb₂O₅-rich rocks. Accordingly to Mariano (1989), the niobium concentration of Catalão I is related to intermediate pulses of carbonatite activity, but Cordeiro (2009 – *Capítulo 2*) showed that the original niobium concentration is related to stockworks of the P2 and P3 nelsonites and associated dolomite carbonatites, the last evolution stages of the phoscoritic-series in Catalão I.

Cordeiro (2009 – *Capítulo 2*) detailed the petrogenesis of the phoscoritic rocks related to the niobium-rich rocks in Catalão I and concluded that the primary niobium concentration depends on the occurrence of nelsonites and related dolomite carbonatites. The REE patterns from the phoscoritic rocks were normalized to the mean composition of the phlogopite picrite from the APIP, which is believed to represent the primitive magma composition of the APIP carbonatite complexes (Brod et al., 2000). The phoscoritic rocks from Catalão I have a M-type tetrad pattern whereas the mirrored W-type tetrad pattern occurs in ultramafic silicate rocks (bebedourites) from Catalão I (Araújo, 1996) and from the Araxá Complex (Traversa et al., 2001). Since very similar Nb-mineralized phoscoritic rocks are describe in Araxá (Silva, 1984), the mirrored tetrad patterns in these rocks indicate a common origin for the bebedouritic-series and the phoscoritic series, as immiscible liquids from a primitive magma similar to the composition of the average phlogopite picrite.

Nb₂O₅ in fresh nelsonite from Catalão I can reach up to 3 wt. percent and the pyrochlore content is up to 13 modal percent (Cordeiro, 2009 – *Capítulo 4*), though even higher Nb concentrations may occur depending on the formation of pyrochlore-rich cumulates. Weathering of the Catalão I rocks originated the residual deposit directly over the stockworks of phoscorite and nelsonite.

All rocks within the Catalão I complex are easily weathered compared with the country-rocks (fenites and quartzites). Furthermore, the deformation of the country rocks by the intrusion results in dome structures with inward drainage patterns that prevent erosion and eventually allow the establishment of a very thick (up to 80 m) soil cover on the alkaline rocks. Weathering-resistant phases such as pyrochlore, apatite, ilmenite, iron-oxide phases and barite remain as constituents of the soil along with clays and secondary phosphates. The final result of this process is a strong enrichment in Nb_2O_5 , P_2O_5 , FeO , TiO_2 and BaSO_4 in the soil.

Although the alteration is not able to destroy completely the structure of the weathering-resistant minerals, composition changes can occur. Mobile elements such as K, Na, Mg, and F are removed from the mineral structure, leaving vacancies or being exchanged by elements with intermediate mobility in such conditions, e.g. Fe, Si, and Ba.

Balaganskaya et al. (2007) described a 200-meter thick weathering crust over phoscorites from Seblyarvr, but shallower alteration in other rock types including carbonatite. In Catalão I, the effects of weathering over phoscorites are observed in some cases up to 150 meters depth, while the soil over the other rock types is up to 80 meters. This gradient of weathering between phoscorites and other rock types might be explained by the occurrence of carbonatite pockets, as well as interstitial carbonate within nelsonites and phoscorites. The dissolution of carbonates with percolation of meteoric water creates a secondary porosity that allows the underground water to reach further depths, comparatively enhancing the weathering effects on these rocks. On the other hand, massive carbonatite stocks in Catalão I develop thinner soils when compared to phoscorites, probably because their porosity is mainly due to cooling fractures and jointing, which would result in less effective systems for water percolation.

Although there are anomalies of niobium in carbonatites from Catalão I, the Nb_2O_5 grade of these rocks is low, which renders them uneconomical under current market and ore processing conditions. The weathering of such rocks could produce a viable deposit if the anomalous carbonatite body were not massive and homogenous, if it were strongly fractured or with a longer and more effective weathering.

CONCLUSIONS

The primary niobium mineralization of the Catalão I carbonatite is related to phoscorites, rather than to carbonatites and can be defined as a Nb-P-Fe deposit. The rocks of the phoscorite series occurring in the complex can be divided into phoscorites (P1), apatite nelsonites (P2), magnetite nelsonites (P3) and dolomite carbonatite (DC). P2, P3 and DC are mineralized in niobium, and since the rocks have also abundant apatite and magnetite, the mineralization system can be classified as Nb-P-Fe-related. Although P1 is pyrochlore-free, it is the primary source for important phosphate mineralization in the complex.

In the APIP, Catalão I and II, and Araxá are the only carbonatite complexes with known niobium mineralization and nelsonite intrusions. Furthermore, the metasomatism in these complexes is more intense, inducing the transformation of former ultramafic rocks into metasomatic phlogopitite. This could indicate that the primitive magmas that intruded bebedourites in these three complexes, produced a more effective metasomatic system compared to other APIP complexes, such as Tapira, Salitre and Serra Negra.

The P1, P2, P3 and DC dikes share similar emplacement style with Catalão I carbonatites, i.e. dominantly stockworks of thin dikes and veins, which indicates similarities in the physical properties of the original magmas, particularly the low viscosity.

The pyrochlore chemical “A” Trend is related to the igneous evolution in fresh rock, following the substitution of Ca by Na-Sr. The Ca-rich end-member of this trend can be related to primitive pyrochlorites, such as those of Salitre and Oka, which were not present in our range of analysed samples from Catalão I. The Na-Sr-rich member is represented by pyrochlore inclusions in ilmenite from dolomite carbonatite (DC). Since DC is the most evolved rock of the phoscorite series in Catalão I, the composition of its pyrochlore is also interpreted as more evolved.

Pyrochlore chemical “B” Trend is related to weathering and can be defined by the substitution of Ca-Na-Nb by Ba-U-Ta-Si. The role of Si in this substitution is also described by Williams et al. (1997) in the Bingo Carbonatite, in Africa.

Ta-U enrichment in fresh-rock bariopyrochlore and high-Ba pyrochlore is a feature of early crystallized pyrochlorites rather than to the evolved pyrochlore composition of Catalão I, while high-Ba-Si is usually associated to lateritization. This feature suggest a more complex evolution for the Catalão I pyrochlore, probably involving primary oscillatory zoning and/or hydrothermal alteration leading to a hybrid composition.

There is no evidence of important substitutions involving Th, REE, Fe, Zr, and Ti neither in the magmatic nor in the weathered pyrochlorites.

The niobium mineralization in Catalão I can be divided into primary and residual. The primary deposit is related to dikes of nelsonites, attesting the igneous origin, usually with the metassomatic phlogopitite and ultramafics as the wallrock.

Secondary porosity is a factor of paramount importance controlling the occurrence of the residual niobium at Catalão I. In phoscorites and nelsonites water percolation and consequent mineral alteration is substantially aided by the early leaching of carbonatite pockets and, most of all, of interstitial carbonate. In other rocks of the complex cooling fractures and joints are the main channels for the meteoric water percolation, resulting in lesser weathering efficiency and conducting to the generation of thinner (albeit still very important) weathered mantle covers.

Acknowledgements

This paper is part of a MSc thesis granted by CNPq—Brazilian Council for Research and Technological Development to the first author and had the support of Mineração Catalão and Anglo American Brazil Exploration Division. The work was further supported by research grants from CNPq to JAB, JCG, RSV, and ESRB. University of Brasília is gratefully acknowledged for fieldwork support and access to laboratory facilities.

REFERENCES

- Araújo, D.P., 1996, Metassomatismo no complexo carbonatítico Catalão-I: implicações para a composição do magma carbonatítico e para o metassomatismo carbonatítico do manto superior: Unpublished MSc Thesis, Brasília, University of Brasília, p. 188.
- Balaganskaya, E.G., Downes, H., and Demaiffe, D., 2007, REE and Sr-Nd isotope compositions of clinopyroxenites, phoscorites, and carbonatites of the Seblyavr Massif, Kola Peninsula, Russia: *Mineralogia Polonica*, v. 38, p. 29-45.
- Brod, J.A., 1999, Petrology and geochemistry of the Tapira alkaline complex, Minas Gerais State, Brazil: Unpublished Ph.D. Thesis, Durham, University of Durham p. 486.
- Brod J.A., Gibson S.A., Thompson R.N., Junqueira-Brod T.C., Seer H.J., Moraes L.C., and Boaventura G.R., 2000, Kamafugite affinity of the Tapira alkaline-carbonatite complex (Minas Gerais, Brazil): *Revista Brasileira de Geociências*, v. 30, p. 404-408.
- Brod, J.A., Gaspar, J.C., Araújo, D.P., Gibson, S.A., Thompson, R.N., and Junqueira-Brod, T.C., 2001, Phlogopite and tetra-ferriphlogopite from Brazilian carbonatite complexes: petrogenetic constraints and implications for mineral-chemistry systematic: *Journal of Asian Earth Sciences*, v. 19, p. 265-296.
- Brod, J.A., Ribeiro, C.C., Gaspar, J.C., Junqueira-Brod, T.C., Barbosa, E.S.R., Riffel, B.F., Silva, J.F., Chaban, N., and Ferrari, A.J.D., 2004, Geologia e Mineralizações dos Complexos Alcalino-Carbonatíticos da Província Ígnea do Alto Paranaíba. In: 42 Congresso Brasileiro de Geologia, Araxá, Minas Gerais, Excursão 1: 1-29 (CD-ROM).
- Caprilli, E., Della Ventura, G., Williams, T.C., Parodi, G.C., and Tuccimei, P., 2006, The crystal chemistry of non-metamict pyrochlore-group minerals from Latium, Italy: *Canadian Mineralogist*, v. 44, p. 1367-1378.
- Carvalho, W.T., and Bressan, S.R., 1981, Depósitos minerais associados ao Complexo ultramáfico-alcalino de Catalão I – Goiás, in Schmaltz W.H., ed., Os principais depósitos minerais da Região Centro Oeste. Brasília: DNPM 6, p. 139-183.
- Chackhmouradian, A.R., and Mitchell, R.H., 1998, Lueshite, pyrochlore and monazite-(Ce) from apatite-dolomite carbonatite, Lesnaya Varaka complex, Kola Peninsula, Russia: *Mineralogical Magazine*, v. 62, p. 769-782.
- Clark, A.H., and Kontak, D.J., 2004, Fe-Ti-P oxide melts generated through magma mixing in the Antauta subvolcanic center, Peru: Implications for the origin of nelsonite and iron oxide-dominated hydrothermal deposits: *ECONOMIC GEOLOGY*, v. 99, p. 377-395.
- Cordeiro, P.F.O., 2009, Petrologia e metalogenia do depósito primário de nióbio do Complexo Carbonatítico-Foscórico de Catalão I, GO. Unpublished M.Sc. Thesis, University of Brasília, p. 140.
- Fava, N., 2001, O manto de intemperismo e a química do pirocloro de Catalão I (GO): Um estudo preliminar: Unpublished MSc Thesis, Brasília, University of Brasília. p. 124.
- Frietsch, R., 1978, On the magmatic origin of iron ores of the Kiruna type: *ECONOMIC GEOLOGY*, v. 73, p. 478-485.
- Geisler, T., Berndt, J., Meyer, H.W., Pollok, K., and Putnis, A., 2004, Low temperature aqueous alteration of crystalline pyrochlore: correspondence between nature and experiment: *Mineralogical Magazine*, v. 68, p. 905-922.
- Gibson, S.A., Thompson, R.N., Leonardos, O.H., Dickin, A.P., and Mitchell, J.G., 1995, The Late Cretaceous impact of the Trindade mantle plume – evidence from large-volume, mafic, potassic magmatism in SE Brazil: *Journal of Petrology*, v. 36, p. 189-229.
- Gierth, E., and Baecker, M.L., 1986, A mineralização de nióbio e as rochas alcalinas associadas no complexo Catalão I, Goiás, in Schobbenhaus, C., ed., Principais depósitos minerais do Brasil: Brasília, MME/DNPM 2, p. 455-462.
- Gold, D.P., Eby, G.N., Bell, K., and Vallee, M., 1986, Carbonatites, diatremes, and ultra-alkaline rocks in the Oka area, Quebec: Geological Association of Canada, Mineralogical Association of Canada, Canadian Geophysical Union, Joint Annual Meeting, Ottawa '86, Field Trip 21: Guidebook, 51p.
- Haggerty, S.E., and Fung, A., 2006, Orbicular oxides in carbonatitic kimberlites: *American Mineralogist*, v. 91, p. 1461–1472.
- Henríquez, F., Naslund, H.R., Nyström, J.O., Vivallo, W., Aguirre, R., Dobbs, F.M., and Lledó, H., 2003, New field evidence bearing on the origin of the El Laco magnetite deposit, northern Chile—a discussion: *ECONOMIC GEOLOGY*, v. 98, p. 1497–1500.
- Hirano, H., Kamitani, M., Sato, T., and Sudo, S., 1990, Niobium mineralization of Catalao I carbonatite complex, Goias, Brazil: *Bulletin of the Geological Survey of Japan*, v. 41, p. 619-626.
- Hogarth, D.D., 1977, Classification and nomenclature of the pyrochlore group: *American Mineralogist*, v. 62, p. 403-410.
- Hogarth, D.D., 1989, Pyrochlore, apatite and amphibole: distinctive minerals in carbonatite, in Bell, K., ed., Carbonatites – Genesis and evolution: London, Unwin Hyman, p. 105-148.
- Hogarth, D.D., Williams, C.T., and Jones, P., 2000, Primary zoning in pyrochlore group minerals from carbonatites: *Mineralogical Magazine*, v. 64, p. 683-697.
- Issa Filho, A., Lima, P.R.A.S., and Souza, O.M., 1984, Aspectos da geologia do complexo carbonatítico do Barreiro, Araxá, MG, Brasil, in CBMM, ed., Complexos Carbonatíticos do Brasil: Geologia: São Paulo, CBMM, p. 20-44.

- Knudsen, C., 1989, Pyrochlore group minerals from the Qaqarssuk carbonatite complex, in Möller, P., Cerný, P., and Saupé, F., eds., Lanthanides, Tantalum and Niobium. Berlin and Heidelberg, Springer-Verlag, p. 80-99.
- Krasnova, N.I., Petrov, T.G., Balaganskaya, E.G., Garcia, D., Moutte, D., Zaitsev, A.N. and Wall, F., 2004a, Introduction to phoscorites: occurrence, composition, nomenclature and petrogenesis, in Wall, F., and Zaitsev, A.N., eds., Phoscorites and Carbonatites from Mantle to Mine: the Key Example of the Kola Alkaline Province: London, Mineralogical Society Series, p. 45-79.
- Krasnova, N.I., Balaganskaya, E.G., and Garcia, D., 2004b, Kovdor – classic phoscorites and carbonatites, in Wall, F., and Zaitsev, A.N., eds., Phoscorites and Carbonatites from Mantle to Mine: the Key Example of the Kola Alkaline Province: London, Mineralogical Society Series, p. 99-132.
- Lapin, A.V., 1982, Carbonatite differentiation processes: International Geology Review, v. 24, p.1079-1090.
- Lapin, A.V., and Vartiainen, H., 1983, Orbicular and spherulitic carbonatites from Sokli and Vuorijarvi: Lithos, v. 16, p. 53–60.
- Lee, M.J., Garcia, D., Moutte, J., Williams, C.T. and Wall, F., 2004, Carbonatites and phoscorites from the Sokli complex, Finland. in Wall, F., and Zaitsev, A.N., eds., Phoscorites and Carbonatites from Mantle to Mine: the Key Example of the Kola Alkaline Province: London, Mineralogical Society Series, p. 133–162.
- Lee, M.J., Lee, J.I., Garcia, D., Moutte, J., Williams, C.T., Wall, F., and Kim, Y., 2006, Pyrochlore chemistry from the Sokli phoscorite-carbonatite complex, Finland: Implications for the genesis of phoscorite and carbonatite association: Geochemical Journal, v. 40, p. 1-13.
- Lumpkin, G.R., and Ewing, R.C., 1995, Geochemical alteration of pyrochlore group minerals: pyrochlore subgroup: American Mineralogist, v. 80, p. 732-743.
- Mariano, A.N., 1989, Nature of economic mineralization in carbonatites and related rocks, in Bell, K., ed., Carbonatites Genesis and Evolution: London, Unwin Hyman, p. 149–176.
- Mücke, A., and Younessi, R., 1994, Magnetite–apatite deposits, Kiruna-type, along the Sanandaj-Sirjan and in the Bafq area, Iran, associated with ultramafic and calcalkaline rocks and carbonatites: Mineralogy and Petrology, v.50, p. 219–44.
- Nasraoui, M. and Bilal, E., 2000, Pyrochlores from the Lueshe carbonatite complex (Democratic Republic of Congo): a geochemical record of different alteration stages: Journal of Asian Earth Sciences, v. 18, p. 237-251.
- Nyström, J.O., and Henríquez, F., 1994, Magmatic Features of Iron Ores of the Kiruna Type in Chile and Sweden: Ore Textures and Magnetite Geochemistry: ECONOMIC GEOLOGY, v. 89, p. 820-839.
- Oliveira I. W. B., Sachs L. L. B., Silva V. A., Batista I. H. 2004. Folha SE.23-Belo Horizonte. In: Schobbenhaus C., Gonçalves J. H., Santos J. O. S., Abram M. B., Leão Neto R., Matos G. M. M., Vidotti R. M., Ramos M. A. B., Jesus J. D. A. (Eds.). *Carta geológica do Brasil ao millionésimo: Sistema de Informações Geográficas – SIG e 46 folhas na escala 1: 1.000.000*. Brasília, Brazil: CPRM 41 CD-ROM Pack.
- Oliveira, R. C., Barbosa, E. S. R., Junqueira-Brod, T. C., Brod, J. A., 2007, Petrografia e mineralogia de estruturas orbiculares do complexo alcalino-carbonatítico de Salitre, MG. In: 4º Congresso de Iniciação Científica do DF/XIII Congresso de Iniciação Científica da UnB, 2007, Brasília, DF. Anais - CD-ROM.
- Palmieri, M., Pereira, G.S. B., Brod, J.A., Junqueira-Brod, T.C., Petrinovic, I.A. and Ferrari, A.J.D., 2008, Orbicular magnetite from the Catalão I phoscorite-carbonatite complex: 9th International Kimberlite Conference Extended Abstract, 9IKC-A-00337.
- Ribeiro, C.C., 2008, Geologia, geometalurgia, controles e gênese dos depósitos de fósforo, terras raras e titânio do complexo carbonatítico Catalão I, GO: Unpublished Ph.D. Thesis. Brasília, University of Brasília, p. 473.
- Rudashevski, N.S., Kretser, Y.L., Rudashevsky, V.N., and Sukharzhevskaya, E.S., 2004, A review and comparison of PGE, noble-metal and sulphide mineralization in phoscorites and carbonatites from Kovdor and Phalaborwa, in Wall, F., and Zaitsev, A.N., eds., Phoscorites and Carbonatites from Mantle to Mine: the Key Example of the Kola Alkaline Province: London, Mineralogical Society Series, p. 375-405.
- Silva, A.B., 1986, Jazida de nióbio de Araxá, Minas Gerais, in Schobbenhaus, C., ed., Principais depósitos minerais do Brasil: Brasília, MME/DNPM 2, p. 435-453.
- Sonoki, I.K., and Garda, G.M., 1988, Idades K-Ar de rochas alcalinas do Brasil Meridional e Paraguai Oriental: compilação e adaptação as novas constantes de decaimento: Boletim IG USP Serie Científica, v. 19, p. 63-85.
- Stoppa, F., and Cundari, A., 1995, A new Italian carbonatite occurrence at Cupaello (Rieti) and its genetic significance: Contributions to Mineralogy and Petrology, v. 122, p. 275-288.
- Stoppa, F., Sharygin, V.V., and Cundari, A., 1997, New data from the carbonatite-kamafugite association: The melilitolite from Pian di Celle, Italy: Mineralogy and Petrology, v. 61, p. 27-45.
- Tither, G. 2001, Progress in Niobium Markets and Technology 1981-2001. In: Proceedings of the International Symposium Niobium, Orlando, Florida, USA, 1-25.
- Thompson, R.N., Gibson, S.A., Mitchell, J.G., Dickin, P., Leonardos, O.H., Brod, J.A., and Greenwood, J.C., 1998, Migrating Cretaceous-Eocene magmatism in the Serra do Mar alkaline province, SE Brazil: melts from the deflected Trindade mantle plume?: Journal of Petrology, v. 39, p. 1439-1526.

Traversa, G., Gomes, C. B., Brotzu, P., Buraglini, N., Morbidelli, L., Principato, M. S., Ronca, S., and Ruberti, E., 2001, Petrography and mineral chemistry of carbonatites and mica-rich rocks from the Araxá complex (Alto Paranaíba Province, Brazil): *Anais da Academia Brasileira de Ciências*, v. 73, p. 71-98.

Williams, C.T., Wall, F., Woolley, A.R., and Phillip, S., 1997, Compositional variation in pyrochlore from the Bingo carbonatite, Zaire: *Journal of African Earth Sciences*, v. 25, p.137-145.

Yang, Z., and Woolley, A., 2006, Carbonatites in China: a review: *Journal of Asian Earth Sciences*, v. 27, p. 559-575.

Yegorov, L.S., 1993, Phoscorites of the Maymecha-Kotuy ijolite-carbonatite association: *International Geology Review*. v. 35, p. 346-358.

Zurevinski, S.E., and Mitchell, R.H., 2004, Extreme compositional variation of pyrochlore-group minerals at the Oka carbonatite complex, Quebec: Evidence of Magma Mixing?: *Canadian Mineralogist*, v. 42, p.1159-1168.

CAPÍTULO 4

Stable O and C isotopes, and carbonate chemistry in phoscorites and Nb-rich nelsonites from the Catalão I carbonatite complex, central Brazil: implications for phosphate-iron-oxide magmas*

Pedro Filipe de Oliveira Cordeiro, José Affonso Brod & Roberto Ventura Santos

Institute of Geosciences, University of Brasília, Brazil

Phone: +55 61 33072873

Email: cordeiro@angloamerican.com.br, brod@unb.br

Abstract The Late-Cretaceous Catalão I contains stockworks of thin dykes of phoscorite-series rocks which can be subdivided into P1 (olivine-bearing, phoscorites) and P2/P3 (olivine-lacking, phlogopite nelsonites). P2 is richer in apatite whereas P3 can vary from nelsonite to magnetitite. Dolomite carbonatites (DC) occurring as pockets within the nelsonites, resemble mingling textures and contain clear (high-SrO) and cloudy (low-SrO) varieties of dolomite. The latter is produced by subsolidus recrystallisation of the former and its presence within a rock may be accompanied of changes in the original isotopic composition. Carbon and oxygen isotopes indicate that DC pockets in nelsonites have a mantle-like stable isotopic composition and evolved by crystal fractionation, liquid immiscibility, fluid percolation and degassing. The occurrence of igneous carbonate shows that the Catalão I phoscorite-series rocks are igneous and that phosphate-iron-oxide magmas can occur in this geological setting. It is likely that other analogous rocks from the so-called Kiruna-type deposits are also products of magmatic crystallisation from similar liquids.

Keywords: Catalão, APIP, Phoscorite, Nelsonite, Magnetitite, Carbonatite, Carbon and Oxygen isotopes

*Submetido ao Contributions to Mineralogy and Petrology em Nov/08

Introduction

Phoscorites are rare igneous rocks with apatite, magnetite, and a magnesian silicate (olivine, diopside, and/or phlogopite). These rocks have been described from only 21 localities worldwide (Krasnova et al., 2004), and are almost always associated with carbonatites. In spite of being well described in terms of contact relations and textural-mineralogical features, the petrogenesis of phoscorites is poorly known and remains inconclusive.

Previous studies have argued that the petrogenesis of phoscorite magma involves assimilation-fractional-crystallisation (AFC) as a form of modifying the melt composition along its magmatic evolution (Krasnova et al. 2004). Those authors have also addressed whether the phoscorite series derived from a carbonatite-silicate parental magma or was generated by an independent primary magma. They concluded that the phoscorite series represents mantle-derived magmas that occur in close spatial and temporal association with carbonatite complexes.

In the Late-Cretaceous Alto Paranaíba Igneous Province (APIP), central Brazil, phoscorite-series rocks are particularly abundant in the Catalão and Araxá carbonatite-bearing complexes. The Catalão I complex, which is the focus of the present study, intrudes schists and quartzites of the Late Proterozoic Brasília Belt, which were fenitized and domed during the emplacement. Phoscorites, nelsonites, and associated dolomite carbonatites occur as small intrusions and stockworks of thin dykes that are clearly observed in outcrops and along more than 20,000 meters of fresh-rock drilling performed by Mineração Catalão Ltda (Anglo American Plc). The alkaline rocks are well preserved in the drill cores and show multiphase phoscorite-carbonatite associations, thus providing a rare opportunity for sampling and describing the contact relationships of the phoscorite series. Furthermore, the phlogopite nelsonites from this complex host an important Nb deposit, whose weathering products have been mined for many years.

This paper focuses on field and textural relations, carbonate chemistry and isotopic characteristics of phoscorite, nelsonite and carbonatite from Catalão I. It aims to establish chemical and textural criteria to identify primary and secondary carbonates, bringing new insights into the discussion of the genesis of phoscorite rocks. The conclusions of the present study might extend to other cases, such as the apatite-magnetite-rich rocks from El Laco, Chile (Nyström & Henríquez, 1994) and nelsonites, and oxide-apatite gabbronorites associated with massif anorthosites in the USA, Canada, and other localities (Dymek and Owens, 2001).

Geological Context

The Late-Cretaceous Alto Paranaiba Igneous Province (APIP) is located in Goiás and Minas Gerais states, central Brazil (Gibson et al. 1995). It occupies a NW-elongated area between the São Francisco Craton and the northeast border of the Paleozoic Paraná Basin (Fig. 4.1). The APIP consists of a variety of ultrapotassic magmas emplaced in metasedimentary rocks of the Late-Proterozoic Brasília mobile belt. It is mainly composed of kamafugites, with subordinate kimberlites, lamproites, and plutonic carbonatite-phoscorite alkaline complexes. The APIP has been related to the impact of the Trindade mantle plume under the Brazilian lithosphere during the Late Cretaceous, which led to melting of K-rich portions of the sub-continental lithospheric mantle (Gibson et al. 1995; Thompson et al. 1998; Brod et al. 2004).

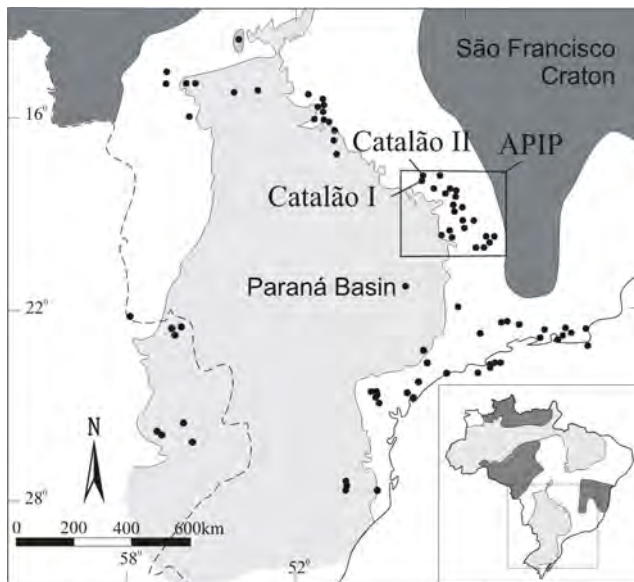


Fig. 4.1 Location of the Alto Paranaíba Igneous Province on the border of the Paraná Basin (modified from Gibson et al. 1995). Black dots represent cretaceous alkaline rocks from different provinces.

The APIP plutonic carbonatite-phoscorite complexes comprise several intrusions from northwest to southeast: Catalão I and Catalão II in the Goiás State; and Serra Negra, Salitre I, Salitre II, Salitre III, Araxá, and Tapira in the Minas Gerais State. In most cases, the intrusions produced a dome structure in the country rocks. Tropical weathering and inward drainage patterns resulting from the external ring of weathering-resistant country-rock produced deep lateritic soil profiles on the alkaline rocks. Therefore, suitable samples for geochemical studies are restricted to drill cores or the lower portions of mining pits. Tropical weathering tends to increase the grade of primary concentrations of niobium, phosphate, titanium, and rare earths in the soil. Some of the complexes have been extensively mined for phosphate (Tapira, Araxá, Catalão I) and niobium (Araxá, Catalão I, and Catalão II).

Except for rare late-stage syenites, the alkaline rocks in the APIP carbonatite-bearing complexes do not contain nepheline. Therefore, they do not belong to the rather common nephelinite (ijolite) – carbonatite association of Le Bas (1985). Instead, they are typically ultrapotassic, leading Brod et al (2000) to define a kamafugite–carbonatite association in the province, similar to that proposed by Stoppa and Cundari (1995) and Stoppa et al. (1997) in Italy.

Three distinct differentiation series are recognized in the APIP plutonic complexes, all generated from a primitive ultrapotassic silicate magma (phlogopite–picrite): bebedourites, phoscorites, and carbonatites (Brod et al. 2004).

Bebedourites are the product of crystal fractionation from a primitive magma and are characterized by variable amounts of essential olivine, diopside, apatite, perovskite, magnetite, and phlogopite. Ti-garnet (melanite) and titanite may also occur, in lesser amounts. These rocks represent the counterparts of the ijolitic series in complexes of potassic rather than sodic affiliation (Brod, 1999; Brod et al. 2004). In the APIP, well preserved bebedourites occur at Tapira and Salitre, whereas at Catalão and Araxá the primary bebedourites were extensively transformed into phlogopitites by carbonatite metasomatism.

Phoscorites are rocks derived from iron-phosphate magmas and are defined by modal variations in apatite, magnetite, and olivine (Yegorov, 1993). Krasnova et al. (2004) recommended that the name phoscorite be applied to plutonic ultramafic rocks comprising apatite, magnetite, and one of the silicates phlogopite, diopside, and forsterite. Common accessories include pyrochlore and dolomite. Rocks from the phoscorite series occur in all complexes of APIP and are particularly common in the Araxá and Catalão I complexes.

The carbonatite series comprises rocks containing over 50% of carbonate minerals and its nomenclature is based on the dominant type of carbonate present. Common carbonates in carbonatites include dolomite, calcite, Fe-dolomite, and ankerite (Woolley and Kempe 1989). At Catalão I, dolomite carbonatites dominate largely over calcite carbonatites.

These three differentiation series occurring in the APIP complexes are related to each other by an intricate combination of recurrent fractional crystallisation and liquid immiscibility processes from a primitive magma of kamafugitic affiliation (Brod 1999; Brod et al. 2000; Brod et al. 2004).

The Catalão I Complex

Catalao I (Fig. 4.2) is located near the city of Catalão, Goiás state. It intrudes quartzites and schists of the Late Proterozoic Brasilia Belt and forms a roughly circular, dome-shaped structure that occupies an area of 27 km². Phlogopite K-Ar dating indicates an intrusion age of 85±6.9 Ma (Sonoki and Garda 1988). Another complex, called Catalão II, is located 15 km north of Catalão I, but their relationship is yet to be detailed. Machado Junior (1992) obtained a Rb-Sr age of 83.4±0.9 Ma for Catalão II. Erosion rates based on apatite fission track (Amaral et al. 1997), together with evidence of the presence of explosive activity within the magma chamber, led Ribeiro et al. (2005) to estimate a depth of intrusion shallower than 2.5 km for the Catalão I and II complexes.

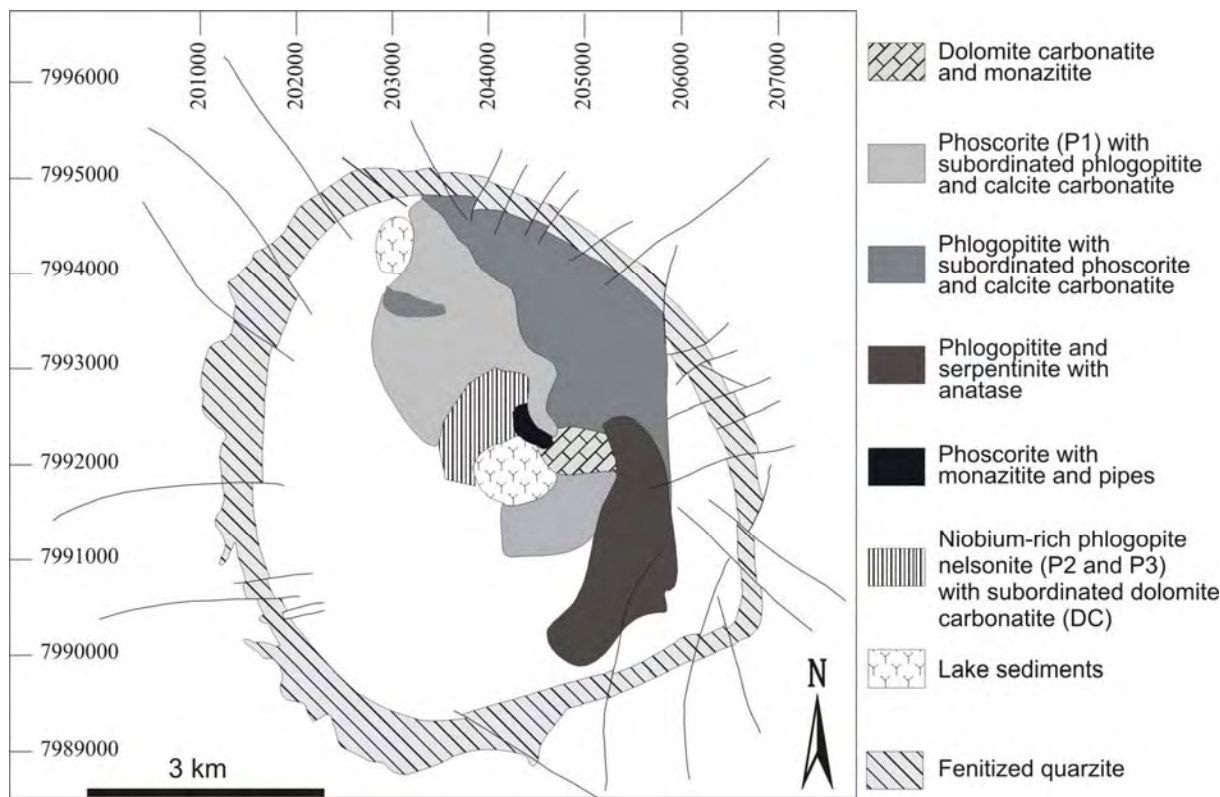


Fig. 4.2 Geological sketch of the Catalão I Complex. The studied samples were obtained from the niobium-rich phlogopite nelsonite and from the phoscorite with subordinated phlogopite and calcite carbonatite units (modified from Ribeiro 2008).

At Catalão I, the common concentric structure of ultramafic-carbonatite complexes is defined by a carbonatite-phoscorite-nelsonite zone in the center and metasomatized ultramafic alkaline rocks in the external portions of the intrusion. The most abundant rock in the complex is metasomatic phlogopite. Common primary magmatic rocks include dunite, clinopyroxenite, bebedourite, carbonatite, phoscorite, nelsonite, apatite, and magnetitite. Dykes of primitive phlogopite-picrite crosscut all other rock types (Brod et al. 2004, Ribeiro et al. 2005).

The predominance of metassomatic phlogopite over primary silicate rocks attests to the importance and intensity of metasomatic events that affected the ultramafic rocks. Metasomatic phlogopites are common in other APIP complexes, such as Tapira, Salitre, and Catalão II, but extremely abundant in the complexes of Catalão I and Araxá. This feature suggests that at Catalão I and Araxá the source of the volatile phase was particularly rich in alkalis relative to the other APIP complexes. The dominance of dolomite carbonatite over calcite carbonatite may be related to this extent of metassomatism.

Common differentiation processes in carbonatite complexes are crystal fractionation, liquid immiscibility, loss of alkalis by degassing, and contamination with adjacent country rocks (Le Bas 1989). Accordingly, several models that include metasomatic, magmatic, hydrothermal, and weathering processes have been proposed for the evolution of the Catalão I complex (Baecker 1983, Araújo 1996, Ribeiro et al. 2005, Brod et al. 2001). But, because of the multi-stage evolution with recurrent magmatism and metassomatism, a single model linking the three distinct petrogenetic series is yet to be developed.

Method and Samples

This study was carried out on drill core samples of phoscorite, nelsonite, and carbonatite rocks from the Catalão I Nb deposit, between the depths of 100 and 500 meters, provided by Mineração Catalão Ltda (Anglo American Plc). Detailed petrographic analysis was used to define the different generations of carbonates and their chronological relationship. Following the petrographic analysis, carbonates were extracted from different rock types, veins, dykes, and pockets with a manual tungsten-carbide drill in order to avoid interference from different carbonate generations or contamination with external sources.

Oxygen and carbon isotope data were obtained by reacting the carbonate samples with 100% H₃PO₄ at 72°C, using a Gas Bench II System connected to a Delta V Advantage gas-source mass spectrometer at the University of Brasília. Results are expressed in delta notation, relatively to the PDB (carbon) and SMOW (oxygen) standards.

Chemical composition of individual carbonate grains was determined by a CAMECA SX-50 electron microprobe equipped with three WD spectrometers and a LINK ED system, at the University of Brasília. Analytical conditions were set at 20 kV and 20 nA.

Rock nomenclature and petrography

The nomenclature of phoscorite-series rocks is not yet firmly established in the literature. The original definition (Yegorov, 1993) was based on a triangular modal-composition diagram involving olivine, apatite and magnetite as the phoscorite essential minerals.

Several authors described phoscorite varieties where diopside or phlogopite, were the essential magnesian silicates, rather than olivine. Krasnova et al. (2004) recommended the extension of the definition of phoscorite to “plutonic ultramafic rocks, comprising magnetite, apatite and one of the silicates, forsterite, diopside or phlogopite”. However, the silicate mineral is probably the best indicator of the differentiation stage of a phoscoritic magma, and assigning the same rock-name to olivine-, diopside- and phlogoptite-bearing rocks has the disadvantage of losing track of the evolution stage of the magma from which the rock crystallised. This has an important bearing, not only petrologically but also from the point of view of ore deposits. For instance, Nb and REE mineralization in the APIP complexes is typically associated with late-stage members of the phoscorite series (Ribeiro et al. 2005, Brod et al. 2004, Ribeiro 2008), such as nelsonites, but apparently absent or sub-economical in “bona fide” olivine-bearing phoscorites.

Krasnova et al. (2004) suggest three alternatives for classifying these rocks: (a) indicate major minerals in the phoscorite by a mineral prefix; (b) the Yegorov (1993) classification scheme, based on the abundances of the major minerals olivine, apatite, and magnetite; (c) the RHA method, a geochemically based classification. In this paper we opted for combining the root names in Yegorov (1993) with the mineral prefixes suggested by Krasnova et al. (2004). This approach allowed us to discriminate rocks of different evolution stages whilst still accounting for the specific dominant silicate mineral.

A similar concept was applied by Yegorov (1993) in the Maymecha-Kotuy carbonatite complex, where the modal content of olivine was used to define the evolution stage of the rock, with olivine-rich phoscorites considered more primitive than olivine-poor phoscorites and nelsonites.

Phoscorite-series rocks from Catalão I may be subdivided into early (P1) and late stage (P2 and P3). The former are olivine-bearing rocks and therefore classified as phoscorite, whereas the latter are nelsonites containing tetra-ferriphlogopite as the dominant magnesian silicate and often mineralized with pyrochlore. P2 and P3 are distinguished on the basis of apatite and magnetite predominance, respectively. Table 4.1 gives the modal composition of representative samples.

Tab. 4.1 Modal composition of the Catalão I phoscorites and nelsonites. The values are expressed as volume percentages.

Sample	Rock	Magnetite	Phlogopite	Apatite	Olivine	Carbonate	Pyrochlore	Barite
N244	P1	11	25	37	25	2	0	0
F4	P1	27	21	5	25	22	0	0
110-46	P1	12	12	18	51	7	0	0
N107	P2	33	11	45	0	6	5	0
N156	P2	33	5	58	0	1	3	0
N157a	P2	31	29	29	0	5	4	2
N178	P2	23	23	34	0	15	5	0
N192B	P2	7	12	43	0	27	11	0
N304 A	P2	35	11	33	0	10	11	0
N103	P3	71	9	6	0	10	4	0
N200	P3	66	12	10	0	6	6	0
N207	P3	59	8	20	0	7	5	1
N230B	P3	69	2	18	0	5	6	0
N206	P3	48	18	12	0	20	2	0
N157b	P3	59	5	19	0	4	13	0

They occur as a stockwork of thin dykes and small plugs crosscutting metassomatic phlogopites and ultramafic alkaline rocks. Large-volume single phoscorite or nelsonite intrusions are unknown in the complex. The associated carbonatites occur as thin dykes or pockets within the phoscorites and nelsonites, and are interpreted as genetically related.

Early-stage phoscorites – P1

P1 rocks occur as centimeter-thick dykes and small plugs with coarse- to medium-grained (average 0.5 mm) magnetite, apatite, olivine, and phlogopite with ultramafic rocks and metassomatic phlogopite as wallrock (Fig. 4.3).

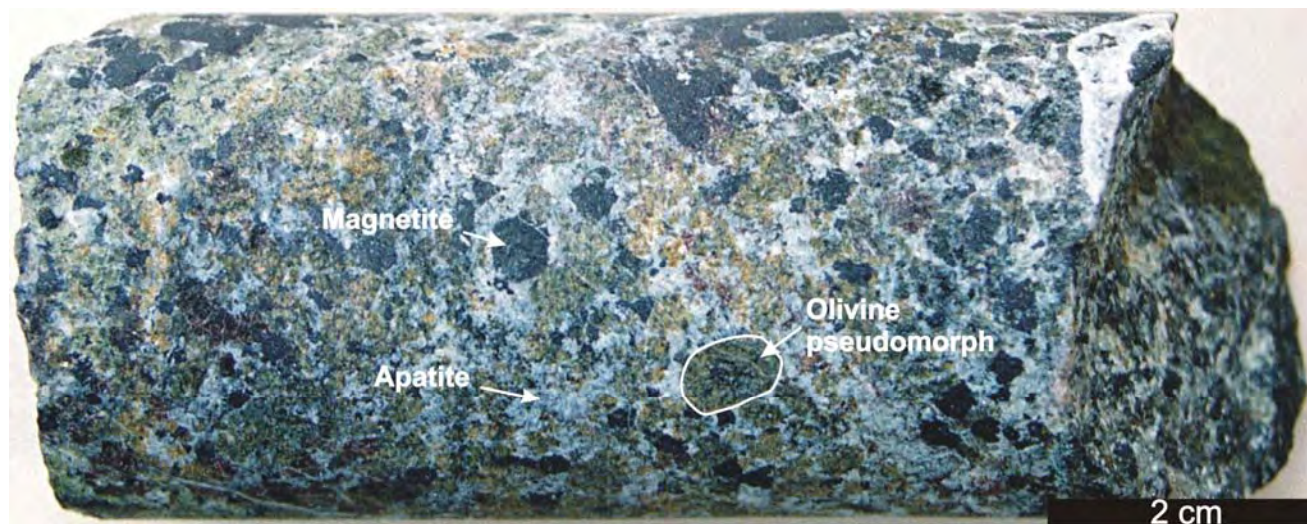


Fig. 4.3 Metassomatised P1 phoscorite. Olivine from this sample was substituted by clino-humite, but the original shapes of olivine grains are still recognizable.

Subhedral to euhedral, coarse- to medium-grained olivine and apatite are the most abundant minerals in P1. Magnetite occurs as anhedral grains and often contains exsolved ilmenite lamellae. Euhedral phlogopite and olivine crystals are commonly replaced by a fine-grained aggregate of tetra-ferriphlogopite, clino-humite, and/or serpentine. Perovskite, ilmenite, rutile, and baddeleyite occur as accessories. Carbonates are often interstitial and related to thin veins that crosscut the rock.

Late-stage phlogopite nelsonites – P2 and P3

Nelsonites occur as stockworks of centimeter- to meter-thick dykes with fine- to medium-grained magnetite, apatite, tetra-ferriphlogopite, and pyrochlore. These rocks intrude both the metassomatic phlogopitite and the early phoscorite. Metasomatic borders in these dykes vary from thin (less than 10 cm) to absent, implying that nelsonitic magmas were not an effective source for the intense metassomatism observed in the ultramafic and early phoscorite rocks.

The Catalão I nelsonites (Fig. 4.4) are subdivided into P2 and P3. P2 rocks are medium- to fine-grained, rich in euhedral apatite grains, with subordinate amounts of euhedral to subhedral magnetite. P3 are medium-grained, dominated by anhedral magnetite with subordinate apatite, and contain abundant dolomite pockets.



Fig. 4.4 P3 dyke (magnetite-rich nelsonite) with slightly metassomatised P2 (apatite-rich nelsonite) as the wallrock and with metassomatic phlogopitite (MP) xenoliths. Note the thin (5 cm) reaction rim in the contact, and the dolomite-carbonatite pockets within the P3 dyke

Magnetite from both P2 and P3 contains thin (ca. 0,01mm) lamellae of exsolved ilmenite. Tetra-ferriphlogopite occurs as euhedral to subhedral grains in both rock types. Crystals with phlogopite cores and tetra-ferriphlogopite rims are common in P2 but rare or absent in P3. Anhedral, fine-grained tetra-ferriphlogopite aggregates may occur as a local product of metassomatism. Apatite occurs as fine-grained, often zoned and oriented crystals in P2 and as monomineralic aggregates in P3. Pyrochlore, columbite, pyrite, chalcopyrite, and sphalerite are common accessories.

Carbonate pockets and dolomite carbonatite (beforsite) dykes – DC

Carbonatite veins and pockets (Figs. 4.4 and 4.5) are usually associated with the nelsonites, mainly P3. Pockets of dolomite carbonatite were also described by Hirano et al. (1990) from the Catalão I complex as lens- and vesiculae-like aggregates of beforsite (dolomite carbonatite) segregated by liquid-immiscibility. The DC pockets in P3 often show a wall composed of magnetite with subordinate tetraferri-phlogopite, apatite, and ilmenite (Fig. 4.5) This was described as “a bunch of grapes texture” and interpreted as liquid immiscibility between phoscorite and carbonatite liquids (Hirano et al., 1990). Alternative interpretations that cannot be ruled out at the present stage of our ongoing work are: a) an origin of the DC pockets as carbonatite segregations from a nelsonitic crystal mush, and b) crystal fractionation of a nelsonitic assemblage at the walls of a carbonatite dyke.



Fig. 4.5 P3 nelsonite with dolomite carbonatite pockets. Note the growth of tetra-ferriphlogopite in the boundary between P3 and the DC pocket, where ilmenite and apatite are also common.

Dolomite carbonatite dykes with the same mineral assemblage also occur spatially associated with nelsonites. They usually have larger and more abundant ilmenite crystals when compared with the carbonate pockets, suggesting that they may represent coalescing dolomite carbonatite exsolved from the nelsonite magmas or, alternatively, from a nelsonitic crystal-mush.

In both pockets and dykes the crystals nucleate on the wall and grow toward the center of the carbonatite. Massive crusts of magnetite, often with thin exsolved ilmenite lamellae, are restricted to the border of the carbonate pockets and DC dykes. Coarse-to-fine grained tetra-ferriphlogopite, ilmenite, pyrochlore, and apatite are associated with the magnetite crust. Sphalerite, chalcopyrite, pyrite, monazite, calcite, barite, and norsethite ($Ba,Mg(CO_3)_2$) occur as common accessories in the dolomite carbonatites.

Dolomite crystals vary from white and brittle to gray and fresh in hand specimen. These correspond, respectively, to dolomite with “cloudy” or “clear” aspect in thin section. These two

varieties often grade into each other. Cloudy dolomite occurs along fractures, cleavages and borders of clear dolomite crystals. It may also be present at the contact between DC pockets and the host nelsonite. Clear dolomite occurs as carbonate grain cores and in the central parts of DC pockets and dykes (Fig. 4.6). The textural properties indicate that the cloudy aspect of dolomite is caused by abundant micro-inclusions, possibly related to exsolution during subsolidus recrystallisation.

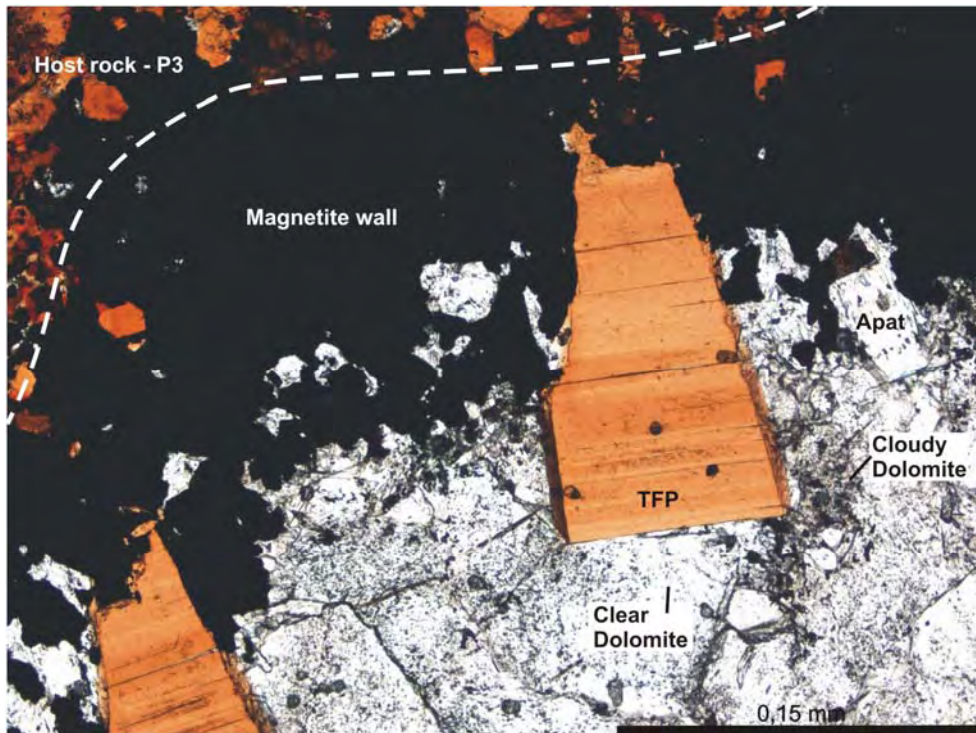


Fig. 4.6 Thin section of dolomite carbonatite pocket in a P3 dyke under transmitted light. Cloudy dolomite is often related to fractures and is common along the boundary between the dolomite carbonatite and the magnetite wall. (Apat=apatite, TFP=tetra-ferriphlogopite)

Carbonate chemistry

Carbonates in P1 rocks can be dolomite and magnesite whereas P2 and P3 rocks contain dolomite and norsethite. In both phoscorites and nelsonites, dolomite is far more abundant than the other carbonates, and only dolomite analyses were used in the chemical characterization of cloudy and clear carbonates. Table 4.2 shows representative analyses.

Tab. 4.2 Representative analyses of dolomites from Catalão I phoscorites, nelsonites, and carbonatites. n.d. = not determined; b.d. = below detection

Sample	304A-1	178-1	200-1	99A-3	183-2	110-46-3	156-3	192A-1	93-1	183-1
Rock	P2	P2	P3	P3	DC	P1	P2	P2	P2	DC
Texture	Clear	Clear	Clear	Clear	Clear	Cloudy	Cloudy	Cloudy	Cloudy	Cloudy
Oxides (wt%)										
CaO	26.38	28.30	28.32	29.74	30.05	29.31	30.41	30.51	29.66	30.85
SrO	4.73	3.16	3.86	2.09	2.772	0.59	0.96	0.61	1.43	0.47
BaO	b.d.	0.09	0.04	0.07	0.116	0.04	b.d.	b.d.	b.d.	0.05
MgO	23.74	22.62	22.58	22.44	22.77	23.06	22.33	22.84	21.92	23.75
FeO _T	0.63	0.93	0.68	1.10	0.668	0.11	0.57	1.45	0.50	0.40
MnO	n.d.	n.d.	0.29	0.28	n.d.	n.d.	0.26	0.97	0.65	n.d.
CO ₂	44.56	44.40	44.65	45.07	45.51	44.09	44.69	46.03	44.10	46.00
Sum	100.04	99.50	100.42	100.78	101.9	97.21	99.21	102.41	98.25	101.52

The SrO content of analysed dolomite from P1 is between 0.59-1.3 wt.%. CaO ranges between 29.3 wt.% and 30.0 wt.% and MgO between 23.1 wt.% and 24.1 wt.%. Other common constituents are present in small quantities, such as FeO (0.11-0.60 wt.%) and BaO (<0.1 wt.%).

Dolomite from DC dykes and P2 and P3 pockets have the same chemical composition. SrO is less than 2.77 wt.%. The CaO content is 30.8 to 26.3 wt.%, and MgO ranges between 23.7 and 20 wt.%. BaO (<0.2 wt.%) and FeO (0.40-1.15 wt.%) are also present.

Norsethite occurs intimately associated with dolomite and barite and is restricted to DC dykes and DC pockets within P3. Calcite is restricted to solid inclusions in other minerals, mainly apatite. Magnesite occurs within altered olivine grains, together with minute anhedral tetra-ferriphlogopite, and may therefore represent post-magmatic alteration (table 4.3).

Tab. 4.3 Chemical compositions of norsethite and magnesite from Catalão I phoscorites and carbonatites. n.d. = not determined; b.d. = below detection

Sample	183-7	339-4	339-1	183-8	339-9	110-1	110-46-2
Rock	DC	DC	DC	DC	DC	P1	P1
Mineral	Norsethite	Norsethite	Norsethite	Norsethite	Norsethite	Magnesite	Magnesite
Oxides (wt%)							
CaO	0.23	0.38	0.55	0.32	0.44	0.54	0.46
SrO	0.32	0.08	0.11	0.21	0.10	b.d.	b.d.
BaO	56.82	57.54	58.32	55.66	57.85	0.13	0.00
MgO	14.18	13.64	12.54	14.11	12.60	40.45	40.12
FeO	0.09	b.d.	0.07	0.22	0.07	7.64	8.34
MnO	n.d.	n.d.	n.d.	n.d.	n.d.	n.d.	n.d.
CO ₂	29.24	28.86	28.13	28.96	27.99	44.82	44.79
Sum	100.89	100.50	99.71	99.48	99.06	93.58	93.71

There is an association between textural features of dolomite and its chemical composition. Cloudy dolomite has less than 1.4 wt.% of SrO whereas in clear dolomite SrO ranges between 1.78

wt.% and 4.76 wt.%. Most analyses are in the range of average carbonate compositions described by Dawson et al. (1996) for several African carbonatite complexes. Their data showed that for most carbonates, the compositions plotted between 1 – 2 wt. % SrO, with rare exceptions of Sr-rich dolomites and calcites. On the other hand, Ahijado et al. (2005) report Sr-rich calcite with up to 7.23 wt. % SrO, interpreted as of igneous origin, from the Fuerteventura basal complex, Canary Islands.

Similarly to Catalão I, Brod (1999) described two separate generations of calcite in the Tapira Complex, also part of the APIP. That author interpreted the crystals with a clear appearance in thin section as primary, magmatic calcite, whereas another, “cloudy” variety of calcite contained exsolved strontianite and opaque minerals (Fig. 4.7). Tapira carbonate chemistry showed that the exsolution-rich calcite crystals with cloudy aspect tend to be near-pure calcite, whereas the clear crystals were Sr-rich calcite. It was concluded that recrystallisation of igneous calcite due to post-magmatic processes induced Sr and Fe exsolution, originating the cloudy aspect and the near-pure calcite host. On the other hand, clear calcite did not undergo recrystallisation, thus retaining the Sr- and Fe-rich composition of the igneous carbonate.

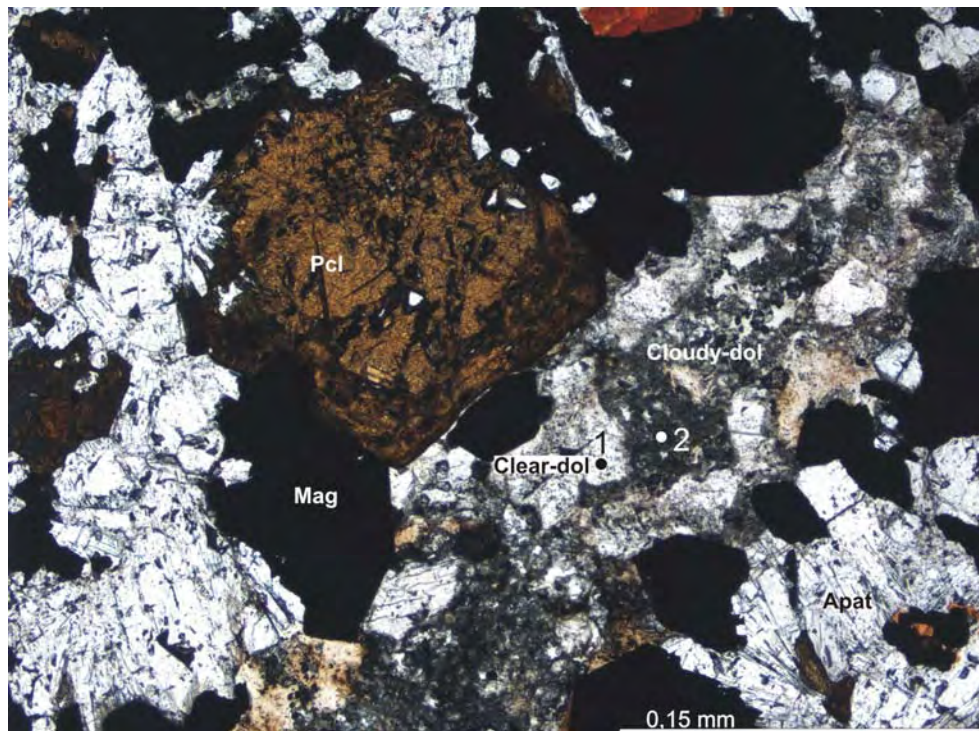


Fig. 4.7 Location of dolomite electron probe microanalyses from a DC pocket in sample NRD-178. Note the different textures between cloudy and clear dolomite, which are attributed to subsolidus alteration. Dots 1 and 2 are represented by arrows in figure 4.8 (Mag = magnetite, Pcl = pyrochlore, Dol = dolomite, Apat = apatite)

The Catalão I dolomites show the same textural features as the Tapira calcite described in Brod (1999). We therefore interpret the strontium content of dolomites from Catalão I as an indicator of origin and post-magmatic processes. Fig. 4.8 shows the SrO content of dolomites from Catalão I rocks.

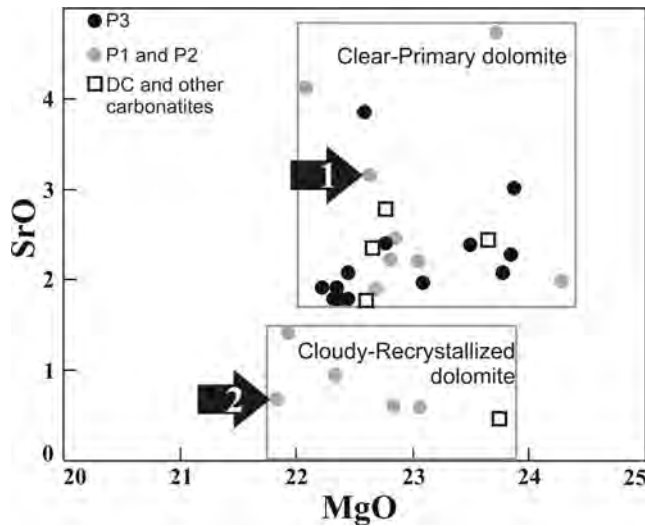


Fig. 4.8 Dolomite compositions from Catalão I phoscorites, nelsonites and dolomite carbonatites. There is a relationship between SrO content and texture, whereby “cloudy” dolomites are SrO poorer than grains with clear aspect. The arrows indicate the composition of both carbonate types from NRD-178 (figure 4.7)

Cloudy dolomites occur in variable degrees depending upon the weathering and the metassomatism imprinted on the rock. In fresh or only slightly altered rocks, cloudy dolomites are restricted to carbonate rims, cleavage, and fractures. This feature is in good agreement with an origin of cloudy dolomite by subsolidus recrystallisation with exsolution of micro-inclusions. Primary carbonates would have a clearer appearance and high SrO content, representing portions preserved from alteration. Textural gradation between both types of dolomite is attributed to variations in the intensity of alteration, and carbonates from DC pockets and dykes are usually a mixture of different proportions of the two textural types.

C-O isotope in the carbonatite and phoscorite-carbonatite association

Table 4.4 summarizes the carbon and oxygen isotope compositions for dolomite carbonate pockets, veins, dykes and interstitial grains of carbonate within phoscorite-series rocks. The data are plotted in Fig 4.9 and show a wide range of composition for these rocks. $\delta^{18}\text{O}_{\text{SMOW}}$ ranges between 8.58‰ and 23.11‰ and $\delta^{13}\text{C}_{\text{PDB}}$ between -3.55‰ and -7.88‰. There is no correlation between rock-type, texture and the isotopic data.

Tab. 4.4 Carbon and oxygen isotopic composition of carbonates from carbonatites, veins, DC dykes, and DC pockets in the Catalão I carbonatite complex

Sample	Type	$\delta^{13}\text{C}_{\text{PDB}}$	$\delta^{18}\text{O}_{\text{SMOW}}$
040V1	Vein	-6.17	17.1592
116V1	Vein	-7.01	21.4919
157G2	Vein	-5.48	22.9982
210V2x	Vein	-7.17	18.6788
252V1	Vein	-5.23	14.8409
309V1	Vein	-5.11	12.4731
339G1	Vein	-6.1	21.4322
103G1	DC-pocket (P3)	-5.91	9.80056
149	DC-pocket (P3)	-5.76	13.0363
157G1	DC-pocket (P3)	-5.61	9.89002
191G1	DC-pocket (P3)	-5.74	9.06029
252G1	DC-pocket (P3)	-5.86	9.6748
257G2	DC-pocket (P3)	-5.53	10.0174
093G1	DC-pocket (P2)	-5.53	10.4194
178G1	DC-pocket (P2)	-5.85	15.9202
178G2	DC-pocket (P2)	-5.16	11.0622
192G1	DC-pocket (P2)	-6.14	8.58781
038G1	DC-dyke	-5.81	10.3455
040G1	DC-dyke	-5.72	9.38799
056B	DC-dyke	-5.53	11.7976
170	DC-dyke	-6.31	12.4396
179G1	DC-dyke	-5.45	10.4394
183G1	DC-dyke	-5.82	11.9047
98	Carbonatite	-6.4	19.0413
210G1x	Carbonatite	-7.6	20.5676
210G2	Carbonatite	-5.87	10.9487
242G1	Carbonatite	-5.77	17.9959
056E	Carbonatite	-5.86	20.2262
91	Carbonatite	-5.85	11.3822
206	Carbonatite	-5.66	10.6184
239	Carbonatite	-5.65	14.522
247A	Carbonatite	-5.45	9.19648
247B	Carbonatite	-5.37	9.52693
250G1	Carbonatite	-5.14	12.3468
250G2	Carbonatite	-3.55	23.1184
250G3	Carbonatite	-4.23	16.4123
334x	Carbonatite	-3.94	19.9417

The isotopic composition of carbonatites and the processes that may affect it are well known (Deines 1989). Primary carbonatites have $\delta^{13}\text{C}_{\text{PDB}}$ values ranging between $-4\text{\textperthousand}$ and $-8\text{\textperthousand}$, and $\delta^{18}\text{O}_{\text{SMOW}}$ values ranging between $+6\text{\textperthousand}$ and $10\text{\textperthousand}$ (Taylor et al. 1967). The isotopic composition of these rocks may be affected by magmatic processes such as degassing and AFC, and by post-magmatic alteration. Assimilation of country rocks is a common process that can explain anomalous

values of carbon and oxygen isotopic composition, such as those observed in the Mato Preto carbonatites, Southern Brazil (Santos and Clayton 1995). Fluid-rock interaction may also affect the isotopic values both at high and low temperatures (Deines 1989; Santos and Clayton 1995). For example, available isotopic data for the APIP carbonatites include many samples with high $\delta^{18}\text{O}$ values and carbonatite-like $\delta^{13}\text{C}$ values, suggesting that they have been variably affected by interaction with water-rich fluids (Morikiyo et al., 1990; Buzzi et al. 1994, Toyoda et al., 1995; Santos and Clayton 1995, and Comin-Chiaromonti et al. 2005).

In contrast to carbonatite, isotopic data on the carbonatite-phoscorite association are scarce, restricted to a few complexes. Available information includes C-O isotope data of phoscorites and carbonatites of the Sokli, Turiy Mys, Vuoriyarvi, and Kovdor complexes from the Kola Alkaline Province (Demeny et al., 2004). In the case of Sokli, Demeny et al. (2004) argue that the data support the liquid immiscibility model between carbonatite and phoscorite liquids proposed by Lapin (1982). Carbon and oxygen isotopes from Sokli fit well along the carbonatite trend. This could indicate that not only phoscorites and carbonatites have the same source, but have similar evolution paths in terms of C-O isotopes. On the other hand, isotopic data for Vuoriyarvi led Dunworth and Bell (2001) to conclude that carbonatite and phoscorite in that complex have different sources. Based on isotopic data from Vuoriyarvi, Demeny et al. (2004) concluded that there is no uniform stable isotope model for the phoscorite-carbonatite association.

The isotopic composition of the Catalão I phoscorites, nelsonites, and associated dolomite carbonatite pockets and dykes varies by ca. 15‰ in $\delta^{18}\text{O}_{\text{SMOW}}$ and ca. 4‰ in $\delta^{13}\text{C}_{\text{PDB}}$ (Fig. 4.9).

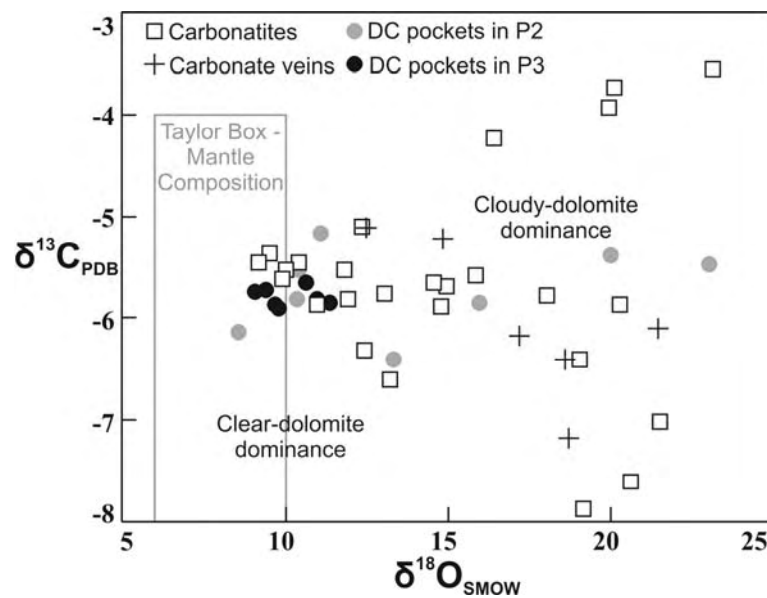


Fig. 4.9 Carbon and oxygen stable isotope data for carbonatites in this study. The isotopic composition of samples dominated by clear- and cloudy-dolomite is indicated, as well as the expected isotopic composition of primary carbonatite (gray box).

The samples can be subdivided into five groups in terms of the C-O isotopic composition (Fig. 4.10).

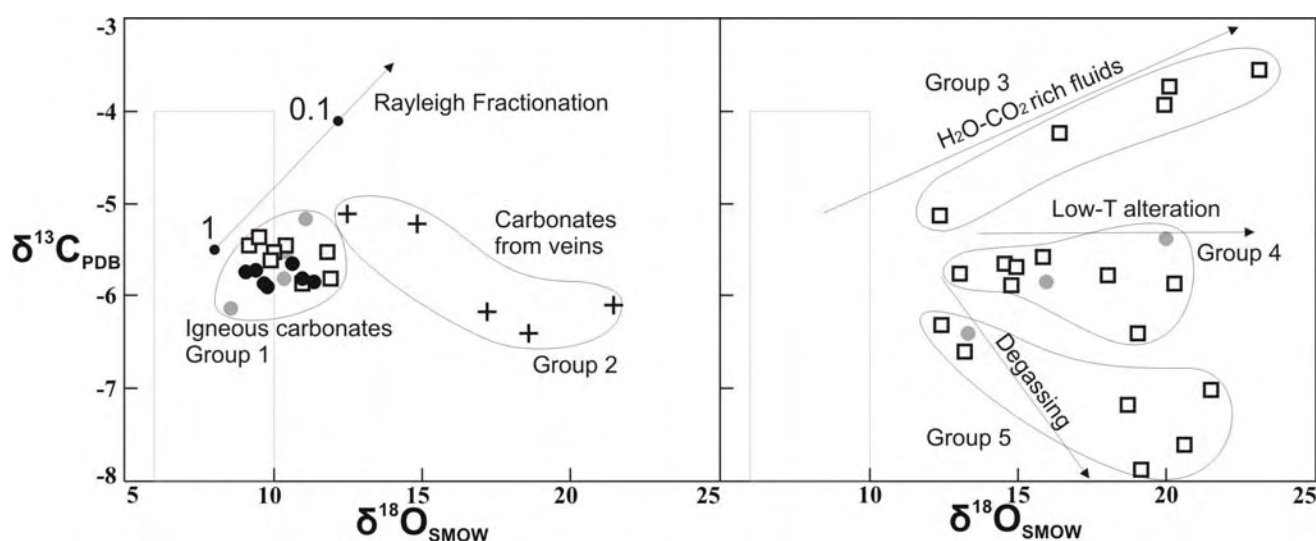


Fig. 4.10 Oxygen and carbon isotopes of different carbonates from the Catalão I complex. Samples were grouped according the isotopic behavior. Key: black = dolomite-carbonatite (DC) pockets in P3; gray = DC pockets in P2; squares = carbonatites; crosses = veins

Group 1 is composed of carbonates with carbonatite-like $\delta^{13}\text{C}$ values, and $\delta^{18}\text{O}$ values slightly higher than those expected for mantle-derived magmas. Under the microscope, these samples are composed of clear carbonate crystals with no signs of post-magmatic or low-temperature alteration. Also, we could not find any petrographic or mineralogical evidence of country-rock assimilation in the studied samples. We therefore interpret these results as representative of primary (igneous) carbonates. A possible explanation for the slightly high oxygen isotope values is that they are related to primary magmatic process such as liquid immiscibility or crystal fractionation. Under these circumstances the oxygen isotopic composition of the carbonate would be a function of the isotopic fractionation between carbonates and other minerals, as well as of the temperature and the isotopic composition of the initial melt. Fig. 4.11 models the expected isotopic composition of calcite in equilibrium with apatite and magnetite considering different temperatures and proportions among these minerals. Since the isotopic fractionation of calcite and dolomite are similar, calcite data was used in the model to estimate the behaviour of dolomite.

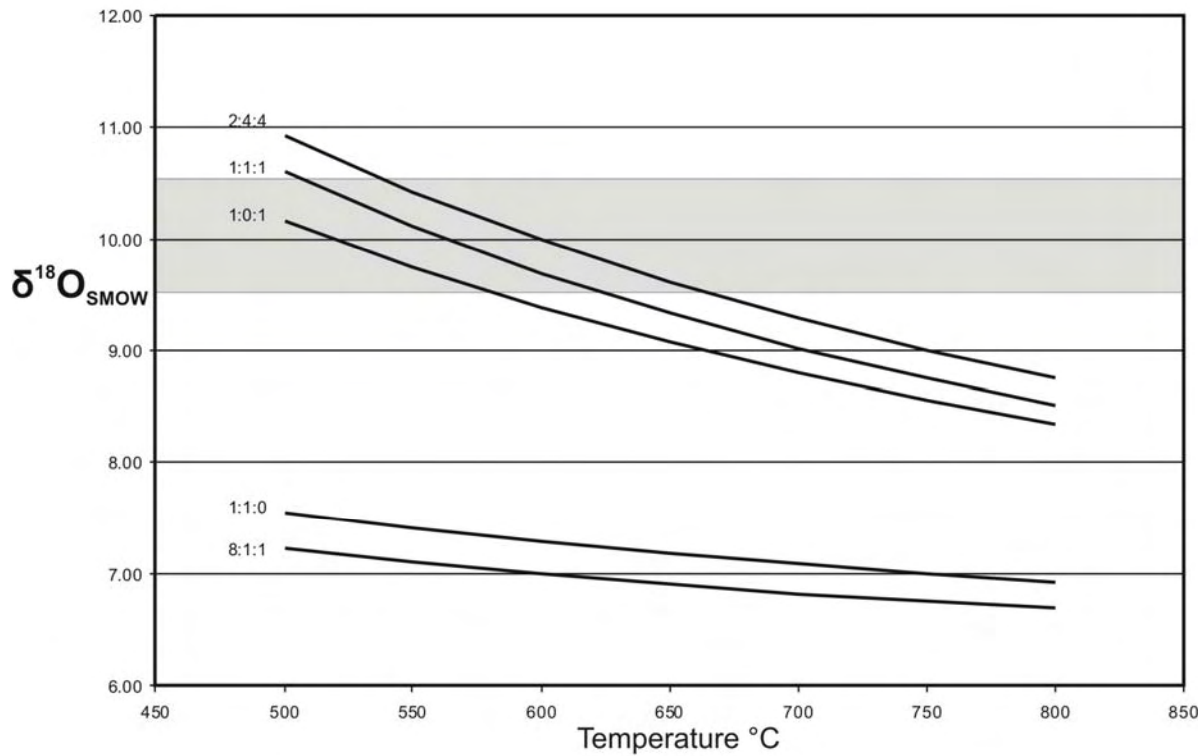


Fig. 4.11 Diagram showing the isotopic composition of calcite in equilibrium with apatite and magnetite at temperatures ranging between 500 and 800°C. The number near the curves indicate the proportion of calcite:apatite:magnetite. The gray area shows the approximate isotopic composition of the carbonates generated by immiscibility. Isotopic fractionations were based on Clayton and Kieffer (1991) and Zhao and Zheng (2003)

The model assumes that the initial isotopic composition of the magma was 6‰ and that liquid immiscibility took place under equilibrium conditions. Anchored in the model, the proportion of carbonate and phosphate + iron oxide generated during immiscibility can be estimated based on the initial isotopic composition of the magma, temperature, and an average isotopic composition for the carbonates. Fig. 4.11 shows that in order to generate carbonate with $\delta^{18}\text{O}$ near 10‰ by immiscibility, it is also necessary to produce significant amounts of magnetite, thus supporting the immiscibility model.

Group 2 is represented by carbonates that occur in veinlets and that are associated with altered minerals and fractures. Although they have a clear aspect in thin section, they are Sr-poor and yield oxygen isotopic ratios significantly higher than those of the primary carbonates. Dolomite of this group is interpreted as a late-stage, low-temperature, metasomatic phase that crystallised directly with a composition near the ideal dolomite end-member. Because it records one of the last events occurring in the complex, and did not contain impurities which could be exsolved, it does not develop the cloudy aspect observed in magmatic dolomites.

Group 3 dolomites have higher $\delta^{18}\text{O}$ and $\delta^{13}\text{C}$ values than expected for primary carbonates. A shift toward higher values in both $\delta^{18}\text{O}$ and $\delta^{13}\text{C}$ could be explained by assimilation of crustal

components or by interaction with meteoric fluids. Since the studied samples were collected in the central portion of the complex (Fig. 4.2), no assimilation of crustal material would be expected, at least during or after emplacement. Based on the modeling by Santos and Clayton (1995), we argue that the high, positively correlated isotopic ratios of this group were produced by low temperature interaction with CO₂-H₂O-fluids.

Group 4 shows high δ¹⁸O values, but carbonatite-like δ¹³C values. These rocks probably interacted with water-rich, CO₂-poor fluids, thus affecting mostly the oxygen isotopes. Most samples contain dolomite crystals with a clear core surrounded by a cloudy rim, thus indicating post-magmatic alteration. Conduits for external fluids are not visible in most samples, suggesting that the alteration may have been produced by self-metasomatism. In some cases, however, there is evidence of mineral alteration related to fractures, indicating that external fluids may also have interacted with these rocks.

Group 5 samples have high oxygen isotopic values but carbon isotopic values lower than those expected for the primary carbonatites. In order to approach the processes that affected the isotopic composition of these rocks, it is necessary to understand the isotopic fractionation between CO₂ and carbonate at different temperatures. For instance, in high temperature systems, above 180°C, the isotopic fractionation between CO₂ and calcite is positive both for carbon and oxygen isotopes (Chacko et al, 1991). Below this temperature, however, there is an inversion on the carbon isotope fractionation, which means that carbon in CO₂ becomes lighter relative to the coexisting carbonate. A possible scenario that may explain the formation of carbonates with high oxygen and low carbon isotopic values in carbonatite environment is the degassing of CO₂ from the carbonate melt. This may occur during decompression and may be accompanied by crystallisation/precipitation of calcite. Similar process was discussed by Zheng (1990) to explain CO₂ degassing accompanied by calcite precipitation in the Kushikino gold occurrence, in Japan. That author showed that degassing processes in which calcite is in equilibrium with HCO₃⁻, may lead to formation of carbonate with progressively negative carbon isotope values. We argue this process may also occur when carbonatite magma is subjected to decompression, thus explaining the negative slope of the trend observed in Group 5 samples. In contrast to carbon, the oxygen values tend to present progressively positive values. Under this circumstance the isotopic fractionation between H₂O and calcite is negative and controls the calcite isotopic composition.

Textural and carbonate chemistry evidence of post-magmatic alteration

Carbonate chemistry, used to distinguish between primary and secondary carbonate, was compared with the isotopic data. Since cloudy dolomite represents recrystallised patches within the rock, isotopic alteration accompanying the recrystallisation is expected. For most of the rocks, carbonate chemistry criteria was applied successfully, which means that $\delta^{18}\text{O}$ -rich samples contain moderate to high modal percentage of cloudy dolomite.

Dolomite carbonatite pockets from P2 were sampled for isotopic analysis in two areas (Fig. 4.12), one containing white, brittle dolomite (cloudy dolomite in thin section), and the other with fresh, gray dolomite (clear dolomite in thin section). The white, brittle DC pocket underwent post-magmatic processes that resulted in $\delta^{18}\text{O}$ enrichment relatively to the expected composition of primary carbonatite. On the other hand, primary compositional features are preserved in the gray, fresh DC pocket. $\delta^{13}\text{C}$ value is basically the same between these two DC pockets, whereas $\delta^{18}\text{O}$ indicates a difference of nearly 5‰, probably because of differential recrystallisation or localized alteration.

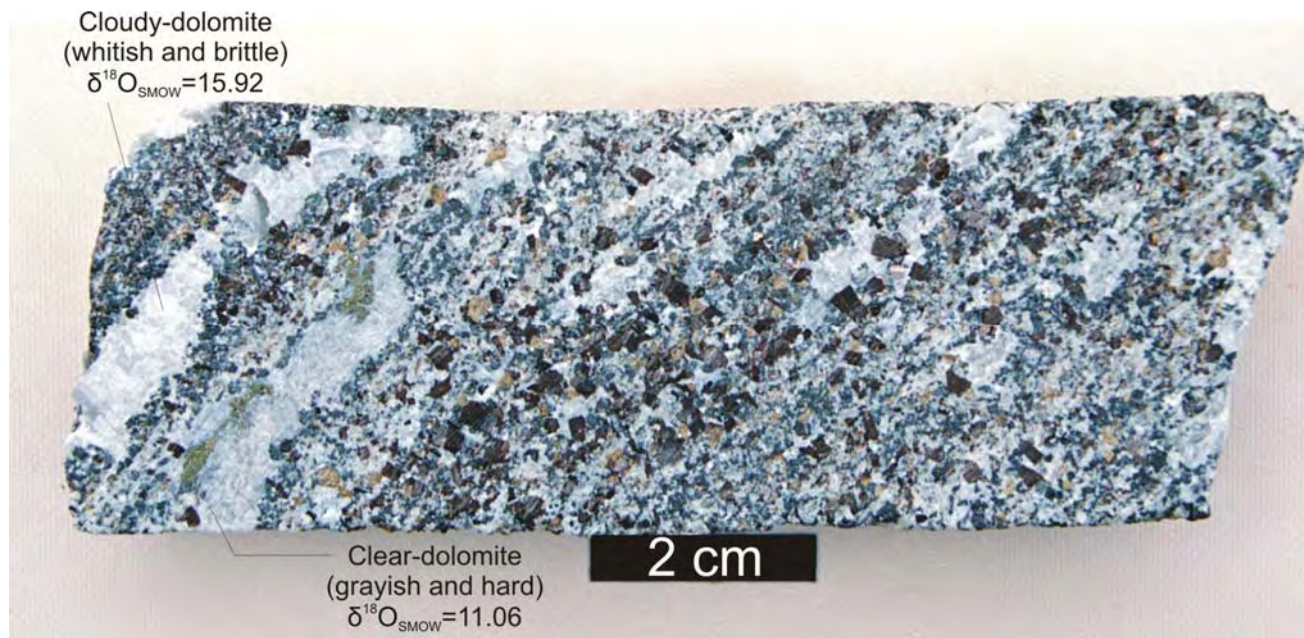


Fig. 4.12 Comparison between the hand-sample aspect of cloudy and clear carbonates in P2 (sample 178). Cloudy dolomite is more white and brittle compared to clear dolomite, and represents the recrystallisation product of primary (high-SrO) carbonates.

Whitish (cloudy) carbonate is common in the border of dolomite pockets and crystals, apparently lacking any connection with veins or other evidence of external carbo-hydrothermal activity. This

carbonate is interpreted as recrystallised patches due to self-metassomatism which mostly affected the contact zones, changing Sr and $\delta^{18}\text{O}$ content in dolomite.

Although gray (clear) dolomite usually represents igneous carbonate, clear carbonate also occurs as thin veins. This variety is $\delta^{18}\text{O}$ rich and Sr-poor, interpreted as of metassomatic origin, contrasting with the igneous clear dolomite. Therefore, textural and chemical criteria must be used together to unequivocally determine carbonate genesis in the studied samples.

A scheme for the occurrence of different types of carbonates is shown in Fig. 4.13.

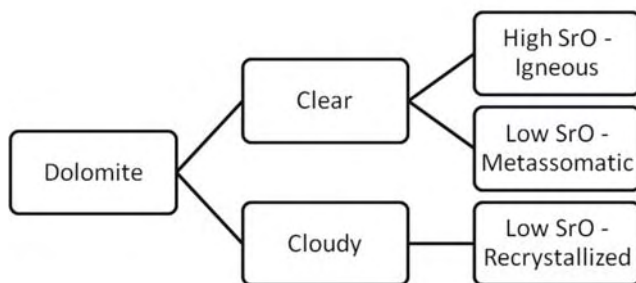


Fig. 4.13 Textural and chemical classification of primary and secondary dolomites from Catalão I

Phosphate-iron-oxide magmas in other environments

Geijer (1910) described the occurrence of magnetite-apatite rich rocks and their contact relations in Kiirunavaara, Sweden, concluding that these rocks are the last stage of magmatic differentiation in the magma chamber and, therefore, of igneous origin. Even at that time, there already was a discussion regarding the genesis of these rocks, with both igneous and hydrothermal sedimentary-exhalative models proposed. Frietsch (1978) and Hildebrand (1986) presented chemical, structural, and textural evidence of the igneous origin for the Kiruna rocks, called Kiruna-type deposits, and for other occurrences in Canada and USA. They concluded that Kiruna-type deposits comprise rocks formed by magnetite, apatite and a Ca-silicate and are most likely associated with plutons of intermediate-composition.

Oxide-apatite rocks are also described in relation with massif anorthosites and several other environments by Dymek and Owens (2001). These rocks were called oxide-apatite gabbronorite when apatite, oxide, plagioclase and pyroxene were the main minerals, and nelsonite, when they did not contain silicate. The authors argued that the most common association of nelsonite is with massif anorthosite, and although nelsonite occurs as dyke-like bodies, which suggest it represents an intrusion of magma, it also forms layers or segregations. Kolker (1982) suggested that nelsonites

represent immiscible liquids and that their common dyke-like occurrence may be explained by the low-viscosity properties of a Fe-oxide-phosphate liquid. Oxide-apatite rocks related to massif anorthosites are Ti-rich, which reflects in the presence of ulvöspinel and ilmenite. In contrast, Kiruna-type rocks as described by Hildebrand (1986) have magnetite as the oxide mineral and are Ti-poor.

Evidence of phosphate-oxide lava flows have been reported in Chile, from the El Laco volcano, (Park, 1961; Henríquez and Martin, 1978 and Nyström and Henríquez, 1994) and Magnetita Pedernales (Grez et al. 1991). These authors describe feeder dykes, textures of rapid crystal growth and columnar magnetite, suggested to be diagnostic of a magmatic origin. Moreover, rapid-growth textures in oxide-apatite rocks indicate emplacement of phosphate-iron-oxide magmas near surface. The El Laco deposit was defined as an extrusive equivalent of the Kiruna-type deposits (Nyström & Henríquez, 1994).

Silitoe & Burrows (2002) proposed that El Laco features do not represent flows from phosphate-iron-oxide magmas but, instead, are the product of metasomatic replacement of previous volcanic structures. The extensive feldspar-destructive alteration is consistent with hydrothermal activity at El Laco, but magmatic origin and fluid-related episodes are not incompatible. Harlov et al. (2002) studied textural and chemistry controls of the ore-rocks and concluded that in Kiirunavaara the oxide-apatite rocks were originally magmatic, but experienced successive stages of fluid-rock interaction.

Kiruna-type oxide-apatite rocks, Ti-oxide nelsonites associated with anorthosites, and phoscorite-series rocks associated with carbonatites share evidence of the existence of phosphate-iron-oxide rocks. These are mostly the dyke-like bodies, intrusive relations, sharp contact and breccias. In the case of phoscorites, the igneous origin is further supported by stable isotopes (Demeny et al., 2004).

The origin of such magmas remains inconclusive, but since Philpotts (1967) and Kolker (1982) the suggestion of liquid immiscibility as a way of generating these liquids has been discussed. Clark and Kontak (2004) reinforced the liquid immiscibility hypothesis by describing Fe-Ti-P rich spheres, interpreted as quenched melts. The mechanism proposed for the generation of iron-phosphatic magmas was mixing of mafic and felsic magmas with vesiculation of Fe-rich oxide melt.

Discussion and conclusions

Phoscorite-series rocks at Catalão I have a clear intrusive, sharp contact with metassomatic phlogopite, which is also the host rock of different carbonatite stages. The intrusion occurred as thin dykes, meter- to centimeter-thick.

The mineralogical and modal difference between phoscorite-series rocks suggests that magma differentiated from early, olivine-bearing phoscorites (P1) to nelsonites, a late stage that can be further divided into apatite-rich (P2) and magnetite-rich (P3).

The contact between P2, P3, and their host rock may be rarely marked by a rather thin metasomatic rim, indicating that nelsonite magma had relatively low metasomatizing capacity or, alternatively, that the chemical gradient between the nelsonite and the previously metasomatized phlogopite was small.

Some P2/P3 dykes contain dolomite carbonatite pockets with a magmatic carbon and oxygen isotopic signature. Hence, it is concluded that these phoscorite-series rocks are of igneous origin, and that phosphate-iron magmas can occur within carbonatite complexes.

After the intrusion of phoscorites and nelsonites, a fluid-related alteration stage affected the isotopic composition of some dolomite carbonatites and DC pockets. This late event caused dolomite to recrystallise preferably along fractures or at the rims of crystals, leaving most of the cores unaltered. More often, recrystallisation of the primary dolomite was complete. Primary dolomite has a clear aspect in thin section and is gray and fresh in hand-sample. Recrystallised dolomite has “cloudy” aspect in thin section and is white and brittle in hand-sample.

Dolomite chemistry was used to distinguish between primary and recrystallised grains. For the Catalão I phoscorites and nelsonites, high SrO content (> 1.4 wt. %), is typical of primary, magmatic carbonate. Dolomite with less than 1.4 wt. % of SrO often exhibits “cloudy” texture which may be attributed to numerous microinclusions produced by the exsolution of Sr, Fe, or other impurities.

Isotopic analysis of C and O was carried out in nelsonites, aiming to determine the genesis of these rocks and their main isotopic characteristics. Carbonate-bearing rocks with high modal content of “cloudy” dolomite also have high $\delta^{18}\text{O}$, if compared with carbonatites containing only dolomite of the clear variety. Nevertheless, since some metassomatic carbonates also show a clear aspect in thin section, both textural and chemical criteria must be used together for a better discrimination of the carbonate genesis.

In both fresh and altered phoscorites, nelsonites and carbonatites, the $\delta^{13}\text{C}$ composition of most samples plots within the mantle composition range, indicating that there was little carbon isotopic

exchange. The wide $\delta^{18}\text{O}$ enrichment is probably due to post-magmatic alteration by water-rich, CO₂-poor fluids.

A set of pristine nelsonites, interpreted as fresh igneous rocks, are slightly enriched in $\delta^{18}\text{O}$. This is probably related to primary magmatic processes such as liquid immiscibility or crystal fractionation, and can be explained by a model constrained by the isotopic fractionation between carbonates and other minerals, temperature, and the initial isotopic composition of the melt.

Carbonates from veins have higher values of $\delta^{18}\text{O}$ compared to the mantle composition, whereas $\delta^{13}\text{C}$ is very similar. These veins represent a fracture-filling metassomatic stage affecting both the studied rocks and their host rocks.

Samples where $\delta^{18}\text{O}$ and $\delta^{13}\text{C}$ are positively correlated and both higher than expected for primary carbonates may be explained by assimilation of crustal components or by interaction with meteoric or carbo-hydrothermal fluids. We argue in favor of low temperature interaction with CO₂-H₂O-rich fluids probably derived from the Catalão I carbonatites, since the studied rocks intrude the core of the complex and are expected to be preserved from the assimilation of crustal components.

Many of the samples analysed in this work show evidence of interaction with water-rich, CO₂-poor fluids shifting the isotopic composition to high $\delta^{18}\text{O}$. Such fluids may derive from the last stages of magma evolution (self-metasomatism) since in most cases there is no visible evidence of conduits on which the fluids could have percolated.

Carbonates with high $\delta^{18}\text{O}$ values and lower $\delta^{13}\text{C}$ than the expected for the primary carbonatites are interpreted as products of degassing at different temperatures.

The occurrence of phosphate-iron-oxide magmas in Catalão I has implications for apatite-oxide rocks in other environments, whose metasomatic or igneous origin is still under debate. The data presented here show that the Catalão I phoscorites and nelsonites are of igneous origin, although some later imprint of metasomatic events is locally observed. Therefore, magmatic liquids composed mostly of phosphate and iron oxide are feasible, and it is possible that rocks of similar composition found in other geological settings are also magmatic. Although major compositional differences occur between carbonatite-related phoscorites/nelsonites, massive anorthosite-related nelsonites, and Kiruna-type magmas, they probably have similar physical properties, such as high density and low-viscosity, and might be generated by similar mechanisms.

Acknowledgements

This paper is part of a MSc thesis granted by CNPq—Brazilian Council for Research and Technological Development to the first author and had the support of Mineração Catalão and Anglo American Brazil Exploration Division. The work was further supported by research grants from CNPq to JAB and RVS. University of Brasília is gratefully acknowledged for fieldwork support and access to laboratory facilities.

References

- Ahijado A, Casillas A, Nagy G, Fernández C (2005) Sr-rich minerals in a carbonatite skarn, Fuerteventura, Canary Islands (Spain). *Miner and Petrol* 84:107-127
- Amaral G, Born H, Hadler JC, Iunes PJ, Kawashita K, Machado DL, Oliveira EP, Paulo SR, Tello CA (1997) Fission track analysis of apatites from São Francisco craton and Mesozoic alkaline-carbonatite complexes from central and southeastern Brazil. *Jour South Amer Earth Sci* 10:285-294
- Araújo DP (1996) Metassomatism no complexo carbonatítico Catalão-I: implicações para a composição do magma carbonatítico e para o metassomatism carbonatítico do manto superior. MSc Thesis University of Brasília
- Baecker ML (1983) A mineralização de nióbio do solo residual laterítico e a petrografia das rochas ultramáficas alcalinas do domo de Catalão I, Goiás. MSc Thesis University of Brasília
- Bizzi LA, Smith BC, De Wit MJ, Macdonald I, Armstrong RA (1994) Isotope characteristics of the lithospheric mantle underlying the SW São Francisco craton margin, Brazil. *Intern Symp on the Phys and Chem of the Upper Mantle* 227-256
- Brod JA (1999) Petrology and geochemistry of the Tapira alkaline complex, Minas Gerais State, Brazil. PhD Thesis, University of Durham
- Brod JA, Gibson SA, Thompson RN, Junqueira-Brod TC, Seer HJ, Moraes LC, Boaventura GR (2000) Kamafugite affinity of the Tapira alkaline-carbonatite complex (Minas Gerais, Brazil). *Rev Bras Geoc* 30:404-408
- Brod JA, Gaspar JC, Araújo DP, Gibson SA, Thompson RN, Junqueira-Brod TC (2001) Phlogopite and tetraferriphlogopite from Brazilian carbonatite complexes: petrogenetic constraints and implications for mineral-chemistry systematics. *J. Southeast Asia Sci.* 19:265-296.
- Brod JA, Ribeiro CC, Gaspar JC, Junqueira-Brod TC, Barbosa ESR, Riffel BF, Silva JF, Chaban N, Ferrarri AJD (2004) Excursion guide: Geologia e Mineralizações dos Complexos Alcalino-Carbonatíticos da Província Ígnea do Alto Paranaíba. Soc Bras Geol
- Chacko T, Mayeda TK, Clayton RN, Goldsmith JR (1991) Oxygen and carbon isotope fractionation between CO₂ and calcite. *Geochim Cosmochim Acta* 55:2867-2882
- Clayton RN and Keiffer SW (1991) Oxygen isotopic thermometer calibrations. In Taylor HP, O'Neil JR and Kaplan IR (eds) Stable Isotope Geochemistry: A tribute to Samuel Epstein, The Geochemical Society, Special Publication 3, pp 3-10
- Clark AH and Kontak DJ (2004) Fe-Ti-P oxide melts generated through magma mixing in the Antauta subvolcanic center, Peru: Implications for the origin of nelsonite and iron oxide-dominated hydrothermal deposits. *Econ Geol* 99:377-395
- Comin-Chiaromonti P, Gomes CB, Censi P, Speziale S (2005) Carbonatites from southeastern Brazil: a model for the carbon and oxygen isotope variations.. In: Comin-Chiaromonti P and Gomes CB (eds) Mesozoic to Cenozoic alkaline magmatism in the Brazilian Platform, 1st edn. Edusp/Fapesp, São Paulo, pp 629-650
- Dawson JB, Steele IM, Smith JV, Rivers ML (1996) Minor and trace element chemistry of carbonates, apatites and magnetites in some African carbonatites. *Miner Magaz* 60:415-425
- Deines P (1989) Stable isotope variations in carbonatites. In: Bell K (ed) Carbonatites: Genesis and Evolution, Unwin Hyman, London, pp 301-359
- Demény A, Sitnikova MA, Karchevsky PI (2004) Stable C and O isotope compositions of carbonatite complexes of the Kola Alkaline Province: phoscorite-carbonatite relationships and source compositions. In: Wall F and Zaitsev AN (eds) Phoscorites and Carbonatites from Mantle to Mine: the Key Example of the Kola Alkaline Province, 1st ed. Mineralogical Society Series, London, pp 407-431
- Dunworth EA and Bell K (2001) The Turiy Massif, Kola Peninsula. Russia: Isotopic and geochemical evidence for multi-source evolution. *J Petrol* 42:377-405
- Dymek RF and Owens BT (2001) Petrogenesis of apatite-rich rocks (nelsonites and oxide-apatite gabbronorites) associated with massif anorthosites. *Econ Geol* 96:797-815
- Frietsch R (1978) On the magmatic origin of iron ores of the Kiruna type. *Econ Geol* 73:478-485

- Geijer P (1910) Igneous rocks and iron ores of Kiirunavaara, Luossavaara and Tuolluvaara. *Econ Geol* 5:699-718
- Gibson SA, Thompson RN, Leonardos OH, Dickin AP, Mitchell JG (1995) The Late Cretaceous impact of the Trindade mantle plume – evidence from large-volume, mafic, potassic magmatism in SE Brazil. *J Petr* 36:189-229
- Grez E, Aguilar A, Henríquez F, Nyström JO (1991) Magnetita Pedernales: A new magmatic iron deposit in northern Chile. *Econ Geol* 86:1346-1349
- Harlov DE, Andersson UB, Nyström JO, Förster HJ, Broman C, Dulski P (2002) Apatite-monazite relations in the Kiirunavaara magnetite-apatite iron ore, northern Sweden. *Chem Geol* 191:47-72
- Henríquez F and Martin RF (1978) Crystal-growth textures in magnetite flows and feeder dykes, El Laco, Chile. *Can Min* 16:581-589
- Hildebrand RS (1986) Kiruna-type deposits: Their origin and relationship to intermediate subvolcanic plutons in the Great Bear magmatic zone, Northwest Canada. *Econ Geol* 81:640-659
- Hirano H, Kamitani M, Sato T, Sudo S (1990) Niobium mineralization of Catalao I carbonatite complex, Goias, Brazil. *Bull Geol Surv Japan* 41:619-626
- Kerr AC, Kempton PD, Thompson RN (1995) Crustal assimilation during turbulent magma ascent (ATA); new isotopic evidence from the Mull Tertiary lava succession, N.W. Scotland. *Contr Min Petrol* 119:142-154
- Kolker A (1982) Mineralogy and geochemistry of Fe-Ti oxide and apatite (nelsonite) deposits and evaluation of the liquid immiscibility hypothesis. *Econ Geol* 77:1146-1158
- Krasnova NI, Petrov TG, Balaganskaya EG, Garcia D, Moutte D, Zaitsev AN, Wall F (2004) Introduction to phoscorites: occurrence, composition, nomenclature and petrogenesis. In: Wall F and Zaitsev AN (eds) Phoscorites and Carbonatites from Mantle to Mine: the Key Example of the Kola Alkaline Province, 1st ed. Mineralogical Society Series, London, pp 45-79
- Lapin, AV (1982) Carbonatite differentiation processes. *Int Geol Rev* 24:1079-1090
- Le Bas MJ (1985) Nephelinites and Carbonatites. *J Geol Soc London* pp 704
- Le Bas MJ (1989) Diversification of carbonatite. In Bell K (ed.) Carbonatites: genesis and evolution. Unwin Hyman, London, pp 1-14.
- Machado Júnior DL (1992) Geologia do complexo alcalino-carbonatítico de Catalão II (GO). 37º Congr Bras Geol, São Paulo pp 94-95
- Mariano AN and Marchetto M (1991) Serra Negra and Salitre – carbonatite alkaline igneous complex. In Leonardos OH, Meyer HOA, Gaspar JC (eds) 5th International Kimberlite Conference (Field Guide Book). CPRM, Special Publication, Brazil 3/91:75-79
- McCrea JM (1950) On the isotopic chemistry of carbonates and paleotemperature scale. *J Chem Phys* 18:849-857
- Morikiyo T, Hirano H, Matsushita Y (1990) Carbon and oxygen isotopic composition of the carbonatites from Jacupiranga and Catalão I carbonatite complexes, Brazil. *Bull Geol Surv Japan* 41:619-626
- Nyström JO and Henríquez F (1994) Magmatic Features of Iron Ores of the Kiruna Type in Chile and Sweden: Ore Textures and Magnetite Geochemistry. *Econ Geol* 89:820-839
- Park CFJ (1961) A magnetite “flow” in northern Chile. *Econ Geol* 56:431-436
- Philpotts AR (1967) Origin of certain iron-titanium oxide and apatite rocks. *Econ Geol* 62:303-315
- Ribeiro, CC (2008) Geologia, geometalurgia, controles e gênese dos depósitos de fósforo, terras raras e titânio do complexo carbonatítico Catalão I, GO. Ph.D. Thesis. University of Brasília
- Ribeiro CC, Brod JA, Junqueira-Brod TC, Gaspar JC, Petrinovic IA (2005) Mineralogical and field aspects of magma-fragmentation deposits in a carbonate-phosphate magma chamber: evidence from the Catalão I Complex, Brazil. *J South Am Earth Sci* 18:355-369
- Santos RV & Clayton RN (1995) Variations of oxygen and carbon isotopes in carbonatites: a study of Brazilian alkaline complexes. *Geoch Cosm Acta* 59:1339-1352
- Sililitoe RH and Burrows DR (2002) New field evidence bearing on the origin of the El Laco magnetite deposit, northern Chile. *Econ Geol* 97:1101-1109
- Sonoki IK and Garda G.M (1988) Idades K-Ar de rochas alcalinas do Brasil Meridional e Paraguai Oriental: compilação e adaptação as novas constantes de decaimento. *Bol. IG USP Serie Científica* 19:63-85
- Stoppa F and Cundari A (1995) A new Italian carbonatite occurrence at Cupaello (Rieti) and its genetic significance. *Contrib Min Petrol* 122:275-288
- Stoppa F, Sharygin VV, Cundari A (1997) New data from the carbonatite-kamafugite association: The melilitolite from Pian di Celle, Italy. *Min and Petrol* 61:27-45
- Taylor HP, Frechen J, Degens ET (1967) Oxygen and carbon isotope studies of carbonatites from the Laacher See District, West Germany and the Alno District, Sweden. *Geoch Cosm Acta* 31: 407-430
- Toyoda K, Horiuchi H, Tokonami M (1994) Dupal anomaly of Brazilian carbonatite: geochemical correlation with hotspots in the South Atlantic and implications for the mantle source. *Earth Plan Sci Let* 126:315-331
- Thompson RN, Gibson SA, Mitchell JG, Dickin P, Leonardos OH, Brod JA, Greenwood JC (1998) Migrating Cretaceous-Eocene magmatism in the Serra do Mar alkaline province, SE Brazil: melts from the deflected Trindade mantle plume? *J Petr* 39:1439-1526

- Woolley AR and Kempe DRC (1989) Carbonatites: nomenclature, average chemical compositions, and element distribution. In: Bell K (ed) Carbonatites: Genesis and Evolution, Unwin Hyman, pp 1-14
- Yegorov LS (1993) Phoscorites of the Maymeha-Kotuy ijolite-carbonatite association. Int Geol Rev 35:346-358
- Zhao ZF and Zheng YF (2003) Calculation of oxygen isotope fractionation in magmatic rocks. Chem Geol 193:59-80
- Zheng YF (1990) Carbon-Oxygen Isotopic Covariation in Hydrothermal Calcite During Degassing of CO₂ - a Quantitative-Evaluation and Application to the Kushikino Gold Mining Area in Japan. Miner Deposit 25:246-250

CAPÍTULO 5

CONCLUSÕES

Rochas ricas em apatita, magnetita, olivina e flogopita em Catalão I classificam-se como foscoritos e nelsonitos, apresentando um contato brusco e claramente intrusivo com o flogopítito metassomático que também hospeda diferentes estágios de carbonatito. Os foscoritos, mas principalmente os nelsonitos, ocorrem como diques centimétricos a métricos e seu estilo intrusivo se assemelha muito ao de carbonatitos indicando que suas propriedades físicas são semelhantes, particularmente a viscosidade baixa. O contato entre nelsonitos e a rocha encaixante é marcado por por zonas de alteração milimétricas a centimétricas, indicando que os magmas nelsoníticos tinham relativamente aos carbonatitos mais primitivos, menor capacidade de metassomatizar a encaixante ou alternativamente, que o gradiente químico entre os nelsonitos e as encaixantes (flogopítito metassomático) é pequeno.

A diferença mineralógica e modal entre rochas da série foscorítica sugere que o magma parental diferenciou-se de foscoritos primitivos com olivina (P1) para nelsonitos, em um estágio tardio que pode ser dividido em apatita nelsonitos (P2) e magnetita nelsonitos (P3). Dolomita carbonatito (DC) ocorre como bolsões em P2 e em P3 e apresenta composição isotópica de carbono e oxigênio de origem magnmática. A composição isotópica, as estruturas intrusivas, a química mineral e as variações contínuas nas proporções modais dos foscoritos primitivos P1, apatita nelsonitos P2 até os magnetita nelsonitos P3 e dolomita carbonatitos DC, comprova que essas rochas originaram-se a partir de um magma foscorítico.

A evolução da fase silicática dos foscoritos de olivina (alterada para Ti-clinohumita) em P1, tetra-ferriflögopita com núcleos de flogopita em P2, até tetra-ferriflögopita em P3 e DC é consistente com observações em foscoritos de outros complexos como Kovdor e Sokli, onde flogopita com Al se torna menos abundante nas fases tardias da série-foscorítica (Krasnova et al. 2004b; Lee et al. 2003; Lee et al. 2004). Se apenas a composição do núcleo dos cristais for levada em consideração, a evolução das micas também acompanhada por aumento na razão Fe/Mg de P1 para DC. A variação química da apatita também é consistente com a evolução magnmática na sequência P1-P2-P3-DC, onde os núcleos de cristais de apatita se tornam progressivamente mais ricos em Sr.

Em P2, zonação mostra enriquecimento de Sr nas bordas de apatitas e empobrecimento em Mg nas bordas de flogopitas. Em P3 a zonação é inversa à de P2, e está relacionada com cristalização em contato com magma carbonatítico (DC). A presença de líquido intersticial carbonatítico reduziria a incorporação de Sr na apatita (Dawson & Hinton, 2003) e formaria micas mais magnesianas

conforme a evolução dos magmas em P3, consistente com o observado em carbonatitos (Brod et al. 2001). Em P2, por outro lado, a formação e extração de DC ocorreram em menor proporção, não sendo capazes de interferir na incorporação esperada de elementos nos minerais do apatita-nelsonito (i.e. enriquecimento em Sr e empobrecimento em Mg do centro pras bordas). Essa afirmação é consistente com a presença de grandes volumes de bolsões de DC em P3 (até 40%) quando comparados aos bolsões em P2, que são menores e mais disseminados.

Ilmenitas variam ao longo da solução sólida geikielita-ilmenita, tornando-se progressivamente menos magnesianas de P1 a P3, em uma evolução similar à descrita por Lee et al. (2005) para os foscoritos em Sokli. A composição da magnetita, por outro lado, não representa um bom indicativo de estágio evolutivo nas rochas da série-foscorítica de Catalão I, pois apesar de mostrar substituições envolvendo Ti e Mg, a composição de magnetita em diferentes rochas se sobrepõe amplamente.

Pirocloro ocorre apenas em P2, P3 e DC e sua evolução ao longo da série foscorítica é difusa mas mostra uma tendência dos pirocloros se tornarem mais ricos em Na e Sr com a evolução. Observa-se um trend composicional ígneo comparando-se pirocloros ricos em Ta e U em magmas foscoríticos primitivos em Sokli e Salitre (Lee et al. 2006; Barbosa et al. 2009) com pirocloros ricos em Ca-Na de Catalão I e pirocloros sódicos inclusos em ilmenitas em DC. Além disso, alteração hidrotermal/intempérica pode sobrepor completamente a assinatura ígnea do mineral por meio da entrada de Ba na estrutura do mineral. O bariopirocloro no depósito residual de nióbio de Catalão I e a ocorrência de núcleos Ca-Na de pirocloro no manto de intemperismo corrobora com essa hipótese. Elementos do sítio B, não apresentam substituições claras, tanto no trend magmático quanto no trend de alteração.

Dolomita não apresenta uma variação composicional clara ao longo da série, mas é um bom indicativo de alteração nas rochas foscoríticas de Catalão I. Enquanto dolomita primária apresenta aspecto límpido em seção delgada, e é cinza e coesa em amostra de mão, dolomita secundária ocorre com aspecto turvo em seção delgada e em amostra de mão é esbranquiçada e friável. Dolomita primária apresenta teores de SrO altos ($> 1.4\%$), típicos de carbonatos magmáticos, enquanto dolomita secundária ocorre com teores de SrO menores ($< 1.4\%$), provavelmente em função de exsolução de Sr, Fe e outras impurezas durante a recristalização. A recristalização dos carbonatos afetou também sua composição isotópica de carbono e oxigênio onde carbonatos secundários apresentam maiores valores de $\delta^{18}\text{O}_{\text{SMOW}}$, sem variações na composição do carbono. Essa associação indica que a recristalização do carbonato se deu por interação com fluidos de baixa temperatura ricos em H₂O e pobres em CO₂ que provocaram recristalização de carbonatos ao longo de fraturas ou nas bordas de cristais, deixando na maior parte dos casos, os núcleos inalterados. De modo geral, carbonatos límpidos representam cristais ígneos inalterados e carbonatos turvos representam indícios

de alteração. A exceção a esse critério textural são os carbonatos gerados por metassomatismo, que são límpidos em seção delgada, mas distinguem-se dos carbonatos magmáticos pelo seu menor teor de SrO. Portanto, os critérios químicos e texturais precisam ser utilizados em conjunto para determinação da evolução isotópica de carbono e oxigênio dos carbonatos de nelsonitos.

A pouca variação de $\delta^{13}\text{C}_{\text{PDB}}$ tanto em carbonatos de nelsonitos e dolomita carbonatitos, indica pouca troca isotópica de carbono na alteração dessas rochas. Portanto, o amplo evento de alteração pós-magmática que influencia a textura e composição química dos carbonatos ocorreu por fluidos ricos em H₂O, provavelmente de origem meteórica. Esses fluidos migraram pelas rochas através de fraturas e da abertura de porosidade secundária pela dissolução do carbonato e alterou minerais mesmo em profundidades maiores que 300 metros. A abertura de porosidade secundária permitiu a formação de solos mais espessos sobre os foscoritos que sobre os demais tipos petrográficos do complexo e consequentemente originou um importante controle metalogenético para a jazida residual de nióbio de Catalão I.

Nelsonitos frescos, onde o carbonato não mostra evidências de recristalização, apresentam-se ligeiramente enriquecidos em $\delta^{18}\text{O}_{\text{SMOW}}$ comparativamente à composição entendida como a composição isotópica do manto (Taylor et al. 1967). Essa variação é provavelmente função de processos magmáticos como imiscibilidade de líquidos e fracionamento isotópico entre minerais, temperatura e a composição inicial do magma. Composições anômalas à de carbonatos magmáticos preservados ocorrem em função de eventos sin-magmáticos (desgasificação) e pós-magmáticos (alteração por fluidos ricos em H₂O e CO₂).

A química de elementos maiores é consistente com a evolução de P1 para P3. Como acontece em outros complexos carbonatíticos-foscoríticos, os magmas foscoríticos em Catalão I são muito pobres em SiO₂ e evoluem na direção do empobrecimento tanto em Si quanto em Mg pelo fracionamento de olivina e flogopita. As rochas silicáticas, por outro lado, evoluem de forma divergente, com enriquecimento em Si.

As evidências de campo, texturais e de química mineral sugerem que, se todo o espectro composicional dos magmas de Catalão I for levado em consideração, os foscoritos e nelsonitos representam um dos estágios finais de formação do complexo. Essa conclusão é suportada pela presença de padrões ETR tetrad tipo-M em todas as rochas da série-foscorítica. Efeito tetrad é relativamente raro e ocorre relacionado a processos hidrotermais (Jahn et al. 2001; Kempe & Götze 2002; Bühn et al. 2003) e intempéricos (Takahashi et al. 2002), mas também relacionado com magmas graníticos tardios (Irber, 1999) e mineralizações associadas (Jahn et al. 2001; Kempe & Göetze, 2002). Além disso, resultados experimentais indicam que padrões tetrad podem ser gerados por processos de imiscibilidade (Veksler et al. 2005).

A normalização ao magma primitivo da APIP (flogopita-picrítico) permitiu um melhor reconhecimento dos padrões tetrad em rochas ultramáficas silicáticas de Catalão I e Araxá (Araújo, 1996; Traversa et al., 2001). Observa-se nessas rochas a ocorrência de padrões tetrad tipo-W que espelham os padrões tetrad tipo-M das rochas da série-foscorítica, indicando que os magmas foscoríticos (e carbonatíticos que derivam dele) foram produzidos por imiscibilidade a partir de um magma parental carbonatado-silicatado, durante os estágios iniciais da evolução do complexo.

Aparentemente existe uma diferença isotópica marcante entre os complexos carbonatíticos-foscoríticos de filiação potássica (i.e. APIP, Brod et al., 2000; Phalabora, Eriksson, 1989; Yuhara et al., 2005) e sódica (i.e. ijolite-bearing, Kola, Zaitsev & Bell, 1995, Dunworth & Bell, 2001). Em diagrama Sr-Nd, os complexos potássicos plotam no quadrante do manto enriquecido enquanto os complexos de filiação sódica plotam no quadrante do manto depletado. Isso pode indicar que os complexos de filiação potássica são principalmente gerados por metassomatismo do manto litosférico enquanto os de filiação sódica são mais fortemente influenciados por fontes astenosféricas e misturas com fontes litosféricas.

A ligação petrogenética entre foscoritos e os carbonatitos coexistentes e as rochas das séries silicáticas permanecem em discussão. As diferenças isotópicas de Sr-Nd entre foscoritos e outras rochas do Complexo de Turiy, na Peninsula de Kola, levaram Dunworth & Bell (2001, 2003) a argumentar multiplas fontes para a origem do complexo, e que carbonatitos, foscoritos e rochas silicáticas não poderiam ter sido geradas por um mesmo magma parental. Por outro lado, evidências de campo, texturais, geoquímicas e de química mineral indicam fortemente um link petrogenético entre foscoritos e rochas associadas. Foscoritos ocorrem exclusivamente em ambientes relacionados com carbonatitos, o que corrobora uma relação genética entre esses dois tipos de rocha, independentemente da assinatura radiogênica da fonte. A ocorrência de pares carbonatito-foscorito em outros complexos (e.g. Krasnova et al. 2004a, Lee et al. 2004, and this work) onde foscoritos e carbonatitos possuem a mesma mineralogia e química mineral semelhante, indica um magma parental comum.

Os padrões ETR tetrad tipo-M descritos em Catalão I e sua contraparte, os padrões ETR tetrad tipo-W da série silicática, sugerem que tanto o magma foscorítico quanto o bebedourítico originaram-se por imiscibilidade a partir de um magma primitivo silicático-carbonatítico (flogopita picrítico). Por outro lado, apesar do processo gerador dos magmas foscoríticos involver imiscibilidade de líquidos, padrões ETR e a química mineral evidenciam que a série evoluiu principalmente por cristalização fracionada. Diagramas multielementares paralelos entre DC e os nelsonitos P2 e P3, sugerem que os dolomita carbonatitos no depósito de Nb estão relacionados entre si apenas por cristalização fracionada e segregação por *filter pressing*.

A ocorrência de magmas ferro-fosfáticos em Catalão I apresenta implicações para rochas ricas em apatita e óxidos de ferro em outros ambientes geológicos, cuja origem ainda é indefinida. Uma vez que líquidos de tal natureza ocorrem em complexos carbonatíticos, é possível que magmas semelhantes ocorram em outros ambientes geológicos. Apesar das diferenças compostionais e modais nos minerais de nelsonitos relacionados com carbonatitos, anortositos e depósitos do tipo Kiruna, os magmas originais provavelmente apresentam propriedades físicas similares, como alta densidade e baixa viscosidade e podem ter sido gerados por mecanismos semelhantes.

Uma vez que a intrusão de magmas nelsoníticos está diretamente relacionada com a ocorrência do depósito primário de nióbio, esse é o principal controle da mineralização em rocha fresca. Além disso, flogopititos metassomáticos são abundantes em Tapira e Salitre, mas são extremamente abundantes em Catalão I e Araxá, onde se encontram depósitos de nióbio. Isso pode significar que o magma primitivo que intrudiu os dois últimos complexos, tinha uma capacidade maior de induzir metassomatismo. Essa característica pode também estar associada com o potencial metalogenético para nióbio dos complexos carbonatíticos, uma vez que a mineralização de nióbio apenas ocorre em complexos com grandes extensões de flogopititos metassomáticos.

A dissolução de bolsões de carbonatito nos nelsonitos mineralizados originou importante porosidade secundária através da qual se formaram espessos perfis de solo. A concentração de minerais resistentes ao intemperismo no solo, dentre eles bariopirocloro, formou o depósito residual de nióbio, com mais alto teor comparativamente ao depósito em rocha fresca e contribuiu para a economicidade do depósito.

A formação dos dois maiores depósitos de nióbio do mundo a partir de rochas mineralizadas em Nb-P-Fe da série foscorítica, tanto em Catalão I quanto em Araxá, é indicativo da importância econômica dessas rochas no cenário mundial do nióbio.

REFERÊNCIAS BIBLIOGRÁFICAS

- Ahijado A, Casillas A, Nagy G, Fernández C (2005) Sr-rich minerals in a carbonatite skarn, Fuerteventura, Canary Islands (Spain). *Miner and Petrol* 84:107-127
- Amaral G, Born H, Hadler JC, Iunes PJ, Kawashita K, Machado DL, Oliveira EP, Paulo SR, Tello CA (1997) Fission track analysis of apatites from São Francisco craton and Mesozoic alkaline-carbonatite complexes from central and southeastern Brazil. *Jour South Amer Earth Sci* 10:285-294
- Araújo DP (1996) Metassomatismo no complexo carbonatítico Catalão-I: implicações para a composição do magma carbonatítico e para o metassomatismo carbonatítico do manto superior. Unpublished MSc Thesis University of Brasília pp 188
- Baecker ML (1983) A mineralização de nióbio do solo residual laterítico e a petrografia das rochas ultramáficas alcalinas do domo de Catalão I, Goiás. MSc Thesis University of Brasília
- Balaganskaya EG, Downes H, Demaiffe D (2007) REE and Sr-Nd isotope compositions of clinopyroxenites, phoscorites, and carbonatites of the Seblyavr Massif, Kola Peninsula, Russia. *Mineralogia Polonica* 38:29-45
- Bizzi LA, Smith BC, De Wit MJ, Macdonald I, Armstrong RA (1994) Isotope characteristics of the lithospheric mantle underlying the SW São Francisco craton margin, Brazil. *Intern Symp on the Phys and Chem of the Upper Mantle* 227-256
- Brod JA (1999) Petrology and geochemistry of the Tapira alkaline complex, Minas Gerais State, Brazil. PhD Thesis, University of Durham pp 486
- Brod JA, Gibson SA, Thompson RN, Junqueira-Brod TC, Seer HJ, Moraes LC, Boaventura GR (2000) Kamafugite affinity of the Tapira alkaline-carbonatite complex (Minas Gerais, Brazil). *Rev Bras Geoc* 30:404-408
- Brod JA, Gaspar JC, Araújo DP, Gibson SA, Thompson RN, Junqueira-Brod TC (2001) Phlogopite and tetra-ferriphlogopite from Brazilian carbonatite complexes: petrogenetic constraints and implications for mineral-chemistry systematics. *J. Southeast Asia Sci.* 19:265-296.
- Brod JA, Ribeiro CC, Gaspar JC, Junqueira-Brod TC, Barbosa ESR, Riffel BF, Silva JF, Chaban N, Ferrari AJD (2004) Geologia e Mineralizações dos Complexos Alcalino-Carbonatíticos da Província Ígnea do Alto Paranaíba. In 42 Congresso Brasileiro de Geologia, Araxá, Minas Gerais, Excursão 1: 1-29 (CD-ROM)
- Brod JA, Gaspar JC, Diniz-Pinto HS, Junqueira Brod TC (2005) Spinel chemistry and petrogenetic processes in the Tapira alkaline-carbonatite complex, Minas Gerais, Brazil. *Rev Bras Geoc* 35:23-32
- Bühn BM, Schneider J, Dulski P, Rankin AH (2003a) Fluid–rock interaction during progressive migration of carbonatitic fluids, derived from small-scale trace element and Sr, Pb isotope distribution in hydrothermal fluorite. *Geochim Cosmochim Acta* 67:4577–4595
- Bühn BM and Trumbull RB (2003b) Comparison of petrogenetic signatures between mantle-derived alkali silicate intrusives with and without associated carbonatite, Namibia. *Lithos* 66:201-221
- Caprilli E, Della Ventura G, Williams TC, Parodi, GC, Tuccimei, P (2006) The crystal chemistry of non-metamict pyrochlore-group minerals from Latium, Italy: *Can Min* 44:1367-1378

Carvalho WT and Bressan SR (1981) Depósitos minerais associados ao Complexo ultramáfico-alcalino de Catalão I – Goiás. In Schmaltz WH (ed) Os principais depósitos minerais da Região Centro Oeste. Brasília: DNPM 6, pp 139-183

Chackhmouradian AR and Mitchell RH (1998) Lueshite, pyrochlore and monazite-(Ce) from apatite-dolomite carbonatite, Lesnaya Varaka complex, Kola Peninsula, Russia. *Min Mag* 62:769-782

Chacko T, Mayeda TK, Clayton RN, Goldsmith JR (1991) Oxygen and carbon isotope fractionation between CO₂ and calcite. *Geochim Cosmochim Acta* 55:2867-2882

Clark AH e Kontak DJ (2004) Fe-Ti-P oxide melts generated through magma mixing in the Antauta subvolcanic center, Peru: Implications for the origin of nelsonite and iron oxide-dominated hydrothermal deposits. *Econ Geol* 99:377-395

Clayton RN and Keiffer SW (1991) Oxygen isotopic thermometer calibrations. In Taylor HP, O'Neil JR and Kaplan IR (eds) Stable Isotope Geochemistry: A tribute to Samuel Epstein, The Geochemical Society, Special Publication 3, pp 3-10

Clark AH and Kontak DJ (2004) Fe-Ti-P oxide melts generated through magma mixing in the Antauta subvolcanic center, Peru: Implications for the origin of nelsonite and iron oxide-dominated hydrothermal deposits. *Econ Geol* 99:377-395

Comin-Chiaromonti P, Gomes CB, Censi P, Speziale S (2005) Carbonatites from southeastern Brazil: a model for the carbon and oxygen isotope variations.. In: Comin-Chiaromonti P and Gomes CB (eds) Mesozoic to Cenozoic alkaline magmatism in the Brazilian Platform, 1st edn. Edusp/Fapesp, São Paulo, pp 629-650

Constanzo A, Moore KR, Wall F, Feely M (2006) Fluid inclusions in apatite from Jacupiranga calcite carbonatites: Evidence for a fluid-stratified carbonatite magma chamber. *Lithos* 91:208-228

Cordeiro PFO (2009) Petrologia e metalogenia do depósito primário de nióbio do Complexo Carbonatítico-Foscorítico de Catalão I, GO. Unpublished MSc thesis. University of Brasília, Brazil, p 140

Dawson JB, Steele IM, Smith JV, Rivers ML (1996) Minor and trace element chemistry of carbonates, apatites and magnetites in some African carbonatites. *Miner Magaz* 60:415-425

Dawson JB and Hinton RW (2003) Trace-element content and partitioning in calcite, dolomite and apatite in carbonatite, Phalaborwa, South Africa. *Min Mag* 67:921-930

Deer WA, Howie RA, Zussman J (1992) Minerais constituintes das rochas uma introdução. Lisboa Lisboa: Fundação Calouste Gulbenkian, pp 358

Deines P (1989) Stable isotope variations in carbonatites. In: Bell K (ed) Carbonatites: Genesis and Evolution, Unwin Hyman, London, pp 301-359

Demény A, Sitnikova MA, Karchevsky PI (2004) Stable C and O isotope compositions of carbonatite complexes of the Kola Alkaline Province: phoscorite-carbonatite relationships and source compositions. In: Wall F and Zaitsev AN (eds) Phoscorites and Carbonatites from Mantle to Mine: the Key Example of the Kola Alkaline Province, 1st ed. Mineralogical Society Series, London, pp 407-431

Downes H, Balaganskaya E, Beard A, Liferovich R, Demaiffe D (2005) Petrogenetic processes in the ultramafic, alkaline and carbonatite magmatism in the Kola Province: A review. *Lithos* 85:48-75

Dunworth EA and Bell K (2001) The Turiy Massif, Kola Peninsula. Russia: Isotopic and geochemical evidence for multi-source evolution. *J Petrol* 42:377-405

Dunworth E and Bell K (2003) The Turiy Massif, Kola Peninsula, Russia. Mineral chemistry of an ultramafic-alkaline-carbonatite intrusion. *Min Mag* 67:423-451

Dymek RF and Owens BT (2001) Petrogenesis of apatite-rich rocks (nelsonites and oxide-apatite gabbronorites) associated with massif anorthosites. *Econ Geol* 96:797-815

Eriksson SC (1989) Phalaborwa: a saga of magmatism, metasomatism and miscibility. In: Bell K (ed) Carbonatites: genesis and evolution, Unwin Hyman, London pp 221-254

Farmer GL and Boetcher AL (1981) Petrologic and crystal-chemical significance of some deep-seated phlogopites. *Am Min* 66:1154-1163

Fava N (2001) O manto de intemperismo e a química do pirocloro de Catalão I (GO): Um estudo preliminar: Unpublished MSc Thesis University of Brasília pp 124

French JE, Heaman LM, Chacko T (2002) Feasibility of chemical U-Th total Pb baddeleyite dating by electron microprobe. *Chem Geol* 188:85-104

Frietsch R (1978) On the magmatic origin of iron ores of the Kiruna type. *Econ Geol* 73:478-485

Fontana J (2006) Phoscorite-carbonatite pipe complexes a promising new platinum group element target in Brazil. *Plat Met Rev* 50:134-142

Gaspar JC and Wyllie PJ (1982) Barium phlogopite from the Jacupiranga carbonatite, Brazil. *Am Min* 67:997-1000

Gaspar JC and Wyllie PJ (1987) The phlogopites from the Jacupiranga carbonatite intrusions. *Min Petr* 36:121-134

Gaspar JC and Wyllie PJ (1983a) Magnetite in the carbonatites from the Jacupiranga complex, Brazil. *Am Min* 68:195-213

Gaspar JC and Wyllie PJ (1983b) Ilmenite (high Mg,Mn,Nb) in the carbonatites from the Jacupiranga complex, Brazil. *Am Min* 68:960-971

Gaspar JC, Araujo DP, Melo MVLC (1998) Olivine in carbonatitic and silicate rocks in carbonatite complexes. 7th Intern Kimberlite Conf Extended Absctract, pp. 239-241

Geijer P (1910) Igneous rocks and iron ores of Kiirunavaara, Luossavaara and Tuolluvaara. *Econ Geol* 5:699-718

Geisler T, Berndt J, Meyer HW, Pollok K, Putnis A (2004) Low temperature aqueous alteration of crystalline pyrochlore: correspondence between nature and experiment: *Min Mag* 68:905-922

Gibson SA, Thompson RN, Leonardos OH, Dickin AP, Mitchell JG (1995) The Late Cretaceous impact of the Trindade mantle plume – evidence from large-volume, mafic, potassic magmatism in SE Brazil. *J Petr* 36:189-229

Gierth E and Baecker ML (1986) A mineralização de nióbio e as rochas alcalinas associadas no complexo Catalão I, Goiás. In Schobbenhaus C (ed) Principais depósitos minerais do Brasil: MME/DNPM 2, Brasília, pp 455-462

Gioia SM and Pimentel MM (2000) A metodologia Sm-Nd no Laboratório de Geocronologia da Universidade de Brasília. An Acad Bras Cien 72:219-245

Gold DP, Eby GN, Bell K, Vallee M (1986) Carbonatites, diatremes, and ultra-alkaline rocks in the Oka area, Quebec. Joint Annual Meeting, Ottawa '86, Field Trip 21: Guidebook, pp 51

Grez E, Aguilar A, Henríquez F, Nyström JO (1991) Magnetita Pedernales: A new magmatic iron deposit in northern Chile. Econ Geol 86:1346-1349

Gullbrandsen RA (1966) Chemical composition of phosphorites of the Phosphoria Formation. Geochim Cosmochim Acta 30:769-778

Haggerty SE and Fung A (2006) Orbicular oxides in carbonatitic kimberlites: Am Min 91:1461–1472

Harlov DE, Andersson UB, Nyström JO, Förster HJ, Broman C, Dulski P (2002) Apatite-monazite relations in the Kiirunavaara magnetite-apatite iron ore, northern Sweden. Chem Geol 191:47-72

Heathcote RC and McCormick GR (1989) Major-cation substitution in phlogopite and evolution of carbonatite in the Potash Sulfur Springs complex, Garland County, Arkansas. Am Min 74: 132-140

Henríquez F and Martin RF (1978) Crystal-growth textures in magnetite flows and feeder dykes, El Laco, Chile. Can Min 16:581-589

Henríquez F, Naslund HR, Nyström JO, Vivallo W, Aguirre R, Dobbs FM, Lledó H (2003) New field evidence bearing on the origin of the El Laco magnetite deposit, northern Chile—a discussion. Econ Geol 98:1497–1500

Hildebrand RS (1986) Kiruna-type deposits: Their origin and relationship to intermediate subvolcanic plutons in the Great Bear magmatic zone, Northwest Canada. Econ Geol 81:640-659

Hirano H, Kamitani M, Sato T, Sudo S (1990) Niobium mineralization of Catalao I carbonatite complex, Goias, Brazil. Bull Geol Surv Japan 41:619-626

Hogarth DD (1977) Classification and nomenclature of the pyrochlore group. Am Min 62: 403-410.

Hogarth DD, Hartree R, Loop J, Solberg TN (1985) Rare-earth element minerals in four carbonatites near Gatineau, Quebec. Am Min 70:1135-1142

Hogarth DD (1989) Pyrochlore, apatite and amphibole: distinctive minerals in carbonatite. In Bell K (ed) Carbonatites – Genesis and evolution, Unwin Hyman, London, pp 105-148

Hogarth DD, Williams CT, Jones P (2000) Primary zoning in pyrochlore group minerals from carbonatites. Min Mag 64:683-697

Irber W (1999) The lanthanide tetrad effect and its correlation with K/Rb, Eu/Eu*, Sr/Eu, Y/Ho, and Zr/Hf of evolving peraluminous granite suites. Geochim Cosmochim Acta 63:489–508

Issa Filho A, Lima PRAS, Souza OM (1984) Aspectos da geologia do complexo carbonatítico do Barreiro, Araxá, MG, Brasil. In CBMM (ed) Complexos Carbonatíticos do Brasil, CBMM, São Paulo, pp 20-44

Jahn B, Wu F, Capdevila R, Martineau F, Zhao Z and Wang Y (2001) Highly evolved juvenile granites with tetrad REE patterns: the Woduhe and Baerzhe granites from the Great Xing'an Mountains in NE China. *Lithos* 59:171-198

Karchevsky PI and Moutte J (2004) The phoscorite-carbonatite complex of Vuorijarvi, northern Karelia. In: Wall F and Zaitsev AN (eds) Phoscorites and Carbonatites from Mantle to Mine: the Key Example of the Kola Alkaline Province, 1st ed. Mineralogical Society Series, London, pp 163-169

Kempe U and Götze J (2002) Cathodoluminescence (CL) behaviour and crystal chemistry of apatite from rare-metal deposits. *Min Mag* 66:135–156

Kerr AC, Kempton PD, Thompson RN (1995) Crustal assimilation during turbulent magma ascent (ATA); new isotopic evidence from the Mull Tertiary lava succession, N.W. Scotland. *Contr Min Petrol* 119:142-154

Klemme S and Dalpe C (2003) Trace-element partitioning between apatite and carbonatite melt. *Am Min* 88:639-646

Knudsen C (1989) Pyrochlore group minerals from the Qaqarssuk carbonatite complex. In Möller P, Cerný P, Saupé F (eds) Lanthanides, Tantalum and Niobium. Springer-Verlag, Berlin and Heidelberg, pp 80-99

Kolker A (1982) Mineralogy and geochemistry of Fe-Ti oxide and apatite (nelsonite) deposits and evaluation of the liquid immiscibility hypothesis. *Econ Geol* 77:1146-1158

Krasnova NI, Petrov TG, Balaganskaya EG, Garcia D, Moutte D, Zaitsev AN, Wall F (2004a) Introduction to phoscorites: occurrence, composition, nomenclature and petrogenesis. In: Wall F and Zaitsev AN (eds) Phoscorites and Carbonatites from Mantle to Mine: the Key Example of the Kola Alkaline Province, 1st ed. Mineralogical Society Series, London, pp 45-79

Krasnova NI, Balaganskaya EG, Garcia D (2004b) Kovdor – classic phoscorites and carbonatites. In: Wall F and Zaitsev AN (eds) Phoscorites and Carbonatites from Mantle to Mine: the Key Example of the Kola Alkaline Province, 1st ed. Mineralogical Society Series, London, pp 99-132

Lapin, AV (1982) Carbonatite differentiation processes. *Int Geol Rev* 24:1079-1090

Lapin AV and Vartiainen H (1983) Orbicular and spherulitic carbonatites from Sokli and Vuorijarvi. *Lithos* 16:53–60

Le Bas MJ (1985) Nephelinites and Carbonatites. *J Geol Soc London* pp 704

Le Bas MJ (1989) Diversification of carbonatite. In Bell K (ed.) Carbonatites: genesis and evolution. Unwin Hyman, London, pp 1-14.

Lee MJ, Garcia D, Moutte J, Lee JI (2003) Phlogopite and tetraferriphlogopite from phoscorite and carbonatite associations in the Sokli massif, Northern Finland. *Geosc Journal* 7:9-20

Lee MJ, Garcia D, Moutte J, Williams CT, Wall F (2004) Carbonatites and phoscorites from the Sokli complex, Finland. In: Wall F and Zaitsev AN (eds) Phoscorites and Carbonatites from Mantle to Mine: the Key Example of the Kola Alkaline Province, 1st ed. Mineralogical Society Series, London, pp 133–162

Lee MJ, Lee JI, Moutte J (2005) Compositional variation of Fe-Ti oxides from the Sokli complex, northeastern Finland. *Geosc Journal* 9:1-13

Lee MJ, Lee JI, Garcia D, Moutte J, Williams CT, Wall F, Kim Y (2006) Pyrochlore chemistry from the Sokli phoscorite-carbonatite complex, Finland: Implications for the genesis of phoscorite and carbonatite association. *Geochem Journal* 40:1-13

Lugmair GW and Marti K (1978) Lunar initial $^{143}\text{Nd}/^{144}\text{Nd}$: Differential evolution of the lunar crust and mantle. *Earth Plan Sci Let* 39:349-357

Lumpkin GR and Ewing RC (1995) Geochemical alteration of pyrochlore group minerals: pyrochlore subgroup. *Am Min* 80:732-743

Machado Júnior DL (1992) Geologia do complexo alcalino-carbonatítico de Catalão II (GO). 37° Congr Bras Geol, São Paulo pp 94-95

Mariano AN (1989) Nature of economic mineralization in carbonatites and related rocks. In Bell K (ed) Carbonatites – Genesis and evolution, Unwin Hyman, London, pp 149–176

Mariano AN and Marchetto M (1991) Serra Negra and Salitre – carbonatite alkaline igneous complex. In Leonardos OH, Meyer HOA, Gaspar JC (eds) 5th International Kimberlite Conference (Field Guide Book). CPRM, Special Publication, Brazil 3/91:75-79

McCrea JM (1950) On the isotopic chemistry of carbonates and paleotemperature scale. *J Chem Phys* 18:849-857

Mitchell RH (1978) Manganese magnesian ilmenite and titanian clinohumite from the Jacupiranga carbonatite, São Paulo, Brazil. *Am Min* 63:544-547

Mitchell RH and Bergman SC (1991) Petrology of Lamproites. New York:Plenum Press, pp 440

Mitchell RH (1995) Kimberlites, Orangeites and Related Rocks. New York:Plenum Press, pp 410

Monecke T, Kempe U, Monecke J, Sala M, Wolf D (2002) Tetrad effect in rare earth element distribution patterns: a method of quantification with application to rock and mineral samples from granite-related rare metal deposits. *Geochim Cosmochim Acta* 66:1185-1196

Morikiyo T, Hirano H, Matsushita Y (1990) Carbon and oxygen isotopic composition of the carbonatites from Jacupiranga and Catalão I carbonatite complexes, Brazil. *Bull Geol Surv Japan* 41:619-626

Mücke A and Younessi R (1994) Magnetite–apatite deposits, Kiruna-type, along the Sanandaj-Sirjan and in the Bafq area, Iran, associated with ultramafic and calcalkaline rocks and carbonatites. *Min Petr* 50:219–44

Nasraoui M and Bilal E (2000) Pyrochlores from the Lueshe carbonatite complex (Democratic Republic of Congo): a geochemical record of different alteration stages. *J Asian Earth Sci* 18:237-251

Nyström JO and Henríquez F (1994) Magmatic Features of Iron Ores of the Kiruna Type in Chile and Sweden: Ore Textures and Magnetite Geochemistry. *Econ Geol* 89:820-839

Oliveira IWB, Sachs LLB, Silva VA, Batista IH (2004) Folha SE.23-Belo Horizonte. In: Schobbenhaus C, Gonçalves JH, Santos JOS, Abram MB, Leão Neto R, Matos GMM, Vicotti RM, Ramos MAB, Jesus JDA (eds) Carta geológica do Brasil ao millionésimo: Sistema de Informações Geográficas – SIG e 46 folhas na escala 1: 1.000.000. CPRM, Brasília, Brazil, CD-ROM Pack

Oliveira RC, Barbosa ESR, Junqueira-Brod TC, Brod JÁ (2007) Petrografia e mineralogia de estruturas orbiculares do complexo alcalino-carbonatítico de Salitre, MG. In: 4º Congresso de Iniciação Científica do DF/XIII Congresso de Iniciação Científica da UnB, Brasília, Anais CD-ROM

Palmieri M, Pereira GSB, Brod JÁ, Junqueira-Brod TC, Petrinovic IA, Ferrari AJD (2008) Orbicular magnetite from the Catalão I phoscorite-carbonatite complex. 9th Intern Kimberlite Conf Extended Abstract, 9IKC-A-00337

Park CFJ (1961) A magnetite “flow” in northern Chile. Econ Geol 56:431-436

Philpotts AR (1967) Origin of certain iron-titanium oxide and apatite rocks. Econ Geol 62:303-315

Ribeiro CC, Brod JA, Gaspar JC, Petrinovic IA, Junqueira-Brod TC (2001) Pipes de Brecha e Atividade Magmática Explosiva no Complexo Carbonatítico de Catalao I, GO. Rev Bras Geoc 31: 417-426

Ribeiro CC, Brod JA, Junqueira-Brod TC, Gaspar JC, Petrinovic IA (2005) Mineralogical and field aspects of magma-fragmentation deposits in a carbonate-phosphate magma chamber: evidence from the Catalão I Complex, Brazil. J South Am Earth Sci 18:355-369

Ribeiro, CC (2008) Geologia, geometalurgia, controles e gênese dos depósitos de fósforo, terras raras e titânio do complexo carbonatítico Catalão I, GO. Unpublished Ph.D. Thesis. University of Brasília pp 478

Rieder M, Cavazzini G, D'Yakonov YS, Frank-Kamenetskii VA, Gottardi G, Guggenheim S, Koval PV, Müller G, Neiva AMR, Radoslovich EW, Robert JL, Sassi FP, Takeda H, Wiss Z, Wones DR (1998) Nomenclature of the micas. Can Min 36:905-912

Rudashevski, N.S., Kretser, Y.L., Rudashevsky, V.N., and Sukharzhevskaya, E.S., 2004, A review and comparison of PGE, noble-metal and sulphide mineralization in phoscorites and carbonatites from Kovdor and Phalaborwa, In: Wall F and Zaitsev AN (eds) Phoscorites and Carbonatites from Mantle to Mine: the Key Example of the Kola Alkaline Province, 1st ed. Mineralogical Society Series, London, pp 375-405

Santos RV & Clayton RN (1995) Variations of oxygen and carbon isotopes in carbonatites: a study of Brazilian alkaline complexes. Geoch Cosm Acta 59:1339-1352

Sililitoe RH and Burrows DR (2002) New field evidence bearing on the origin of the El Laco magnetite deposit, northern Chile. Econ Geol 97:1101-1109

Silva AB (1986) Jazida de nióbio de Araxá, Minas Gerais. In Schobbenhaus C (ed) Principais depósitos minerais do Brasil, MME/DNPM 2, Brasília, pp 435-453

Sonoki IK and Garda G.M (1988) Idades K-Ar de rochas alcalinas do Brasil Meridional e Paraguai Oriental: compilação e adaptação as novas constantes de decaimento. Bol. IG USP Serie Científica 19:63-85

Stoppa F and Cundari A (1995) A new Italian carbonatite occurrence at Cupaello (Rieti) and its genetic significance. Contrib Min Petrol 122:275-288

Stoppa F, Sharygin VV, Cundari A (1997) New data from the carbonatite-kamafugite association: The melilitolite from Pian di Celle, Italy. *Min and Petrol* 61:27-45

Takahashi Y, Yoshida H, Sato N, Hama K, Yusa Y, Shimizu H (2002) W- and M-type tetrad effects in REE patterns for water-rock systems in Tono uranium deposit, central Japan. *Chem Geol* 184:311-335

Takahashi Y, Châtelier X, Hattori KH, Kato K, Fortin D (2005) Adsorption of rare earth elements onto bacterial cells and its implication for REE sorption onto natural microbial mats. *Chem Geol* 219:53-67

Tither G (2001) Progress in Niobium Markets and Technology 1981-2001. In: Proceedings of the International Symposium Niobium, Orlando, Florida, USA, 1-25

Taylor HP, Frechen J, Degens ET (1967) Oxygen and carbon isotope studies of carbonatites from the Laacher See District, West Germany and the Alno District, Sweden. *Geoch Cosm Acta* 31: 407-430

Thompson RN, Gibson SA, Mitchell JG, Dickin P, Leonardos OH, Brod JA, Greenwood JC (1998) Migrating Cretaceous-Eocene magmatism in the Serra do Mar alkaline province, SE Brazil: melts from the deflected Trindade mantle plume? *J Petr* 39:1439-1526

Toledo MCM and Pereira VP (2001) A variabilidade de composição da apatita associada a carbonatitos. *Rev Instituto Geológico* 22:27-64

Torres MG (1996) Caracterização mineralógica do minério fosfático da Arafértil S.A., no Complexo Carbonatítico de Barreiro, Araxá, MG. Unpublished M.Sc. Thesis, University of Brasília, 149 pp

Toyoda K, Horiuchi H, Tokonami M (1994) Dupal anomaly of Brazilian carbonatite: geochemical correlation with hotspots in the South atlantic and implications for the mantle source. *Earth Plan Sci Let* 126:315-331

Traversa G, Gomes CB, Brotzu P, Buraglini N, Morbidelli L, Principato MS, Ronca S, Ruberti E (2001) Petrography and mineral chemistry of carbonatites and mica-rich rocks from the Araxá complex (Alto Paranaíba Province, Brazil). *An Acad Bras Cien* 73:71-98

Veksler IV, Dorfman AM, Kamenetsky M, Dulski P and Dingwell DB (2005) Partitioning of lanthanides and Y between immiscible silicate and fluoride melts, fluorite and cryolite and the origin of the lanthanide tetrad effect in igneous rocks. *Geochim Cosmochim Acta* 69: 2847-2860

Verhulst A, Balaganskaya E, Kirnarsky Y, Demaiffe D (2000) Petrological and geochemical (trace elements and Sr-Nd isotopes) characteristics of the Paleozoic Kovdor ultramafic, alkaline and carbonatite intrusion (Kola Peninsula, NW Russia). *Lithos* 51:1-25

Williams CT, Wall F, Woolley AR, Phillip S (1997) Compositional variation in pyrochlore from the Bingo carbonatite, Zaire. *J African Earth Sci* 25:137-145

Woolley AR and Kempe DRC (1989) Carbonatites: nomenclature, average chemical compositions, and element distribution. In: Bell K (ed) *Carbonatites: Genesis and Evolution*, Unwin Hyman, pp 1-14

Yang Z and Woolley A (2006) Carbonatites in China: a review. *J Asian Earth Sci* 27:559-575

Yegorov LS (1993) Phoscorites of the Maymecha-Kotuy ijolite-carbonatite association. *Int Geol Rev* 35:346-358

Yuhara M, Hirahara Y, Nishi N, Kagami H (2005) Rb-Sr, Sm-Nd of the Phalaborwa Carbonatite Complex, South Africa. *Polar Geosc* 18:101-113

Zaitsev A and Bell K (1995) Sr and Nd isotope data of apatite, calcite and dolomite as indicators of source, and the relationships of phoscorites and carbonatites. *Contrib Min Petr* 121:324–335

Zhao ZF and Zheng YF (2003) Calculation of oxygen isotope fractionation in magmatic rocks. *Chem Geol* 193:59-80

Zheng YF (1990) Carbon-Oxygen Isotopic Covariation in Hydrothermal Calcite During Degassing of CO₂ - a Quantitative-Evaluation and Application to the Kushikino Gold Mining Area in Japan. *Miner Deposit* 25:246-250

Zurevinski SE and Mitchell RH (2004) Extreme compositional variation of pyrochlore-group minerals at the Oka carbonatite complex, Quebec: Evidence of Magma Mixing? *Can Min* 42:1159-1168

ANEXOS

Tabela A – Composição química da apatita

Tabela B- Composição química da flogopita e tetra-ferriflogopita

Tabela C- Composição química da magnetita

Tabela D- Composição química da clino-humita

Tabela E- Composição química da ilmenita

Tabela F- Composição química do pirocloro

Tabela G- Composição química do carbonato

Tabela H – Análises de Rocha Total

Tabela I – Análises de isótopos estáveis de C-O e radiogênicos Sr-Sm-Nd

Tabela A – Análises de apatita de rochas foscoríticas e glimerito de Catalão I. As análises foram recalculadas para 25 oxigênios.

Amostra	110-														056-1-						
	110- 46-2-1	110- 46-2-2	110- 46-2-3	110- 46-2-4	110- 46-5-5	46-2- 6B	110- 46-2-7	F4-2-1	F4-2-2	F4-2-3	F4-2-4	F4-2-5	F4-2-6	F4-2-7	1B	056-1- 2	056-1- 3	056-1- 4	093-3- 1B	093-3-2	
Coord	0	10	19	33		58	71	0	10	19	25	34	43	53	0	10	14	19	5	14	
Unidade	P1	P1	P1	P1	P1	P1	P1	P1	P1	P1	P1	P1	P1	P1	DC	DC	DC	DC	DC	DC	
Posição	interm	interm	núcleo	núcleo	interm	borda	borda	borda	interm	interm	núcleo	núcleo	interm	borda	núcleo	interm	interm	interm	borda	interm	
Oxidos (%)																					
P ₂ O ₅	41.42	40.78	41.13	40.16	40.72	40.89	41.43	42.08	42.91	42.24	42.47	42.05	42.41	42.35	40.40	39.82	40.37	39.91	40.56	41.71	
SiO ₂	1.05	1.06	1.01	1.02	0.97	0.89	0.70	0.19	0.05	0.16	0.12	0.09	0.05	0.09	0.00	0.00	0.00	0.00	0.00	0.00	
Na ₂ O	0.00	0.00	0.00	0.00	0.00	0.00	0.00	0.00	0.00	0.00	0.00	0.00	0.00	0.00	0.00	0.51	0.06	0.51	0.48	0.00	
K ₂ O	0.02	0.01	0.00	0.00	0.00	0.00	0.00	0.02	0.00	0.02	0.00	0.01	0.01	0.00	0.04	0.06	0.04	0.03	0.01	0.00	
MgO	0.01	0.04	0.07	0.02	0.03	0.05	0.00	0.14	0.03	0.02	0.09	0.07	0.04	0.01	0.12	0.17	0.11	0.08	0.03	0.00	
FeO	0.00	0.00	0.04	0.01	0.03	0.08	0.02	0.22	0.01	0.05	0.03	0.03	0.03	0.16	1.09	0.09	0.10	0.04	0.04	0.01	
CaO	51.99	51.74	51.81	52.05	51.19	52.29	52.59	53.18	53.99	53.35	53.70	53.88	53.17	53.11	50.76	50.70	51.28	50.79	48.18	50.11	
SrO	0.86	0.87	1.04	0.94	1.00	0.69	0.62	0.82	0.80	0.72	0.93	0.76	0.72	0.84	3.09	4.00	3.30	3.58	3.34	2.98	
BaO	0.03	0.00	0.00	0.03	0.00	0.00	0.00	0.00	0.04	0.08	0.00	0.00	0.00	0.00	0.03	0.19	0.05	0.04	0.22	0.03	
La ₂ O ₃	0.48	0.36	0.47	0.38	0.61	0.64	0.35	0.14	0.24	0.21	0.26	0.10	0.18	0.35	0.65	0.28	0.51	0.49	1.17	0.58	
Ce ₂ O ₃	1.18	1.05	1.00	1.26	0.91	0.88	0.92	0.55	0.32	0.62	0.47	0.38	0.53	0.59	0.90	0.82	0.64	0.69	1.79	1.41	
Al ₂ O ₃	0.00	0.01	0.04	0.00	0.00	0.02	0.00	0.00	0.00	0.01	0.00	0.00	0.00	0.01	0.00	0.00	0.03	0.01	0.01	0.00	
Total	97.02	95.91	96.61	95.85	95.44	96.41	96.65	97.33	98.39	97.47	98.09	97.37	97.11	97.50	97.08	96.62	96.45	96.18	95.83	96.84	
Cations (p.f.u.)																					
P	5.9433	5.9226	5.9348	5.8656	5.9480	5.9206	5.9648	6.0196	6.0635	6.0324	6.0317	6.0158	6.0661	6.0494	5.9331	5.8995	5.9499	5.9197	6.0211	6.0662	
Si	0.1778	0.1810	0.1715	0.1755	0.1670	0.1529	0.1189	0.0314	0.0088	0.0277	0.0205	0.0159	0.0081	0.0157	0.0000	0.0000	0.0000	0.0000	0.0000	0.0000	
Na	0.0000	0.0000	0.0000	0.0000	0.0000	0.0000	0.0000	0.0000	0.0000	0.0000	0.0000	0.0000	0.0000	0.0000	0.1727	0.0216	0.1733	0.1625	0.0000	0.0000	
K	0.0045	0.0013	0.0009	0.0000	0.0000	0.0000	0.0000	0.0047	0.0002	0.0041	0.0000	0.0015	0.0011	0.0000	0.0095	0.0129	0.0080	0.0072	0.0031	0.0000	
Mg	0.0025	0.0097	0.0170	0.0049	0.0064	0.0135	0.0005	0.0358	0.0085	0.0048	0.0228	0.0184	0.0091	0.0018	0.0300	0.0444	0.0286	0.0219	0.0073	0.0000	
Fe ²⁺	0.0000	0.0000	0.0105	0.0014	0.0072	0.0220	0.0057	0.0630	0.0031	0.0141	0.0070	0.0076	0.0076	0.0454	0.3162	0.0252	0.0277	0.0126	0.0126	0.0037	
Ca	9.4410	9.5094	9.4608	9.6203	9.4631	9.5822	9.5820	9.6283	9.6561	9.6430	9.6508	9.7549	9.6246	9.6015	9.4333	9.5059	9.5654	9.5339	9.0524	9.2216	
Sr	0.0845	0.0867	0.1028	0.0937	0.0998	0.0682	0.0615	0.0803	0.0775	0.0707	0.0908	0.0743	0.0701	0.0822	0.3111	0.4057	0.3328	0.3637	0.3393	0.2971	
Ba	0.0019	0.0000	0.0000	0.0020	0.0000	0.0000	0.0000	0.0000	0.0026	0.0053	0.0000	0.0000	0.0000	0.0000	0.0018	0.0127	0.0036	0.0027	0.0153	0.0018	
La	0.0299	0.0229	0.0292	0.0241	0.0388	0.0404	0.0219	0.0087	0.0145	0.0129	0.0163	0.0060	0.0113	0.0216	0.0416	0.0179	0.0329	0.0313	0.0755	0.0367	
Ce	0.1393	0.1261	0.1195	0.1515	0.1100	0.1048	0.1089	0.0647	0.0369	0.0734	0.0555	0.0449	0.0624	0.0697	0.1095	0.1003	0.0780	0.0838	0.2187	0.1686	
Al	0.0000	0.0010	0.0072	0.0000	0.0000	0.0048	0.0000	0.0000	0.0008	0.0028	0.0000	0.0000	0.0000	0.0010	0.0000	0.0000	0.0062	0.0017	0.0028		
Sum	15.825	15.861	15.854	15.939	15.840	15.905	15.869	15.936	15.872	15.889	15.898	15.939	15.860	15.887	16.187	16.197	16.048	16.156	15.910	15.799	

Tabela A – Análises de apatita de rochas foscoríticas e glimerito de Catalão I. As análises foram recalculadas com base em 25 O. (Cont. I)

Amostra	093-3-3	093-3-4	093-3-5	093-3-6	099A-5-1	099A-5-2	099A-5-3	099A-5-4	099A-5-5	099A-5-5B	099B-4L-01	099B-4L-02	099B-4L-04	099B-4L-05	099B-4L-06	099B-4L-07	099B-4L-08	099B-4L-09	099B-4L-10	116-1L-1
Coord	14	22	30	36	0	3	6	9	12	12.5	1	4	12	17	21	25	30	34	38	0
Unidade	DC	DC	DC	DC	DC	DC	DC	DC	DC	DC	DC	DC	DC	DC	DC	DC	DC	DC	DC	DC
Posição	núcleo	núcleo	interm	borda	borda	interm	núcleo	núcleo	interm	interm	borda	borda	núcleo	núcleo	núcleo	núcleo	borda	borda	borda	borda
Oxidos (%)																				
P ₂ O ₅	41.84	41.95	42.39	39.95	42.09	40.81	41.86	42.02	40.79	40.29	41.07	41.73	42.05	43.44	41.96	42.75	42.34	41.05	41.94	39.94
SiO ₂	0.05	0.03	0.00	0.00	0.00	0.00	0.00	0.00	0.00	0.00	0.00	0.00	0.04	0.02	0.00	0.00	0.01	0.03	0.00	0.00
Na ₂ O	0.00	0.00	0.10	0.64	0.00	0.00	0.00	0.30	0.00	0.33	0.00	0.00	0.00	0.00	0.00	0.00	0.09	0.00	0.19	0.07
K ₂ O	0.00	0.00	0.01	0.04	0.02	0.00	0.02	0.01	0.04	0.01	0.02	0.02	0.00	0.00	0.01	0.00	0.02	0.05	0.02	0.02
MgO	0.05	0.00	0.02	0.05	0.00	0.11	0.09	0.06	0.03	0.10	0.04	0.07	0.09	0.06	0.00	0.04	0.00	0.04	0.03	0.06
FeO	0.00	0.00	0.03	0.07	0.47	0.00	0.02	0.00	0.07	0.01	0.65	0.15	0.03	0.00	0.00	0.05	0.38	0.43	0.29	
CaO	54.06	53.66	53.06	47.47	50.64	50.53	50.08	50.17	49.40	48.65	50.32	50.51	53.17	53.86	53.68	53.74	51.33	49.19	49.79	49.29
SrO	0.81	0.90	1.15	3.32	3.45	4.05	3.59	3.63	3.45	3.73	3.40	3.61	1.30	1.18	1.50	1.38	3.48	3.72	3.57	4.84
BaO	0.09	0.00	0.11	0.12	0.11	0.07	0.06	0.09	0.04	0.16	0.00	0.01	0.00	0.07	0.12	0.01	0.11	0.03	0.12	0.00
La ₂ O ₃	0.11	0.24	0.31	0.98	0.37	0.16	0.37	0.23	0.71	0.83	0.55	0.49	0.08	0.11	0.23	0.31	0.19	0.33	0.53	0.38
Ce ₂ O ₃	0.22	0.60	0.42	1.94	0.85	0.59	0.81	0.65	1.37	1.27	1.27	1.08	0.31	0.40	0.47	0.41	0.82	1.21	1.37	1.30
Al ₂ O ₃	0.00	0.00	0.00	0.00	0.01	0.02	0.00	0.00	0.03	0.00	0.03	0.00	0.01	0.01	0.00	0.01	0.06	0.01	0.00	
Total	97.24	97.38	97.59	94.56	97.99	96.32	96.91	97.16	95.90	95.41	97.31	97.70	97.07	99.13	97.98	98.64	98.44	96.07	97.99	96.18
Cations (p.f.u.)																				
P	6.0061	6.0147	6.0606	6.0085	6.0650	6.0078	6.0842	6.0908	6.0272	6.0072	5.9929	6.0399	6.0413	6.0896	6.0051	6.0517	6.0625	6.0436	6.0570	5.9479
Si	0.0083	0.0042	0.0000	0.0007	0.0000	0.0000	0.0000	0.0000	0.0000	0.0000	0.0000	0.0000	0.0059	0.0033	0.0000	0.0000	0.0020	0.0056	0.0000	0.0000
Na	0.0000	0.0000	0.0314	0.2208	0.0000	0.0000	0.0000	0.0992	0.0000	0.1141	0.0000	0.0000	0.0000	0.0000	0.0000	0.0000	0.0289	0.0000	0.0612	0.0225
K	0.0000	0.0000	0.0013	0.0079	0.0046	0.0000	0.0046	0.0020	0.0085	0.0018	0.0040	0.0044	0.0002	0.0002	0.0019	0.0006	0.0037	0.0118	0.0037	0.0045
Mg	0.0129	0.0000	0.0053	0.0119	0.0000	0.0283	0.0228	0.0145	0.0081	0.0252	0.0095	0.0173	0.0233	0.0148	0.0005	0.0087	0.0000	0.0099	0.0066	0.0147
Fe ²⁺	0.0000	0.0000	0.0076	0.0193	0.1327	0.0000	0.0055	0.0000	0.0210	0.0041	0.1876	0.0426	0.0094	0.0000	0.0000	0.0000	0.0150	0.1096	0.1227	0.0850
Ca	9.8199	9.7370	9.6004	9.0344	9.2344	9.4137	9.2126	9.2029	9.2388	9.1808	9.2910	9.2527	9.6670	9.5550	9.7221	9.6270	9.3025	9.1647	9.0995	9.2884
Sr	0.0791	0.0887	0.1126	0.3418	0.3405	0.4085	0.3573	0.3606	0.3490	0.3811	0.3395	0.3576	0.1278	0.1128	0.1465	0.1334	0.3409	0.3751	0.3533	0.4932
Ba	0.0062	0.0000	0.0070	0.0083	0.0076	0.0048	0.0038	0.0057	0.0029	0.0108	0.0000	0.0009	0.0000	0.0043	0.0078	0.0009	0.0075	0.0017	0.0079	0.0000
La	0.0070	0.0147	0.0190	0.0641	0.0230	0.0099	0.0232	0.0143	0.0454	0.0539	0.0350	0.0309	0.0049	0.0064	0.0145	0.0189	0.0117	0.0209	0.0336	0.0244
Ce	0.0264	0.0713	0.0498	0.2406	0.1011	0.0720	0.0976	0.0782	0.1670	0.1559	0.1531	0.1291	0.0365	0.0465	0.0558	0.0481	0.0966	0.1463	0.1627	0.1600
Al	0.0000	0.0000	0.0000	0.0000	0.0016	0.0045	0.0000	0.0000	0.0062	0.0000	0.0054	0.0000	0.0020	0.0026	0.0000	0.0018	0.0113	0.0014	0.0008	
Sum	15.966	15.931	15.895	15.958	15.909	15.947	15.816	15.868	15.941	16.012	15.881	15.916	15.835	15.957	15.889	15.873	15.900	15.910	16.041	

Tabela A – Análises de apatita de rochas foscoríticas e glimerito de Catalão I. As análises foram recalculadas com base em 25 O. (Cont. II)

Amostra	116-1L-2	116-1L-3	116-1L-4	116-1L-5	116-1L-6	116-1L-7	116-2-1	116-2-2	116-2-3	116-2-4	116-2-5	116-2-6	149-4L-02	149-4L-05	149-4L-06	149-4L-09	149-4L-10	149-4L-12	149-4L-13	149-4L-14
Coord	6	11	17	22	27	32	5	12	19	25	31	35								
Unidade	DC	DC	DC	DC	DC	DC	DC	DC	DC	DC	DC	DC	DC	DC	DC	DC	DC	DC	DC	
Posição	núcleo	núcleo	núcleo	interm	interm	borda	borda	interm	interm	núcleo	núcleo	borda								
Oxidos (%)																				
P ₂ O ₅	42.09	41.43	42.24	40.43	41.74	38.16	41.52	42.49	42.44	43.17	43.18	41.90	40.46	40.76	40.30	40.64	40.57	40.13	40.66	41.19
SiO ₂	0.00	0.00	0.00	0.02	0.02	0.00	0.00	0.00	0.00	0.00	0.00	0.00	0.43	0.00	0.02	0.00	0.00	0.16	0.00	0.13
Na ₂ O	0.00	0.00	0.00	0.00	0.00	0.18	0.06	0.00	0.00	0.00	0.00	0.09	0.00	0.00	0.44	0.00	0.27	0.35	0.00	0.00
K ₂ O	0.00	0.05	0.00	0.03	0.02	0.02	0.01	0.00	0.00	0.00	0.00	0.02	0.13	0.03	0.04	0.00	0.01	0.15	0.01	0.06
MgO	0.03	0.06	0.01	0.08	0.00	0.15	0.07	0.03	0.00	0.02	0.04	0.01	0.15	0.08	0.03	0.00	0.01	0.13	0.00	0.13
FeO	0.08	0.11	0.12	0.10	0.16	0.52	0.09	0.01	0.03	0.00	0.06	0.00	1.05	0.12	0.08	0.00	0.02	0.48	0.00	0.20
CaO	51.99	52.59	53.44	48.67	50.57	47.49	49.81	51.70	52.33	53.35	53.75	49.93	46.70	48.86	48.21	48.51	48.03	46.41	47.73	46.44
SrO	1.63	1.49	1.77	3.91	3.65	6.23	4.10	1.75	1.71	1.68	1.49	4.67	5.36	5.93	5.06	5.43	5.13	5.36	5.42	5.40
BaO	0.00	0.18	0.00	0.00	0.00	0.10	0.17	0.08	0.00	0.00	0.11	0.09	0.28	0.15	0.01	0.07	0.00	0.09	0.00	0.03
La ₂ O ₃	0.30	0.21	0.17	0.47	0.23	0.32	0.43	0.30	0.43	0.08	0.09	0.01	0.33	0.94	0.54	0.72	0.94	1.00	0.91	0.83
Ce ₂ O ₃	0.77	0.52	0.67	1.25	0.56	1.25	1.20	0.94	0.56	0.38	0.38	0.03	1.58	1.92	1.21	1.82	2.00	1.71	2.40	1.64
Al ₂ O ₃	0.00	0.06	0.00	0.12	0.10	0.01	0.00	0.00	0.01	0.00	0.01	0.03	0.62	0.00	0.06	0.02	0.01	0.16	0.00	0.04
Total	96.89	96.69	98.42	95.06	97.05	94.43	97.45	97.30	97.50	98.67	99.10	96.78	97.10	98.79	96.00	97.21	97.00	96.11	97.12	96.09
Cations (p.f.u.)																				
P	6.0679	6.0086	6.0169	6.0254	6.0624	5.8676	6.0431	6.0946	6.0798	6.0929	6.0738	6.1103	5.9519	5.9545	5.9998	5.9940	5.9951	5.9916	6.0029	6.0974
Si	0.0000	0.0000	0.0000	0.0032	0.0038	0.0000	0.0000	0.0000	0.0000	0.0000	0.0000	0.0000	0.0752	0.0000	0.0042	0.0000	0.0000	0.0275	0.0000	0.0226
Na	0.0000	0.0000	0.0000	0.0000	0.0000	0.0644	0.0203	0.0000	0.0000	0.0000	0.0000	0.0304	0.0000	0.0000	0.1514	0.0000	0.0917	0.1210	0.0000	0.0000
K	0.0002	0.0101	0.0000	0.0058	0.0044	0.0044	0.0022	0.0000	0.0000	0.0000	0.0000	0.0033	0.0284	0.0070	0.0087	0.0000	0.0018	0.0340	0.0013	0.0136
Mg	0.0076	0.0143	0.0018	0.0205	0.0000	0.0398	0.0172	0.0066	0.0000	0.0047	0.0107	0.0033	0.0391	0.0196	0.0071	0.0010	0.0018	0.0337	0.0010	0.0341
Fe ²⁺	0.0222	0.0327	0.0346	0.0297	0.0450	0.1570	0.0259	0.0020	0.0093	0.0000	0.0178	0.0000	0.3051	0.0352	0.0238	0.0012	0.0058	0.1425	0.0000	0.0594
Ca	9.4845	9.6516	9.6333	9.1798	9.2961	9.2410	9.1748	9.3844	9.4869	9.5275	9.5696	9.2162	8.6946	9.0327	9.0832	9.0533	8.9803	8.7689	8.9184	8.6991
Sr	0.1606	0.1476	0.1723	0.3988	0.3632	0.6564	0.4084	0.1722	0.1673	0.1623	0.1433	0.4665	0.5401	0.5933	0.5159	0.5489	0.5196	0.5477	0.5477	0.5479
Ba	0.0000	0.0123	0.0000	0.0000	0.0000	0.0074	0.0114	0.0052	0.0000	0.0000	0.0068	0.0061	0.0190	0.0103	0.0009	0.0044	0.0000	0.0061	0.0000	0.0018
La	0.0190	0.0131	0.0102	0.0303	0.0146	0.0215	0.0270	0.0186	0.0265	0.0048	0.0056	0.0008	0.0210	0.0599	0.0350	0.0461	0.0606	0.0647	0.0584	0.0533
Ce	0.0918	0.0622	0.0785	0.1534	0.0672	0.1584	0.1435	0.1109	0.0665	0.0436	0.0435	0.0038	0.1920	0.2312	0.1483	0.2209	0.2441	0.2103	0.2916	0.2001
Al	0.0000	0.0123	0.0000	0.0251	0.0198	0.0024	0.0004	0.0000	0.0014	0.0004	0.0018	0.0055	0.1272	0.0000	0.0120	0.0041	0.0027	0.0322	0.0000	0.0078
Sum	15.854	15.965	15.948	15.872	15.877	16.220	15.874	15.794	15.838	15.836	15.873	15.846	15.994	15.944	15.990	15.874	15.903	15.980	15.821	15.737

Tabela A – Análises de apatita de rochas foscoríticas e glimerito de Catalão I. As análises foram recalculadas com base em 25 O. (Cont. III)

Amostra	149-4L-	149-4L-	149-4L-	149-4L-	149-4L-	149-3L-	156-3-	156-3-	156-3-											
	15	16	17	18	19	20	01	02	03	04	05	06	07	08	09	10	08	09	10	11
Coord							1	10	20	30	40	50	60	70	80	90	1	7	15	22
Unidade	DC	DC	DC	P2	P2	P2	P2													
Posição							núcleo	interm	interm	interm	interm	interm	interm	interm	interm	borda				
Oxidos (%)																				
P ₂ O ₅	40.47	40.77	40.70	40.34	40.67	41.58	42.16	42.12	41.80	38.77	41.56	41.93	41.57	42.80	43.32	42.40	41.91	41.72	42.79	41.49
SiO ₂	0.00	0.00	0.00	0.00	0.00	0.00	0.00	0.00	0.00	0.00	0.00	0.00	0.00	0.01	0.00	0.00	0.00	0.00	0.04	0.00
Na ₂ O	0.00	0.00	0.00	0.24	0.18	0.00	0.00	0.00	0.09	0.51	0.00	0.00	0.00	0.00	0.00	0.00	0.00	0.00	0.00	0.00
K ₂ O	0.02	0.02	0.02	0.03	0.04	0.01	0.00	0.00	0.00	0.14	0.00	0.03	0.00	0.00	0.00	0.01	0.02	0.00	0.02	0.03
MgO	0.07	0.01	0.02	0.01	0.04	0.04	0.01	0.00	0.00	0.26	0.03	0.05	0.05	0.09	0.00	0.00	0.04	0.00	0.00	0.00
FeO	0.04	0.01	0.02	0.00	0.00	0.01	0.09	0.02	0.04	0.05	0.02	0.13	0.06	0.00	0.07	0.00	0.15	0.05	0.00	0.01
CaO	47.86	47.73	47.58	47.38	48.45	47.93	51.23	51.86	50.46	47.74	50.54	49.71	51.46	52.15	51.72	52.25	52.32	51.90	51.91	51.34
SrO	5.30	5.18	5.42	5.27	5.39	5.31	3.76	3.75	3.68	6.50	6.28	4.09	4.14	3.36	3.90	3.44	2.10	2.75	2.32	2.56
BaO	0.10	0.03	0.21	0.13	0.26	0.05	0.00	0.00	0.00	0.14	0.04	0.30	0.10	0.06	0.00	0.10	0.16	0.14	0.00	0.17
La ₂ O ₃	1.08	1.13	1.21	1.17	0.88	0.66	0.63	0.55	0.90	0.42	0.05	0.52	0.19	0.48	0.25	0.18	0.13	0.28	0.17	0.38
Ce ₂ O ₃	2.25	2.11	2.34	2.12	1.64	1.99	0.97	0.93	1.65	0.72	0.80	1.22	0.76	0.85	0.59	0.46	0.48	0.51	0.52	0.79
Al ₂ O ₃	0.00	0.02	0.02	0.00	0.01	0.02	0.00	0.01	0.00	0.01	0.01	0.02	0.01	0.02	0.00	0.04	0.01	0.03	0.00	0.00
Total	97.19	97.00	97.54	96.67	97.56	97.59	98.85	99.24	98.63	95.27	99.33	97.98	98.35	99.82	99.85	98.86	97.34	97.35	97.79	96.76
Cations (p.f.u.)																				
P	5.9838	6.0196	6.0004	5.9968	5.9899	6.0686	6.0389	6.0158	6.0177	5.9014	5.9957	6.0662	6.0018	6.0484	6.1058	6.0490	6.0393	6.0354	6.1063	6.0378
Si	0.0000	0.0000	0.0000	0.0000	0.0000	0.0000	0.0000	0.0000	0.0000	0.0000	0.0000	0.0000	0.0010	0.0000	0.0000	0.0000	0.0000	0.0000	0.0069	0.0003
Na	0.0000	0.0000	0.0000	0.0807	0.0611	0.0000	0.0000	0.0000	0.0293	0.1767	0.0000	0.0000	0.0000	0.0000	0.0000	0.0000	0.0000	0.0000	0.0000	0.0000
K	0.0045	0.0044	0.0047	0.0067	0.0082	0.0013	0.0000	0.0000	0.0007	0.0330	0.0000	0.0057	0.0002	0.0000	0.0004	0.0026	0.0041	0.0007	0.0037	0.0057
Mg	0.0177	0.0023	0.0062	0.0013	0.0101	0.0105	0.0023	0.0000	0.0010	0.0705	0.0079	0.0127	0.0119	0.0234	0.0000	0.0000	0.0112	0.0005	0.0000	0.0000
Fe ²⁺	0.0102	0.0038	0.0067	0.0000	0.0000	0.0020	0.0258	0.0048	0.0108	0.0144	0.0057	0.0369	0.0180	0.0000	0.0184	0.0006	0.0427	0.0143	0.0000	0.0020
Ca	8.9551	8.9184	8.8775	8.9142	9.0310	8.8536	9.2868	9.3729	9.1929	9.1963	9.2266	9.1021	9.4023	9.3267	9.2240	9.4344	9.5401	9.5021	9.3757	9.4560
Sr	0.5368	0.5235	0.5476	0.5365	0.5437	0.5312	0.3689	0.3667	0.3631	0.6775	0.6200	0.4056	0.4093	0.3253	0.3768	0.3363	0.2074	0.2723	0.2270	0.2550
Ba	0.0070	0.0017	0.0146	0.0087	0.0176	0.0035	0.0000	0.0000	0.0099	0.0026	0.0200	0.0069	0.0042	0.0000	0.0069	0.0103	0.0094	0.0000	0.0112	
La	0.0698	0.0728	0.0777	0.0760	0.0566	0.0419	0.0391	0.0340	0.0567	0.0278	0.0033	0.0325	0.0120	0.0295	0.0155	0.0112	0.0080	0.0176	0.0103	0.0242
Ce	0.2746	0.2569	0.2840	0.2597	0.1997	0.2395	0.1151	0.1100	0.1955	0.0906	0.0954	0.1452	0.0901	0.0989	0.0680	0.0544	0.0570	0.0611	0.0614	0.0949
Al	0.0000	0.0043	0.0031	0.0000	0.0025	0.0039	0.0004	0.0016	0.0000	0.0017	0.0018	0.0042	0.0018	0.0031	0.0000	0.0078	0.0010	0.0056	0.0000	
Sum	15.860	15.808	15.823	15.881	15.920	15.756	15.877	15.906	15.868	16.200	15.959	15.831	15.954	15.861	15.809	15.895	15.928	15.914	15.797	15.887

Tabela A – Análises de apatita de rochas foscoríticas e glimerito de Catalão I. As análises foram recalculadas com base em 25 O. (Cont. IV)

Amostra	156-3-12	156-3-13	156-3-14	156-3-14B	156-3-15	156-3-16	156-3-17	156-3-18	156-3L-1	156-3L-2	156-3L-3	156-3L-4	156-3L-5	157A-5-1B	157A-5-2B	157A-5-3	157A-5-4	157A-5-5	157A-5-6	157A-5-6B
Coord	30	36	44	45	51	59	65	71	4	8	12	15	20	1	7	10	17	22	27	27
Unidade	P2	P2	P2	P2	P2	P2	P2	P2	P2	P2	P2	P2	P2	P2	P2	P2	P2	P2	P2	P2
Posição														núcleo	borda	interm	núcleo	núcleo	núcleo	interm
Oxidos (%)																				
P ₂ O ₅	42.58	41.85	41.49	42.02	42.20	42.27	42.89	42.50	42.53	42.63	42.74	42.37	42.61	40.95	41.24	42.21	42.37	42.52	41.28	42.03
SiO ₂	0.00	0.00	0.00	0.00	0.00	0.00	0.00	0.00	0.00	0.00	0.00	0.03	0.00	0.00	0.02	0.01	0.00	0.03	0.04	0.01
Na ₂ O	0.00	0.00	0.00	0.00	0.00	0.00	0.00	0.00	0.00	0.00	0.00	0.00	0.00	0.00	0.00	0.00	0.00	0.00	0.00	0.00
K ₂ O	0.00	0.01	0.00	0.01	0.01	0.00	0.02	0.00	0.01	0.00	0.00	0.00	0.00	0.00	0.02	0.03	0.01	0.01	0.00	0.01
MgO	0.00	0.01	0.04	0.03	0.01	0.01	0.03	0.03	0.02	0.02	0.02	0.03	0.07	0.04	0.00	0.02	0.01	0.03	0.10	0.07
FeO	0.00	0.01	0.00	0.00	0.00	0.04	0.17	0.00	0.01	0.11	0.19	0.57	0.13	0.10	0.04	0.10	0.08	0.00	0.08	0.00
CaO	51.75	52.27	51.37	51.84	51.92	52.58	52.12	51.26	53.35	53.27	53.01	52.43	52.47	49.59	49.31	52.41	51.59	51.46	51.37	51.22
SrO	2.38	2.14	2.01	2.24	2.12	1.91	1.93	2.56	1.94	2.14	2.05	2.34	2.04	3.98	3.65	0.88	1.12	1.19	1.07	1.07
BaO	0.00	0.00	0.00	0.00	0.00	0.01	0.00	0.03	0.00	0.00	0.00	0.00	0.05	0.01	0.00	0.15	0.01	0.09	0.05	0.01
La ₂ O ₃	0.32	0.22	0.34	0.04	0.19	0.14	0.24	0.27	0.01	0.33	0.13	0.42	0.10	0.39	0.45	0.08	0.05	0.33	0.30	0.08
Ce ₂ O ₃	0.76	0.45	0.65	0.66	0.49	0.47	0.30	0.65	0.29	0.46	0.43	0.71	0.41	0.82	1.03	0.15	0.51	0.33	0.32	0.25
Al ₂ O ₃	0.02	0.02	0.00	0.03	0.01	0.02	0.00	0.03	0.00	0.04	0.01	0.00	0.00	0.00	0.00	0.02	0.02	0.05	0.00	0.01
Total	97.80	96.96	95.89	96.85	96.96	97.41	97.57	97.48	98.17	98.89	98.49	98.52	98.32	95.93	95.84	95.98	95.79	96.09	94.54	94.85
Cations (p.f.u.)																				
P	6.0916	6.0476	6.0590	6.0675	6.0830	6.0639	6.1228	6.1015	6.0555	6.0431	6.0678	6.0407	6.0657	6.0453	6.0735	6.1027	6.1293	6.1380	6.0759	6.1357
Si	0.0000	0.0000	0.0000	0.0000	0.0000	0.0000	0.0000	0.0000	0.0000	0.0000	0.0000	0.0044	0.0000	0.0000	0.0038	0.0022	0.0000	0.0044	0.0068	0.0019
Na	0.0000	0.0000	0.0000	0.0000	0.0000	0.0000	0.0000	0.0000	0.0000	0.0000	0.0000	0.0000	0.0000	0.0000	0.0000	0.0000	0.0000	0.0000	0.0000	0.0000
K	0.0004	0.0020	0.0000	0.0024	0.0028	0.0006	0.0049	0.0000	0.0030	0.0000	0.0002	0.0009	0.0000	0.0042	0.0055	0.0026	0.0013	0.0000	0.0013	0.0022
Mg	0.0000	0.0023	0.0095	0.0066	0.0013	0.0033	0.0063	0.0066	0.0055	0.0047	0.0042	0.0078	0.0173	0.0112	0.0010	0.0061	0.0023	0.0076	0.0270	0.0180
Fe ²⁺	0.0000	0.0037	0.0000	0.0000	0.0000	0.0000	0.0110	0.0474	0.0000	0.0025	0.0303	0.0530	0.1612	0.0385	0.0282	0.0103	0.0297	0.0240	0.0006	0.0231
Ca	9.3690	9.5592	9.4932	9.4732	9.4711	9.5464	9.4144	9.3132	9.6116	9.5569	9.5223	9.4610	9.4535	9.2645	9.1902	9.5898	9.4457	9.4002	9.5694	9.4617
Sr	0.2332	0.2118	0.2005	0.2215	0.2093	0.1879	0.1885	0.2514	0.1893	0.2077	0.1991	0.2288	0.1988	0.4026	0.3685	0.0875	0.1105	0.1172	0.1083	0.1074
Ba	0.0000	0.0000	0.0000	0.0000	0.0000	0.0009	0.0000	0.0017	0.0000	0.0000	0.0000	0.0000	0.0034	0.0009	0.0000	0.0097	0.0009	0.0061	0.0036	0.0009
La	0.0199	0.0137	0.0218	0.0024	0.0121	0.0088	0.0150	0.0168	0.0009	0.0206	0.0080	0.0261	0.0063	0.0250	0.0291	0.0050	0.0033	0.0204	0.0193	0.0050
Ce	0.0894	0.0532	0.0777	0.0785	0.0585	0.0554	0.0354	0.0766	0.0344	0.0533	0.0505	0.0838	0.0484	0.0992	0.1255	0.0178	0.0612	0.0392	0.0390	0.0303
Al	0.0032	0.0030	0.0000	0.0050	0.0024	0.0036	0.0000	0.0064	0.0004	0.0071	0.0012	0.0000	0.0000	0.0000	0.0034	0.0034	0.0090	0.0000	0.0022	
Sum	15.807	15.896	15.862	15.857	15.840	15.871	15.798	15.822	15.900	15.896	15.884	15.906	15.955	15.891	15.825	15.837	15.788	15.766	15.851	15.788

Tabela A – Análises de apatita de rochas foscoríticas e glimerito de Catalão I. As análises foram recalculadas com base em 25 O. (Cont. V)

	157A-5-7	157A-5-8	157B-5-1C	157B-5-2	157B-5-2B	157B-5-3	157B-5-4	157B-5-6	170-3L-03	170-3L-04	170-3L-05	170-3L-06	170-3L-07	170-3L-08	170-3L-09	170-3L-10	178-2-1	178-2-2	178-2-3	178-2-4
Amostra									núcleo	interm	interm	interm	interm	interm	interm	borda	interm	interm	interm	núcleo
Coord	34	43	0.4	4.2	4.8	7	9.4	17	16	24	32	40	48	56	64	72	0	5	10	18
Unidade	P2	P2	P3	P3	P3	P3	P3	P3	DC	P2	P2	P2	P2							
Posição	interm	borda																		
Oxidos (%)																				
P ₂ O ₅	40.77	39.34	41.36	40.19	40.27	40.42	39.85	41.21	38.21	39.13	35.16	38.94	39.13	40.35	40.07	38.13	42.11	40.23	40.95	40.97
SiO ₂	0.00	0.15	0.00	0.00	0.01	0.00	0.00	0.00	0.00	0.00	0.00	0.00	0.00	0.00	0.00	0.00	0.00	0.00	0.00	0.04
Na ₂ O	0.00	0.34	0.00	0.00	0.06	0.00	0.00	0.00	0.29	0.48	0.19	0.16	0.00	0.13	0.00	0.57	0.00	0.15	0.21	0.00
K ₂ O	0.02	0.08	0.00	0.01	0.02	0.01	0.11	0.02	0.02	0.00	0.06	0.01	0.02	0.02	0.02	0.06	0.00	0.02	0.03	0.02
MgO	0.06	0.13	0.02	0.03	0.10	0.05	0.06	0.00	0.00	0.00	0.08	0.00	0.06	0.04	0.05	0.10	0.03	0.06	0.06	0.04
FeO	0.00	0.79	0.74	0.35	0.45	0.16	0.06	0.22	0.01	0.08	0.13	0.00	0.00	0.03	0.05	0.00	0.05	0.00	0.02	0.00
CaO	47.69	45.47	48.10	48.78	48.47	48.87	49.02	49.77	43.35	44.96	43.87	46.29	47.23	48.12	47.64	43.98	48.67	48.11	48.75	49.75
SrO	3.51	4.19	4.08	3.66	3.55	3.42	3.80	3.26	5.31	5.37	5.80	5.45	5.10	5.27	4.82	6.13	3.78	4.07	3.98	1.97
BaO	0.13	0.00	0.00	0.00	0.00	0.26	0.00	0.00	0.12	0.00	0.08	0.00	0.20	0.00	0.13	0.04	0.18	0.09	0.00	0.14
La ₂ O ₃	0.42	0.81	0.44	0.48	0.74	0.40	0.47	0.39	1.52	1.26	1.10	1.14	0.92	0.66	0.50	1.27	0.30	0.66	0.63	0.43
Ce ₂ O ₃	0.99	1.15	0.97	1.10	0.88	1.17	0.86	0.62	2.60	2.86	2.01	1.92	1.71	1.37	1.23	2.74	1.11	1.19	1.20	0.91
Al ₂ O ₃	0.00	0.07	0.00	0.00	0.04	0.04	0.00	0.03	0.00	0.25	0.01	0.00	0.03	0.01	0.00	0.01	0.00	0.00	0.01	0.01
Total	93.59	92.52	95.70	94.59	94.54	94.80	94.27	95.49	91.46	94.14	88.73	93.91	94.37	96.01	94.51	93.02	96.24	94.59	95.82	94.26
Cations (p.f.u.)																				
P	6.1267	6.0458	6.1073	6.0239	6.0375	6.0361	6.0032	6.0783	6.0186	5.9874	5.7946	5.9730	5.9643	6.0105	6.0404	5.9469	6.1480	6.0401	6.0549	6.0830
Si	0.0002	0.0270	0.0000	0.0000	0.0023	0.0000	0.0000	0.0000	0.0000	0.0000	0.0000	0.0000	0.0000	0.0000	0.0000	0.0000	0.0000	0.0000	0.0000	0.0067
Na	0.0000	0.1193	0.0000	0.0000	0.0213	0.0000	0.0000	0.0000	0.1039	0.1678	0.0728	0.0559	0.0000	0.0433	0.0000	0.2047	0.0000	0.0526	0.0725	0.0000
K	0.0038	0.0178	0.0000	0.0020	0.0036	0.0020	0.0241	0.0051	0.0052	0.0002	0.0156	0.0014	0.0048	0.0038	0.0039	0.0148	0.0004	0.0034	0.0069	0.0045
Mg	0.0148	0.0355	0.0044	0.0069	0.0264	0.0142	0.0162	0.0000	0.0000	0.0000	0.0229	0.0005	0.0150	0.0097	0.0119	0.0264	0.0072	0.0159	0.0151	0.0092
Fe ²⁺	0.0006	0.2383	0.2150	0.1048	0.1330	0.0457	0.0176	0.0626	0.0034	0.0230	0.0410	0.0000	0.0000	0.0085	0.0149	0.0000	0.0133	0.0000	0.0053	0.0000
Ca	9.0706	8.8436	8.9872	9.2530	9.1963	9.2355	9.3452	9.2908	8.6425	8.7054	9.1497	8.9844	9.1112	9.0724	9.0885	8.6809	8.9927	9.1418	9.1220	9.3485
Sr	0.3617	0.4413	0.4124	0.3756	0.3646	0.3493	0.3922	0.3294	0.5729	0.5631	0.6544	0.5721	0.5327	0.5372	0.4975	0.6545	0.3783	0.4185	0.4030	0.1999
Ba	0.0091	0.0000	0.0000	0.0000	0.0181	0.0000	0.0000	0.0086	0.0000	0.0060	0.0000	0.0140	0.0000	0.0092	0.0028	0.0123	0.0063	0.0000	0.0099	
La	0.0272	0.0543	0.0282	0.0314	0.0483	0.0262	0.0306	0.0251	0.1044	0.0841	0.0790	0.0762	0.0613	0.0430	0.0326	0.0865	0.0188	0.0431	0.0408	0.0276
Ce	0.1224	0.1456	0.1182	0.1362	0.1082	0.1441	0.1068	0.0749	0.3375	0.3609	0.2732	0.2422	0.2147	0.1688	0.1528	0.3525	0.1340	0.1470	0.1461	0.1108
Al	0.0000	0.0156	0.0004	0.0000	0.0004	0.0089	0.0075	0.0000	0.0070	0.0000	0.0583	0.0028	0.0000	0.0060	0.0029	0.0000	0.0022	0.0000	0.0000	0.0012
Sum	15.737	15.984	15.873	15.934	15.942	15.880	15.943	15.866	15.804	15.892	16.168	15.909	15.918	15.903	15.855	15.970	15.707	15.871	15.867	15.801

Tabela A – Análises de apatita de rochas foscoríticas e glimerito de Catalão I. As análises foram recalculadas com base em 25 O. (Cont. VI)

Amostra	178-2-5	178-2-6B	183-1L-01	183-1L-02	183-1L-03	183-1L-04	183-1L-05	183-1L-06	183-1L-07	183-1L-08	183-1L-09	183-1L-10	183-2-2	183-2-3	183-2-4	183-2-5B	183-2L-01	183-2L-03	183-2L-04	183-2L-05
Coord	27	35	0	3	5.5	8	11	14	16.5	19	21.5	25	4.5	9	14	19	0	5	8	10
Unidade	P2	P2	DC	P3	P3	P3	P3	P3	P3	P3	P3									
Posição	interm	borda	núcleo	interm	borda				borda	borda	interm	núcleo								
Oxidos (%)																				
P ₂ O ₅	41.53	40.35	41.37	42.20	41.04	41.10	41.22	40.09	41.39	40.62	40.69	42.37	41.91	42.75	42.50	41.91	42.12	43.06	41.82	42.19
SiO ₂	0.03	0.00	0.01	0.00	0.00	0.04	0.01	0.00	0.00	0.00	0.01	0.00	0.00	0.01	0.00	0.02	0.08	0.05	0.05	0.00
Na ₂ O	0.00	0.30	0.00	0.00	0.00	0.03	0.00	0.00	0.00	0.15	0.00	0.00	0.00	0.00	0.00	0.00	0.00	0.00	0.00	0.00
K ₂ O	0.01	0.03	0.00	0.01	0.04	0.03	0.01	0.03	0.02	0.03	0.03	0.02	0.02	0.00	0.01	0.03	0.00	0.02	0.00	0.00
MgO	0.02	0.12	0.05	0.07	0.05	0.07	0.09	0.08	0.02	0.08	0.01	0.04	0.04	0.04	0.01	0.09	0.06	0.04	0.05	0.03
FeO	0.00	0.09	0.20	0.04	0.00	0.03	0.05	0.04	0.03	0.00	0.00	0.00	0.15	0.02	0.08	0.26	0.58	0.26	0.12	0.10
CaO	51.15	47.92	51.01	51.92	49.45	50.28	50.77	50.51	51.69	51.01	51.77	52.12	53.14	53.18	52.71	52.61	53.38	52.85	53.01	51.53
SrO	2.18	4.44	3.50	2.93	4.85	3.93	3.77	3.70	3.66	3.97	3.61	3.40	2.20	1.58	2.12	1.80	2.13	2.25	2.82	3.67
BaO	0.00	0.16	0.07	0.00	0.08	0.24	0.00	0.16	0.18	0.18	0.00	0.05	0.00	0.13	0.14	0.09	0.05	0.16	0.05	0.00
La ₂ O ₃	0.27	0.67	0.49	0.12	0.73	0.67	0.30	0.58	0.25	0.32	0.39	0.35	0.39	0.23	0.17	0.03	0.13	0.12	0.12	0.42
Ce ₂ O ₃	0.55	1.22	0.91	0.36	1.30	1.00	0.83	0.88	0.61	0.84	0.88	0.66	0.64	0.71	0.41	0.38	0.53	0.36	0.23	0.83
Al ₂ O ₃	0.00	0.00	0.01	0.00	0.00	0.02	0.02	0.00	0.01	0.00	0.00	0.00	0.00	0.00	0.02	0.00	0.02	0.01	0.01	0.01
Total	95.75	95.29	97.62	97.64	97.53	97.44	97.08	96.07	97.87	97.19	97.39	99.00	98.48	98.65	98.14	97.23	99.05	99.18	98.27	98.77
Cations (p.f.u.)																				
P	6.0704	6.0319	6.0069	6.0667	6.0089	6.0018	6.0118	5.9504	5.9977	5.9565	5.9446	6.0405	5.9938	6.0569	6.0656	6.0346	5.9853	6.0762	5.9993	6.0382
Si	0.0057	0.0000	0.0021	0.0000	0.0000	0.0069	0.0022	0.0000	0.0003	0.0000	0.0021	0.0000	0.0000	0.0015	0.0000	0.0034	0.0126	0.0090	0.0081	0.0000
Na	0.0000	0.1041	0.0000	0.0000	0.0000	0.0100	0.0000	0.0000	0.0507	0.0000	0.0000	0.0000	0.0000	0.0000	0.0000	0.0000	0.0000	0.0000	0.0000	0.0000
K	0.0026	0.0072	0.0007	0.0011	0.0079	0.0068	0.0029	0.0067	0.0033	0.0057	0.0066	0.0041	0.0034	0.0000	0.0011	0.0074	0.0000	0.0047	0.0000	0.0000
Mg	0.0062	0.0303	0.0123	0.0182	0.0132	0.0172	0.0241	0.0199	0.0061	0.0199	0.0028	0.0103	0.0088	0.0097	0.0018	0.0218	0.0148	0.0092	0.0124	0.0086
Fe ²⁺	0.0000	0.0266	0.0568	0.0105	0.0000	0.0087	0.0135	0.0117	0.0094	0.0000	0.0000	0.0000	0.0418	0.0042	0.0228	0.0728	0.1628	0.0711	0.0340	0.0280
Ca	9.4612	9.0645	9.3728	9.4458	9.1627	9.2913	9.3720	9.4893	9.4799	9.4668	9.5707	9.4027	9.6191	9.5349	9.5183	9.5858	9.6005	9.4367	9.6234	9.3332
Sr	0.2187	0.4542	0.3483	0.2880	0.4868	0.3929	0.3765	0.3766	0.3636	0.3986	0.3612	0.3317	0.2150	0.1529	0.2076	0.1779	0.2072	0.2172	0.2769	0.3597
Ba	0.0000	0.0108	0.0044	0.0000	0.0052	0.0163	0.0000	0.0108	0.0123	0.0123	0.0000	0.0034	0.0000	0.0086	0.0094	0.0061	0.0034	0.0102	0.0035	0.0000
La	0.0173	0.0435	0.0311	0.0073	0.0466	0.0424	0.0193	0.0376	0.0155	0.0204	0.0251	0.0218	0.0243	0.0144	0.0104	0.0016	0.0078	0.0071	0.0072	0.0260
Ce	0.0657	0.1509	0.1085	0.0429	0.1570	0.1204	0.0998	0.1078	0.0729	0.1015	0.1058	0.0772	0.0751	0.0833	0.0477	0.0445	0.0618	0.0419	0.0266	0.0979
Al	0.0004	0.0000	0.0018	0.0000	0.0004	0.0047	0.0043	0.0000	0.0028	0.0000	0.0000	0.0006	0.0000	0.0038	0.0000	0.0045	0.0010	0.0022		
Sum	15.848	15.924	15.946	15.881	15.889	15.919	15.927	16.011	15.964	16.032	16.019	15.892	15.982	15.866	15.885	15.960	16.056	15.888	15.992	15.894

Tabela A – Análises de apatita de rochas foscoríticas e glimerito de Catalão I. As análises foram recalcadas com base em 25 O. (Cont. VII)

	183-2L-06	183-2L-07	183-2L-09	183-2L-10	192B-3-1	192B-3-2	192B-3-3	192B-3-4	192B-3-5	192B-3-6	192B-3-7	206-2-1	206-2-2	206-2-3	206-2-4	206-2-5	207-1-1	207-1-2	207-1-3	207-1-4
Amostra	núcleo	núcleo	interm	borda	borda	núcleo	núcleo	núcleo	interm	interm	interm	borda	borda	núcleo	borda	borda	interm	interm	interm	
Oxidos (%)																				
P ₂ O ₅	42.20	41.98	41.76	41.19	42.13	42.99	42.20	42.54	41.75	42.16	42.04	42.18	40.90	42.33	41.14	41.25	41.98	42.23	42.76	42.19
SiO ₂	0.00	0.00	0.01	0.02	0.00	0.00	0.00	0.00	0.01	0.04	0.00	0.00	0.06	0.03	0.05	0.06	0.00	0.00	0.00	0.00
Na ₂ O	0.00	0.00	0.00	0.00	0.00	0.00	0.00	0.00	0.28	0.00	0.00	0.09	0.00	0.00	0.00	0.00	0.00	0.00	0.00	0.00
K ₂ O	0.00	0.01	0.00	0.01	0.02	0.00	0.01	0.00	0.00	0.01	0.02	0.00	0.01	0.02	0.01	0.03	0.01	0.01	0.00	0.03
MgO	0.05	0.03	0.06	0.02	0.02	0.03	0.05	0.06	0.03	0.05	0.01	0.05	0.11	0.05	0.11	0.08	0.00	0.00	0.08	0.00
FeO	0.11	0.13	0.19	0.15	0.01	0.06	0.04	0.04	0.00	0.00	0.10	0.29	0.21	0.22	0.26	0.52	0.28	0.05	0.06	0.07
CaO	51.89	51.86	52.54	52.14	50.49	51.86	51.40	51.59	50.54	50.69	50.15	52.06	51.18	51.25	50.55	50.82	51.85	51.90	51.23	51.57
SrO	3.51	3.18	2.87	2.30	2.86	1.41	1.43	1.49	2.35	2.08	2.52	1.99	1.94	2.95	2.29	1.86	2.33	2.68	3.36	3.20
BaO	0.00	0.00	0.00	0.00	0.00	0.00	0.00	0.01	0.07	0.17	0.00	0.01	0.00	0.07	0.00	0.00	0.00	0.06	0.00	0.00
La ₂ O ₃	0.30	0.33	0.26	0.19	0.31	0.24	0.05	0.16	0.36	0.18	0.24	0.39	0.28	0.22	0.36	0.42	0.10	0.19	0.26	0.40
Ce ₂ O ₃	0.49	0.49	0.47	0.72	0.83	0.60	0.47	0.38	0.67	0.36	0.48	0.29	0.74	0.61	0.78	0.69	0.26	0.52	0.62	0.62
Al ₂ O ₃	0.02	0.00	0.03	0.00	0.00	0.01	0.01	0.00	0.00	0.05	0.00	0.00	0.01	0.01	0.02	0.00	0.00	0.06	0.00	0.02
Total	98.57	98.00	98.18	96.74	96.67	97.20	95.65	96.27	96.05	95.79	95.56	97.35	95.42	97.75	95.57	95.72	96.81	97.71	98.36	98.09
Cations (p.f.u.)																				
P	6.0425	6.0395	6.0006	5.9942	6.1070	6.1379	6.1240	6.1341	6.0890	6.1314	6.1403	6.0673	6.0145	6.0806	6.0431	6.0428	6.0725	6.0647	6.1027	6.0594
Si	0.0000	0.0000	0.0020	0.0031	0.0000	0.0000	0.0000	0.0000	0.0009	0.0067	0.0000	0.0000	0.0101	0.0046	0.0090	0.0097	0.0000	0.0000	0.0000	0.0000
Na	0.0000	0.0000	0.0000	0.0000	0.0000	0.0000	0.0000	0.0000	0.0918	0.0000	0.0000	0.0306	0.0000	0.0000	0.0000	0.0000	0.0000	0.0000	0.0000	0.0000
K	0.0002	0.0024	0.0000	0.0029	0.0052	0.0000	0.0011	0.0009	0.0000	0.0020	0.0040	0.0007	0.0022	0.0037	0.0022	0.0068	0.0026	0.0026	0.0000	0.0058
Mg	0.0113	0.0068	0.0139	0.0062	0.0046	0.0083	0.0123	0.0140	0.0080	0.0128	0.0015	0.0137	0.0287	0.0132	0.0272	0.0214	0.0000	0.0000	0.0206	0.0010
Fe ²⁺	0.0300	0.0378	0.0534	0.0431	0.0020	0.0166	0.0118	0.0114	0.0006	0.0000	0.0283	0.0810	0.0596	0.0627	0.0749	0.1517	0.0792	0.0148	0.0178	0.0196
Ca	9.4026	9.4434	9.5549	9.6028	9.2620	9.3712	9.4388	9.4136	9.3282	9.3280	9.2688	9.4774	9.5240	9.3169	9.3956	9.4211	9.4916	9.4323	9.2532	9.3713
Sr	0.3442	0.3136	0.2825	0.2294	0.2835	0.1380	0.1417	0.1471	0.2345	0.2071	0.2525	0.1958	0.1951	0.2906	0.2306	0.1861	0.2308	0.2632	0.3282	0.3144
Ba	0.0000	0.0000	0.0000	0.0000	0.0000	0.0000	0.0000	0.0000	0.0009	0.0044	0.0114	0.0000	0.0009	0.0000	0.0044	0.0000	0.0000	0.0000	0.0043	0.0000
La	0.0187	0.0206	0.0162	0.0122	0.0195	0.0152	0.0032	0.0097	0.0229	0.0114	0.0155	0.0246	0.0176	0.0138	0.0232	0.0267	0.0064	0.0120	0.0159	0.0248
Ce	0.0582	0.0577	0.0561	0.0859	0.0996	0.0702	0.0564	0.0457	0.0800	0.0432	0.0581	0.0339	0.0902	0.0726	0.0947	0.0830	0.0305	0.0621	0.0724	0.0728
Al	0.0034	0.0000	0.0054	0.0000	0.0000	0.0010	0.0010	0.0000	0.0000	0.0107	0.0000	0.0000	0.0020	0.0010	0.0037	0.0008	0.0000	0.0126	0.0000	0.0038
Sum	15.911	15.922	15.985	15.980	15.784	15.758	15.790	15.777	15.860	15.765	15.769	15.926	15.944	15.864	15.904	15.950	15.914	15.868	15.811	15.873

Tabela A – Análises de apatita de rochas foscoríticas e glimerito de Catalão I. As análises foram recalculadas com base em 25 O. (Cont. VIII)

	207-1- Amostra 5	207-1- 6B	207- 1b-07	207- 1b-07B	207- 1b-08	207- 1b-09	207- 1b-10	207- 1b-11	225-2- 1	225-2- 2	225-2- 3	225-2- 4	225-2- 5	225-2- 6	225-2- 7	230A- 1-1	230A- 1-2	230A- 1-3	230A- 1-4	230A- 1-5
Coord	21	27	0	1	5	8	10	14	2	7	12	16	21		0	4	9	13	19	
Unidade	DC	DC	P3	P3	P3	P3	P3	P3	GLIM	GLIM	GLIM	GLIM	GLIM	GLIM	P2	P2	P2	P2	P2	
Posição	núcleo	interm	interm	núcleo	núcleo	núcleo	borda	borda	interm	interm	núcleo	interm	interm	interm	borda	borda	núcleo	interm	borda	
Oxidos (%)																				
P ₂ O ₅	41.86	42.39	40.61	40.87	41.70	42.36	42.70	41.16	41.84	40.84	42.10	41.24	41.69	41.63	40.96	42.31	41.91	42.80	42.97	41.28
SiO ₂	0.00	0.01	0.00	0.03	0.11	0.06	0.03	0.00	0.28	0.19	0.03	0.46	0.51	0.58	0.96	0.00	0.00	0.01	0.00	0.01
Na ₂ O	0.00	0.00	0.00	0.00	0.00	0.00	0.00	0.00	0.00	0.00	0.00	0.00	0.00	0.00	0.00	0.00	0.00	0.00	0.00	0.00
K ₂ O	0.00	0.04	0.03	0.28	0.00	0.00	0.00	0.01	0.03	0.04	0.09	0.00	0.01	0.00	0.01	0.00	0.01	0.01	0.01	0.02
MgO	0.03	0.03	0.08	0.02	0.09	0.04	0.06	0.03	0.03	0.09	0.05	0.07	0.05	0.08	0.00	0.02	0.01	0.00	0.01	0.06
FeO	0.18	0.16	0.75	0.59	0.15	0.09	0.06	0.20	0.04	0.02	0.11	0.00	0.02	0.10	0.07	0.17	0.04	0.11	0.09	0.54
CaO	51.64	51.09	49.85	50.34	53.21	52.84	52.57	50.75	52.52	51.36	50.98	53.24	52.76	53.29	52.57	51.05	51.21	52.58	51.90	51.02
SrO	2.68	2.67	3.20	2.45	0.87	1.09	1.31	2.73	0.92	0.86	1.22	0.79	1.00	0.80	0.99	3.63	3.18	1.54	2.45	3.39
BaO	0.15	0.00	0.12	0.00	0.01	0.00	0.03	0.03	0.10	0.05	0.13	0.01	0.00	0.00	0.14	0.07	0.20	0.00	0.05	0.01
La ₂ O ₃	0.12	0.33	0.42	0.14	0.23	0.12	0.15	0.41	0.45	0.51	0.84	0.04	0.19	0.21	0.31	0.09	0.37	0.28	0.29	0.31
Ce ₂ O ₃	0.60	0.67	0.83	0.78	0.06	0.36	0.51	0.74	0.42	0.81	1.55	0.49	0.70	0.59	0.99	0.49	0.85	0.71	0.49	0.48
Al ₂ O ₃	0.00	0.00	0.00	0.05	0.01	0.00	0.00	0.01	0.00	0.01	0.01	0.01	0.02	0.00	0.00	0.00	0.00	0.00	0.00	0.02
Total	97.26	97.39	95.89	95.56	96.42	96.95	97.42	96.05	96.63	94.77	97.09	96.35	96.94	97.27	97.01	97.83	97.78	98.04	98.27	97.14
Cations (p.f.u.)																				
P	6.0505	6.0984	6.0056	6.0235	6.0270	6.0750	6.0945	6.0362	6.0343	6.0166	6.0670	5.9640	5.9891	5.9632	5.9032	6.0873	6.0492	6.0867	6.1128	6.0139
Si	0.0000	0.0014	0.0000	0.0056	0.0181	0.0102	0.0046	0.0000	0.0482	0.0338	0.0053	0.0784	0.0869	0.0981	0.1636	0.0000	0.0000	0.0020	0.0000	0.0015
Na	0.0000	0.0000	0.0000	0.0000	0.0000	0.0000	0.0000	0.0000	0.0000	0.0000	0.0000	0.0000	0.0000	0.0000	0.0000	0.0000	0.0000	0.0000	0.0000	0.0000
K	0.0004	0.0076	0.0071	0.0611	0.0002	0.0000	0.0000	0.0018	0.0063	0.0095	0.0189	0.0009	0.0011	0.0000	0.0028	0.0000	0.0022	0.0017	0.0026	0.0042
Mg	0.0069	0.0084	0.0201	0.0062	0.0221	0.0088	0.0148	0.0072	0.0071	0.0228	0.0119	0.0176	0.0114	0.0202	0.0010	0.0061	0.0023	0.0005	0.0033	0.0159
Fe ²⁺	0.0514	0.0463	0.2179	0.1724	0.0431	0.0246	0.0172	0.0585	0.0105	0.0044	0.0307	0.0000	0.0051	0.0269	0.0202	0.0477	0.0120	0.0317	0.0256	0.1543
Ca	9.4473	9.3021	9.3286	9.3888	9.7321	9.5896	9.4965	9.4191	9.5871	9.5735	9.2976	9.7428	9.5912	9.6598	9.5890	9.2945	9.3545	9.4612	9.3449	9.4062
Sr	0.2651	0.2632	0.3240	0.2474	0.0858	0.1072	0.1280	0.2739	0.0911	0.0872	0.1201	0.0777	0.0980	0.0782	0.0980	0.3575	0.3145	0.1498	0.2387	0.3380
Ba	0.0103	0.0000	0.0079	0.0000	0.0009	0.0000	0.0017	0.0018	0.0069	0.0035	0.0087	0.0009	0.0000	0.0000	0.0096	0.0044	0.0132	0.0000	0.0035	0.0009
La	0.0072	0.0208	0.0270	0.0091	0.0145	0.0072	0.0095	0.0261	0.0284	0.0325	0.0527	0.0025	0.0121	0.0130	0.0196	0.0057	0.0230	0.0170	0.0177	0.0199
Ce	0.0716	0.0796	0.1016	0.0950	0.0067	0.0423	0.0605	0.0894	0.0497	0.0979	0.1840	0.0582	0.0832	0.0698	0.1174	0.0579	0.1006	0.0831	0.0574	0.0577
Al	0.0000	0.0000	0.0000	0.0098	0.0012	0.0000	0.0000	0.0027	0.0000	0.0010	0.0026	0.0018	0.0046	0.0000	0.0000	0.0004	0.0006	0.0037		
Sum	15.911	15.828	16.040	16.019	15.952	15.865	15.827	15.917	15.870	15.883	15.799	15.945	15.883	15.929	15.925	15.861	15.871	15.834	15.807	16.016

Tabela A – Análises de apatita de rochas foscoríticas e glimerito de Catalão I. As análises foram recalculadas com base em 25 O. (Cont. IX)

Amostra	230B-5-1	230B-5-2	230B-5-3	230B-5-4	230B-5-5	230B-5-6	230B-5-7	230B-6-1	230B-6-2	230B-6-3	230B-6-4	244-2-1	244-2-2	244-2-3	244-3-1	244-3-3	244-3-4	244-3-5	244-3-6	244-3-7
Coord	0	9	18	28	37	45	55	0	4	6.5	9.5	0	9	16	2	16	23	29	35	41
Unidade	P3	P1																		
Posição	borda	interm	núcleo	núcleo	interm	interm	borda	interm	núcleo	borda	borda				borda	núcleo	núcleo	interm	interm	borda
Oxidos (%)																				
P ₂ O ₅	41.87	42.19	42.60	42.59	41.78	42.06	41.73	41.97	41.92	41.43	41.98	40.90	41.61	41.87	42.67	42.75	42.25	42.56	42.33	42.13
SiO ₂	0.00	0.00	0.00	0.00	0.00	0.00	0.00	0.00	0.00	0.00	0.00	0.44	0.27	0.34	0.04	0.18	0.08	0.04	0.06	0.00
Na ₂ O	0.71	0.00	0.09	0.00	0.43	0.00	0.00	0.00	0.00	0.00	0.00	0.00	0.00	0.00	0.07	0.00	0.00	0.00	0.00	0.07
K ₂ O	0.00	0.00	0.00	0.01	0.01	0.00	0.02	0.01	0.01	0.00	0.02	0.00	0.00	0.00	0.00	0.01	0.00	0.00	0.02	0.01
MgO	0.05	0.02	0.00	0.02	0.01	0.00	0.01	0.03	0.06	0.06	0.01	0.03	0.02	0.05	0.00	0.07	0.00	0.02	0.06	0.11
FeO	0.10	0.05	0.21	0.11	0.05	0.07	0.42	0.23	0.01	0.00	0.05	0.06	0.03	0.00	0.04	0.00	0.04	0.00	0.04	0.00
CaO	48.42	50.43	51.17	50.92	49.57	51.56	49.76	50.69	49.33	50.95	51.39	52.42	52.50	52.50	52.97	53.42	53.30	53.33	52.64	52.27
SrO	4.08	3.82	3.44	3.19	4.47	3.49	4.68	3.77	4.31	3.47	3.38	0.93	1.17	0.83	1.02	0.98	0.94	1.01	1.28	1.28
BaO	0.08	0.11	0.03	0.07	0.07	0.01	0.00	0.00	0.33	0.00	0.00	0.16	0.07	0.27	0.09	0.00	0.00	0.00	0.14	0.00
La ₂ O ₃	0.84	0.30	0.33	0.52	0.83	0.27	0.34	0.54	0.70	0.59	0.48	0.39	0.31	0.23	0.65	0.11	0.18	0.43	0.48	0.33
Ce ₂ O ₃	1.95	0.96	0.64	0.76	1.22	0.60	1.12	0.92	1.36	0.87	0.66	0.65	0.51	0.30	0.80	0.93	0.58	0.86	1.03	0.99
Al ₂ O ₃	0.00	0.00	0.00	0.02	0.02	0.00	0.00	0.00	0.01	0.00	0.01	0.01	0.00	0.01	0.00	0.04	0.02	0.00	0.00	0.00
Total	98.10	97.88	98.50	98.19	98.47	98.06	98.08	98.14	98.02	97.37	97.97	95.99	96.48	96.39	98.35	98.49	97.40	98.24	98.07	97.18
Cations (p.f.u.)																				
P	6.0597	6.0817	6.0881	6.0989	6.0396	6.0505	6.0456	6.0500	6.0714	6.0221	6.0484	5.9610	6.0188	6.0422	6.0587	6.0375	6.0411	6.0437	6.0386	6.0515
Si	0.0000	0.0000	0.0000	0.0000	0.0002	0.0000	0.0000	0.0000	0.0000	0.0000	0.0000	0.0754	0.0461	0.0578	0.0064	0.0305	0.0140	0.0074	0.0094	0.0000
Na	0.2337	0.0000	0.0301	0.0000	0.1420	0.0000	0.0000	0.0000	0.0000	0.0000	0.0000	0.0000	0.0000	0.0000	0.0218	0.0000	0.0000	0.0000	0.0000	0.0220
K	0.0007	0.0007	0.0000	0.0017	0.0030	0.0000	0.0052	0.0026	0.0013	0.0007	0.0037	0.0000	0.0009	0.0000	0.0000	0.0026	0.0000	0.0000	0.0032	0.0013
Mg	0.0135	0.0051	0.0000	0.0043	0.0033	0.0000	0.0023	0.0066	0.0148	0.0159	0.0018	0.0072	0.0046	0.0130	0.0000	0.0172	0.0000	0.0050	0.0153	0.0268
Fe ²⁺	0.0277	0.0151	0.0590	0.0297	0.0151	0.0202	0.1196	0.0644	0.0031	0.0011	0.0128	0.0167	0.0074	0.0000	0.0107	0.0000	0.0110	0.0000	0.0110	0.0000
Ca	8.8683	9.1989	9.2532	9.2277	9.0686	9.3865	9.1245	9.2478	9.0424	9.3713	9.3694	9.6686	9.6115	9.5886	9.5180	9.5481	9.6454	9.5829	9.5017	9.5003
Sr	0.4041	0.3772	0.3365	0.3126	0.4428	0.3435	0.4648	0.3721	0.4277	0.3454	0.3334	0.0925	0.1157	0.0815	0.0992	0.0945	0.0920	0.0983	0.1248	0.1262
Ba	0.0052	0.0070	0.0017	0.0044	0.0044	0.0009	0.0000	0.0000	0.0219	0.0000	0.0000	0.0106	0.0048	0.0181	0.0057	0.0000	0.0000	0.0000	0.0094	0.0000
La	0.0531	0.0187	0.0204	0.0327	0.0524	0.0171	0.0213	0.0336	0.0441	0.0371	0.0304	0.0250	0.0196	0.0142	0.0402	0.0070	0.0115	0.0263	0.0300	0.0203
Ce	0.2326	0.1145	0.0754	0.0893	0.1451	0.0714	0.1332	0.1099	0.1622	0.1037	0.0789	0.0785	0.0604	0.0352	0.0940	0.1080	0.0687	0.1001	0.1209	0.1171
Al	0.0000	0.0000	0.0000	0.0034	0.0036	0.0000	0.0000	0.0000	0.0020	0.0000	0.0014	0.0028	0.0000	0.0024	0.0000	0.0079	0.0040	0.0000	0.0000	0.0000
Sum	15.899	15.819	15.864	15.805	15.920	15.890	15.917	15.887	15.791	15.897	15.880	15.938	15.890	15.853	15.853	15.888	15.864	15.866	15.866	

Tabela A – Análises de apatita de rochas foscoríticas e glimerito de Catalão I. As análises foram recalculadas com base em 25 O. (Cont. X)

	304A- 3-3	304A- 3-4	304A- 3-5	304A- 3-6	304A- 3-7	304A- 3-8	304A- 3-9	304B- 2-1	304B- 2-2	304B- 2-3	304B- 2-4	304B- 2-5	319-2- 1	319-2- 2	319-2- 3	319-2- 4	319-2- 5	319-2- 6	319-2- 7	319-2- 8
Amostra	borda	interm	interm	interm	núcleo	interm	interm	borda	interm	núcleo	interm	interm	borda	interm	interm	interm	núcleo	núcleo	interm	
Oxidos (%)																				
P ₂ O ₅	41.61	42.23	41.92	42.15	41.38	41.28	41.40	40.13	40.82	41.73	42.09	41.13	42.41	41.94	41.77	41.52	42.30	42.75	41.83	42.25
SiO ₂	0.00	0.00	0.03	0.00	0.03	0.02	0.02	0.09	0.00	0.06	0.04	0.05	0.04	0.52	0.53	0.45	0.65	0.22	0.59	0.58
Na ₂ O	0.09	0.00	0.00	0.00	0.00	0.00	0.00	0.12	0.00	0.00	0.03	0.00	0.00	0.00	0.00	0.00	0.00	0.00	0.00	0.00
K ₂ O	0.00	0.00	0.01	0.01	0.02	0.03	0.09	0.09	0.05	0.01	0.00	0.01	0.00	0.00	0.01	0.00	0.00	0.00	0.00	0.01
MgO	0.01	0.02	0.00	0.04	0.10	0.06	0.07	0.12	0.05	0.04	0.00	0.10	0.06	0.06	0.01	0.04	0.04	0.06	0.08	0.05
FeO	0.14	0.05	0.06	0.10	0.07	0.13	0.15	0.24	0.17	0.22	0.30	1.50	0.01	0.05	0.00	0.01	0.04	0.00	0.00	0.00
CaO	49.76	52.19	51.09	51.87	52.21	51.53	50.92	51.09	51.64	53.06	52.02	51.90	53.03	51.33	52.21	52.46	52.36	51.65	52.17	52.83
SrO	4.21	2.77	3.65	2.37	1.55	1.94	3.00	3.14	2.34	1.49	2.64	2.06	1.35	1.24	1.06	0.83	0.87	1.15	0.96	0.88
BaO	0.03	0.00	0.00	0.09	0.00	0.12	0.12	0.13	0.01	0.01	0.10	0.09	0.00	0.13	0.12	0.00	0.00	0.05	0.00	0.00
La ₂ O ₃	0.53	0.17	0.37	0.27	0.28	0.33	0.23	0.57	0.36	0.27	0.29	0.27	0.09	0.48	0.34	0.28	0.42	0.49	0.26	0.28
Ce ₂ O ₃	1.25	0.60	0.95	0.48	0.50	1.19	0.78	0.88	0.78	0.44	0.51	0.35	0.37	0.63	0.83	0.51	0.64	0.65	0.67	0.66
Al ₂ O ₃	0.02	0.02	0.00	0.00	0.02	0.00	0.02	0.00	0.02	0.00	0.02	0.00	0.00	0.00	0.01	0.01	0.01	0.00	0.00	0.00
Total	97.65	98.04	98.07	97.38	96.15	96.63	96.77	96.48	96.36	97.31	98.02	97.49	97.36	96.37	96.87	96.10	97.31	97.02	96.60	97.53
Cations (p.f.u.)																				
P	6.0447	6.0498	6.0405	6.0691	6.0232	6.0077	6.0329	5.9235	5.9787	6.0083	6.0417	5.9647	6.0658	6.0545	6.0082	6.0099	6.0316	6.1127	6.0174	6.0172
Si	0.0000	0.0000	0.0051	0.0000	0.0052	0.0038	0.0036	0.0150	0.0000	0.0097	0.0064	0.0091	0.0069	0.0880	0.0896	0.0769	0.1095	0.0365	0.0996	0.0979
Na	0.0299	0.0000	0.0000	0.0000	0.0000	0.0000	0.0000	0.0000	0.0406	0.0000	0.0000	0.0103	0.0000	0.0000	0.0000	0.0000	0.0000	0.0000	0.0000	0.0000
K	0.0000	0.0000	0.0020	0.0028	0.0033	0.0066	0.0189	0.0196	0.0106	0.0015	0.0009	0.0015	0.0000	0.0000	0.0017	0.0000	0.0000	0.0006	0.0000	0.0013
Mg	0.0018	0.0061	0.0010	0.0101	0.0244	0.0151	0.0177	0.0315	0.0132	0.0096	0.0000	0.0263	0.0141	0.0158	0.0028	0.0107	0.0108	0.0151	0.0193	0.0113
Fe ²⁺	0.0396	0.0133	0.0159	0.0279	0.0187	0.0368	0.0417	0.0709	0.0483	0.0617	0.0862	0.4309	0.0037	0.0131	0.0000	0.0000	0.0031	0.0099	0.0000	0.0000
Ca	9.1490	9.4636	9.3152	9.4508	9.6173	9.4891	9.3889	9.5423	9.5719	9.6680	9.4491	9.5245	9.5999	9.3769	9.5053	9.6094	9.4489	9.3471	9.4969	9.5223
Sr	0.4190	0.2714	0.3602	0.2341	0.1544	0.1931	0.2992	0.3176	0.2349	0.1470	0.2595	0.2044	0.1326	0.1222	0.1043	0.0818	0.0848	0.1128	0.0943	0.0858
Ba	0.0017	0.0000	0.0000	0.0060	0.0000	0.0078	0.0078	0.0088	0.0009	0.0009	0.0068	0.0060	0.0000	0.0088	0.0079	0.0000	0.0000	0.0035	0.0000	0.0000
La	0.0337	0.0103	0.0232	0.0168	0.0178	0.0210	0.0145	0.0368	0.0228	0.0168	0.0184	0.0169	0.0057	0.0302	0.0214	0.0174	0.0260	0.0308	0.0165	0.0171
Ce	0.1499	0.0709	0.1123	0.0570	0.0604	0.1432	0.0935	0.1071	0.0942	0.0517	0.0608	0.0414	0.0431	0.0745	0.0981	0.0604	0.0754	0.0765	0.0791	0.0769
Al	0.0044	0.0040	0.0000	0.0000	0.0049	0.0000	0.0030	0.0000	0.0047	0.0000	0.0034	0.0000	0.0000	0.0002	0.0000	0.0018	0.0026	0.0000	0.0000	0.0000
Sum	15.874	15.889	15.875	15.875	15.930	15.924	15.922	16.073	16.021	15.975	15.933	16.236	15.872	15.784	15.839	15.868	15.793	15.745	15.827	15.830

Tabela A – Análises de apatita de rochas foscoríticas e glimerito de Catalão I. As análises foram recalculadas com base em 25 O. (Cont. XI)

	319-2- 9	339-2- 1B	339-2- 2	339-2- 3	339-2- 4	339-2- 5	339-4L- 1	339-4L- 2	339-4L- 3	339-4L- 4	339-4L- 5
Amostra											
Coord	17	2	6	11	16	20	2	10	18	27	36
Unidade	P1	P2	P2	P2	P2	DC	DC	DC	DC	DC	DC
Posição	borda	borda	núcleo	interm	interm	borda	borda	interm	núcleo	interm	borda
Oxidos (%)											
P ₂ O ₅	42.98	40.69	41.79	41.82	41.53	41.91	41.37	42.04	43.35	42.01	42.26
SiO ₂	0.02	0.00	0.00	0.01	0.00	0.00	0.00	0.01	0.00	0.02	0.03
Na ₂ O	0.00	0.00	0.00	0.00	0.13	0.00	0.19	0.00	0.00	0.00	0.00
K ₂ O	0.00	0.04	0.01	0.01	0.01	0.01	0.01	0.02	0.02	0.01	0.01
MgO	0.03	0.01	0.02	0.06	0.02	0.05	0.04	0.07	0.05	0.00	0.02
FeO	0.00	0.20	0.17	0.17	0.12	0.08	0.57	0.18	0.16	0.05	0.14
CaO	52.31	49.15	50.06	50.58	50.23	50.59	50.27	53.00	52.55	53.00	51.92
SrO	1.03	3.40	3.18	3.05	2.59	3.36	3.14	0.97	1.18	1.58	2.61
BaO	0.13	0.00	0.03	0.18	0.06	0.00	0.00	0.00	0.00	0.00	0.00
La ₂ O ₃	0.07	0.47	0.24	0.41	0.46	0.34	0.38	0.18	0.20	0.28	0.44
Ce ₂ O ₃	0.48	0.84	0.67	0.62	0.80	0.56	0.94	0.24	0.36	0.35	0.70
Al ₂ O ₃	0.00	0.00	0.00	0.00	0.02	0.01	0.02	0.02	0.02	0.00	0.01
Total	97.05	94.80	96.15	96.90	95.97	96.92	96.94	96.72	97.88	97.29	98.14
Cations (p.f.u.)											
P	6.1344	6.0605	6.1021	6.0763	6.0779	6.0841	6.0299	6.0532	6.1386	6.0393	6.0527
Si	0.0039	0.0000	0.0000	0.0021	0.0000	0.0000	0.0000	0.0015	0.0000	0.0036	0.0042
Na	0.0000	0.0000	0.0000	0.0000	0.0436	0.0000	0.0648	0.0000	0.0000	0.0000	0.0000
K	0.0000	0.0090	0.0013	0.0013	0.0026	0.0020	0.0026	0.0037	0.0032	0.0028	0.0022
Mg	0.0070	0.0026	0.0059	0.0141	0.0062	0.0125	0.0105	0.0188	0.0127	0.0000	0.0043
Fe ²⁺	0.0011	0.0600	0.0482	0.0479	0.0335	0.0232	0.1644	0.0509	0.0442	0.0128	0.0396
Ca	9.4485	9.2644	9.2506	9.3009	9.3013	9.2944	9.2724	9.6574	9.4168	9.6424	9.4102
Sr	0.1003	0.3471	0.3177	0.3032	0.2595	0.3344	0.3134	0.0957	0.1143	0.1552	0.2564
Ba	0.0087	0.0000	0.0018	0.0120	0.0037	0.0000	0.0000	0.0000	0.0000	0.0000	0.0000
La	0.0041	0.0303	0.0154	0.0259	0.0296	0.0216	0.0243	0.0114	0.0126	0.0175	0.0274
Ce	0.0566	0.1032	0.0807	0.0743	0.0965	0.0670	0.1133	0.0283	0.0417	0.0420	0.0827
Al	0.0000	0.0000	0.0000	0.0000	0.0037	0.0020	0.0045	0.0036	0.0030	0.0000	0.0020
Sum	15.765	15.877	15.824	15.858	15.858	15.841	16.000	15.924	15.787	15.915	15.882

Tabela B – Análises de flogopita e tetra-ferriflogopita de rochas foscoríticas e glimerito de Catalão I. As análises foram recalculadas com base em 22 O.

	110-46-1b-06	110-46-1b-07	110-46-1b-08	110-46-1b-09	110-46-1b-10	110-46-1-01B	46-1-02	110-46-1-03	110-46-1-04	110-46-1-05	F4-1-1	F4-1-2	F4-1-3	F4-1-4	F4-1-5	056-1-1C	056-1-2	056-1-3	056-1-4	056-1-5
Amostra	5	9	14	17	22	3	7	12	16	23	1	8	13.5	22	29	3	31	55	81	105
Coord	interm	núcleo	núcleo	interm	borda	interm	interm	núcleo	interm	borda						núcleo	interm	interm	interm	borda
Posição	P1	P1	P1	P1	P1	P1	P1	P1	P1	P1	P1	P1	P1	P1	P1	DC	DC	DC	DC	DC
Unidade																				
Oxidos (%)																				
SiO₂	40.92	41.07	40.65	41.80	40.90	41.35	41.13	41.10	41.11	39.99	40.88	40.97	41.11	40.26	42.03	41.31	40.98	41.26	41.12	40.35
TiO₂	0.81	0.87	0.75	0.58	0.23	0.66	0.76	0.99	0.79	0.74	0.23	2.53	2.50	2.54	0.24	0.06	0.13	0.13	0.13	0.10
Al₂O₃	9.80	9.94	9.59	9.18	3.03	9.43	9.80	10.07	9.87	8.76	1.63	10.50	11.08	10.87	0.13	0.00	0.01	0.02	0.08	0.02
Fe₂O₃	3.70	3.55	4.20	4.44	12.31	4.23	3.76	3.54	3.77	5.90	13.68	3.34	2.65	3.17	15.75	15.55	16.70	16.77	16.55	16.46
FeO	2.53	2.72	2.59	2.41	0.99	2.47	2.76	2.92	2.98	2.08	3.16	2.67	2.24	1.86	1.62	3.51	2.51	2.97	3.50	3.09
MnO	0.05	0.10	0.06	0.05	0.05	0.06	0.02	0.03	0.06	0.05	0.10	0.06	0.01	0.06	0.11	0.07	0.09	0.08	0.06	0.07
MgO	25.76	25.63	25.73	26.19	26.19	26.39	25.76	25.26	25.58	26.55	25.11	25.02	25.61	25.56	26.71	24.38	25.63	25.49	25.10	24.68
Na₂O	0.03	0.00	0.06	0.09	0.07	0.00	0.00	0.49	0.00	0.00	0.06	0.23	0.17	0.20	0.03	0.06	0.00	0.00	0.00	0.19
K₂O	10.68	10.75	10.66	11.05	10.54	10.24	10.92	10.84	11.08	9.52	9.07	9.09	8.92	8.57	8.46	10.52	10.31	10.45	10.27	10.36
BaO	0.25	0.41	0.34	0.17	0.00	0.01	0.20	0.17	0.28	0.21	0.00	0.00	0.00	0.00	0.19	0.00	0.00	0.00	0.00	0.00
CaO	0.00	0.00	0.01	0.01	0.08	0.03	0.00	0.00	0.00	0.00	0.09	0.06	0.05	0.09	0.13	0.01	0.01	0.00	0.01	0.04
H₂O	4.11	4.12	4.09	4.15	3.91	4.13	4.12	4.13	4.13	4.05	3.85	4.15	4.18	4.13	3.90	3.83	3.85	3.89	3.87	3.80
Total	98.65	99.16	98.74	100.11	98.29	99.01	99.22	99.54	99.65	97.84	97.85	98.61	98.51	97.31	99.28	99.29	100.21	101.05	100.69	99.17
Cl⁻	0.000	0.000	0.006	0.007	0.007	0.000	0.004	0.009	0.000	0.000	0.000	0.007	0.018	0.001	0.017	0.000	0.034	0.005	0.003	0.018
Cations (p.f.u.)																				
Si	5.924	5.925	5.900	5.976	6.089	5.945	5.927	5.910	5.917	5.843	6.156	5.867	5.856	5.808	6.213	6.229	6.115	6.118	6.125	6.113
Al	1.672	1.690	1.641	1.547	0.532	1.598	1.665	1.707	1.674	1.508	0.288	1.773	1.860	1.848	0.022	0.000	0.001	0.003	0.013	0.004
Fe³⁺	0.404	0.386	0.459	0.477	1.380	0.458	0.408	0.383	0.409	0.649	1.555	0.360	0.284	0.344	1.764	1.770	1.884	1.879	1.861	1.883
Ti	0.089	0.094	0.081	0.062	0.025	0.071	0.082	0.107	0.085	0.081	0.026	0.272	0.268	0.276	0.026	0.006	0.014	0.014	0.014	0.012
Oct	0.039	0.054	0.030	0.060	0.035	0.000	0.049	0.122	0.060	0.000	0.000	0.062	0.026	0.000	0.000	0.066	0.000	0.000	0.000	0.022
Fe²⁺	0.307	0.328	0.314	0.288	0.122	0.297	0.333	0.351	0.359	0.254	0.393	0.319	0.267	0.224	0.188	0.437	0.305	0.361	0.430	0.384
Mn	0.006	0.012	0.008	0.007	0.006	0.007	0.002	0.004	0.008	0.006	0.012	0.007	0.001	0.008	0.014	0.009	0.011	0.010	0.007	0.009
Mg	5.559	5.512	5.567	5.583	5.812	5.655	5.534	5.416	5.488	5.783	5.638	5.340	5.438	5.497	5.886	5.481	5.700	5.635	5.574	5.574
Ba	0.014	0.023	0.019	0.009	0.000	0.001	0.011	0.009	0.016	0.012	0.000	0.000	0.000	0.000	0.011	0.000	0.000	0.000	0.000	0.000
Ca	0.000	0.000	0.002	0.001	0.013	0.005	0.000	0.000	0.000	0.000	0.014	0.009	0.007	0.014	0.020	0.001	0.001	0.000	0.002	0.006
Na	0.009	0.000	0.017	0.026	0.019	0.000	0.000	0.136	0.000	0.000	0.018	0.065	0.048	0.057	0.009	0.019	0.000	0.000	0.000	0.056
K	1.973	1.979	1.974	2.015	2.002	1.879	2.009	1.988	2.035	1.775	1.742	1.661	1.621	1.577	1.596	2.023	1.962	1.977	1.952	2.003
OH⁻	3.967	3.968	3.960	3.958	3.882	3.962	3.965	3.966	3.946	3.871	3.968	3.971	3.971	3.849	3.853	3.835	3.843	3.844	3.839	
Sum	15.996	16.003	16.012	16.051	16.035	15.916	16.020	16.133	16.051	15.911	15.843	15.734	15.677	15.652	15.749	16.043	15.992	15.998	15.979	16.065

Tabela B – Análises de flogopita e tetra-ferriflogopita de rochas foscoríticas e glimerito de Catalão I. As análises foram recalculadas com base em 22 O. (Cont. I)

	091-3-1	091-3-2	091-3-3	091-3-4	091-3-5	091x-1-1	091x-1-2	091x-1-3	091x-1-4	091x-1-5	091x-1-6	091x-1-7	091x-1-8	093-1-1	093-1-2	093-1-3	093-1-4	093-1-5	093-1-6	093-1-1B
Amostra	1	2	3	4	5	1	2	3	4	5	6	7	8	1	2	3	4	5	6	1B
Coord	1	4	9	13	17									1	20	35	49	67	81	4
Posição	borda	interm	núcleo	interm	borda	núcleo	P2													
Unidade																				
Oxidos (%)																				
SiO₂	40.17	42.23	42.76	42.38	40.17	42.81	42.67	42.67	43.30	41.44	41.20	40.53	42.19	40.95	41.00	41.39	41.28	41.69	41.39	40.83
TiO₂	0.05	0.06	0.04	0.06	0.19	0.05	0.03	0.08	0.07	0.08	0.10	0.06	0.07	0.05	0.10	0.10	0.06	0.09	0.11	0.09
Al₂O₃	0.06	9.62	9.62	10.49	0.42	10.53	9.51	8.98	8.97	0.42	0.03	0.59	9.98	0.01	0.07	0.09	0.55	0.12	0.03	12.14
Fe₂O₃	17.34	4.27	3.42	2.02	16.52	1.88	3.47	4.27	4.41	15.69	16.08	15.65	2.41	16.16	16.43	15.25	15.25	15.62	15.27	0.78
FeO	2.80	0.63	1.14	1.20	2.27	2.34	1.99	1.65	2.67	2.43	2.52	2.54	2.04	3.54	3.30	3.93	3.40	3.76	4.51	2.24
MnO	0.13	0.03	0.01	0.02	0.08	0.02	0.03	0.03	0.05	0.10	0.04	0.09	0.00	0.05	0.08	0.07	0.03	0.13	0.11	0.03
MgO	25.34	28.18	27.78	27.38	25.21	27.29	27.43	27.60	27.46	25.76	25.32	25.33	26.96	24.46	24.73	24.18	24.37	24.40	23.71	26.79
Na₂O	0.00	0.00	0.00	0.00	0.24	0.13	0.01	0.00	0.02	0.00	0.00	0.08	0.19	0.48	0.57	0.03	0.79	0.41	0.13	0.00
K₂O	10.49	11.23	11.05	11.24	10.51	10.41	10.56	10.33	10.46	9.83	10.21	9.95	10.31	10.08	10.17	10.17	10.17	10.30	10.16	10.90
BaO	0.16	0.43	0.10	0.25	0.00	0.17	0.05	0.14	0.00	0.11	0.08	0.09	0.10	0.00	0.01	0.00	0.00	0.00	0.00	0.74
CaO	0.01	0.01	0.06	0.01	0.02	0.02	0.01	0.07	0.00	0.00	0.00	0.06	0.07	0.09	0.04	0.03	0.15	0.01	0.03	0.05
H₂O	3.83	4.21	4.21	4.20	3.82	4.23	4.20	4.19	4.25	3.88	3.84	3.83	4.15	3.83	3.85	3.83	3.86	3.87	3.82	4.17
Total	100.37	100.89	100.18	99.25	99.46	99.87	99.95	100.00	101.66	99.75	99.44	98.80	98.47	99.70	100.36	99.07	99.92	100.39	99.26	98.75
Cl⁻	0.005	0.005	0.013	0.006	0.013	0.000	0.009	0.024	0.002	0.009	0.010	0.000	0.031	0.014	0.011	0.013	0.000	0.007	0.013	0.022
Cations (p.f.u.)																				
Si	6.031	5.950	6.036	6.026	6.052	6.047	6.043	6.045	6.057	6.169	6.179	6.117	6.053	6.162	6.132	6.246	6.180	6.219	6.254	5.861
Al	0.010	1.598	1.601	1.758	0.074	1.753	1.588	1.499	1.479	0.074	0.006	0.105	1.687	0.002	0.012	0.017	0.097	0.022	0.006	2.054
Fe³⁺	1.959	0.452	0.363	0.216	1.873	0.200	0.370	0.456	0.464	1.757	1.815	1.778	0.260	1.836	1.855	1.737	1.724	1.759	1.741	0.084
Ti	0.005	0.007	0.004	0.006	0.021	0.005	0.004	0.009	0.007	0.009	0.011	0.006	0.007	0.006	0.011	0.012	0.006	0.010	0.012	0.010
Oct	0.000	0.000	0.015	0.044	0.019	0.000	0.000	0.000	0.000	0.007	0.000	0.000	0.060	0.058	0.048	0.132	0.085	0.068	0.000	
Fe²⁺	0.351	0.074	0.134	0.143	0.286	0.277	0.235	0.196	0.313	0.302	0.316	0.321	0.245	0.440	0.407	0.491	0.420	0.463	0.565	0.269
Mn	0.016	0.003	0.001	0.003	0.010	0.003	0.003	0.003	0.006	0.013	0.005	0.012	0.000	0.006	0.010	0.009	0.004	0.016	0.014	0.003
Mg	5.672	5.919	5.846	5.804	5.664	5.745	5.791	5.828	5.725	5.715	5.661	5.698	5.766	5.488	5.515	5.441	5.438	5.426	5.341	5.734
Ba	0.009	0.024	0.006	0.014	0.000	0.009	0.003	0.008	0.000	0.007	0.004	0.005	0.006	0.000	0.001	0.000	0.000	0.000	0.000	0.042
Ca	0.002	0.001	0.009	0.001	0.004	0.002	0.001	0.010	0.000	0.000	0.000	0.010	0.010	0.015	0.007	0.005	0.024	0.001	0.006	0.007
Na	0.000	0.000	0.000	0.000	0.071	0.035	0.002	0.000	0.005	0.000	0.000	0.023	0.054	0.139	0.166	0.009	0.230	0.120	0.038	0.000
K	2.010	2.019	1.990	2.039	2.020	1.875	1.909	1.866	1.866	1.867	1.954	1.915	1.886	1.935	1.940	1.958	1.943	1.960	1.958	1.996
OH⁻	3.835	3.961	3.966	3.981	3.840	3.986	3.967	3.956	3.961	3.851	3.845	3.851	3.972	3.844	3.843	3.851	3.857	3.852	3.851	3.992
Sum	16.065	16.047	16.005	16.054	16.094	15.951	15.949	15.920	15.922	15.913	15.958	15.990	15.974	16.089	16.114	15.972	16.196	16.080	16.001	16.061

Tabela B – Análises de flogopita e tetra-ferriflogopita de rochas foscoríticas e glimerito de Catalão I. As análises foram recalculadas com base em 22 O. (Cont. II)

	093-3- 2B	093-3- 3	093-1- 1	093-1- 2	093-1- 3	093-1- 5	093-1- 6	093-1- 7	093-1- 8	093-1- 9	099A- 5-1	099A- 5-3	099A- 5-4	099A- 5-5	099A-1- 10	099A-1- 11	099A-1- 12	099A-1- 13	099A-1- 14	099A-1- 15
Amostra	21	36	5	24	42	53	65	84	85	1	7	10	13							
Coord	borda	interm	interm	núcleo	interm	interm	borda			interm	núcleo	interm	borda							
Posição	P2	P2	P2	P2	P2	P2	P2	P2	P2	P3	P3	P3	P3	P3	P3	P3	P3	P3	P3	
Unidade																				
Oxidos (%)																				
SiO ₂	39.87	41.00	41.00	41.67	41.44	41.09	41.80	41.17	40.76	41.07	41.13	41.75	41.25	41.23	41.18	40.92	41.07	40.18	40.90	39.80
TiO ₂	0.05	0.03	0.05	0.15	0.07	0.00	0.10	0.13	0.13	0.10	0.09	0.11	0.12	0.13	0.11	0.09	0.10	0.03	0.07	0.11
Al ₂ O ₃	12.46	12.50	0.08	0.05	0.02	11.69	0.07	0.08	0.05	0.03	0.07	0.05	0.03	0.02	0.05	0.07	0.11	0.03	1.67	0.09
Fe ₂ O ₃	0.85	0.71	15.15	14.66	14.66	0.56	14.31	14.76	15.20	14.94	16.63	16.52	16.77	17.08	15.65	16.32	15.83	16.01	14.05	15.73
FeO	2.15	1.95	4.32	4.66	4.12	1.59	4.53	3.71	4.53	4.55	3.14	3.39	3.10	2.91	3.39	2.90	2.96	2.55	3.08	3.07
MnO	0.04	0.07	0.09	0.06	0.06	0.00	0.04	0.08	0.08	0.04	0.09	0.09	0.04	0.08	0.08	0.10	0.10	0.13	0.05	0.12
MgO	26.63	27.48	23.80	23.57	23.76	27.28	23.46	24.11	23.54	23.37	25.00	25.14	24.91	25.55	24.52	25.04	24.80	24.78	25.14	24.05
Na ₂ O	0.14	0.00	0.20	0.09	0.00	0.10	0.05	0.26	0.23	0.00	0.20	0.00	0.63	0.00	0.04	0.07	0.02	0.00	0.09	0.04
K ₂ O	10.45	10.27	9.79	9.81	9.87	9.32	10.04	9.36	9.81	10.15	10.66	10.72	10.53	10.59	10.09	10.25	10.38	10.00	10.28	10.10
BaO	1.75	1.55	0.10	0.00	0.05	1.21	0.00	0.10	0.00	0.15	0.04	0.08	0.00	0.00	0.06	0.00	0.05	0.18	0.00	0.06
CaO	0.00	0.00	0.04	0.00	0.03	0.14	0.01	0.03	0.01	0.00	0.00	0.01	0.00	0.02	0.08	0.14	0.04	0.08	0.05	0.11
H ₂ O	4.13	4.21	3.80	3.82	3.80	4.14	3.81	3.79	3.78	3.79	3.87	3.91	3.88	3.89	3.83	3.84	3.83	3.76	3.85	3.72
Total	98.51	99.78	98.42	98.52	97.88	97.10	98.22	97.57	98.11	98.19	100.91	101.77	101.26	101.52	99.07	99.74	99.28	97.72	99.24	97.00
Cl	0.000	0.000	0.000	0.021	0.002	0.013	0.000	0.010	0.017	0.015	0.002	0.000	0.007	0.007	0.004	0.013	0.016	0.015	0.073	0.031
Cations (p.f.u.)																				
Si	5.779	5.829	6.248	6.319	6.314	5.946	6.351	6.288	6.239	6.276	6.124	6.158	6.123	6.096	6.215	6.144	6.185	6.150	6.122	6.153
Al	2.129	2.095	0.015	0.009	0.004	1.993	0.012	0.015	0.009	0.005	0.012	0.009	0.005	0.004	0.008	0.012	0.020	0.006	0.295	0.016
Fe ³⁺	0.092	0.076	1.737	1.672	1.681	0.061	1.637	1.697	1.751	1.718	1.864	1.833	1.873	1.900	1.777	1.844	1.795	1.844	1.583	1.831
Ti	0.005	0.003	0.006	0.017	0.007	0.000	0.011	0.015	0.015	0.011	0.010	0.012	0.013	0.015	0.012	0.011	0.011	0.003	0.007	0.013
Oct	0.000	0.000	0.024	0.056	0.064	0.000	0.094	0.011	0.023	0.079	0.038	0.030	0.085	0.000	0.033	0.009	0.036	0.000	0.000	0.032
Fe ²⁺	0.260	0.232	0.550	0.591	0.524	0.193	0.575	0.473	0.580	0.581	0.391	0.418	0.385	0.360	0.428	0.364	0.373	0.326	0.385	0.396
Mn	0.005	0.008	0.012	0.008	0.008	0.000	0.005	0.010	0.011	0.006	0.011	0.011	0.005	0.011	0.011	0.013	0.013	0.017	0.007	0.016
Mg	5.753	5.824	5.408	5.328	5.397	5.886	5.315	5.491	5.371	5.323	5.550	5.529	5.512	5.631	5.516	5.603	5.567	5.654	5.610	5.543
Ba	0.099	0.086	0.006	0.000	0.003	0.068	0.000	0.006	0.000	0.009	0.002	0.005	0.000	0.000	0.004	0.000	0.003	0.011	0.000	0.004
Ca	0.000	0.000	0.006	0.000	0.005	0.021	0.001	0.006	0.001	0.000	0.000	0.001	0.000	0.003	0.013	0.023	0.007	0.013	0.008	0.018
Na	0.040	0.000	0.059	0.027	0.000	0.027	0.015	0.076	0.067	0.000	0.058	0.000	0.182	0.000	0.011	0.021	0.006	0.000	0.027	0.013
K	1.932	1.863	1.903	1.897	1.919	1.720	1.946	1.823	1.915	1.978	2.024	2.018	1.994	1.997	1.942	1.962	1.994	1.952	1.963	1.993
OH ⁻	3.992	3.993	3.860	3.860	3.861	3.995	3.866	3.856	3.856	3.858	3.841	3.844	3.841	3.840	3.851	3.843	3.848	3.842	3.848	3.841
Sum	16.095	16.017	15.974	15.924	15.915	15.962	15.911	15.982	15.986	16.084	16.024	16.177	16.017	15.970	16.006	16.010	15.976	16.007	16.028	

Tabela B – Análises de flogopita e tetra-ferriflogopita de rochas foscoríticas e glimerito de Catalão I. As análises foram recalculadas com base em 22 O. (Cont. III)

Amostra	099A- 1-16	099A- 1-17	099A- 1-19	099A- 1-2	099A- 1-20	099A- 1-21	099A- 1-3	099A- 1-4	099A- 1-8	099A- 1-9	099A- 4-1	099A- 4-2	099B- 2-1	099B- 2-1B	099B- 2-2	099B- 2-3	099B- 2-3B	099B- 2-4	099B- 2-5	099B- 2-6
Coord	P3	P3	P3	P3	P3	P3	P3	P3	P3	DC	DC	P2	P2	P2	P2	P2	P2	P2	P2	P2
Posição												borda	borda	interm	interm	interm	núcleo	núcleo	interm	
Unidade												P2	P2	P2	P2	P2	P2	P2	P2	P2
Oxidos (%)																				
SiO ₂	40.25	40.70	41.46	41.79	40.72	40.68	40.61	41.62	40.68	41.18	40.63	41.19	39.94	40.38	40.55	39.35	40.64	41.39	41.85	40.41
TiO ₂	0.06	0.11	0.06	0.05	0.08	0.05	0.13	0.08	0.10	0.10	0.08	0.09	0.05	0.05	0.10	0.11	0.12	0.04	0.05	0.08
Al ₂ O ₃	0.10	0.06	0.07	0.03	0.03	0.07	0.06	0.04	0.08	0.06	0.01	0.05	0.01	0.03	0.00	0.03	0.05	8.09	11.27	0.07
Fe ₂ O ₃	15.99	16.16	15.29	15.21	15.49	15.61	16.47	15.79	16.06	15.90	16.01	16.07	15.95	15.96	16.25	15.70	15.83	5.68	1.33	15.43
FeO	3.11	3.32	3.13	2.97	3.45	4.20	3.33	3.02	2.92	3.31	3.06	3.13	3.28	3.07	3.30	3.58	3.24	1.83	2.02	3.68
MnO	0.07	0.05	0.07	0.06	0.03	0.08	0.03	0.14	0.06	0.11	0.09	0.02	0.04	0.08	0.06	0.02	0.06	0.03	0.02	0.06
MgO	24.51	24.67	24.77	24.79	24.30	23.94	24.83	25.05	24.91	24.80	24.60	24.98	24.33	24.63	24.76	23.65	24.55	27.01	27.17	24.05
Na ₂ O	0.13	0.16	0.00	0.28	0.15	0.00	0.00	0.32	0.04	0.05	0.27	0.00	0.00	0.01	0.37	0.18	0.11	0.29	0.17	0.06
K ₂ O	10.13	10.24	9.89	10.29	9.89	9.98	10.25	10.15	10.02	10.02	10.25	10.17	9.87	10.03	9.94	9.79	9.84	10.28	10.58	9.86
BaO	0.13	0.00	0.05	0.13	0.04	0.00	0.00	0.11	0.00	0.00	0.05	0.00	0.08	0.00	0.00	0.18	0.20	0.10	0.52	0.03
CaO	0.07	0.02	0.04	0.01	0.05	0.06	0.00	0.01	0.06	0.05	0.06	0.06	0.06	0.03	0.01	0.01	0.06	0.04	0.00	0.02
H ₂ O	3.77	3.82	3.83	3.85	3.78	3.79	3.82	3.87	3.82	3.84	3.80	3.85	3.74	3.77	3.80	3.69	3.80	4.08	4.20	3.76
Total	98.30	99.29	98.65	99.45	98.00	98.45	99.53	100.20	98.74	99.40	98.91	99.60	97.32	98.03	99.14	96.32	98.48	98.81	99.20	97.48
Cl ⁻	0.036	0.003	0.023	0.008	0.019	0.010	0.003	0.000	0.009	0.010	0.010	0.013	0.011	0.018	0.000	0.037	0.015	0.016	0.000	0.005
Cations (p.f.u.)																				
Si	6.146	6.151	6.252	6.275	6.216	6.198	6.121	6.218	6.156	6.191	6.168	6.178	6.150	6.162	6.146	6.148	6.179	5.999	5.965	6.205
Al	0.017	0.011	0.013	0.006	0.005	0.012	0.010	0.007	0.015	0.010	0.002	0.008	0.002	0.005	0.000	0.006	0.009	1.382	1.893	0.012
Fe ³⁺	1.837	1.838	1.735	1.719	1.779	1.790	1.869	1.775	1.829	1.799	1.830	1.814	1.848	1.833	1.854	1.846	1.811	0.619	0.143	1.782
Ti	0.007	0.012	0.006	0.005	0.009	0.006	0.014	0.009	0.011	0.011	0.010	0.010	0.005	0.006	0.011	0.013	0.014	0.004	0.005	0.009
Oct	0.008	0.002	0.024	0.065	0.018	0.011	0.000	0.020	0.000	0.001	0.021	0.010	0.000	0.000	0.010	0.003	0.000	0.000	0.000	0.007
Fe ²⁺	0.397	0.419	0.394	0.372	0.440	0.535	0.419	0.377	0.369	0.416	0.389	0.392	0.423	0.392	0.418	0.468	0.412	0.222	0.241	0.472
Mn	0.009	0.007	0.008	0.008	0.004	0.010	0.004	0.017	0.007	0.014	0.012	0.002	0.006	0.010	0.008	0.002	0.007	0.003	0.002	0.008
Mg	5.579	5.560	5.568	5.550	5.529	5.438	5.580	5.577	5.620	5.558	5.568	5.586	5.584	5.604	5.594	5.507	5.564	5.835	5.772	5.504
Ba	0.008	0.000	0.003	0.007	0.002	0.000	0.000	0.007	0.000	0.000	0.003	0.000	0.005	0.000	0.000	0.011	0.012	0.006	0.029	0.002
Ca	0.011	0.003	0.007	0.002	0.008	0.009	0.000	0.002	0.010	0.008	0.009	0.010	0.005	0.001	0.002	0.009	0.006	0.000	0.004	0.000
Na	0.038	0.045	0.000	0.080	0.045	0.000	0.000	0.092	0.011	0.013	0.081	0.000	0.000	0.004	0.108	0.055	0.033	0.082	0.047	0.018
K	1.972	1.974	1.903	1.970	1.926	1.940	1.972	1.934	1.934	1.921	1.985	1.945	1.938	1.953	1.921	1.951	1.908	1.901	1.923	1.932
OH ⁻	3.838	3.849	3.853	3.854	3.853	3.851	3.843	3.852	3.853	3.848	3.845	3.852	3.843	3.842	3.846	3.845	3.849	3.947	3.995	3.854
Sum	16.029	16.022	15.913	16.059	15.981	15.949	15.989	16.035	15.962	15.942	16.078	15.955	15.966	15.970	16.062	16.026	15.958	16.053	16.024	15.951

Tabela B – Análises de flogopita e tetra-ferriflogopita de rochas foscoríticas e glimerito de Catalão I. As análises foram recalculadas com base em 22 O. (Cont. IV)

	099B-2-6B	099B-2-7	099B-2-7B	099B-2-8	103-1-1	103-1-2	103-1-3	103-1-4	103-1-5	103-3-1	103-3-2	103-3-3B	103-3-4	103-3-5	103-3-6	107-3b-5	107-3b-6	107-3b-7	107-3b-8	107-3-1
Amostra																				
Coord	72	86	84	112	7	43	74	92												5
Posição	interm	interm	interm	borda	núcleo	interm	interm	borda												borda
Unidade	P2	P2	P2	P2	DC	DC	DC	DC	P3	P3	P3	P3	P3	P3	P2	P2	P2	P2	P2	
Oxidos (%)																				
SiO₂	40.48	39.91	39.92	39.92	41.36	41.15	42.75	40.78	41.28	40.47	40.14	40.94	40.56	41.15	41.23	41.21	40.50	40.73	40.64	41.00
TiO₂	0.08	0.09	0.10	0.04	0.04	0.10	0.05	0.06	0.03	0.11	0.06	0.10	0.07	0.14	0.07	0.05	0.10	0.08	0.10	0.07
Al₂O₃	0.06	0.06	0.02	0.02	0.00	0.01	0.18	0.01	0.01	0.04	0.01	0.03	0.04	0.06	0.04	0.10	0.02	0.02	0.08	0.10
Fe₂O₃	15.39	15.73	15.52	15.79	15.96	15.59	14.61	16.08	16.41	16.03	15.89	16.03	15.59	16.30	15.83	15.21	16.27	16.27	15.39	15.31
FeO	3.31	3.30	3.15	2.37	2.94	2.99	2.96	3.12	2.74	2.52	2.47	3.09	2.64	3.37	2.61	4.09	2.59	4.52	3.86	4.17
MnO	0.07	0.06	0.04	0.06	0.06	0.04	0.12	0.05	0.11	0.09	0.00	0.14	0.12	0.02	0.08	0.08	0.10	0.06	0.08	0.07
MgO	24.20	24.12	24.09	24.58	25.13	24.72	25.10	24.90	25.46	24.94	24.81	24.94	24.63	25.07	25.28	24.06	25.07	24.22	24.05	23.93
Na₂O	0.00	0.04	0.00	0.06	0.17	0.20	0.20	0.00	0.05	0.00	0.00	0.08	0.10	0.00	0.03	0.14	0.09	0.18	0.14	0.07
K₂O	9.90	9.95	9.90	10.17	10.16	10.18	10.12	9.96	10.13	10.11	9.96	9.85	10.08	9.88	9.87	9.84	9.98	9.74	9.65	9.94
BaO	0.14	0.03	0.01	0.15	0.04	0.01	0.00	0.01	0.13	0.01	0.14	0.00	0.08	0.10	0.00	0.06	0.09	0.13	0.01	0.14
CaO	0.02	0.06	0.00	0.03	0.00	0.00	0.00	0.00	0.04	0.01	0.00	0.00	0.04	0.04	0.04	0.08	0.04	0.07	0.07	0.05
H₂O	3.76	3.73	3.72	3.73	3.85	3.82	3.91	3.82	3.87	3.79	3.75	3.82	3.78	3.85	3.84	3.81	3.80	3.82	3.78	3.79
Total	97.40	97.07	96.48	96.91	99.71	98.82	99.99	98.79	100.24	98.11	97.23	99.03	97.72	99.97	98.90	98.73	98.64	99.84	97.84	98.66
Cl	0.000	0.013	0.016	0.023	0.000	0.007	0.015	0.011	0.006	0.000	0.018	0.019	0.012	0.011	0.005	0.005	0.006	0.000	0.017	0.037
Cations (p.f.u.)																				
Si	6.212	6.161	6.186	6.163	6.199	6.223	6.338	6.168	6.157	6.158	6.163	6.175	6.199	6.155	6.201	6.247	6.140	6.148	6.215	6.231
Al	0.010	0.011	0.004	0.003	0.000	0.002	0.032	0.002	0.001	0.006	0.001	0.005	0.008	0.010	0.008	0.017	0.003	0.004	0.014	0.018
Fe³⁺	1.777	1.828	1.810	1.834	1.801	1.775	1.630	1.830	1.842	1.836	1.836	1.820	1.793	1.835	1.792	1.735	1.856	1.848	1.771	1.751
Ti	0.009	0.011	0.011	0.004	0.004	0.011	0.005	0.007	0.003	0.013	0.007	0.012	0.008	0.015	0.007	0.006	0.011	0.009	0.012	0.008
Oct	0.022	0.005	0.010	0.025	0.004	0.033	0.066	0.000	0.000	0.000	0.000	0.000	0.028	0.000	0.000	0.027	0.000	0.000	0.000	0.033
Fe²⁺	0.425	0.425	0.407	0.306	0.368	0.378	0.366	0.394	0.342	0.320	0.316	0.390	0.337	0.421	0.328	0.518	0.328	0.570	0.494	0.530
Mn	0.009	0.008	0.006	0.008	0.008	0.005	0.015	0.007	0.013	0.011	0.000	0.018	0.015	0.002	0.010	0.010	0.013	0.008	0.011	0.008
Mg	5.535	5.551	5.566	5.657	5.616	5.573	5.548	5.613	5.661	5.658	5.680	5.609	5.612	5.591	5.439	5.667	5.448	5.484	5.421	
Ba	0.008	0.002	0.001	0.009	0.002	0.001	0.000	0.001	0.008	0.001	0.009	0.000	0.005	0.006	0.000	0.004	0.005	0.007	0.001	0.008
Ca	0.003	0.009	0.001	0.005	0.000	0.000	0.000	0.000	0.006	0.001	0.000	0.000	0.006	0.006	0.013	0.006	0.011	0.011	0.009	
Na	0.000	0.013	0.000	0.018	0.049	0.058	0.058	0.000	0.015	0.000	0.000	0.022	0.030	0.000	0.008	0.040	0.026	0.051	0.041	0.021
K	1.937	1.959	1.958	2.004	1.943	1.964	1.914	1.922	1.927	1.963	1.952	1.896	1.966	1.885	1.893	1.903	1.930	1.876	1.882	1.928
OH⁻	3.853	3.843	3.845	3.840	3.852	3.854	3.865	3.850	3.845	3.848	3.842	3.845	3.850	3.844	3.850	3.857	3.845	3.850	3.851	3.846
Sum	15.947	15.983	15.960	16.036	15.994	16.023	15.972	15.944	15.975	15.967	15.964	15.947	16.007	15.926	15.959	15.985	15.980	15.936	15.966	

Tabela B – Análises de flogopita e tetra-ferriflogopita de rochas foscoríticas e glimerito de Catalão I. As análises foram recalculadas com base em 22 O. (Cont. V)

	099B-2-6B	099B-2-7	099B-2-7B	099B-2-8	103-1-1	103-1-2	103-1-3	103-1-4	103-1-5	103-3-1	103-3-2	103-3-3B	103-3-4	103-3-5	103-3-6	107-3b-5	107-3b-6	107-3b-7	107-3b-8	107-3-1
Amostra																				
Coord	72	86	84	112	7	43	74	92												5
Posição	interm	interm	interm	borda	núcleo	interm	interm	borda												borda
Unidade	P2	P2	P2	P2	DC	DC	DC	DC	P3	P3	P3	P3	P3	P3	P2	P2	P2	P2	P2	
Oxidos (%)																				
SiO ₂	40.48	39.91	39.92	39.92	41.36	41.15	42.75	40.78	41.28	40.47	40.14	40.94	40.56	41.15	41.23	41.21	40.50	40.73	40.64	41.00
TiO ₂	0.08	0.09	0.10	0.04	0.04	0.10	0.05	0.06	0.03	0.11	0.06	0.10	0.07	0.14	0.07	0.05	0.10	0.08	0.10	0.07
Al ₂ O ₃	0.06	0.06	0.02	0.02	0.00	0.01	0.18	0.01	0.01	0.04	0.01	0.03	0.04	0.06	0.04	0.10	0.02	0.02	0.08	0.10
Fe ₂ O ₃	15.39	15.73	15.52	15.79	15.96	15.59	14.61	16.08	16.41	16.03	15.89	16.03	15.59	16.30	15.83	15.21	16.27	16.27	15.39	15.31
FeO	3.31	3.30	3.15	2.37	2.94	2.99	2.96	3.12	2.74	2.52	2.47	3.09	2.64	3.37	2.61	4.09	2.59	4.52	3.86	4.17
MnO	0.07	0.06	0.04	0.06	0.06	0.04	0.12	0.05	0.11	0.09	0.00	0.14	0.12	0.02	0.08	0.08	0.10	0.06	0.08	0.07
MgO	24.20	24.12	24.09	24.58	25.13	24.72	25.10	24.90	25.46	24.94	24.81	24.94	24.63	25.07	25.28	24.06	25.07	24.22	24.05	23.93
Na ₂ O	0.00	0.04	0.00	0.06	0.17	0.20	0.20	0.00	0.05	0.00	0.00	0.08	0.10	0.00	0.03	0.14	0.09	0.18	0.14	0.07
K ₂ O	9.90	9.95	9.90	10.17	10.16	10.18	10.12	9.96	10.13	10.11	9.96	9.85	10.08	9.88	9.87	9.84	9.98	9.74	9.65	9.94
BaO	0.14	0.03	0.01	0.15	0.04	0.01	0.00	0.01	0.13	0.01	0.14	0.00	0.08	0.10	0.00	0.06	0.09	0.13	0.01	0.14
CaO	0.02	0.06	0.00	0.03	0.00	0.00	0.00	0.04	0.01	0.00	0.00	0.04	0.04	0.04	0.08	0.04	0.07	0.07	0.05	
H ₂ O	3.76	3.73	3.72	3.73	3.85	3.82	3.91	3.82	3.87	3.79	3.75	3.82	3.78	3.85	3.84	3.81	3.80	3.82	3.78	3.79
Total	97.40	97.07	96.48	96.91	99.71	98.82	99.99	98.79	100.24	98.11	97.23	99.03	97.72	99.97	98.90	98.73	98.64	99.84	97.84	98.66
Cl ⁻	0.000	0.013	0.016	0.023	0.000	0.007	0.015	0.011	0.006	0.000	0.018	0.019	0.012	0.011	0.005	0.006	0.000	0.017	0.037	
Cations (p.f.u.)																				
Si	6.212	6.161	6.186	6.163	6.199	6.223	6.338	6.168	6.157	6.158	6.163	6.175	6.199	6.155	6.201	6.247	6.140	6.148	6.215	6.231
Al	0.010	0.011	0.004	0.003	0.000	0.002	0.032	0.002	0.001	0.006	0.001	0.005	0.008	0.010	0.008	0.017	0.003	0.004	0.014	0.018
Fe ³⁺	1.777	1.828	1.810	1.834	1.801	1.775	1.630	1.830	1.842	1.836	1.836	1.820	1.793	1.835	1.792	1.735	1.856	1.848	1.771	1.751
Ti	0.009	0.011	0.011	0.004	0.004	0.011	0.005	0.007	0.003	0.013	0.007	0.012	0.008	0.015	0.007	0.006	0.011	0.009	0.012	0.008
Oct	0.022	0.005	0.010	0.025	0.004	0.033	0.066	0.000	0.000	0.000	0.000	0.000	0.028	0.000	0.000	0.027	0.000	0.000	0.000	0.033
Fe ²⁺	0.425	0.425	0.407	0.306	0.368	0.378	0.366	0.394	0.342	0.320	0.316	0.390	0.337	0.421	0.328	0.518	0.328	0.570	0.494	0.530
Mn	0.009	0.008	0.006	0.008	0.008	0.005	0.015	0.007	0.013	0.011	0.000	0.018	0.015	0.002	0.010	0.010	0.013	0.008	0.011	0.008
Mg	5.535	5.551	5.566	5.657	5.616	5.573	5.548	5.613	5.661	5.658	5.680	5.609	5.612	5.591	5.669	5.439	5.667	5.448	5.484	5.421
Ba	0.008	0.002	0.001	0.009	0.002	0.001	0.000	0.001	0.008	0.001	0.009	0.000	0.005	0.006	0.000	0.004	0.005	0.007	0.001	0.008
Ca	0.003	0.009	0.001	0.005	0.000	0.000	0.000	0.006	0.001	0.000	0.000	0.006	0.006	0.006	0.013	0.006	0.011	0.011	0.009	
Na	0.000	0.013	0.000	0.018	0.049	0.058	0.058	0.000	0.015	0.000	0.000	0.022	0.030	0.000	0.008	0.040	0.026	0.051	0.041	0.021
K	1.937	1.959	1.958	2.004	1.943	1.964	1.914	1.922	1.927	1.963	1.952	1.896	1.966	1.885	1.893	1.903	1.930	1.876	1.882	1.928
OH ⁻	3.853	3.843	3.845	3.840	3.852	3.854	3.865	3.850	3.845	3.848	3.842	3.845	3.850	3.844	3.850	3.857	3.845	3.850	3.851	3.846
Sum	15.947	15.983	15.960	16.036	15.994	16.023	15.972	15.944	15.975	15.967	15.964	15.947	16.007	15.926	15.922	15.959	15.985	15.980	15.936	15.966

Tabela B – Análises de flogopita e tetra-ferriflogopita de rochas foscoríticas e glimerito de Catalão I. As análises foram recalculadas com base em 22 O. (Cont. VI)

Amostra	107-3-2	107-3-3	107-3-4	116-2-1	116-2-2	116-2-3	116-2-4	116-2-5	116-2-6	116-4-1	116-4-2	116-4-3	116-4-4	116-4-5	116-4-6	149-1b-01	149-1b-02	149-1b-03	149-1b-04	149-1b-05	149-1b-06
	Coord	13	17	26	2	14	21	26	35	42	3	22	65	100	125	5	10	15	20	25	30
Posição	núcleo	interm	interm	borda	interm	núcleo	interm	borda	núcleo	interm	interm	borda	interm	borda	interm	interm	interm	núcleo	interm	interm	
Unidade	P2	DC	DC	DC	DC	DC															
Oxidos (%)																					
SiO ₂	40.46	40.38	42.13	39.96	41.12	40.38	40.94	40.73	40.81	41.29	41.13	40.78	40.82	39.83	40.41	40.98	41.02	41.15	40.92	40.32	
TiO ₂	0.00	0.05	0.03	0.04	0.09	0.10	0.04	0.11	0.10	0.13	0.07	0.11	0.06	0.10	0.07	0.08	0.08	0.06	0.06	0.04	
Al ₂ O ₃	0.02	0.02	0.07	0.34	0.07	0.32	0.18	0.09	0.05	0.02	0.09	0.01	0.06	0.03	0.03	0.05	0.07	0.05	0.05	0.02	0.06
Fe ₂ O ₃	16.91	16.45	15.03	15.85	15.95	16.40	16.81	15.00	15.76	15.43	16.05	16.58	16.56	16.68	15.76	15.32	15.69	15.55	15.75	15.40	
FeO	1.72	2.71	3.60	3.09	3.13	2.24	2.43	3.73	3.23	3.09	3.60	2.97	3.15	3.64	3.68	3.31	3.24	3.36	3.60	3.14	
MnO	0.11	0.02	0.03	0.13	0.11	0.10	0.05	0.08	0.06	0.04	0.13	0.06	0.11	0.07	0.02	0.05	0.04	0.12	0.10		
MgO	26.08	25.14	24.73	24.21	24.39	25.44	25.62	23.63	24.34	24.28	24.53	24.95	24.73	24.22	24.08	24.23	24.47	24.38	24.26	24.02	
Na ₂ O	0.09	0.00	0.09	0.12	0.37	0.00	0.21	0.00	0.06	0.21	0.06	0.03	0.46	0.00	0.00	0.00	0.00	0.00	0.00	0.00	
K ₂ O	9.95	10.02	9.93	10.70	10.72	10.45	10.63	10.47	10.60	10.65	10.50	10.60	10.46	10.59	10.30	10.42	10.57	10.51	10.51	10.25	
BaO	0.10	0.10	0.00	0.00	0.13	0.03	0.03	0.03	0.00	0.00	0.04	0.06	0.00	0.04	0.00	0.04	0.04	0.00	0.00	0.13	
CaO	0.02	0.05	0.03	0.08	0.00	0.00	0.00	0.00	0.00	0.00	0.01	0.00	0.00	0.00	0.01	0.01	0.01	0.00	0.00	0.11	
H ₂ O	3.83	3.80	3.87	3.77	3.84	3.82	3.87	3.77	3.80	3.82	3.85	3.84	3.84	3.77	3.77	3.79	3.82	3.82	3.81	3.74	
Total	99.29	98.73	99.53	98.27	99.91	99.26	100.80	97.63	98.81	98.96	100.06	99.99	100.24	98.97	98.12	98.27	99.05	98.99	99.03	97.31	
Cl ⁻	0.012	0.000	0.005	0.005	0.000	0.013	0.013	0.004	0.000	0.000	0.000	0.002	0.006	0.000	0.000	0.013	0.007	0.005	0.025		
Cations (p.f.u.)																					
Si	6.083	6.120	6.297	6.114	6.183	6.084	6.087	6.251	6.191	6.241	6.172	6.125	6.121	6.079	6.181	6.236	6.202	6.222	6.200	6.205	
Al	0.004	0.004	0.013	0.060	0.012	0.056	0.032	0.017	0.009	0.004	0.016	0.001	0.011	0.006	0.005	0.009	0.012	0.009	0.003	0.011	
Fe ³⁺	1.913	1.876	1.690	1.825	1.805	1.860	1.881	1.732	1.799	1.755	1.812	1.874	1.868	1.915	1.814	1.755	1.786	1.769	1.796	1.783	
Ti	0.000	0.005	0.003	0.005	0.010	0.011	0.004	0.013	0.011	0.014	0.008	0.012	0.007	0.011	0.008	0.009	0.010	0.006	0.004	0.007	
Oct	0.000	0.000	0.034	0.060	0.117	0.000	0.010	0.093	0.067	0.119	0.037	0.020	0.057	0.004	0.028	0.068	0.059	0.058	0.045	0.067	
Fe ²⁺	0.215	0.343	0.450	0.395	0.393	0.282	0.302	0.478	0.410	0.390	0.451	0.373	0.395	0.465	0.470	0.421	0.410	0.425	0.456	0.403	
Mn	0.013	0.003	0.004	0.017	0.014	0.012	0.006	0.011	0.007	0.005	0.017	0.008	0.013	0.009	0.003	0.006	0.005	0.015	0.016	0.013	
Mg	5.845	5.680	5.509	5.523	5.466	5.714	5.678	5.405	5.505	5.472	5.487	5.587	5.528	5.511	5.491	5.496	5.516	5.496	5.479	5.510	
Ba	0.006	0.006	0.000	0.000	0.007	0.001	0.001	0.002	0.000	0.002	0.004	0.000	0.002	0.000	0.002	0.000	0.000	0.000	0.000	0.008	
Ca	0.004	0.007	0.005	0.013	0.000	0.000	0.001	0.000	0.000	0.002	0.000	0.000	0.000	0.001	0.001	0.002	0.000	0.000	0.000	0.018	
Na	0.027	0.000	0.026	0.036	0.107	0.000	0.061	0.000	0.018	0.062	0.018	0.009	0.133	0.000	0.000	0.000	0.000	0.000	0.000	0.000	
K	1.908	1.937	1.893	2.088	2.057	2.009	2.016	2.051	2.052	2.053	2.011	2.030	2.001	2.061	2.010	2.022	2.038	2.028	2.032	2.012	
OH ⁻	3.839	3.844	3.859	3.846	3.849	3.841	3.839	3.855	3.850	3.853	3.849	3.843	3.842	3.840	3.848	3.850	3.849	3.851	3.849	3.844	
Sum	16.018	15.981	15.924	16.136	16.171	16.029	16.079	16.053	16.069	16.115	16.033	16.043	16.134	16.063	16.011	16.025	16.042	16.028	16.031	16.037	

Tabela B – Análises de flogopita e tetra-ferriflogopita de rochas foscoríticas e glimerito de Catalão I. As análises foram recalculadas com base em 22 O. (Cont. VII)

	149-1b-	149-1-	149-1-	149-1-	149-1-	149-1-	149-1-	149-1-	149-1-	149-1-	149-1-	152-1-	152-1-	152-1-	152-1-	156-1-	156-1-	156-1-	156-1-3	
Amostra	07	01	02	03	04	05	06	07	08	09	10	1	2	3	4	5	6	1	2	
Coord	35	10	20	30	40	50	60	70	80	90	100	4	27	50	49	9	20	30		
Posição	borda	núcleo	interm	borda	borda	borda	borda	borda	interm	núcleo										
Unidade	DC	DC	DC	DC	DC	DC	DC	DC	DC	DC	DC	P2								
Oxidos (%)																				
SiO ₂	41.39	41.19	39.51	40.87	41.30	41.20	40.82	41.21	40.99	40.82	39.94	41.46	40.56	39.53	40.34	42.12	41.43	41.46	41.25	43.21
TiO ₂	0.07	0.12	0.09	0.04	0.06	0.06	0.04	0.11	0.08	0.09	0.04	0.08	0.11	0.01	0.06	0.11	0.07	0.05	0.06	0.06
Al ₂ O ₃	0.04	0.00	0.21	0.03	0.00	0.04	0.07	0.03	0.08	0.09	0.07	0.03	0.03	0.61	0.44	0.02	0.01	2.53	0.76	10.33
Fe ₂ O ₃	15.94	15.86	15.25	16.02	15.72	15.64	15.34	15.67	15.83	15.20	15.39	15.35	15.58	15.37	15.69	14.81	15.23	12.14	15.04	2.17
FeO	2.57	2.97	3.22	2.98	3.65	3.57	3.50	3.78	3.63	3.11	3.22	4.00	3.59	4.08	4.39	3.69	4.15	2.79	3.54	1.52
MnO	0.08	0.06	0.06	0.06	0.07	0.07	0.03	0.07	0.10	0.06	0.03	0.06	0.12	0.11	0.07	0.12	0.10	0.05	0.05	0.04
MgO	25.13	24.64	23.60	24.58	24.24	24.44	24.09	24.18	24.19	24.21	23.83	24.28	24.14	24.02	24.19	24.44	24.02	25.31	25.00	27.79
Na ₂ O	0.00	0.18	0.51	0.21	0.15	0.00	0.00	0.03	0.18	0.09	0.22	0.29	0.29	0.03	0.12	0.12	0.01	0.00	0.00	0.12
K ₂ O	10.66	10.44	9.56	10.70	10.60	10.35	10.47	10.52	10.55	10.23	10.18	9.86	9.89	9.60	9.77	9.77	10.06	10.10	9.90	10.72
BaO	0.04	0.09	0.13	0.01	0.00	0.00	0.03	0.06	0.11	0.12	0.05	0.00	0.00	0.00	0.00	0.00	0.00	0.00	0.00	0.17
CaO	0.00	0.00	0.07	0.00	0.00	0.00	0.00	0.00	0.00	0.00	0.00	0.03	0.02	0.03	0.05	0.00	0.00	0.00	0.00	0.00
H ₂ O	3.85	3.83	3.68	3.82	3.83	3.83	3.79	3.83	3.82	3.77	3.72	3.84	3.78	3.74	3.80	3.86	3.82	3.90	3.87	4.25
Total	99.77	99.38	95.89	99.31	99.62	99.18	98.18	99.49	99.55	97.77	96.69	99.28	98.10	97.11	98.90	99.06	98.89	98.32	99.46	100.38
Cl ⁻	0.015	0.012	0.054	0.008	0.000	0.003	0.003	0.000	0.011	0.037	0.011	0.007	0.003	0.002	0.007	0.004	0.008	0.001	0.000	0.011
Cations (p.f.u.)																				
Si	6.197	6.202	6.169	6.173	6.219	6.217	6.227	6.216	6.188	6.237	6.192	6.253	6.202	6.104	6.128	6.322	6.265	6.190	6.173	6.063
Al	0.007	0.000	0.039	0.006	0.000	0.007	0.012	0.005	0.014	0.015	0.013	0.006	0.006	0.110	0.079	0.004	0.001	0.446	0.134	1.708
Fe ³⁺	1.796	1.798	1.792	1.821	1.781	1.776	1.761	1.779	1.798	1.747	1.795	1.742	1.792	1.786	1.794	1.673	1.733	1.364	1.694	0.229
Ti	0.008	0.013	0.011	0.004	0.007	0.006	0.005	0.012	0.009	0.010	0.005	0.009	0.013	0.002	0.006	0.012	0.008	0.006	0.007	0.007
Oct	0.050	0.074	0.068	0.076	0.083	0.037	0.065	0.067	0.077	0.072	0.067	0.020	0.011	0.000	0.000	0.041	0.039	0.004	0.000	0.000
Fe ²⁺	0.321	0.374	0.420	0.377	0.459	0.450	0.447	0.476	0.458	0.397	0.418	0.504	0.459	0.526	0.557	0.463	0.525	0.349	0.443	0.178
Mn	0.011	0.008	0.008	0.008	0.009	0.009	0.004	0.009	0.012	0.008	0.004	0.008	0.015	0.014	0.008	0.015	0.012	0.007	0.004	
Mg	5.610	5.531	5.493	5.535	5.442	5.498	5.479	5.436	5.444	5.513	5.506	5.459	5.502	5.528	5.477	5.469	5.416	5.634	5.576	5.812
Ba	0.002	0.005	0.008	0.001	0.000	0.001	0.004	0.006	0.007	0.003	0.000	0.000	0.000	0.000	0.000	0.000	0.000	0.000	0.009	
Ca	0.000	0.000	0.012	0.000	0.000	0.000	0.000	0.000	0.001	0.000	0.000	0.004	0.004	0.005	0.007	0.000	0.000	0.000	0.000	
Na	0.000	0.054	0.154	0.061	0.045	0.000	0.000	0.009	0.052	0.027	0.066	0.086	0.087	0.007	0.036	0.036	0.004	0.000	0.000	0.033
K	2.036	2.006	1.904	2.062	2.037	1.992	2.038	2.025	2.032	1.993	2.014	1.897	1.930	1.891	1.894	1.872	1.942	1.923	1.890	1.920
OH ⁻	3.846	3.847	3.835	3.846	3.851	3.851	3.852	3.852	3.847	3.843	3.848	3.860	3.857	3.851	3.862	3.854	3.886	3.859	3.980	
Sum	16.038	16.065	16.078	16.124	16.082	15.992	16.039	16.038	16.091	16.026	16.083	15.988	16.021	15.973	15.986	15.907	15.945	15.923	15.924	15.963

Tabela B – Análises de flogopita e tetra-ferriflogopita de rochas foscoríticas e glimerito de Catalão I. As análises foram recalculadas com base em 22 O. (Cont. VIII)

Amostra	156-1-4	156-1-5	156-2-1	156-2-2	156-2-3	157a-1-1	157a-1-2	157a-1-3	157a-1-4	157a-1-5	157B-5-1B	157B-5-2	157B-5-3B	157B-5-4	157B-5-5	157B-5-6B	157b-2-a-1	157b-2-a-2	157b-2-a-3
	Coord	41	58	2	27	59	3	16	27	40	57	1	6	11	15	19	26	6	14
Posição	midddl	borda	borda	núcleo		borda	interm	núcleo	interm	borda	borda	interm	interm	núcleo	interm	borda	borda	núcleo	núcleo
Unidade	P2	P2	P2	P2	P2	P2	P2	P2	P2	P2	P3	P3	P3	P3	P3	P3	P3	P3	P3
Oxidos (%)																			
SiO ₂	41.36	41.32	40.93	41.98	41.67	40.75	40.42	42.45	40.67	41.08	41.88	40.93	40.19	40.32	40.56	40.68	40.99	40.77	41.09
TiO ₂	0.06	0.06	0.09	0.06	0.06	0.08	0.10	0.03	0.07	0.07	0.12	0.08	0.07	0.11	0.08	0.11	0.08	0.07	0.10
Al ₂ O ₃	3.21	4.12	2.49	9.18	4.39	0.00	0.00	10.80	0.02	0.10	0.02	0.00	0.09	0.01	0.03	0.00	0.06	0.00	0.02
Fe ₂ O ₃	12.10	10.60	12.95	4.24	10.53	15.84	16.20	1.74	15.58	15.14	16.81	16.89	16.18	16.01	16.34	16.70	15.81	15.39	15.71
FeO	2.92	3.12	3.01	1.89	2.50	2.81	3.33	1.62	3.28	3.59	2.64	3.16	3.41	3.43	3.02	2.78	2.88	3.37	3.21
MnO	0.06	0.04	0.06	0.00	0.12	0.02	0.08	0.00	0.04	0.08	0.10	0.06	0.10	0.08	0.09	0.05	0.09	0.07	0.05
MgO	25.72	25.62	25.38	27.25	26.19	24.95	24.68	27.60	24.65	24.34	25.91	25.11	24.30	24.07	24.43	25.01	24.91	24.25	24.73
Na ₂ O	0.00	0.00	0.05	0.00	0.00	0.00	0.00	0.00	0.09	0.00	0.00	0.00	0.03	0.00	0.25	0.15	0.14	0.07	0.00
K ₂ O	10.27	10.03	9.93	10.70	10.36	9.82	9.75	10.54	9.44	9.76	10.28	10.76	10.52	10.69	10.78	10.61	10.06	10.04	9.93
BaO	0.09	0.00	0.20	0.03	0.00	0.00	0.10	0.40	0.00	0.00	0.16	0.05	0.00	0.04	0.00	0.06	0.00	0.09	0.09
CaO	0.00	0.03	0.02	0.00	0.02	0.00	0.00	0.00	0.03	0.00	0.06	0.00	0.00	0.03	0.07	0.02	0.00	0.00	0.01
H ₂ O	3.95	3.96	3.90	4.16	4.00	3.80	3.79	4.22	3.78	3.80	3.93	3.86	3.78	3.77	3.81	3.83	3.82	3.78	3.82
Total	99.73	98.89	98.99	99.48	99.84	98.07	98.45	99.40	97.64	97.96	101.91	100.89	98.69	98.52	99.48	99.94	98.90	97.81	98.76
Cl ⁻	0.003	0.012	0.000	0.000	0.010	0.000	0.005	0.009	0.001	0.000	0.018	0.000	0.010	0.014	0.011	0.014	0.000	0.006	0.013
Cations (p.f.u.)																			
Si	6.100	6.104	6.107	5.998	6.087	6.190	6.146	6.012	6.207	6.249	6.142	6.104	6.127	6.158	6.136	6.112	6.193	6.230	6.210
Al	0.557	0.717	0.438	1.546	0.755	0.000	0.000	1.803	0.004	0.018	0.003	0.001	0.017	0.002	0.004	0.000	0.010	0.000	0.004
Fe ³⁺	1.343	1.178	1.455	0.456	1.158	1.810	1.854	0.185	1.789	1.734	1.855	1.896	1.856	1.840	1.860	1.888	1.797	1.770	1.786
Ti	0.006	0.007	0.010	0.006	0.007	0.010	0.012	0.003	0.008	0.007	0.013	0.009	0.008	0.012	0.010	0.013	0.010	0.008	0.012
Oct	0.000	0.000	0.000	0.000	0.000	0.000	0.000	0.000	0.000	0.007	0.000	0.008	0.023	0.061	0.089	0.031	0.005	0.029	0.005
Fe ²⁺	0.360	0.385	0.375	0.226	0.305	0.357	0.423	0.192	0.419	0.457	0.324	0.394	0.434	0.438	0.382	0.349	0.364	0.430	0.406
Mn	0.007	0.006	0.008	0.000	0.015	0.002	0.010	0.000	0.005	0.010	0.013	0.007	0.012	0.011	0.011	0.006	0.011	0.009	0.006
Mg	5.655	5.642	5.645	5.804	5.704	5.651	5.595	5.828	5.608	5.519	5.664	5.582	5.523	5.478	5.508	5.601	5.610	5.524	5.571
Ba	0.005	0.000	0.012	0.001	0.000	0.000	0.006	0.022	0.000	0.000	0.009	0.003	0.000	0.000	0.002	0.000	0.004	0.000	0.005
Ca	0.000	0.005	0.003	0.000	0.003	0.000	0.000	0.000	0.004	0.000	0.010	0.000	0.001	0.004	0.011	0.003	0.000	0.000	0.001
Na	0.000	0.000	0.014	0.000	0.000	0.000	0.000	0.001	0.026	0.000	0.000	0.000	0.009	0.000	0.072	0.045	0.040	0.021	0.000
K	1.932	1.891	1.889	1.951	1.931	1.903	1.892	1.905	1.837	1.893	1.923	2.048	2.046	2.082	2.080	2.033	1.939	1.958	1.915
OH ⁻	3.887	3.899	3.880	3.962	3.900	3.849	3.844	3.982	3.852	3.855	3.840	3.842	3.842	3.842	3.839	3.853	3.848		
Sum	15.96	15.93	15.95	15.99	15.96	15.923	15.938	15.951	15.907	15.894	15.956	16.052	16.056	16.086	16.165	16.081	15.983	15.979	15.921

Tabela B – Análises de flogopita e tetra-ferriflogopita de rochas foscoríticas e glimerito de Catalão I. As análises foram recalculadas com base em 22 O. (Cont. IX)

Amostra	157b- 2b-6	157b- 2b-7	157b- 2b-8	170-1-1	170-1- 2	170-1- 3	170-1- 4	170-1- 5	178-1- 1	178-1- 2	178-1- 3	178-1- 4	178-1- 6	178-1- 7	178-1- 8B	183- 1Lb-1	183- 1Lb-2	183- 1Lb-3	183- 1Lb-4	183- 1Lb-5	
	Coord	4	8		1	7	14	21	27	1	11	26	40	61	72	85	1	11	21	31	41
Posição	núcleo	borda								borda	interm	núcleo	núcleo	núcleo	interm	borda	borda	interm	interm	borda	
Unidade	P3	P3	P3	DC	DC	DC	DC	DC	P2	P2	P2	P2	P2	P2	DC	DC	DC	DC	DC	DC	
Oxidos (%)																					
SiO ₂	41.304	40.76	40.87	41.39	41.42	41.56	41.74	42.16	40.24	39.67	42.08	41.76	41.82	40.40	41.12	41.53	40.25	40.62	40.62	40.52	
TiO ₂	0.067	0.11	0.10	0.07	0.08	0.09	0.09	0.07	0.06	0.06	0.02	0.02	0.02	0.10	0.02	0.04	0.04	0.07	0.09	0.06	
Al ₂ O ₃	2.603	0.01	0.04	0.06	0.04	0.01	0.08	0.12	0.12	0.04	8.82	7.68	7.68	0.01	0.04	0.02	0.07	0.01	0.02	0.04	
Fe ₂ O ₃	12.399	15.69	15.73	15.32	15.60	15.54	15.49	16.32	15.86	16.17	4.80	6.39	5.91	16.35	15.52	15.47	16.27	16.42	16.06	15.80	
FeO	2.614	3.18	3.72	3.20	2.89	3.59	3.93	3.24	3.73	3.10	1.37	1.45	1.31	2.17	3.21	2.40	2.51	2.54	2.74	2.60	
MnO	0.067	0.14	0.11	0.09	0.04	0.07	0.12	0.07	0.12	0.04	0.00	0.03	0.04	0.07	0.02	0.09	0.05	0.01	0.07	0.10	
MgO	25.628	24.52	24.38	24.17	24.62	24.72	24.52	25.44	24.15	24.22	27.45	27.20	26.79	25.35	24.35	24.93	24.91	25.12	24.61	24.43	
Na ₂ O	0	0.03	0.00	0.60	0.51	0.00	0.00	0.54	0.00	0.00	0.00	0.00	0.33	0.03	0.28	0.09	0.18	0.00	0.12	0.15	
K ₂ O	9.83	9.91	9.81	10.42	10.42	9.95	10.15	10.16	10.03	10.43	11.17	10.96	10.92	9.92	10.39	10.60	10.35	10.61	10.62	10.73	
BaO	0.038	0.00	0.09	0.04	0.00	0.00	0.06	0.00	0.09	0.00	0.03	0.09	0.09	0.05	0.00	0.00	0.00	0.00	0.10	0.05	
CaO	0.031	0.02	0.04	0.00	0.00	0.00	0.00	0.00	0.04	0.03	0.00	0.01	0.01	0.02	0.05	0.06	0.00	0.00	0.00	0.03	
H ₂ O	3.909	3.79	3.80	3.83	3.85	3.85	3.87	3.94	3.77	3.74	4.16	4.11	4.09	3.79	3.82	3.84	3.79	3.82	3.80	3.78	
Total	98.49	98.15	98.69	99.20	99.45	99.38	100.03	102.05	98.19	97.51	99.89	99.67	99.00	98.25	98.81	99.08	98.43	99.21	98.85	98.28	
Cl ⁻	0	0.000	0.014	0.005	0.000	0.000	0.002	0.008	0.016	0.000	0.017	0.011	0.003	0.012	0.000	0.008	0.000	0.004	0.002	0.000	
Cations (p.f.u.)																					
Si	6.153	6.203	6.197	6.244	6.222	6.237	6.239	6.174	6.153	6.117	6.002	6.007	6.048	6.131	6.225	6.245	6.123	6.132	6.163	6.180	
Al	0.457	0.001	0.008	0.011	0.008	0.002	0.013	0.021	0.022	0.007	1.483	1.301	1.309	0.001	0.007	0.004	0.013	0.002	0.003	0.006	
Fe ³⁺	1.39	1.796	1.795	1.745	1.770	1.761	1.748	1.805	1.825	1.877	0.515	0.692	0.643	1.868	1.768	1.751	1.863	1.865	1.834	1.814	
Ti	0.008	0.012	0.011	0.008	0.009	0.010	0.010	0.007	0.007	0.007	0.002	0.002	0.002	0.011	0.002	0.004	0.005	0.008	0.010	0.007	
Oct	0	0.004	0.000	0.148	0.116	0.004	0.025	0.041	0.000	0.018	0.000	0.000	0.060	0.000	0.093	0.094	0.019	0.018	0.066	0.094	
Fe ²⁺	0.326	0.404	0.471	0.398	0.356	0.445	0.486	0.390	0.477	0.400	0.163	0.174	0.158	0.275	0.406	0.302	0.319	0.320	0.348	0.331	
Mn	0.008	0.018	0.014	0.012	0.005	0.009	0.015	0.008	0.016	0.006	0.000	0.003	0.004	0.009	0.003	0.012	0.007	0.001	0.009	0.013	
Mg	5.691	5.562	5.510	5.434	5.514	5.532	5.463	5.553	5.504	5.569	5.835	5.833	5.776	5.736	5.496	5.588	5.650	5.653	5.567	5.555	
Ba	0.002	0.000	0.005	0.002	0.000	0.000	0.004	0.000	0.005	0.000	0.001	0.005	0.005	0.003	0.000	0.000	0.000	0.006	0.003		
Ca	0.005	0.003	0.006	0.000	0.000	0.000	0.000	0.000	0.006	0.005	0.000	0.001	0.001	0.003	0.009	0.010	0.001	0.000	0.000	0.004	
Na	0	0.009	0.000	0.177	0.148	0.000	0.000	0.153	0.000	0.000	0.000	0.000	0.093	0.009	0.081	0.027	0.053	0.000	0.035	0.045	
K	1.868	1.924	1.896	2.006	1.996	1.905	1.935	1.899	1.956	2.052	2.033	2.012	2.015	1.920	2.007	2.034	2.009	2.042	2.055	2.087	
OH ⁻	3.884	3.851	3.846	3.854	3.853	3.853	3.854	3.847	3.843	3.844	3.953	3.939	3.945	3.841	3.853	3.852	3.844	3.844	3.847	3.849	
Sum	15.908	15.936	15.913	16.185	16.144	15.905	15.939	16.052	15.971	16.058	16.034	16.030	16.114	15.966	16.097	16.071	16.062	16.041	16.096	16.139	

Tabela B – Análises de flogopita e tetra-ferriflogopita de rochas foscoríticas e glimerito de Catalão I. As análises foram recalculadas com base em 22 O. (Cont. X)

	183-1L-01	183-1L-02	183-1L-03	183-1L-04	183-1L-05	183-1L-06	183-1L-07	183-1L-08	183-1L-09	183-1L-10	183-1-1	183-1-2	183-1-3	183-1-4	183-1-5	183-1-6	183-1-7	192B-3-01	192B-3-02	192B-3-03
Amostra	DC	P2	P2	P2																
Coord	1	11	21	31	41	51	61	71	81	91	1	7	15	22	28	37	45	1	3	9
Posição	núcleo	interm	borda	interm	interm	núcleo	interm	interm	borda	interm	interm	interm	interm							
Unidade	DC	P2	P2	P2																
Oxidos (%)																				
SiO ₂	40.75	40.109	39.99	40.32	39.64	40.47	40.86	40.32	40.17	40.53	41.04	40.16	40.09	40.73	42.07	40.71	40.17	40.33	40.71	40.59
TiO ₂	0.08	0.121	0.08	0.11	0.08	0.09	0.11	0.04	0.09	0.08	0.16	0.09	0.08	0.06	0.14	0.07	0.10	0.05	0.07	0.06
Al ₂ O ₃	0.02	0.04	0.00	0.08	0.07	0.02	0.06	0.05	0.00	0.17	0.02	0.06	0.07	0.17	0.00	0.06	0.03	0.13	0.16	0.20
Fe ₂ O ₃	15.61	15.775	16.40	16.95	16.37	16.43	16.71	16.10	16.62	16.94	16.42	16.89	17.06	16.78	15.89	16.48	16.06	16.11	15.89	15.81
FeO	2.60	3.451	2.87	2.86	2.97	2.42	2.17	3.31	2.31	1.55	2.24	2.22	2.35	1.80	2.54	3.24	3.39	1.66	1.87	1.76
MnO	0.08	0.053	0.03	0.10	0.10	0.03	0.06	0.07	0.09	0.06	0.08	0.06	0.01	0.06	0.10	0.09	0.09	0.08	0.08	0.04
MgO	24.54	23.834	24.43	25.15	24.36	25.07	25.55	24.32	25.06	25.95	25.04	25.34	25.44	25.89	25.20	24.82	24.16	25.31	25.23	25.29
Na ₂ O	0.00	0.089	0.24	0.00	0.09	0.00	0.12	0.00	0.00	0.51	0.00	0.00	0.15	0.30	0.00	0.00	0.03	0.00	0.03	0.03
K ₂ O	10.57	10.579	10.49	10.47	10.42	10.64	10.57	10.62	10.51	10.81	10.55	10.62	10.59	10.53	10.53	10.54	10.49	10.58	10.65	10.42
BaO	0.05	0	0.11	0.03	0.00	0.06	0.00	0.09	0.09	0.20	0.10	0.10	0.00	0.00	0.04	0.00	0.05	0.01	0.05	0.05
CaO	0.07	0	0.00	0.00	0.00	0.02	0.00	0.01	0.00	0.00	0.00	0.00	0.00	0.00	0.02	0.01	0.06	0.05	0.11	
H ₂ O	3.79	3.75	3.77	3.83	3.75	3.81	3.85	3.78	3.79	3.85	3.85	3.81	3.81	3.86	3.90	3.83	3.77	3.79	3.81	3.80
Total	98.15	97.801	98.42	99.88	97.85	99.03	100.05	98.70	98.72	100.14	100.03	99.34	99.49	100.04	100.70	99.86	98.30	98.13	98.58	98.15
Cl ⁻	0.007	0.005	0.002	0.000	0.004	0.001	0.006	0.000	0.001	0.000	0.011	0.011	0.000	0.000	0.013	0.000	0.018	0.000	0.013	0.013
Cations (p.f.u.)																				
Si	6.207	6.167	6.113	6.067	6.094	6.125	6.110	6.145	6.101	6.062	6.145	6.069	6.050	6.083	6.230	6.124	6.146	6.133	6.161	6.159
Al	0.004	0.007	0.000	0.013	0.012	0.003	0.010	0.008	0.000	0.030	0.004	0.010	0.012	0.031	0.000	0.010	0.005	0.023	0.029	0.035
Fe ³⁺	1.789	1.825	1.887	1.919	1.894	1.872	1.880	1.846	1.899	1.907	1.851	1.921	1.938	1.886	1.770	1.866	1.849	1.844	1.810	1.806
Ti	0.009	0.014	0.010	0.013	0.010	0.010	0.012	0.005	0.010	0.009	0.018	0.010	0.009	0.007	0.015	0.008	0.011	0.005	0.008	0.007
Oct	0.079	0.072	0.053	0.000	0.013	0.023	0.015	0.038	0.014	0.004	0.101	0.000	0.000	0.000	0.096	0.006	0.034	0.035	0.053	0.043
Fe ²⁺	0.331	0.444	0.366	0.360	0.381	0.306	0.271	0.421	0.293	0.193	0.281	0.281	0.296	0.224	0.314	0.408	0.433	0.211	0.237	0.223
Mn	0.010	0.007	0.004	0.013	0.014	0.004	0.007	0.009	0.011	0.007	0.011	0.008	0.001	0.008	0.013	0.011	0.012	0.010	0.010	0.005
Mg	5.571	5.463	5.567	5.642	5.582	5.657	5.695	5.527	5.672	5.787	5.589	5.709	5.722	5.765	5.562	5.567	5.510	5.739	5.692	5.722
Ba	0.003	0	0.007	0.001	0.000	0.004	0.000	0.005	0.005	0.012	0.006	0.006	0.000	0.000	0.002	0.000	0.003	0.001	0.003	0.003
Ca	0.011	0	0.000	0.001	0.001	0.000	0.002	0.000	0.002	0.000	0.000	0.000	0.000	0.000	0.003	0.001	0.010	0.008	0.018	
Na	0.000	0.027	0.072	0.000	0.027	0.000	0.035	0.000	0.000	0.000	0.149	0.000	0.000	0.044	0.087	0.000	0.000	0.009	0.000	0.009
K	2.053	2.075	2.046	2.010	2.044	2.054	2.015	2.065	2.036	2.063	2.014	2.046	2.039	2.006	1.989	2.023	2.047	2.052	2.056	2.016
OH ⁻	3.848	3.846	3.842	3.840	3.841	3.843	3.841	3.846	3.841	3.841	3.845	3.837	3.835	3.843	3.852	3.841	3.845	3.841	3.849	3.845
Sum	16.067	16.101	16.125	16.039	16.072	16.058	16.052	16.069	16.043	16.074	16.169	16.060	16.067	16.054	16.078	16.026	16.051	16.072	16.067	16.046

Tabela B – Análises de flogopita e tetra-ferriflogopita de rochas foscoríticas e glimerito de Catalão I. As análises foram recalculadas com base em 22 O. (Cont. XI)

	192B-3-04	192B-3-05	192B-3-06	192B-3-07	192B-3-08	192B-3-09	192B-3-10	192B-3-11	192B-1-1	192B-1-2	192B-1-3	192B-1-4	192B-1-5	200-1-1	200-1-2	200-1-3	200-1-4	200-1-5	200-1-6	200-2-1
Amostra	12	15	18	21	24	27	30	31						7	14	27	37	51	33	
Coord	interm	núcleo	núcleo	interm	interm	interm	interm	borda	núcleo					borda	interm	interm	interm	interm	núcleo	
Posição	P2	P2	P2	P2	P2	P2	P3	P3	P3	P3	P3	DC								
Unidade	Oxidos(%)																			
SiO ₂	39.75	39.94	39.87	40.56	40.56	39.28	39.79	39.56	40.47	43.12	41.17	40.55	40.67	40.56	40.52	40.89	41.18	41.76	41.08	40.87
TiO ₂	0.12	0.11	0.13	0.08	0.14	0.08	0.09	0.10	0.07	0.13	0.17	0.08	0.10	0.07	0.08	0.09	0.11	0.07	0.14	0.10
Al ₂ O ₃	0.14	0.12	0.109	0.20	0.26	0.00	0.01	0.00	0.17	9.58	0.16	0.00	0.05	0.08	0.01	0.03	0.02	0.11	0.02	0.05
Fe ₂ O ₃	17.03	16.34	16.029	16.48	15.67	16.40	16.13	16.07	16.25	3.18	16.21	16.48	16.51	15.88	16.43	15.59	15.58	14.81	15.34	15.60
FeO	1.69	2.30	2.002	2.00	2.53	2.19	2.16	2.52	2.18	1.81	1.95	2.65	2.47	2.62	2.99	3.46	3.59	3.25	3.89	3.25
MnO	0.05	0.05	0.067	0.06	0.00	0.07	0.05	0.02	0.06	0.01	0.07	0.01	0.03	0.03	0.06	0.03	0.06	0.04	0.05	0.09
MgO	25.42	24.89	24.859	25.43	24.89	24.52	24.68	24.27	25.52	27.51	25.81	25.36	25.47	24.86	25.09	24.43	24.50	24.66	24.04	24.65
Na ₂ O	0.28	0.00	0.031	0.10	0.03	0.00	0.00	0.00	0.11	0.17	0.07	0.12	0.00	0.04	0.03	0.00	0.00	0.14	0.00	0.00
K ₂ O	10.39	10.54	10.358	10.71	10.25	10.35	10.55	10.56	9.91	10.64	9.96	9.82	10.03	10.18	9.90	9.95	9.84	9.77	10.01	9.71
BaO	0.00	0.12	0	0.04	0.00	0.01	0.05	0.14	0.10	0.00	0.08	0.04	0.00	0.09	0.00	0.09	0.05	0.00	0.01	0.00
CaO	0.15	0.03	0.027	0.04	0.04	0.23	0.02	0.04	0.03	0.03	0.05	0.01	0.01	0.06	0.00	0.00	0.00	0.01	0.01	0.01
H ₂ O	3.78	3.77	3.748	3.83	3.79	3.71	3.74	3.72	3.80	4.22	3.86	3.81	3.83	3.79	3.81	3.80	3.82	3.84	3.80	3.80
Total	98.79	98.20	97.23	99.53	98.17	96.84	97.26	96.99	98.65	100.39	99.55	98.92	99.17	98.24	98.91	98.36	98.76	98.46	98.38	98.14
Cl ⁻	0.050	0.004	0.013	0.006	0.041	0.022	0.011	0.005	0.042	0.038	0.025	0.016	0.000	0.009	0.000	0.014	0.007	0.011	0.014	0.011
Cations (p.f.u.)																				
Si	6.030	6.099	6.126	6.099	6.162	6.087	6.129	6.127	6.121	6.073	6.150	6.126	6.121	6.169	6.128	6.212	6.224	6.299	6.243	6.207
Al	0.026	0.022	0.02	0.035	0.047	0.000	0.001	0.000	0.030	1.589	0.028	0.001	0.009	0.013	0.002	0.006	0.004	0.019	0.003	0.009
Fe ³⁺	1.945	1.878	1.854	1.866	1.791	1.913	1.870	1.873	1.850	0.337	1.822	1.873	1.870	1.818	1.870	1.782	1.772	1.682	1.754	1.783
Ti	0.014	0.012	0.015	0.009	0.016	0.009	0.010	0.012	0.007	0.014	0.019	0.009	0.012	0.008	0.009	0.010	0.013	0.008	0.016	0.012
Oct	0.016	0.023	0.025	0.030	0.027	0.036	0.039	0.055	0.000	0.000	0.000	0.000	0.000	0.019	0.000	0.012	0.003	0.031	0.036	0.000
Fe ²⁺	0.214	0.293	0.257	0.252	0.321	0.283	0.277	0.327	0.275	0.214	0.243	0.334	0.311	0.332	0.377	0.440	0.454	0.410	0.495	0.412
Mn	0.007	0.006	0.009	0.008	0.000	0.009	0.007	0.002	0.007	0.001	0.008	0.001	0.003	0.004	0.008	0.004	0.008	0.005	0.006	0.012
Mg	5.749	5.666	5.694	5.701	5.636	5.663	5.667	5.604	5.753	5.775	5.748	5.712	5.715	5.637	5.656	5.534	5.522	5.546	5.447	5.580
Ba	0.000	0.007	0	0.002	0.000	0.001	0.003	0.008	0.006	0.000	0.004	0.002	0.000	0.005	0.000	0.005	0.003	0.000	0.001	0.000
Ca	0.024	0.005	0.004	0.006	0.007	0.039	0.003	0.006	0.004	0.004	0.008	0.001	0.002	0.010	0.000	0.000	0.000	0.001	0.001	0.002
Na	0.082	0.000	0.009	0.028	0.009	0.000	0.000	0.000	0.033	0.047	0.021	0.034	0.000	0.011	0.008	0.000	0.000	0.041	0.000	0.000
K	2.010	2.053	2.03	2.055	1.986	2.045	2.073	2.086	1.912	1.911	1.897	1.892	1.927	1.975	1.909	1.929	1.898	1.881	1.941	1.882
OH ⁻	3.824	3.843	3.842	3.843	3.839	3.834	3.841	3.842	3.836	3.965	3.843	3.842	3.844	3.846	3.844	3.847	3.851	3.860	3.850	3.848
Sum	16.117	16.064	16.043	16.091	16.002	16.085	16.079	16.100	15.998	15.965	15.948	15.985	15.970	16.001	15.967	15.934	15.901	15.923	15.943	15.899

Tabela B – Análises de flogopita e tetra-ferriflogopita de rochas foscoríticas e glimerito de Catalão I. As análises foram recalculadas com base em 22 O. (Cont. XII)

Amostra	200-2-2	206-1-	206-1-	206-1-	206-1-	206-1-	206-2-	206-2-	206-2-	206-2-	207-4-	207-4-1	207-4-2	207-4-3	207-4-4	207-4-5	207-5-1	207-5-2	207-5-	
		1	2	3B	4	5B	1	2B	3	4	5B								3	
Coord		1	3	4	8	10	1	6	9	10	16									
Posição	borda	núcleo	interm	interm	interm	borda	interm	interm	interm	interm										
Unidade	DC	P3	DC	DC	DC	DC	DC	DC	P3	P3	P3									
Oxidos (%)																				
SiO₂	40.83	40.94	40.43	40.708	40.79	42.00	40.60	40.61	41.89	41.72	40.93	40.60	40.72	41.35	40.97	40.21	40.76	41.55	40.46	40.06
TiO₂	0.39	0.06	0.07	0.105	0.09	0.05	0.07	0.05	0.11	0.11	0.11	0.09	0.12	0.04	0.13	0.10	0.08	0.07	0.11	0.09
Al₂O₃	0.05	0.04	0.09	0.028	0.06	0.00	0.10	0.05	0.02	0.25	0.06	0.05	0.02	0.04	0.00	0.00	0.02	0.03	0.00	0.04
Fe₂O₃	15.66	15.97	15.61	14.911	15.57	15.02	15.67	15.61	15.41	15.44	15.51	15.27	15.63	15.77	15.21	15.52	15.45	15.33	16.15	15.65
FeO	2.76	1.91	2.40	1.98	2.09	1.76	1.85	2.08	1.66	1.81	1.45	2.46	2.31	2.69	3.16	3.23	3.59	3.26	2.94	3.16
MnO	0.07	0.05	0.07	0.036	0.09	0.04	0.06	0.08	0.08	0.01	0.06	0.13	0.07	0.05	0.04	0.09	0.05	0.10	0.08	0.08
MgO	24.58	25.31	24.42	24.167	24.82	25.35	24.96	24.90	25.50	25.48	25.33	24.48	24.78	25.28	24.43	24.22	24.30	24.79	24.85	24.26
Na₂O	0.00	0.00	0.27	0.306	0.00	0.00	0.00	0.00	0.03	0.00	0.00	0.00	0.18	0.00	0.15	0.01	0.05	0.13	0.00	0.00
K₂O	9.90	10.65	10.49	10.618	10.60	10.53	10.68	10.42	10.58	10.61	10.26	10.13	10.12	9.89	9.65	9.60	9.69	9.79	9.75	9.76
BaO	0.00	0.01	0.00	0.084	0.00	0.06	0.11	0.11	0.00	0.01	0.00	0.03	0.04	0.00	0.01	0.01	0.00	0.09	0.18	
CaO	0.01	0.02	0.10	0.092	0.08	0.01	0.05	0.03	0.02	0.23	0.13	0.10	0.16	0.06	0.06	0.07	0.04	0.00	0.06	0.02
H₂O	3.80	3.82	3.77	3.748	3.79	3.85	3.79	3.78	3.87	3.87	3.80	3.77	3.79	3.84	3.79	3.74	3.78	3.84	3.79	3.74
Total	98.04	98.78	97.72	96.783	97.98	98.65	97.96	97.72	99.16	99.54	97.63	97.11	97.94	99.00	97.60	96.80	97.80	98.87	98.27	97.01
Cl⁻	0.012	0.018	0.008	0.026	0.000	0.000	0.000	0.000	0.010	0.007	0.000	0.000	0.015	0.003	0.009	0.002	0.003	0.008	0.012	
Cations (p.f.u.)																				
Si	6.201	6.180	6.186	6.267	6.207	6.303	6.185	6.198	6.262	6.222	6.217	6.227	6.205	6.211	6.253	6.200	6.223	6.258	6.152	6.177
Al	0.009	0.006	0.016	0.005	0.010	0.000	0.018	0.009	0.004	0.044	0.010	0.009	0.003	0.007	0.000	0.000	0.003	0.005	0.000	0.006
Fe³⁺	1.790	1.814	1.798	1.728	1.783	1.697	1.797	1.793	1.734	1.733	1.773	1.763	1.793	1.783	1.747	1.800	1.775	1.737	1.848	1.816
Ti	0.045	0.007	0.008	0.012	0.011	0.005	0.008	0.006	0.012	0.012	0.013	0.010	0.013	0.004	0.015	0.011	0.009	0.007	0.013	0.010
Oct	0.031	0.050	0.107	0.182	0.081	0.099	0.080	0.055	0.087	0.098	0.061	0.060	0.055	0.000	0.020	0.000	0.000	0.006	0.000	0.000
Fe²⁺	0.350	0.241	0.307	0.255	0.266	0.220	0.235	0.265	0.207	0.225	0.184	0.315	0.294	0.337	0.403	0.417	0.458	0.410	0.374	0.407
Mn	0.008	0.006	0.009	0.005	0.012	0.005	0.008	0.010	0.010	0.001	0.007	0.017	0.009	0.006	0.005	0.011	0.007	0.012	0.011	0.010
Mg	5.566	5.696	5.569	5.546	5.630	5.671	5.669	5.664	5.684	5.664	5.735	5.598	5.629	5.661	5.557	5.568	5.530	5.565	5.632	5.576
Ba	0.000	0.001	0.000	0.005	0.000	0.003	0.007	0.007	0.000	0.001	0.000	0.002	0.000	0.001	0.001	0.000	0.000	0.005	0.011	
Ca	0.002	0.004	0.016	0.015	0.013	0.001	0.009	0.005	0.003	0.036	0.021	0.017	0.027	0.010	0.010	0.012	0.006	0.000	0.009	0.004
Na	0.000	0.000	0.081	0.091	0.000	0.000	0.000	0.000	0.009	0.000	0.000	0.000	0.053	0.000	0.045	0.004	0.015	0.039	0.000	0.000
K	1.917	2.050	2.047	2.085	2.057	2.015	2.076	2.028	2.017	2.019	1.987	1.981	1.967	1.894	1.879	1.887	1.887	1.880	1.890	1.920
OH⁻	3.847	3.844	3.848	3.849	3.851	3.858	3.850	3.850	3.855	3.853	3.850	3.853	3.855	3.847	3.857	3.848	3.853	3.858	3.844	3.845
Sum	15.919	16.055	16.144	16.196	16.070	16.019	16.092	16.040	16.029	16.055	16.008	15.999	16.050	15.913	15.935	15.911	15.913	15.919	15.934	15.937

Tabela B – Análises de flogopita e tetra-ferriflogopita de rochas foscoríticas e glimerito de Catalão I. As análises foram recalculadas com base em 22 O. (Cont. XIII)

Amostra	207-5-4	207-5-5	207-5-6	207-5-8	207-5-9	225-1-2	225-1-3	225-1-4	225-1-5	225-1-6	225-1-7	225-1-8	225-2-1	225-2-2	225-2-3	225-2-4	225-2-5	225-2-6	225-2-7	230A-1-1B
	Coord					borda	interm	núcleo	interm	interm	interm	interm	borda	interm	núcleo	interm	interm	interm	interm	
Posição	P3	P3	P3	P3	GLIM	P2														
Oxidos (%)																				
SiO ₂	41.64	41.00	40.33	40.99	40.334	40.37	40.17	40.04	39.79	39.67	39.84	40.40	40.92	39.96	39.38	39.01	39.51	41.53	41.57	40.62
TiO ₂	0.04	0.09	0.10	0.05	0.077	0.47	0.87	1.11	1.15	1.25	1.22	0.67	0.17	1.22	1.50	1.46	1.19	0.24	0.28	0.04
Al ₂ O ₃	9.22	0.00	0.01	0.05	0.265	11.49	11.07	11.26	11.47	11.70	11.34	11.29	11.40	11.76	11.84	11.99	11.53	12.44	12.40	0.11
Fe ₂ O ₃	3.87	15.57	15.73	15.69	15.579	1.19	1.76	2.10	2.10	2.25	2.31	1.39	0.72	1.49	1.80	1.44	1.89	0.53	0.41	16.80
FeO	2.05	3.81	2.87	3.10	3.42	4.22	5.25	5.69	5.44	5.45	5.22	4.83	2.86	6.01	5.87	6.22	5.35	3.90	2.99	2.22
MnO	0.03	0.03	0.07	0.06	0.062	0.06	0.11	0.04	0.13	0.09	0.08	0.07	0.08	0.11	0.15	0.08	0.07	0.04	0.05	0.12
MgO	26.90	24.47	24.51	24.73	24.415	24.78	23.70	23.60	23.63	23.84	23.81	24.10	25.69	23.27	23.09	22.68	23.49	25.46	26.01	25.32
Na ₂ O	0.01	0.15	0.00	0.00	0.126	0.00	0.08	0.00	0.17	0.00	0.03	0.25	0.00	0.00	0.00	0.00	0.00	0.00	0.00	0.22
K ₂ O	10.22	9.44	9.95	9.90	9.88	11.07	10.83	10.90	10.83	10.91	10.78	10.84	11.21	10.93	10.79	10.75	10.80	11.17	11.43	10.81
BaO	0.23	0.00	0.14	0.05	0.127	0.22	0.09	0.16	0.15	0.40	0.43	0.29	0.00	0.32	0.40	0.48	0.60	0.00	0.05	0.00
CaO	0.06	0.03	0.01	0.14	0	0.01	0.00	0.01	0.00	0.00	0.00	0.00	0.02	0.00	0.00	0.00	0.00	0.00	0.00	0.07
H ₂ O	4.12	3.81	3.76	3.81	3.781	4.09	4.07	4.09	4.09	4.11	4.09	4.09	4.11	4.10	4.08	4.05	4.06	4.20	4.21	3.84
Total	98.39	98.39	97.49	98.56	98.066	97.96	97.99	99.00	98.96	99.68	99.15	98.22	97.18	99.18	98.89	98.15	98.48	99.50	99.41	100.18
Cl ⁻	0.000	0.000	0.000	0.000	0.004	0.018	0.014	0.012	0.018	0.016	0.020	0.016	0.006	0.009	0.000	0.000	0.017	0.022	0.000	0.010
Cations (p.f.u.)																				
Si	6.011	6.222	6.183	6.204	6.161	5.892	5.892	5.836	5.799	5.754	5.801	5.902	5.963	5.819	5.760	5.755	5.797	5.929	5.923	6.086
Al	1.569	0.000	0.002	0.008	0.048	1.977	1.914	1.934	1.970	2.000	1.946	1.944	1.958	2.018	2.042	2.085	1.994	2.093	2.083	0.019
Fe ³⁺	0.420	1.778	1.815	1.788	1.791	0.131	0.194	0.231	0.231	0.246	0.253	0.153	0.079	0.163	0.198	0.159	0.208	0.057	0.057	1.895
Ti	0.004	0.010	0.011	0.005	0.009	0.051	0.096	0.121	0.126	0.137	0.134	0.074	0.019	0.134	0.165	0.162	0.131	0.025	0.030	0.004
Oct	0.000	0.000	0.010	0.014	0	0.036	0.064	0.054	0.061	0.035	0.053	0.080	0.041	0.069	0.065	0.072	0.066	0.088	0.000	0.046
Fe ²⁺	0.247	0.483	0.368	0.392	0.437	0.515	0.644	0.693	0.663	0.661	0.635	0.590	0.349	0.732	0.718	0.768	0.656	0.465	0.464	0.278
Mn	0.004	0.004	0.009	0.008	0.008	0.007	0.013	0.005	0.016	0.012	0.010	0.009	0.010	0.014	0.018	0.010	0.009	0.004	0.006	0.016
Mg	5.788	5.536	5.602	5.581	5.56	5.391	5.183	5.127	5.134	5.155	5.168	5.247	5.581	5.051	5.034	4.988	5.138	5.418	5.524	5.656
Ba	0.013	0.000	0.008	0.003	0.008	0.012	0.005	0.009	0.009	0.023	0.024	0.017	0.000	0.018	0.023	0.028	0.034	0.000	0.003	0.000
Ca	0.010	0.006	0.001	0.023	0	0.001	0.000	0.002	0.000	0.000	0.000	0.000	0.002	0.000	0.000	0.000	0.000	0.000	0.012	
Na	0.002	0.043	0.000	0.000	0.037	0.000	0.024	0.000	0.048	0.000	0.008	0.071	0.000	0.000	0.000	0.000	0.000	0.000	0.063	
K	1.882	1.827	1.946	1.911	1.925	2.061	2.027	2.027	2.013	2.019	2.002	2.019	2.084	2.031	2.013	2.024	2.023	2.034	2.077	2.066
OH ⁻	3.965	3.856	3.849	3.851	3.853	3.984	3.980	3.977	3.976	3.975	3.973	3.982	3.992	3.984	3.983	3.986	3.978	3.996	4.000	3.839
Sum	15.950	15.909	15.955	15.937	15.984	16.074	16.056	16.039	16.070	16.042	16.034	16.106	16.086	16.049	16.036	16.051	16.056	16.113	16.167	16.141

Tabela B – Análises de flogopita e tetra-ferriflogopita de rochas foscoríticas e glimerito de Catalão I. As análises foram recalculadas com base em 22 O. (Cont. XIV)

Amostra	230A-1-2	230A-1-3	230A-1-4	230A-1-5	230A-1-6	230A-1-7	230B-4-1B	230B-4-2	230B-4-3	230B-4-4	230B-4-5	230B-4-6	230B-4-7	244-2-1	244-2-2	244-2-3	244-2-4	244-2-5	244-3-1	244-3-2
Coord	8	14	21	27	32	38	1	10	18	25	35	43	50	2	6	10	14	19	1	9
Posição	interm	interm	núcleo	interm	borda	borda	borda	borda	interm	núcleo	interm	interm	borda	borda	interm	núcleo	interm	interm	borda	interm
Unidade	P2	P3	P3	P3	P3	P3	P1	P1	P1	P1	P1	P1	P1	P1						
Oxidos (%)																				
SiO ₂	41.15	40.88	40.04	40.56	41.06	41.433	41.38	40.57	41.02	40.91	41.75	41.32	41.29	40.66	41.76	41.53	41.71	41.20	41.23	41.52
TiO ₂	0.09	0.08	0.05	0.13	0.09	0.05	0.12	0.15	0.12	0.09	0.06	0.06	0.17	0.05	0.37	0.46	0.51	0.34	0.16	0.40
Al ₂ O ₃	0.21	0.04	0.38	0.16	0.03	0.048	0.03	0.00	0.00	0.04	0.02	0.02	0.00	0.34	5.57	5.66	5.77	5.70	3.12	5.81
Fe ₂ O ₃	17.15	16.55	16.59	16.66	16.41	16.481	16.46	16.38	16.65	16.35	16.49	16.12	16.64	16.30	9.56	9.45	9.31	8.96	12.49	8.94
FeO	2.59	2.70	3.35	2.45	2.37	2.076	2.90	2.73	2.57	2.52	2.08	2.58	2.47	1.70	1.36	1.82	1.43	1.51	2.11	1.37
MnO	0.04	0.11	0.08	0.09	0.06	0.105	0.11	0.01	0.08	0.00	0.06	0.09	0.08	0.05	0.05	0.07	0.06	0.00	0.05	0.05
MgO	25.90	25.20	24.85	25.41	25.58	25.809	25.17	24.73	25.20	25.18	25.73	25.14	25.54	25.84	26.69	26.35	26.71	26.36	25.98	26.68
Na ₂ O	0.00	0.00	0.00	0.00	0.00	0	0.00	0.06	0.00	0.06	0.15	0.00	0.00	0.00	0.43	0.25	0.19	0.06	0.00	0.00
K ₂ O	10.81	10.58	10.55	10.33	10.16	10.596	10.76	10.79	10.83	10.59	10.93	10.75	10.46	10.33	10.68	10.64	10.65	10.57	10.67	10.66
BaO	0.00	0.04	0.00	0.08	0.00	0.012	0.00	0.06	0.19	0.00	0.04	0.08	0.01	0.03	0.08	0.11	0.00	0.15	0.12	0.00
CaO	0.00	0.00	0.00	0.04	0.00	0.03	0.00	0.00	0.00	0.04	0.00	0.00	0.01	0.17	0.00	0.06	0.02	0.07	0.03	0.03
H ₂ O	3.91	3.85	3.81	3.84	3.85	3.885	3.88	3.81	3.86	3.83	3.90	3.85	3.87	3.84	4.07	4.06	4.07	4.01	3.95	4.04
Total	101.85	100.03	99.70	99.75	99.62	100.53	100.81	99.29	100.51	99.61	101.20	99.99	100.56	99.29	100.62	100.44	100.45	98.94	99.89	99.49
Cl ⁻	0.003	0.002	0.000	0.010	0.000	0	0.000	0.000	0.007	0.024	0.016	0.013	0.015	0.012	0.006	0.006	0.000	0.006	0.000	0.023
Cations (p.f.u.)																				
Si	6.062	6.127	6.047	6.089	6.146	6.15	6.153	6.135	6.128	6.145	6.164	6.182	6.138	6.100	6.018	6.007	6.010	6.030	6.075	6.029
Al	0.036	0.006	0.067	0.029	0.005	0.008	0.005	0.001	0.001	0.007	0.003	0.003	0.000	0.060	0.946	0.965	0.980	0.984	0.541	0.994
Fe ³⁺	1.902	1.867	1.886	1.882	1.849	1.841	1.842	1.864	1.872	1.848	1.833	1.815	1.862	1.840	1.036	1.028	1.010	0.987	1.384	0.977
Ti	0.010	0.009	0.005	0.015	0.011	0.006	0.014	0.017	0.013	0.011	0.007	0.007	0.019	0.006	0.040	0.050	0.056	0.038	0.018	0.044
Oct	0.000	0.008	0.000	0.000	0.000	0.013	0.033	0.061	0.043	0.035	0.064	0.053	0.005	0.000	0.058	0.041	0.026	0.026	0.012	0.008
Fe ²⁺	0.318	0.338	0.423	0.307	0.296	0.257	0.360	0.345	0.321	0.316	0.257	0.322	0.307	0.213	0.164	0.220	0.172	0.184	0.259	0.166
Mn	0.005	0.014	0.010	0.012	0.008	0.013	0.014	0.001	0.010	0.000	0.007	0.011	0.010	0.006	0.006	0.009	0.008	0.000	0.006	0.006
Mg	5.688	5.631	5.594	5.685	5.709	5.711	5.579	5.576	5.613	5.638	5.665	5.607	5.659	5.779	5.732	5.680	5.738	5.752	5.705	5.776
Ba	0.000	0.002	0.000	0.004	0.000	0.001	0.000	0.004	0.011	0.000	0.002	0.004	0.001	0.002	0.005	0.006	0.000	0.009	0.007	0.000
Ca	0.000	0.000	0.001	0.007	0.000	0.005	0.000	0.000	0.000	0.007	0.000	0.000	0.001	0.027	0.000	0.009	0.003	0.012	0.004	0.004
Na	0.000	0.000	0.000	0.000	0.000	0	0.000	0.018	0.000	0.018	0.044	0.000	0.000	0.000	0.121	0.069	0.052	0.018	0.000	0.000
K	2.032	2.022	2.032	1.979	1.941	2.007	2.041	2.082	2.064	2.028	2.058	2.053	1.984	1.977	1.964	1.962	1.957	1.972	2.005	1.974
OH ⁻	3.841	3.844	3.842	3.840	3.846	3.847	3.846	3.845	3.842	3.839	3.843	3.845	3.840	3.843	3.912	3.913	3.916	3.916	3.885	3.912
Sum	16.053	16.024	16.065	16.009	15.965	16.012	16.041	16.104	16.076	16.053	16.104	16.057	15.986	16.010	16.090	16.046	16.012	16.016	15.978	

Tabela B – Análises de flogopita e tetra-ferriflogopita de rochas foscoríticas e glimerito de Catalão I. As análises foram recalculadas com base em 22 O. (Cont. XV)

Amostra	244-3-3		244-3-4	244-3-5	304A-1-1	304A-1-10	304A-1-2	304A-1-3	304A-1-4	304A-1-6	304A-1-8	304A-1-9	304A-2-1	304A-2-2	304B-1-10	304B-1-2	304B-1-3	304B-1-4	304B-1-5	304B-1-6	304B-1-7
	P1	P1	P1	P2	P2	P2	P2	P2	P2	P2	P2	P2	DC	DC	P3	P3	P3	P3	P3	P3	P3
Coord	15	21	23																		
Posição	núcleo	mid	mid																		
Unidade																					
Oxidos (%)																					
SiO ₂	41.50	41.56	40.61	40.29	40.78	40.77	40.454	40.41	39.45	42.83	39.97	42.83	43.43	41.66	41.68	41.69	40.80	41.88	42.76	40.32	
TiO ₂	0.34	0.29	0.16	0.05	0.07	0.03	0.089	0.07	0.06	0.10	0.11	0.04	0.03	0.04	0.10	0.07	0.08	0.04	0.08	0.05	
Al ₂ O ₃	5.83	5.65	2.67	0.54	0.27	1.90	0.165	1.21	1.47	10.72	0.35	0.03	0.00	0.00	0.01	0.03	0.04	0.00	0.02		
Fe ₂ O ₃	9.16	9.72	13.44	15.27	15.53	13.24	16.081	14.33	14.03	1.44	15.23	14.08	13.66	14.92	15.58	15.69	16.27	16.06	15.68	16.51	
FeO	1.41	1.29	1.46	2.58	2.85	1.89	2.38	2.56	1.51	2.09	2.41	2.31	2.06	2.29	2.09	3.12	2.73	2.72	2.86	2.95	
MnO	0.05	0.08	0.02	0.02	0.09	0.05	0.039	0.09	0.06	0.02	0.05	0.11	0.03	0.03	0.09	0.02	0.05	0.08	0.08	0.06	
MgO	26.72	27.06	26.18	25.01	24.96	25.69	25.236	25.02	25.24	27.29	24.73	25.06	25.22	25.20	25.47	25.15	25.25	25.60	25.62	25.12	
Na ₂ O	0.00	0.00	0.00	0.16	0.13	0.00	0.015	0.00	0.18	0.39	0.13	0.00	0.00	0.17	0.00	0.08	0.00	0.14	0.00	0.12	
K ₂ O	10.82	10.99	10.53	9.86	9.74	9.76	10.077	9.98	9.76	10.38	9.62	9.87	10.14	9.64	10.13	9.91	9.86	10.11	10.17	9.79	
BaO	0.28	0.01	0.29	0.00	0.00	0.00	0	0.01	0.14	0.12	0.08	0.00	0.00	0.00	0.00	0.01	0.00	0.16	0.10	0.05	
CaO	0.04	0.01	0.12	0.04	0.07	0.06	0.013	0.04	0.10	0.04	0.04	0.10	0.00	0.04	0.00	0.00	0.08	0.00	0.01	0.00	
H ₂ O	4.05	4.07	3.91	3.78	3.81	3.84	3.803	3.77	3.74	4.23	3.74	3.87	3.90	3.82	3.86	3.86	3.83	3.90	3.94	3.80	
Total	100.	100.7	99.36	97.59	98.30	97.23	98.352	97.49	95.73	99.63	96.45	98.31	98.47	97.81	99.00	99.61	98.96	100.71	101.30	98.78	
Cl	0.01	0.001	0.006	0.006	0.007	0.017	0	0.175	0.020	0.000	0.006	0.016	0.000	0.022	0.013	0.019	0.014	0.000	0.003	0.007	
Cations (p.f.u.)																					
Si	6.01	5.987	6.031	6.150	6.181	6.157	6.135	6.143	6.099	6.059	6.168	6.410	6.468	6.301	6.243	6.232	6.150	6.203	6.270	6.113	
Al	1	0.959	0.467	0.097	0.047	0.338	0.029	0.217	0.268	1.787	0.064	0.005	0.001	0.001	0.000	0.002	0.005	0.007	0.000	0.003	
Fe ³⁺	1	1.054	1.502	1.754	1.771	1.505	1.835	1.639	1.633	0.154	1.769	1.586	1.532	1.698	1.757	1.765	1.846	1.790	1.730	1.884	
Ti	0.04	0.032	0.018	0.006	0.008	0.004	0.01	0.008	0.006	0.011	0.013	0.005	0.003	0.005	0.011	0.008	0.009	0.004	0.009	0.006	
Oct	0.02	0.000	0.002	0.000	0.000	0.000	0	0.000	0.000	0.000	0.000	0.102	0.138	0.022	0.028	0.000	0.000	0.000	0.029	0.000	
Fe ²⁺	0.17	0.155	0.181	0.329	0.361	0.239	0.302	0.325	0.195	0.247	0.311	0.288	0.256	0.289	0.262	0.390	0.343	0.337	0.351	0.374	
Mn	0.01	0.010	0.002	0.002	0.011	0.006	0.005	0.011	0.008	0.002	0.007	0.014	0.004	0.003	0.012	0.003	0.007	0.009	0.010	0.008	
Mg	5.77	5.812	5.797	5.690	5.640	5.783	5.705	5.669	5.817	5.756	5.688	5.591	5.599	5.681	5.687	5.604	5.674	5.653	5.601	5.678	
Ba	0.02	0.001	0.017	0.000	0.000	0.000	0	0.001	0.009	0.006	0.005	0.000	0.000	0.000	0.000	0.001	0.000	0.009	0.006	0.003	
Ca	0.01	0.001	0.019	0.006	0.011	0.010	0.002	0.007	0.016	0.006	0.007	0.017	0.000	0.006	0.000	0.000	0.012	0.000	0.001	0.000	
Na	0.00	0.000	0.000	0.047	0.039	0.000	0.004	0.000	0.054	0.106	0.038	0.000	0.000	0.048	0.000	0.023	0.000	0.041	0.000	0.034	
K	2	2.019	1.994	1.920	1.884	1.879	1.95	1.936	1.925	1.873	1.894	1.885	1.926	1.860	1.935	1.890	1.895	1.910	1.903	1.894	
OH ⁻	3.91	3.912	3.873	3.852	3.852	3.870	3.847	3.819	3.858	3.990	3.851	3.863	3.876	3.857	3.852	3.848	3.845	3.854	3.855	3.843	
Sum	16.0	16.03	16.03	16.001	15.953	15.921	15.977	15.956	16.030	16.007	15.964	15.903	15.927	15.914	15.935	15.918	15.941	15.963	15.910	15.997	

Tabela B – Análises de flogopita e tetra-ferriflogopita de rochas foscoríticas e glimerito de Catalão I. As análises foram recalculadas com base em 22 O. (Cont. XVI)

Amostra	304B-1-8	339-2-		339-2-	339-2-	339-2-	339-3-	339-3-	339-3-	339-3-	
		1	339-2-2								
Coord				núcleo		borda	núcleo	interm	interm	interm	
Posição					P2	P2	P2	P2	P2	P2	
Unidade	P3	P2	P2	P2	P2	P2	P2	P2	P2	P2	
Oxidos (%)											
SiO₂	40.55	39.18	39.95	40.22	40.04	39.29	41.93	41.77	41.39	40.74	41.40
TiO₂	0.45	0.08	0.06	0.07	0.07	0.06	0.05	0.015	0.08	0.05	0.06
Al₂O₃	0.00	0.06	0.14	3.49	0.05	0.05	0.01	11.128	4.73	2.96	2.34
Fe₂O₃	15.54	16.72	15.44	11.92	15.88	16.95	15.31	1.519	9.91	13.14	13.45
FeO	2.40	2.03	2.70	2.02	3.22	1.48	2.81	1.856	1.85	1.72	1.97
MnO	0.07	0.09	0.12	0.03	0.08	0.05	0.01	0.007	0.05	0.06	0.05
MgO	24.47	25.08	24.29	25.84	24.29	25.56	25.14	27.199	26.33	26.52	26.26
Na₂O	0.00	0.00	0.08	0.00	0.04	0.00	0.25	0	0.05	0.00	0.00
K₂O	9.88	9.97	10.02	10.25	9.98	10.21	10.01	10.726	10.42	10.31	10.34
BaO	0.00	0.00	0.06	0.00	0.00	0.03	0.00	0.448	0.00	0.00	0.13
CaO	0.00	0.08	0.08	0.03	0.09	0.03	0.03	0.053	0.03	0.02	0.00
H₂O	3.77	3.72	3.73	3.88	3.75	3.75	3.87	4.179	3.99	3.93	3.94
Total	97.13	97.01	96.68	97.74	97.50	97.44	99.41	98.9	98.81	99.45	99.95
Cl⁻	0.005	0.017	0.006	0.023	0.018	0.000	0.011	0.021	0.003	0.010	0.009
Cations (p.f.u.)											
Si	6.209	6.047	6.179	6.037	6.154	6.033	6.275	5.964	6.085	6.023	6.101
Al	0.000	0.010	0.025	0.617	0.009	0.008	0.002	1.873	0.819	0.515	0.407
Fe³⁺	1.791	1.943	1.796	1.347	1.837	1.959	1.724	0.163	1.096	1.462	1.492
Ti	0.052	0.009	0.006	0.007	0.009	0.007	0.005	0.002	0.009	0.005	0.007
Oct	0.046	0.000	0.028	0.000	0.002	0.000	0.032	0	0.000	0.000	0.000
Fe²⁺	0.307	0.262	0.349	0.254	0.414	0.189	0.352	0.222	0.227	0.213	0.242
Mn	0.009	0.012	0.016	0.004	0.010	0.007	0.002	0.001	0.006	0.007	0.006
Mg	5.586	5.771	5.601	5.780	5.565	5.850	5.609	5.789	5.771	5.844	5.770
Ba	0.000	0.000	0.004	0.000	0.000	0.002	0.000	0.025	0.000	0.000	0.007
Ca	0.000	0.013	0.013	0.004	0.015	0.005	0.004	0.008	0.005	0.004	0.000
Na	0.000	0.000	0.025	0.000	0.012	0.000	0.071	0	0.014	0.000	0.001
K	1.930	1.963	1.978	1.962	1.956	1.999	1.910	1.954	1.954	1.944	1.945
OH⁻	3.849	3.833	3.851	3.881	3.843	3.837	3.860	3.98	3.909	3.875	3.873
Sum	15.930	16.030	16.020	16.012	15.983	16.059	15.986	16.001	15.986	16.017	15.978

Tabela C – Análises de magnetita de rochas foscoríticas de Catalão I. Análises recalculadas na base de 32 O.

Amostra	38-1-1	38-2-1	38-2-2	38-2-3	38-2-4	56-1-1	56-1-2	56-1-3	87-1-4	87-1-5	87-1-6	87-1-9	91-1-1	91-1-11	91-1-2	91-1-3	91-1-4	91-1-5	91-1-6
Unidade	DC	DC	DC	DC	DC														
Oxidos (%)																			
Nb ₂ O ₅	0.05	0	0	0.02	0.11	0.177	0	0.057	0	0	0	0	0.05	0	0	0	0.05	0.07	0.09
SiO ₂	0	0	0.02	0.03	0	0.068	0	0.007	0.1	0	0	0.04	0	0.03	0.04	0.02	0.04	0.04	0
TiO ₂	1.11	5.59	6.33	3.51	5.13	1.617	1.879	1.882	3.63	1.98	1.07	1.59	1.13	1.5	1.86	1.48	1.34	1.66	1.17
Al ₂ O ₃	0	0.02	0	0.01	0	0.055	0	0	0.02	0	0.03	0	0	0.01	0.08	0	0	0	0.06
Cr ₂ O ₃	0	0	0.04	0.01	0	0	0	0.002	0.03	0	0	0.02	0	0.02	0	0.07	0.04	0.01	0.02
Fe ₂ O ₃	67.38	59.21	57.53	63.09	59.96	65.428	65.65	65.279	62.32	65.69	67.25	66.48	67.04	66.92	66.77	67.13	67.09	66.54	67.64
FeO	29.92	32.71	32.77	31.19	32.28	32.34	31.18	32.594	32.28	31.2	30.78	30.95	30.89	29.38	28.3	29.23	29.61	29.83	29.1
MnO	0.28	0.7	0.81	0.49	0.56	0.151	0.346	0.118	0.4	0.2	0.21	0.2	0.02	0.47	0.63	0.5	0.42	0.37	0.41
MgO	1.22	1.69	2.17	1.6	1.91	0.156	0.584	0.069	1.07	0.94	0.67	0.69	0.46	1.54	2.21	1.47	1.41	1.5	1.47
CaO	0.01	0.03	0.02	0.04	0.01	0.029	0.171	0	0.01	0	0.01	0.04	0.37	0.03	0.02	0	0.01	0.01	0.08
Total	99.97	99.95	99.69	99.99	99.96	100.02	99.81	100.01	99.86	100.01	100.02	100.01	99.91	99.95	99.91	99.9	99.96	100.01	99.94
Cations (p.f.u.)																			
Nb	0.007	0	0	0.002	0.015	0.024	0	0.008	0	0	0	0	0.007	0	0	0	0.007	0.009	0.012
Si	0	0	0.006	0.009	0	0.021	0	0.002	0.031	0	0	0.011	0	0.009	0.013	0.007	0.011	0.011	0
Ti	0.258	1.277	1.48	0.801	1.171	0.37	0.458	0.433	0.852	0.454	0.245	0.362	0.27	0.346	0.427	0.345	0.311	0.378	0.272
Al	0	0.006	0	0.002	0.001	0.02	0	0	0.006	0	0.011	0	0	0.004	0.029	0.001	0	0.001	0.02
Cr	0	0	0.01	0.003	0	0	0	0	0.007	0	0	0.006	0	0.004	0	0.017	0.01	0.002	0
Fe ³⁺	15.465	13.467	13.026	14.391	13.629	15.13	15.107	15.108	14.258	15.095	15.5	15.292	15.459	15.296	15.156	15.339	15.361	15.22	15.472
Fe ²⁺	7.632	8.266	8.245	7.908	8.155	8.311	7.974	8.383	8.206	7.968	7.884	7.912	7.916	7.464	7.139	7.421	7.533	7.582	7.397
Mn	0.074	0.179	0.214	0.126	0.143	0.039	0.095	0.031	0.105	0.051	0.054	0.052	0.005	0.123	0.164	0.131	0.109	0.095	0.107
Mg	0.56	0.766	1.007	0.722	0.865	0.071	0.282	0.031	0.497	0.428	0.305	0.311	0.221	0.703	1.002	0.679	0.645	0.681	0.675
Ca	0.003	0.01	0.005	0.013	0.003	0.009	0.059	0	0.002	0	0.002	0.012	0.128	0.009	0.007	0	0.003	0.002	0.027
Sum	23.998	23.973	23.992	23.978	23.982	23.996	23.976	23.997	23.964	23.997	24	23.957	24	23.964	23.936	23.939	23.984	23.979	23.958

Tabela C – Análises de magnetita de rochas foscoríticas de Catalão I. As análises foram recalculadas com base em 32 O. (Cont. I)

Amostra	91-1-7	91-1-7	91-1-8	91-1-9	93-1-1	93-1-1	93-1-1	93-1-1	93-1-11	93-1-2	93-1-2	93-1-2	93-1-3	93-1-3	93-1-3	93-1-4	93-1-4	93-1-5	93-1-5	93-1-6
Unidade				P2min	P2min	P2min	P2min	P2min	P2min	P2min	P2min	P2min	P2min	P2min	P2min	P2min	P2min	P2min	P2min	P2min
Oxidos (%)																				
Nb ₂ O ₅	0	0	0	0	0.13	0.02	0	0	0.09	0.13	0.13	0	0.17	0.04	0.15	0	0.12	0.09	0	0
SiO ₂	0	0.05	0	0	0.06	0	0	0	0	0.03	0.08	0.05	0.1	0	0.03	0.02	0.03	0	0.04	0
TiO ₂	1.27	6.36	4.67	1.01	9.63	2.05	0.72	2.66	0.56	8.11	2.94	4.1	1.44	4.38	1.59	7.09	4.68	3.71	4.95	1.29
Al ₂ O ₃	0.02	0.04	0.02	0	0.01	0.03	0.02	0.05	0	0	0	0	0	0	0	0.04	0.01	0	0	0.04
Cr ₂ O ₃	0	0.02	0	0.02	0	0.01	0.02	0	0	0.03	0	0.08	0.05	0	0.03	0.02	0	0.03	0.03	0.02
Fe ₂ O ₃	66.92	58.17	61.21	67.92	51.56	65.11	68.48	64.36	68.26	54.01	63.04	61.13	66.22	60.91	65.72	55.57	60.01	61.93	59.7	66.8
FeO	30.7	31.16	30.31	29.45	35.51	32.15	29.24	31.96	30.06	34.98	32.88	33.45	31.23	33.26	31.93	35.31	33.74	33.23	33.81	31.28
MnO	0.21	1.1	0.94	0.34	0.89	0.21	0.2	0.3	0.13	0.69	0.28	0.37	0.17	0.41	0.15	0.71	0.47	0.38	0.55	0.13
MgO	0.83	3.01	2.58	1.12	2.36	0.36	1.28	0.61	0.85	1.97	0.54	0.69	0.59	0.91	0.36	1.09	0.85	0.6	0.87	0.41
CaO	0.03	0.03	0.02	0.12	0	0	0	0.01	0.04	0	0	0.02	0	0	0.02	0	0	0	0	0
Total	99.98	99.94	99.75	99.98	100.15	99.94	99.96	99.95	99.99	99.95	99.89	99.89	99.97	99.91	99.98	99.85	99.91	99.97	99.95	99.97
Cations (p.f.u.)																				
Nb	0	0	0	0	0.017	0.002	0	0	0.012	0.018	0.018	0	0.024	0.006	0.02	0	0.016	0.012	0	0
Si	0	0.015	0.001	0	0.018	0	0	0	0	0.009	0.025	0.017	0.03	0	0.01	0.006	0.008	0	0.013	0
Ti	0.295	1.437	1.085	0.232	2.145	0.483	0.166	0.616	0.129	1.845	0.697	0.959	0.332	1.017	0.369	1.643	1.087	0.859	1.142	0.297
Al	0.008	0.016	0.008	0	0.004	0.009	0.007	0.018	0	0	0	0	0	0	0	0.013	0.005	0	0	0.016
Cr	0	0.004	0	0.004	0	0.003	0.006	0	0.001	0.006	0	0.019	0.013	0	0.008	0.006	0	0.007	0.006	0.005
Fe ³⁺	15.401	13.087	13.836	15.576	11.633	15.023	15.695	14.795	15.717	12.24	14.512	14.037	15.244	13.964	15.178	12.685	13.762	14.247	13.684	15.41
Fe ²⁺	7.852	7.791	7.613	7.506	8.904	8.245	7.448	8.165	7.691	8.809	8.412	8.535	7.989	8.474	8.196	8.958	8.599	8.496	8.613	8.021
Mn	0.056	0.279	0.247	0.088	0.222	0.056	0.052	0.078	0.033	0.177	0.075	0.096	0.044	0.108	0.04	0.185	0.123	0.099	0.144	0.034
Mg	0.379	1.349	1.186	0.511	1.041	0.168	0.587	0.278	0.39	0.89	0.252	0.322	0.272	0.418	0.167	0.5	0.392	0.274	0.398	0.189
Ca	0.009	0.011	0.006	0.04	0	0	0	0.004	0.013	0	0	0.006	0	0	0.006	0	0	0	0	0
Sum	24	23.989	23.983	23.957	23.985	23.991	23.96	23.954	23.987	23.993	23.99	23.992	23.948	23.985	23.994	23.997	23.993	23.993	24	23.97

Tabela C – Análises de magnetita de rochas foscoríticas de Catalão I. As análises foram recalculadas com base em 32 O. (Cont. II)

Amostra	93-1-7	93-1-7	93-1-8	93-1-8	93-1-9	93-1-9	99a1-1	99a1-2	99a1-3	99a1-4	99a1-5	99a1-6	99a2-1	99a2-2	99a2-3	99a3-1	99a4-3	99a4-4	99a4-5	
Unidade	P2min	P2min	P2min	P2min	P2min	P2bar	DC	DC	DC	DC										
Oxidos (%)																				
Nb ₂ O ₅	0.08	0	0.01	0.04	0	0.03	0.01	0.76	0.07	0	0.74	0	0.05	0.03	0.05	0	0	0.17	0.02	0.11
SiO ₂	0.01	0	0	0	0	0.02	0	0	0	0.06	0.07	0.03	0	0	0	0.03	0.02	0.03	0	0.04
TiO ₂	6.66	7.43	0.6	5.16	0.65	5.79	3.33	2.89	1.16	1.17	5.93	1.34	2.29	1.71	2.78	2.03	1.24	1.71	2.57	3.3
Al ₂ O ₃	0	0	0	0	0.03	0.05	0	0.03	0.02	0	0.01	0	0	0	0.02	0.03	0	0.05	0	0.04
Cr ₂ O ₃	0	0	0	0	0	0	0.01	0.02	0.02	0	0.04	0	0.02	0.02	0	0	0.03	0	0.02	0.02
Fe ₂ O ₃	56.47	55.78	68	59.61	68.26	58.41	63.09	62.45	66.73	66.91	56.48	66.7	64.78	66.02	63.93	65.33	66.9	65.32	64.33	62.67
FeO	35.27	34.53	31.03	33.65	29.73	33.84	32.28	32.4	31.63	31.46	35.15	31.23	31.99	31.13	32.18	31.96	30.93	32.13	32.14	32.83
MnO	0.56	0.65	0.09	0.38	0.2	0.61	0.44	0.33	0.13	0.1	0.69	0.17	0.28	0.34	0.35	0.17	0.15	0.27	0.31	0.42
MgO	0.8	1.54	0.24	1.17	1.1	1.17	0.85	1	0.21	0.25	0.79	0.44	0.5	0.7	0.69	0.46	0.4	0.23	0.53	0.53
CaO	0.05	0.01	0.02	0.01	0	0.01	0	0.07	0	0.02	0.07	0.07	0.04	0.05	0	0	0.28	0.04	0.04	0.05
Total	99.9	99.94	99.99	100.02	99.97	99.93	100.01	99.95	99.97	99.97	99.97	99.98	99.95	100	100	100.01	99.95	99.95	99.96	100.01
Cations (p.f.u.)																				
Nb	0.011	0	0.001	0.005	0	0.004	0.001	0.105	0.01	0	0.102	0	0.007	0.004	0.007	0	0	0.025	0.003	0.015
Si	0.004	0.001	0	0	0	0.005	0	0	0	0.019	0.022	0.009	0	0	0	0.008	0.007	0.008	0	0.011
Ti	1.539	1.694	0.14	1.178	0.152	1.333	0.763	0.67	0.27	0.271	1.362	0.31	0.534	0.393	0.639	0.464	0.289	0.403	0.596	0.759
Al	0	0	0	0	0.012	0.018	0	0.011	0.009	0.001	0.003	0	0	0	0.005	0.01	0	0.017	0	0.013
Cr	0	0	0.001	0	0	0.003	0.004	0.006	0	0.009	0	0.005	0.005	0	0	0.008	0	0.005	0.005	
Fe ³⁺	12.916	12.668	15.729	13.632	15.684	13.33	14.485	14.348	15.43	15.452	12.948	15.384	14.925	15.202	14.707	15.06	15.426	15.094	14.813	14.418
Fe ²⁺	8.966	8.715	7.976	8.553	7.592	8.583	8.235	8.273	8.127	8.075	8.957	8.005	8.19	7.968	8.227	8.188	7.927	8.252	8.225	8.393
Mn	0.145	0.167	0.024	0.097	0.052	0.157	0.112	0.086	0.035	0.026	0.178	0.045	0.072	0.088	0.09	0.045	0.04	0.071	0.081	0.109
Mg	0.366	0.694	0.109	0.528	0.508	0.532	0.385	0.46	0.098	0.115	0.362	0.202	0.233	0.319	0.316	0.21	0.183	0.108	0.244	0.241
Ca	0.017	0.002	0.006	0.004	0	0.002	0	0.024	0	0.006	0.024	0.022	0.014	0.016	0	0	0.094	0.014	0.012	0.017
Sum	23.964	23.942	23.986	23.997	24	23.964	23.984	23.981	23.985	23.966	23.965	23.978	23.98	23.995	23.99	23.985	23.974	23.992	23.98	23.98

Tabela C – Análises de magnetita de rochas foscoríticas de Catalão I. As análises foram recalculadas com base em 32 O. (Cont. III)

Amostra	99a4-6	99a4-6	99a4-8	99b1-1	99b1-1	99b1-11	99b1-2	99b1-3	99b1-4	99b1-5	99b1-6	99b1-7	99b1-8	99b1-9	99b2-1	13-3-1	13-3-2	13-3-3	13-3-4		
Unidade	DC	DC	DC	P3min	P3min	P3min	P3min	P3min	P3min	P3min	P3min	P3min	P3min	P3min	P3min	P3bar	P3bar	P3bar	P3bar		
Oxidos (%)																					
Nb ₂ O ₅	0.03	0.43	0.24	0.09	0	0	0.08	0	0	0.22	0	0	0	0.06	1.06	0.46	0.13	0	0.02	0.01	
SiO ₂	0	0.07	0.02	0.04	0	0.04	0.04	0.01	0	0.03	0.02	0.04	0	0.06	0.07	0.08	0.05	0.02	0.04	0	
TiO ₂	3.01	3.05	1.91	0.76	0.94	1.15	0.54	2.88	2.41	4.42	1.37	1.71	1.77	4.08	5.07	2.63	2.56	2.53	2.67	1.88	
Al ₂ O ₃	0	0.03	0	0.03	0	0.03	0	0.02	0	0	0.03	0.01	0	0	0	0.04	0	0	0	0.03	
Cr ₂ O ₃	0.04	0	0	0	0	0	0.03	0.02	0	0.04	0	0.01	0.04	0.03	0	0.01	0.03	0.03	0	0.02	
Fe ₂ O ₃	63.45	62.28	65.28	67.32	67.51	67.14	67.83	64.02	64.77	60.41	66.52	65.9	65.93	61.41	57.59	63.22	64.72	64.87	64.59	66.04	
FeO	32.19	33.28	31.7	31.42	30.69	30.73	31.08	31.69	31.59	33.09	31.26	31.34	31.29	32.81	34.05	32.11	30.43	30.61	31.03	30.87	
MnO	0.36	0.34	0.29	0.1	0.19	0.17	0.08	0.46	0.32	0.68	0.16	0.22	0.3	0.55	0.67	0.36	0.46	0.45	0.51	0.32	
MgO	0.78	0.47	0.54	0.23	0.64	0.74	0.21	0.82	0.76	0.89	0.44	0.53	0.55	0.87	1.35	0.99	1.59	1.43	1.12	0.8	
CaO	0.09	0.01	0.02	0.01	0.03	0	0.11	0.06	0.06	0.1	0.19	0.21	0.1	0.01	0.03	0.01	0.03	0.02	0.04		
Total	99.95	99.96	100	100	100	100	99.98	99.91	99.88	99.99	99.97	99.98	99.88	99.89	99.91	100	99.97	100	100.01		
Cations (p.f.u.)																					
Nb	0.004	0.06	0.033	0.013	0	0	0.011	0	0	0.03	0	0	0	0.008	0.147	0.065	0.017	0	0.002	0.001	
Si	0	0.021	0.006	0.013	0	0.012	0.011	0.004	0	0.008	0.005	0.011	0	0.018	0.021	0.025	0.016	0.005	0.011	0	
Ti	0.699	0.71	0.438	0.175	0.216	0.265	0.125	0.66	0.567	1.028	0.318	0.399	0.411	0.951	1.173	0.613	0.582	0.583	0.611	0.426	
Al	0	0.01	0.001	0.009	0.001	0.01	0	0.007	0	0	0.01	0.004	0	0	0	0.015	0	0	0	0.012	
Cr	0.011	0.001	0.001	0	0.001	0	0.006	0.006	0	0.011	0	0.002	0.009	0.008	0	0.003	0.008	0.007	0	0.005	
Fe ³⁺	14.581	14.357	15.044	15.575	15.568	15.454	15.694	14.694	14.885	13.847	15.344	15.181	15.188	14.07	13.181	14.518	14.778	14.835	14.792	15.174	
Fe ²⁺	8.221	8.525	8.12	8.077	7.864	7.861	7.991	8.083	8.069	8.43	8.015	8.024	8.011	8.355	8.662	8.195	7.721	7.78	7.897	7.883	
Mn	0.094	0.089	0.075	0.026	0.048	0.044	0.02	0.119	0.084	0.179	0.041	0.057	0.078	0.144	0.175	0.094	0.117	0.115	0.131	0.083	
Mg	0.358	0.216	0.244	0.107	0.291	0.337	0.097	0.372	0.357	0.412	0.205	0.247	0.251	0.401	0.62	0.458	0.718	0.653	0.507	0.359	
Ca	0.029	0.003	0.006	0.004	0.009	0	0.036	0.02	0.019	0.033	0.062	0.069	0.033	0.002	0.011	0.004	0.009	0.007	0.013		
Sum	23.997	23.991	23.967	24	23.998	23.982	23.993	23.966	23.981	23.978	24	23.993	23.981	23.959	23.989	23.991	23.967	23.984	23.958	23.955	

Tabela C – Análises de magnetita de rochas foscoríticas de Catalão I. As análises foram recalculadas com base em 32 O. (Cont. IV)

Amostra	103-3-4	103-3-6	103-3-7	107-1-1	107-1-2	107-3-1	107-3-3	107-3-4	107-3-5	107-3-6	107-3-7	152-1-1	152-1-10	152-1-2	152-1-5	152-1-6	152-1-7	152-1-9	152-2-1	152-2-2	
Unidade	P3bar	P3bar	P3bar	P2bar	P2bar	P2bar	P2bar	P2bar	P2bar	P2bar	DC	DC									
Oxidos (%)																					
Nb ₂ O ₅	0	0	0.12	0	0.01	0	0	0	0.02	0	0	0	0.04	0.09	0	0.04	0	0	0	0.1	
SiO ₂	0	0.06	0	0.04	0.05	0.03	0	0.02	0	0.03	0	0	0.01	0	0	0.06	0	0.02	0.06	0.02	
TiO ₂	1.79	2.1	1.47	1.13	1.01	1.52	2.65	1.21	1.04	0.9	2.66	6.73	0.94	2.96	0.45	0.65	0.51	0.61	1.3	0.7	
Al ₂ O ₃	0	0	0	0	0	0.04	0	0.02	0.02	0	0	0	0.01	0	0.01	0.03	0	0	0	0	
Cr ₂ O ₃	0	0.04	0.06	0	0.05	0	0	0.03	0.03	0	0	0.06	0.02	0.01	0	0.01	0	0	0	0	
Fe ₂ O ₃	66.22	65.97	66.59	67.25	67.3	66.2	64.27	66.71	67.3	67.61	64.26	55.84	67.55	63.53	68.78	67.97	68.05	67.92	66.82	67.77	
FeO	30.47	29.62	30.23	30.49	30.45	31.75	32.26	31.57	30.66	30.52	32.19	35.82	30.72	32.55	29.5	30.84	30.83	30.91	31.12	30.86	
MnO	0.35	0.43	0.29	0.21	0.24	0.17	0.31	0.19	0.23	0.12	0.32	0.5	0.22	0.31	0.18	0.05	0.13	0.17	0.16	0.09	
MgO	1.15	1.75	1.21	0.83	0.85	0.26	0.43	0.24	0.72	0.75	0.49	0.65	0.47	0.51	0.96	0.33	0.28	0.31	0.47	0.43	
CaO	0	0	0	0.03	0.02	0.02	0.05	0	0	0.03	0.08	0	0.04	0.03	0.02	0.06	0.12	0.06	0.01	0.01	
Total	99.98	99.97	99.97	99.98	99.98	99.99	99.97	99.99	100	99.98	100	99.6	99.97	99.95	99.98	99.98	99.99	100	99.94	99.98	
Cations (p.f.u.)																					
Nb	0	0	0.016	0	0.002	0	0	0	0.003	0	0	0	0.005	0.012	0	0.005	0	0	0.014		
Si	0.001	0.019	0	0.011	0.016	0.01	0	0.005	0	0.008	0	0.001	0.004	0	0	0.019	0	0.006	0.017	0.006	
Ti	0.412	0.479	0.339	0.261	0.234	0.353	0.615	0.281	0.24	0.208	0.611	1.615	0.217	0.689	0.104	0.151	0.118	0.142	0.304	0.163	
Al	0	0	0	0	0	0.013	0	0.008	0.009	0	0	0	0.004	0	0.004	0.01	0	0	0		
Cr	0	0.01	0.014	0	0.012	0	0	0.008	0.007	0	0	0.014	0.005	0.002	0	0.003	0	0	0		
Fe ³⁺	15.189	15.04	15.277	15.471	15.486	15.284	14.804	15.422	15.505	15.571	14.799	12.784	15.581	14.623	15.808	15.691	15.739	15.704	15.399	15.646	
Fe ²⁺	7.766	7.504	7.708	7.796	7.788	8.147	8.257	8.111	7.849	7.812	8.237	9.114	7.876	8.328	7.535	7.912	7.925	7.942	7.971	7.918	
Mn	0.091	0.11	0.075	0.054	0.063	0.044	0.08	0.048	0.06	0.031	0.082	0.136	0.058	0.081	0.046	0.013	0.035	0.044	0.043	0.022	
Mg	0.526	0.791	0.553	0.383	0.389	0.118	0.196	0.109	0.33	0.345	0.225	0.307	0.217	0.234	0.439	0.15	0.128	0.143	0.218	0.198	
Ca	0	0	0.001	0.008	0.006	0.005	0.015	0	0	0.011	0.025	0	0.012	0.01	0.005	0.021	0.041	0.02	0.005	0.002	
Sum	23.985	23.954	23.983	23.984	23.996	23.975	23.966	23.991	24	23.988	23.979	23.971	23.971	23.976	23.948	23.963	24	24	23.957	23.971	

Tabela C – Análises de magnetita de rochas foscoríticas de Catalão I. As análises foram recalculadas com base em 32 O. (Cont. V)

Amostra	152-2-3	156-1-01	156-1-02	156-1-03	156-1-04	156-1-05	156-1-06	156-1-07	156-1-08	156-1-09	156-1-10	156-1-11	156-1-12	156-1-13	156-1-14	156-1-15	156-1-16	156-1-17	156-1-18	156-1-19
Unidade	DC	P2bar																		
Oxidos (%)																				
Nb ₂ O ₅	0	0	0	0	0.07	0	0.06	0	0	0	0.01	0	0	0.02	0.02	0.04	0	0	0	
SiO ₂	0	0.02	0	0	0.01	0	0	0	0	0.03	0.01	0.04	0.05	0.07	0.02	0	0	0	0	
TiO ₂	0.5	0.6	1.02	0.9	1.69	0.73	0.83	1.08	0.99	1.93	2.62	0.58	1.98	2.34	0.8	1.29	0.66	0.76	0.82	0.88
Al ₂ O ₃	0.01	0.02	0	0	0.04	0.02	0	0	0	0	0.06	0.01	0.01	0	0.02	0.03	0	0.01	0	
Cr ₂ O ₃	0	0.07	0.02	0	0.03	0.02	0.07	0.38	0.03	0.06	0.06	0.01	0.04	0.01	0	0.02	0.04	0	0.04	0.02
Fe ₂ O ₃	68.28	68.4	67.67	68.01	66.3	68.13	67.8	67.17	67.8	66.21	64.77	68.3	65.76	64.82	67.83	67.3	68.16	68.05	67.96	67.97
FeO	30.55	29.57	29.94	29.77	30.25	29.78	29.82	30.19	29.63	30.03	30.57	30	30.36	31.05	30.1	29.93	29.98	30	29.94	29.93
MnO	0.09	0.21	0.34	0.25	0.33	0.27	0.29	0.24	0.28	0.41	0.54	0.23	0.36	0.42	0.22	0.26	0.2	0.28	0.32	0.25
MgO	0.52	0.74	0.94	1.02	1.32	1.03	1.12	0.87	1.25	1.31	1.44	0.14	0.94	0.95	0.85	1.06	0.83	0.87	0.87	0.9
CaO	0.04	0.32	0.04	0.01	0	0	0	0.06	0	0.04	0	0.57	0.44	0.3	0.15	0.09	0.07	0.05	0.07	0.05
Total	99.99	99.95	99.97	99.96	100	100	100.01	99.99	99.98	100.02	100.01	99.94	99.94	99.97	99.99	99.99	100.01	100.01	100.03	100
Cations (p.f.u.)																				
Nb	0	0	0	0	0.01	0	0.008	0	0	0	0.002	0	0	0.003	0.003	0.005	0	0	0	
Si	0	0.006	0	0	0.002	0	0	0	0	0.009	0.002	0.013	0.016	0.021	0.006	0	0	0	0	
Ti	0.116	0.139	0.238	0.209	0.386	0.168	0.191	0.249	0.227	0.436	0.598	0.135	0.458	0.54	0.184	0.295	0.15	0.173	0.187	0.201
Al	0.004	0.009	0	0	0.016	0.006	0	0	0	0	0.023	0.003	0.003	0	0.007	0.01	0	0.003	0	
Cr	0	0.017	0.004	0	0.007	0.005	0.016	0.091	0.007	0.014	0.013	0.002	0.011	0.002	0	0.005	0.01	0	0.009	0.005
Fe ³⁺	15.84	15.726	15.55	15.62	15.196	15.657	15.578	15.44	15.554	15.148	14.81	15.748	15.073	14.873	15.612	15.438	15.685	15.663	15.634	15.626
Fe ²⁺	7.838	7.556	7.646	7.599	7.707	7.605	7.614	7.712	7.554	7.636	7.766	7.687	7.733	7.919	7.7	7.629	7.668	7.674	7.654	7.648
Mn	0.024	0.056	0.088	0.065	0.085	0.069	0.075	0.063	0.073	0.104	0.138	0.061	0.093	0.11	0.058	0.068	0.051	0.072	0.081	0.063
Mg	0.241	0.342	0.432	0.466	0.598	0.468	0.508	0.397	0.569	0.587	0.65	0.065	0.434	0.434	0.388	0.478	0.376	0.393	0.392	0.409
Ca	0.013	0.108	0.013	0.005	0	0	0	0.02	0	0.013	0.001	0.189	0.146	0.098	0.048	0.028	0.024	0.017	0.021	0.016
Sum	24	23.958	23.97	23.963	23.991	23.987	23.995	23.971	23.985	23.947	23.978	23.926	23.966	24	23.998	23.951	23.979	23.991	23.98	23.968

Tabela C – Análises de magnetita de rochas foscoríticas de Catalão I. As análises foram recalculadas com base em 32 O. (Cont. VI)

Amostra	156-1-20	156-1-21	156-1-22	156-1-23	156-1-24	156-1-25	156-2-1	156-2-2	156-2-3	156-2-4	156-2-5	157a2-1	157a2-2	157a2-3	157a2-4	157a2-5	157b1-01	157b1-02	157b1-03	157b1-04
Unidade	P2bar	P2bar	P2bar	P2bar	P2bar	P2bar	P2bar	P2bar	P2bar	P2bar	P2bar	P2bar	P2bar	P2bar	P2bar	P2bar	P3min	P3min	P3min	P3min
Oxidos (%)																				
Nb ₂ O ₅	0.02	0	0.02	0	0.01	0.05	0	0.07	0	0.02	0	0.01	0	0.14	0.07	0	0.2	0.2	0.02	0.06
SiO ₂	0.03	0.03	0	0	0	0.03	0.09	0.03	0.04	0.02	0	0	0.05	0.04	0	0.03	0.1	0.1	0	0.01
TiO ₂	1.02	1.04	1.05	0.96	1.05	0.93	0.46	0.66	0.76	2.7	0.58	1.42	0.86	1.28	1.28	1.64	0.79	5.49	3.97	1.26
Al ₂ O ₃	0	0	0	0.01	0	0	0.06	0	0	0	0	0	0.01	0.06	0.04	0.12	0	0.01	0.01	0.01
Cr ₂ O ₃	0.02	0.01	0	0	0.05	0.02	0.01	0.22	0.04	0.02	0.06	0.01	0.03	0	0.06	0	0	0.03	0.01	0
Fe ₂ O ₃	67.58	67.62	67.48	67.84	67.5	67.81	68.04	68	68.2	64.5	68.39	66.4	67.5	66.43	66.73	66.09	67.52	58.44	62.04	66.87
FeO	30.09	30.04	30.19	29.91	30.09	29.83	30.68	29.72	29.47	30.71	29.76	31.49	30.74	31.34	30.76	31.31	29.59	33.76	32.02	31.19
MnO	0.28	0.27	0.34	0.3	0.32	0.31	0.19	0.22	0.27	0.48	0.21	0.14	0.18	0.21	0.28	0.21	0.28	0.57	0.48	0.14
MgO	0.91	0.99	0.91	0.91	0.92	0.91	0.47	0.96	1.17	1.41	0.96	0.47	0.6	0.42	0.65	0.63	1.36	1.34	1.31	0.42
CaO	0.06	0.02	0.03	0.08	0.08	0.12	0	0.1	0.01	0.07	0.02	0.01	0.03	0.09	0.08	0.04	0	0.03	0	0
Total	100.01	100.02	100.02	100.01	100.02	100.01	100	99.98	99.96	99.93	99.98	99.95	99.99	99.96	99.97	99.99	99.96	99.96	99.86	99.96
Cations (p.f.u.)																				
Nb	0.003	0	0.003	0	0.001	0.007	0	0.01	0	0.003	0	0.002	0	0.02	0.01	0	0.027	0.028	0.003	0.008
Si	0.01	0.008	0.001	0	0	0.008	0.028	0.009	0.011	0.005	0	0	0.015	0.012	0	0.01	0.032	0.029	0	0.004
Ti	0.232	0.236	0.239	0.219	0.24	0.212	0.106	0.151	0.176	0.625	0.134	0.334	0.2	0.299	0.296	0.378	0.183	1.26	0.925	0.292
Al	0	0	0	0.002	0	0	0.023	0.001	0	0	0	0	0	0.005	0.021	0.013	0.042	0	0.004	0.005
Cr	0.004	0.002	0	0	0.011	0.006	0.003	0.054	0.01	0.006	0.014	0.002	0.007	0	0.016	0.001	0	0.006	0.002	0
Fe ³⁺	15.534	15.536	15.521	15.592	15.522	15.58	15.707	15.627	15.647	14.745	15.729	15.324	15.566	15.329	15.366	15.22	15.466	13.339	14.17	15.423
Fe ²⁺	7.687	7.671	7.717	7.639	7.688	7.616	7.87	7.589	7.513	7.801	7.606	8.076	7.878	8.037	7.871	8.014	7.532	8.563	8.129	7.993
Mn	0.073	0.069	0.087	0.078	0.082	0.079	0.048	0.057	0.071	0.124	0.055	0.037	0.047	0.056	0.073	0.054	0.072	0.149	0.125	0.036
Mg	0.409	0.444	0.41	0.413	0.415	0.41	0.215	0.437	0.537	0.646	0.442	0.222	0.276	0.195	0.297	0.287	0.626	0.61	0.604	0.194
Ca	0.019	0.007	0.009	0.024	0.027	0.039	0	0.032	0.005	0.024	0.007	0.004	0.008	0.03	0.027	0.012	0	0.009	0.001	0.001
Sum	23.97	23.973	23.988	23.967	23.985	23.955	24	23.967	23.97	23.98	23.988	24	23.997	23.983	23.976	23.989	23.98	23.993	23.964	23.956

Tabela C – Análises de magnetita de rochas foscoríticas de Catalão I. As análises foram recalculadas com base em 32 O. (Cont. VII)

Amostra	157b1-05	157b1-06	157b1-08	157b1-09	157b1-10	157b3-1	157b3-2	157b3-5	157b3-6	157b3-7	192b2-1	192b2-2	192b2-3	192b2-4	192b2-5	192b2-6	200-1-1	200-1-10	200-1-11	200-1-2
Unidade	P3min	P3min	P3min	P3min	P3min	P3min	P3min	P3min	P3min	P3min	P2min	P2min	P2min	P2min	P2min	P3bar	P3bar	P3bar	P3bar	
Oxidos (%)																				
Nb ₂ O ₅	0.04	0	0.18	0.04	0	0	0.41	0.21	0.24	0.36	0.02	0	0.09	0.09	0.11	0.12	0.04	0	0.36	0.02
SiO ₂	0	0.01	0.03	0.01	0.03	0.02	0.06	0.02	0.01	0.08	0.03	0.07	0.08	0.02	0.01	0	0.01	0.01	0.07	0.02
TiO ₂	2.37	3.28	3.18	4.17	1.41	0.53	4.99	5.32	5.51	2.97	2.41	2.64	1.76	2.77	5.26	2.36	0.78	6.54	7.13	1.15
Al ₂ O ₃	0	0	0.02	0	0	0	0.04	0	0.03	0	0	0.02	0.02	0	0	0.04	0	0	0	0
Cr ₂ O ₃	0.01	0	0	0.01	0	0	0.04	0.04	0.02	0.03	0	0.02	0	0.04	0	0	0	0.03	0	0
Fe ₂ O ₃	64.77	63.26	63.03	61.71	66.73	68.52	59.41	58.65	58.56	63	64.41	64.38	65.51	63.81	59.05	64.41	68.1	56.87	54.99	67.31
FeO	31.64	31.81	31.71	32.32	30.75	29.96	32.58	34.12	33.38	32.1	32.23	30.99	31.85	32.09	34.15	32.35	29.77	34.83	35.38	30.28
MnO	0.25	0.42	0.49	0.61	0.23	0.15	0.59	0.7	0.56	0.4	0.22	0.41	0.19	0.29	0.46	0.25	0.24	0.72	0.74	0.12
MgO	0.83	1.07	1.16	1.18	0.8	0.74	1.92	0.72	1.48	0.99	0.54	1.26	0.45	0.81	0.88	0.39	1.02	0.97	1.1	1.06
CaO	0.02	0.02	0.18	0.02	0.01	0.09	0.02	0.08	0.02	0.02	0.06	0.18	0.06	0.05	0.06	0.06	0	0	0.02	0
Total	99.93	99.87	99.98	100.07	99.96	100.01	100.06	99.86	99.81	99.95	99.92	99.97	100.01	99.97	99.98	99.98	99.96	99.97	99.79	99.96
Cations (p.f.u.)																				
Nb	0.006	0	0.024	0.005	0	0	0.056	0.03	0.034	0.05	0.003	0	0.012	0.012	0.015	0.017	0.006	0	0.051	0.003
Si	0.001	0.003	0.01	0.003	0.01	0.005	0.017	0.006	0.002	0.025	0.01	0.02	0.023	0.005	0.002	0.001	0.004	0.002	0.021	0.006
Ti	0.553	0.768	0.73	0.941	0.326	0.122	1.128	1.24	1.286	0.685	0.566	0.608	0.406	0.64	1.209	0.545	0.181	1.499	1.657	0.267
Al	0.001	0	0.008	0	0	0	0.015	0	0.011	0	0	0.007	0.006	0	0	0.016	0	0	0	0.001
Cr	0.003	0	0	0.002	0	0	0.009	0.01	0.004	0.007	0.001	0.005	0.001	0.009	0	0	0.007	0	0	0
Fe ³⁺	14.885	14.488	14.44	14.118	15.349	15.776	13.521	13.445	13.342	14.453	14.837	14.734	15.107	14.667	13.534	14.854	15.646	13.003	12.543	15.46
Fe ²⁺	8.081	8.097	8.074	8.216	7.861	7.665	8.239	8.692	8.453	8.185	8.251	7.883	8.162	8.197	8.699	8.291	7.601	8.851	8.969	7.728
Mn	0.065	0.11	0.128	0.155	0.061	0.038	0.149	0.184	0.146	0.104	0.057	0.106	0.048	0.077	0.119	0.065	0.062	0.185	0.192	0.032
Mg	0.384	0.496	0.527	0.53	0.366	0.335	0.861	0.331	0.683	0.455	0.253	0.575	0.207	0.371	0.401	0.177	0.467	0.441	0.508	0.486
Ca	0.007	0.008	0.06	0.007	0.003	0.028	0.006	0.025	0.006	0.006	0.021	0.06	0.019	0.018	0.02	0.019	0	0	0.007	0
Sum	23.986	23.97	24	23.977	23.977	23.97	24	23.963	23.966	23.97	24	23.998	23.991	23.997	24	23.986	23.967	23.988	23.948	23.984

Tabela C – Análises de magnetita de rochas foscoríticas de Catalão I. As análises foram recalculadas com base em 32 O. (Cont. VIII)

Amostra	200-1-3	200-1-4	200-1-5	200-1-6	200-1-7	200-1-8	200-2-4	200-2-5	200-2-6	200-2-7	200-2-8	200-2-9	207-1-1	207-4-1	207-4-2	207-4-3	207-4-4	207-4-5	207-5-3	207-5-5	
Unidade	P3bar	P3bar	P3bar	P3bar	P3bar	P3bar	DC	P3bar	P3bar												
Oxidos (%)																					
Nb ₂ O ₅	0.12	0.07	0	0.01	0	0.15	0.05	0.06	0.04	0.51	0.01	0	0.1	0.01	0	0.01	0.19	0.04	0	0.12	
SiO ₂	0.01	0	0.02	0.03	0.01	0.04	0	0	0.03	0.01	0	0.01	0.03	0	0.05	0.01	0.01	0.02	0.04	0.03	
TiO ₂	4.85	0.91	1.88	2.05	2.45	0.73	2.1	2.13	1.41	4.02	2.41	1.88	1.94	3.39	6.29	2.2	4.02	0.94	0.98	5.96	
Al ₂ O ₃	0	0	0.02	0	0	0.02	0.02	0.02	0.01	0	0	0.01	0.01	0	0.08	0	0	0	0.04	0	
Cr ₂ O ₃	0	0	0	0.01	0.01	0.04	0	0.07	0	0.01	0	0.04	0	0.01	0	0	0	0	0.02	0	
Fe ₂ O ₃	60	67.5	66.02	65.55	64.72	67.22	65.4	65.08	66.53	60.89	64.73	65.74	65.66	63.11	58.08	65.5	61.49	67.36	67.3	57.6	
FeO	33.2	30.97	30.55	31.01	31.88	31.44	31.26	31.55	31.31	32.92	31.74	31.57	30.51	31.6	32.35	30.45	32.01	30.78	30.81	33.61	
MnO	0.56	0.1	0.4	0.28	0.27	0.06	0.32	0.3	0.18	0.42	0.34	0.17	0.42	0.55	0.92	0.49	0.64	0.22	0.14	0.73	
MgO	1.22	0.43	1.1	1.06	0.6	0.23	0.77	0.8	0.45	1.06	0.74	0.45	1.26	1.21	2.18	1.32	1.37	0.63	0.47	1.59	
CaO	0.02	0	0	0	0.01	0.06	0.05	0	0.02	0.05	0.01	0.09	0.04	0.08	0.08	0.04	0	0	0.18	0.04	
Total	99.98	99.98	99.99	100	99.95	99.99	99.97	100.01	99.98	99.89	99.98	99.96	99.97	99.96	100.03	100.02	99.73	99.99	99.98	99.68	
Cations (p.f.u.)																					
Nb	0.017	0.01	0	0.001	0	0.021	0.007	0.008	0.005	0.071	0.001	0	0.014	0.001	0	0.001	0.027	0.006	0	0.017	
Si	0.002	0	0.007	0.008	0.004	0.012	0	0	0.009	0.002	0	0.002	0.008	0	0.015	0.004	0.003	0.007	0.012	0.008	
Ti	1.112	0.211	0.431	0.47	0.57	0.171	0.485	0.49	0.327	0.936	0.557	0.439	0.448	0.782	1.417	0.5	0.954	0.217	0.227	1.41	
Al	0	0	0.006	0	0	0.006	0.008	0.006	0.005	0	0	0.003	0.002	0	0.029	0	0	0	0.016	0	
Cr	0	0	0	0.003	0.002	0.011	0	0.017	0	0.002	0	0.009	0	0.003	0	0	0	0	0.004	0	
Fe ³⁺	13.722	15.581	15.142	15.046	14.887	15.553	15.032	14.974	15.341	13.951	14.889	15.144	15.051	14.443	13.142	15.001	14.041	15.535	15.518	13.113	
Fe ²⁺	8.44	7.944	7.786	7.91	8.151	8.085	7.986	8.066	8.023	8.382	8.114	8.083	7.771	8.038	8.135	7.751	8.122	7.89	7.894	8.503	
Mn	0.145	0.025	0.102	0.073	0.07	0.017	0.083	0.077	0.046	0.11	0.088	0.044	0.11	0.143	0.233	0.124	0.172	0.057	0.038	0.194	
Mg	0.554	0.196	0.499	0.483	0.276	0.104	0.351	0.362	0.206	0.487	0.34	0.206	0.576	0.553	0.971	0.594	0.644	0.288	0.217	0.743	
Ca	0.006	0	0	0	0.003	0.02	0.015	0.001	0.008	0.015	0.003	0.03	0.012	0.025	0.024	0.014	0	0	0.058	0.012	
Sum	23.998	23.968	23.974	23.993	23.963	24	23.968	24	23.968	23.957	23.994	23.961	23.993	23.987	23.966	23.989	23.963	24	23.983	24	

Tabela C – Análises de magnetita de rochas foscoríticas de Catalão I. As análises foram recalculadas com base em 32 O. (Cont. IX)

Amostra	207-5-6	207-5-6	207-5-8	225-1-3	225-1-4	225-1-5	225-1-6	225-4-2	225-4-3	225-4-4	244-1-1	244-1-2	244-1-3	304a1-1	304a1-2	304a1-3	304a1-4	304a1-5	304a1-6	
Unidade	P3bar	P3bar	P3bar	glim	P1	P1	P1	P2min	P2min	P2min	P2min	P2min	P2min							
Oxidos (%)																				
Nb ₂ O ₅	0	0.01	0	0.093	0.243	0.015	0.128	0.876	0.064	0.014	0	0.042	0	0.028	0.1	0.01	0.02	0.05	0	0
SiO ₂	0.05	0	0	0	0.061	0.341	0.358	0.054	0.234	0.008	0.159	0.098	0.003	0.303	0	0.06	0.03	0	0.03	0
TiO ₂	1.21	2.11	1.53	3.494	5.801	6.67	6.674	7.392	7.599	7.89	10.57	13.263	13.378	14.886	0.77	0.71	0.7	0.46	1.02	0.79
Al ₂ O ₃	0	0.02	0.02	0	0	0.002	0	0	0	0.004	0.035	0	0.042	0	0	0	0	0.01	0	
Cr ₂ O ₃	0	0.03	0.04	0.029	0.043	0.024	0.036	0.007	0.051	0.004	0	0	0.065	0.028	0.04	0.03	0	0.02	0.02	
Fe ₂ O ₃	66.75	65.74	66.7	62.704	57.597	55.957	55.739	53.364	54.616	54.961	49.272	41.731	44.162	38.137	68.05	68.15	68.15	68.7	67.62	67.89
FeO	31.39	30.32	30.43	32.49	34.684	34.337	33.409	36.068	33.616	32.778	31.656	41.988	37.528	44.636	29.86	29.43	29.86	29.37	30.05	30.3
MnO	0.2	0.52	0.3	0.448	0.666	0.274	0.417	0.777	0.414	0.753	0.724	0.221	0.711	0.149	0.19	0.33	0.29	0.26	0.3	0.19
MgO	0.37	1.2	0.95	0.715	0.835	1.987	2.656	1.278	2.951	2.967	5.479	1.369	3.537	0.797	0.61	1.23	0.86	1.07	0.85	0.73
CaO	0.03	0	0.02	0.087	0.065	0.011	0.001	0.056	0	0.01	0.083	0.011	0	0.012	0.32	0.03	0.06	0.06	0.09	0.09
Total	100	99.95	99.99	100.06	99.995	99.618	99.418	99.872	99.545	99.389	97.978	98.723	99.426	98.976	99.94	99.98	99.97	99.99	99.99	100.01
Cations (p.f.u.)																				
Nb	0	0.001	0	0.013	0.033	0.002	0.018	0.122	0.009	0.002	0	0.006	0	0.004	0.014	0.001	0.002	0.007	0	0
Si	0.015	0	0	0	0.019	0.107	0.113	0.017	0.073	0.003	0.052	0.032	0.001	0.097	0	0.017	0.01	0	0.009	0
Ti	0.28	0.487	0.35	0.79	1.329	1.568	1.586	1.708	1.774	1.858	2.579	3.249	3.071	3.581	0.18	0.164	0.162	0.105	0.234	0.181
Al	0	0.005	0.006	0	0	0.001	0	0	0	0.001	0.013	0	0.015	0	0	0	0	0.002	0	
Cr	0	0.007	0.009	0.007	0.01	0.006	0.009	0.002	0.013	0.001	0	0	0.016	0.007	0.011	0.008	0	0.005	0.005	
Fe ³⁺	15.415	15.054	15.318	14.404	13.199	12.659	12.546	12.188	12.266	12.325	10.761	9.429	9.825	8.638	15.655	15.636	15.676	15.787	15.544	15.641
Fe ²⁺	8.056	7.717	7.768	8.294	8.833	8.633	8.357	9.155	8.391	8.169	7.684	10.544	9.279	11.235	7.636	7.505	7.634	7.5	7.677	7.757
Mn	0.052	0.136	0.078	0.114	0.172	0.073	0.112	0.202	0.109	0.2	0.199	0.061	0.184	0.04	0.049	0.085	0.075	0.068	0.078	0.048
Mg	0.17	0.551	0.432	0.32	0.379	0.926	1.251	0.585	1.365	1.384	2.649	0.665	1.609	0.38	0.281	0.566	0.394	0.485	0.386	0.33
Ca	0.009	0	0.005	0.028	0.021	0.004	0	0.018	0	0.003	0.029	0.004	0	0.004	0.106	0.01	0.02	0.02	0.029	0.03
Sum	23.996	23.958	23.966	23.971	23.995	23.978	23.992	23.997	24	23.946	23.965	23.99	24	23.987	23.932	23.992	23.973	23.977	23.963	23.992

Tabela C – Análises de magnetita de rochas foscoríticas de Catalão I. As análises foram recalculadas com base em 32 O. (Cont. X)

Amostra	304a1-8	304a2-1	304a2-2	304a2-3	304a2-4	304a2-5	304a2-6	304a2-7	304a2-10	304a3-11	304a3-8	304a3-9	304b3-1	304b3-2	304b3-3	304b3-4	304b3-5	304b3-6	304b3-7	339-2-2
Unidade	P2min	DC	DC	DC	DC	P3bar	P2bar													
Oxidos (%)																				
Nb ₂ O ₅	0	0.1	0	0.03	0.01	0	0	0	0.01	1.15	0.08	0.05	0	0	0.1	0.02	0.16	0	0.35	
SiO ₂	0.01	0.03	0.05	0	0	0.02	0.01	0	0.01	0.04	0.13	0	0.02	0.02	0	0.05	0	0.02	0.01	0.05
TiO ₂	0.31	1.64	5.34	5.24	0.43	0.51	1.26	1.07	0.52	0.37	5.28	1.67	6.58	2.03	0.6	0.63	0.57	0.73	0.66	1.47
Al ₂ O ₃	0.05	0.03	0.03	0	0.01	0.01	0	0	0.01	0	0	0	0.02	0	0	0.04	0.05	0.02	0	
Cr ₂ O ₃	0.03	0	0	0.03	0	0	0.02	0.04	0.03	0.03	0.01	0	0.05	0	0	0	0	0	0.04	0
Fe ₂ O ₃	68.82	66.41	59.52	59.73	68.69	68.49	67.1	67.36	68.27	68.67	57.27	66.08	56.9	65.54	68.12	67.87	68.35	67.76	68.18	66
FeO	29.69	30.27	32.79	32.41	29.72	29.94	30.44	30.5	30.41	29.92	32.95	30.93	34.17	31.21	30.53	30.71	29.99	30.09	30.2	31.04
MnO	0.17	0.34	0.6	0.66	0.2	0.21	0.2	0.26	0.18	0.17	0.86	0.28	0.79	0.35	0.2	0.16	0.19	0.29	0.19	0.23
MgO	0.77	1.07	1.64	1.79	0.92	0.82	0.95	0.75	0.54	0.74	2.03	0.9	1.41	0.77	0.55	0.47	0.82	0.86	0.65	0.76
CaO	0.15	0.09	0	0.03	0	0	0	0.01	0.02	0.04	0.08	0.03	0.06	0.03	0	0.02	0.01	0.03	0.02	0.03
Total	100	99.98	99.97	99.92	99.98	100	99.98	99.99	99.99	99.99	99.76	99.97	100.03	99.97	100	100.01	99.99	99.99	99.97	99.93
Cations (p.f.u.)																				
Nb	0	0.014	0	0.004	0.001	0	0	0	0.001	0.161	0.011	0.007	0	0	0.013	0.003	0.022	0	0.049	
Si	0.003	0.008	0.014	0	0	0.005	0.004	0	0.003	0.012	0.04	0	0.005	0.007	0	0.014	0.001	0.006	0.004	0.016
Ti	0.071	0.375	1.219	1.202	0.1	0.117	0.29	0.247	0.122	0.085	1.228	0.387	1.497	0.47	0.138	0.145	0.13	0.169	0.154	0.344
Al	0.017	0.012	0.009	0.001	0.004	0.003	0	0	0.004	0	0	0	0.007	0	0	0.014	0.017	0.005	0	
Cr	0.007	0.001	0	0.007	0	0	0.005	0.01	0.006	0.008	0.003	0	0.011	0	0	0	0	0.009	0	
Fe ³⁺	15.845	15.227	13.546	13.587	15.808	15.77	15.423	15.51	15.753	15.817	13.019	15.196	12.967	15.066	15.724	15.666	15.735	15.591	15.706	15.182
Fe ²⁺	7.597	7.714	8.293	8.193	7.602	7.662	7.776	7.806	7.798	7.659	8.323	7.904	8.654	7.974	7.833	7.879	7.673	7.696	7.732	7.936
Mn	0.044	0.088	0.155	0.171	0.053	0.053	0.051	0.067	0.047	0.044	0.225	0.073	0.202	0.09	0.052	0.04	0.049	0.074	0.049	0.061
Mg	0.35	0.484	0.74	0.812	0.419	0.374	0.436	0.344	0.248	0.339	0.934	0.415	0.637	0.351	0.252	0.213	0.373	0.39	0.299	0.354
Ca	0.049	0.029	0	0.011	0	0	0	0.002	0.005	0.014	0.026	0.01	0.018	0.011	0.001	0.007	0.004	0.011	0.007	0.008
Sum	23.983	23.951	23.977	23.988	23.986	23.984	23.984	23.986	23.987	23.979	23.959	23.996	23.997	23.974	24	23.977	23.981	23.976	23.964	23.95

Tabela C – Análises de magnetita de rochas foscoríticas de Catalão I. As análises foram recalculadas com base em 32 O. (Cont. XI)

Amostra	339-2-3	339-2-4	339-2-5	339-2-6	339-2-7	339-3-1	339-3-2	F4-1-1	F4-1-2	F4-1-3	F4-1-4	F4-1-5
Unidade	P2bar	P1	P1	P1	P1	P1						
Oxidos (%)												
Nb ₂ O ₅	0.02	0.09	0	0.23	0	0	0	0.043	0	0.057	1.161	0
SiO ₂	0.04	0	0.01	0.03	0	0.05	0.02	0	0.023	0	0.06	0.044
TiO ₂	1.1	0.89	0.76	3.61	0.92	0.24	1.2	1.066	1.07	1.094	1.434	1.483
Al ₂ O ₃	0.01	0.01	0	0	0.03	0.03	0.01	0.071	0.044	0	0	0.029
Cr ₂ O ₃	0	0	0	0	0	0	0	0	0.062	0	0	0.002
Fe ₂ O ₃	67.16	67.46	67.84	61.84	67.61	68.53	66.93	67.221	67.334	67.054	64.362	66.346
FeO	30.68	30.71	30.75	32.92	30.89	30.98	31.08	30.434	30.663	31.38	31.897	31.524
MnO	0.23	0.12	0.1	0.51	0.14	0.07	0.25	0.172	0.096	0.122	0.099	0.186
MgO	0.74	0.6	0.35	0.71	0.32	0.02	0.46	0.826	0.715	0.129	0.807	0.361
CaO	0	0.09	0.16	0.02	0.06	0.07	0.04	0.045	0.001	0.146	0.001	0.031
Total	99.98	99.97	99.97	99.87	99.97	99.99	99.99	99.878	100.008	99.982	99.821	100.006
Cations (p.f.u.)												
Nb	0.002	0.012	0	0.033	0	0	0	0.006	0	0.008	0.168	0
Si	0.012	0	0.002	0.009	0.001	0.016	0.007	0	0.007	0	0.019	0.013
Ti	0.257	0.208	0.177	0.849	0.214	0.057	0.278	0.258	0.243	0.253	0.344	0.339
Al	0.002	0.004	0	0.001	0.012	0.011	0.005	0.027	0.016	0	0	0.01
Cr	0	0	0	0	0	0	0	0	0.015	0	0	0
Fe ³⁺	15.463	15.554	15.664	14.209	15.604	15.868	15.44	15.457	15.498	15.503	14.83	15.308
Fe ²⁺	7.849	7.87	7.891	8.405	7.922	7.972	7.97	7.777	7.844	8.063	8.168	8.083
Mn	0.06	0.032	0.027	0.135	0.037	0.018	0.065	0.047	0.025	0.032	0.027	0.048
Mg	0.343	0.278	0.163	0.329	0.145	0.011	0.209	0.396	0.322	0.059	0.384	0.164
Ca	0	0.029	0.052	0.007	0.019	0.022	0.012	0.015	0	0.048	0	0.01
Sum	23.989	23.988	23.977	23.977	23.954	23.975	23.985	23.982	23.97	23.966	23.94	23.976

Tabela D – Análises de clinohumita de foscorito (P1) de Catalão I

Amostra	n319-1-1	n319-2-2	n319-1-3	n319-2-1	n319-2-2	n319-2-3	n319-2-4	n319-2-5	n319-1-4	n319-1-5	n319-1-6
Unidade	P1										
SiO ₂	37.893	37.459	41.969	38.746	38.736	39.15	38.62	39.41	38.667	38.757	39.966
TiO ₂	1.92	1.482	0.198	1.148	1.092	1.301	1.197	1.25	1.437	2.094	1.297
Cr ₂ O ₃	0.006	0.012	0	0	0.024	0	0.04	0.012	0.003	0	0.006
MgO	51.971	52.839	53.165	55.756	55.341	55.981	56.386	56.205	54.575	54.002	54.608
FeO	4.568	4.457	5.198	3.309	3.236	3.39	3.279	2.886	4.884	4.53	4.729
MnO	0.287	0.304	0.369	0.226	0.33	0.271	0.265	0.247	0.316	0.387	0.494
CaO	0.021	0.02	0.017	0.011	0.007	0	0	0.08	0.033	0.011	0.037
NiO	0	0.02	0.015	0.01	0.059	0.041	0	0	0	0.013	0
Total	96.666	96.593	100.931	99.206	98.825	100.134	99.787	100.09	99.915	99.794	101.137

Tabela E – Análises de ilmenita de rochas foscoríticas de Catalão I. Fórmula recalculada com base em 6 O.

Amostra	116-1	116-2	116-3	116-4	116-5	116-6	116-7	116-1	116-2	116-3	116-4	116-5	149-01	149-02	149-03	149-04	149-05	149-06	149-07	149-08	149-09	149-10
Coord	2	10	19	27	35	43	51	3	28	51	70	92	0	10	20	30	40	50	60	70	80	90
Posição								core	middle	middle	middle	rim	rim	middle								
Unidade	P2	DC	DC	DC	DC	DC	DC	DC	DC	DC	DC	DC	DC	DC	DC	DC						
Oxides (%)																						
SiO₂	0.00	0.01	0.04	0.00	0.00	0.00	0.01	0.00	0.00	0.01	0.02	0.00	0.01	0.00	0.00	0.00	0.00	0.02	0.13	0.03	0.02	0.00
TiO₂	51.98	52.33	51.80	51.32	53.01	49.82	51.71	50.55	53.71	51.93	52.31	53.30	53.45	52.93	53.80	53.22	52.10	50.68	53.29	54.20	52.98	52.61
Al₂O₃	0.02	0.00	0.00	0.01	0.05	0.01	0.01	0.01	0.00	0.00	0.00	0.01	0.00	0.02	0.04	0.02	0.04	0.02	0.06	0.00	0.02	0.01
Cr₂O₃	0.00	0.00	0.00	0.00	0.01	0.00	0.00	0.00	0.01	0.04	0.00	0.00	0.03	0.02	0.02	0.01	0.01	0.01	0.00	0.00	0.00	0.00
FeO	41.53	40.15	39.12	39.14	39.49	40.42	41.89	40.60	38.14	37.68	37.90	41.49	37.81	38.32	39.86	39.77	41.17	38.76	37.48	36.98	39.78	38.50
Fe₂O₃	0.00	0.25	0.95	1.71	0.73	2.51	1.32	2.51	0.42	0.79	1.17	0.00	0.00	0.00	0.00	0.00	0.00	1.48	0.00	0.00	0.00	0.00
MnO	2.54	2.41	2.42	2.38	2.61	2.41	2.77	2.28	2.56	2.47	2.39	2.79	1.87	2.22	2.09	3.74	3.20	1.84	2.51	1.99	1.91	1.90
MgO	1.55	3.02	3.65	3.24	3.43	2.44	1.20	2.40	4.48	4.64	4.57	1.87	4.78	4.40	3.35	1.37	1.93	3.89	3.78	4.73	3.51	4.36
CaO	0.07	0.00	0.00	0.02	0.02	0.03	0.07	0.01	0.01	0.01	0.00	0.10	0.00	0.00	0.01	0.00	0.01	0.06	0.01	0.00	0.00	0.00
Nb₂O₅	0.75	0.84	1.33	1.10	0.57	2.27	0.39	1.60	0.40	1.62	1.30	0.39	0.87	1.03	0.68	0.10	1.06	1.82	0.58	0.56	1.18	1.32
Total	98.45	99.01	99.31	98.91	99.92	99.91	99.38	99.95	99.73	99.18	99.65	99.95	98.81	98.94	99.83	98.24	99.52	98.52	97.88	98.50	99.40	98.71
Cations (p.f.u.)																						
Si	0.000	0.000	0.002	0.000	0.000	0.000	0.001	0.000	0.000	0.000	0.001	0.000	0.001	0.000	0.000	0.000	0.001	0.006	0.001	0.001	0.000	
Ti	1.982	1.967	1.936	1.931	1.966	1.876	1.961	1.899	1.979	1.930	1.935	1.995	1.981	1.969	1.992	2.023	1.965	1.909	1.999	2.007	1.972	1.963
Al	0.001	0.000	0.000	0.000	0.003	0.000	0.000	0.001	0.000	0.000	0.000	0.000	0.000	0.001	0.002	0.001	0.002	0.001	0.003	0.000	0.001	0.001
Cr	0.000	0.000	0.000	0.000	0.000	0.000	0.000	0.000	0.000	0.002	0.000	0.000	0.001	0.001	0.001	0.000	0.000	0.000	0.000	0.000	0.000	
Fe²⁺	1.761	1.677	1.625	1.637	1.628	1.692	1.766	1.695	1.562	1.557	1.558	1.726	1.558	1.584	1.641	1.681	1.726	1.623	1.563	1.522	1.647	1.597
Fe³⁺	0.000	0.010	0.035	0.064	0.027	0.095	0.050	0.094	0.016	0.029	0.043	0.000	0.000	0.000	0.000	0.000	0.056	0.000	0.000	0.000	0.000	0.000
Mn	0.109	0.102	0.102	0.101	0.109	0.102	0.118	0.096	0.106	0.103	0.099	0.118	0.078	0.093	0.087	0.160	0.136	0.078	0.106	0.083	0.080	0.080
Mg	0.117	0.225	0.270	0.241	0.252	0.182	0.091	0.179	0.327	0.342	0.335	0.139	0.351	0.324	0.246	0.103	0.144	0.291	0.281	0.347	0.259	0.323
Ca	0.004	0.000	0.000	0.001	0.001	0.001	0.004	0.000	0.001	0.000	0.000	0.005	0.000	0.000	0.000	0.000	0.000	0.003	0.000	0.000	0.000	
Nb	0.017	0.019	0.030	0.025	0.013	0.051	0.009	0.036	0.009	0.036	0.029	0.009	0.019	0.023	0.015	0.002	0.024	0.041	0.013	0.012	0.026	0.030
Sum	3.990	4.000	4.000	4.000	4.000	4.000	4.000	4.000	4.000	4.000	4.000	3.990	3.990	4.000	3.980	3.970	4.000	3.970	3.990	3.990	3.990	

Tabela E – Análises de ilmenita de rochas foscoríticas de Catalão I (Cont. I). Fórmula recalculada com base em 6 O.

Amostra	149-11	149-12	178-1	178-2	178-3	183-1	183-2	183-3	225-1	225-4	225-5	230A-2	230A-3	230A-4	244-1	244-2	244-3	319-1	319-2	319-3	319-4	319-5
Coord	100	110	0	2.5	5				0	9	12	11	17	23								
Posição	middle	middle	rim	core	rim																	
Unidade	DC	DC	P2	P2	P2	DC	DC	GLIM	GLIM	GLIM	P2	P2	P2	P1	P1	P1	P1	P1	P1	P1	P1	P1
Oxides (%)																						
SiO ₂	0.02	0.25	0.00	0.03	0.02	0.06	0.00	0.01	0.00	0.16	0.00	0.00	0.03	0.00	0.04	0.00	0.01	0.00	0.00	0.00	0.05	0.01
TiO ₂	54.84	49.21	51.10	52.54	52.83	49.59	51.03	50.57	51.01	49.30	50.67	49.99	50.53	50.53	56.96	57.02	57.03	55.21	56.99	57.38	57.15	57.43
Al ₂ O ₃	0.00	0.78	0.00	0.05	0.01	0.02	0.00	0.02	0.02	0.06	0.00	0.01	0.02	0.03	0.00	0.02	0.00	0.00	0.01	0.00	0.03	0.00
Cr ₂ O ₃	0.00	0.00	0.00	0.00	0.00	0.00	0.01	0.02	0.00	0.00	0.05	0.03	0.00	0.02	0.02	0.01	0.00	0.03	0.00	0.00	0.00	0.08
FeO	36.46	34.75	35.75	36.61	36.21	39.74	40.00	40.58	41.83	40.68	40.53	40.29	40.25	40.50	25.59	24.56	24.67	21.73	21.15	21.00	20.86	20.70
Fe ₂ O ₃	0.00	0.00	2.98	0.44	0.69	0.52	0.00	0.15	1.51	1.83	2.89	1.63	1.57	1.11	0.43	1.10	0.00	0.00	0.00	0.00	0.00	0.00
MnO	1.89	1.47	4.09	4.20	4.60	4.90	4.38	4.67	3.78	3.69	3.59	4.73	4.82	4.81	4.45	4.31	4.32	2.46	2.30	2.45	2.51	2.47
MgO	5.00	5.05	3.93	4.04	4.01	1.36	1.89	1.26	0.62	0.76	0.93	0.99	1.28	1.01	12.02	12.63	12.51	15.52	15.49	15.45	15.90	16.38
CaO	0.01	0.13	0.00	0.03	0.01	0.02	0.00	0.01	0.05	0.01	0.00	0.06	0.03	0.00	0.00	0.05	0.00	0.13	0.03	0.02	0.02	0.10
Nb ₂ O ₅	0.32	1.29	0.87	0.76	0.47	2.31	1.99	1.92	0.89	1.17	0.23	1.83	1.83	1.61	0.24	0.20	0.27	2.29	0.94	1.00	1.48	1.25
Total	98.54	92.91	98.71	98.70	98.84	98.52	99.31	99.18	99.71	97.66	98.90	99.56	100.36	99.62	99.76	99.90	98.82	97.37	96.91	97.31	98.00	98.41
Cations (p.f.u.)																						
Si	0.001	0.013	0.000	0.001	0.001	0.003	0.000	0.000	0.008	0.000	0.000	0.002	0.000	0.002	0.000	0.001	0.000	0.000	0.000	0.000	0.002	0.000
Ti	2.021	1.926	1.915	1.963	1.970	1.906	1.935	1.930	1.940	1.914	1.936	1.905	1.906	1.923	1.983	1.974	1.994	1.928	1.985	1.990	1.967	1.966
Al	0.000	0.048	0.000	0.003	0.000	0.001	0.000	0.001	0.001	0.003	0.000	0.001	0.001	0.002	0.000	0.001	0.000	0.000	0.000	0.000	0.002	0.000
Cr	0.000	0.000	0.000	0.000	0.000	0.000	0.001	0.001	0.000	0.000	0.002	0.001	0.000	0.001	0.001	0.000	0.000	0.001	0.000	0.000	0.000	0.003
Fe ²⁺	1.494	1.512	1.489	1.521	1.502	1.699	1.686	1.722	1.769	1.756	1.721	1.707	1.688	1.713	0.990	0.945	0.959	0.844	0.819	0.809	0.798	0.788
Fe ³⁺	0.000	0.000	0.112	0.017	0.026	0.020	0.000	0.006	0.058	0.071	0.111	0.062	0.059	0.042	0.015	0.038	0.000	0.000	0.000	0.000	0.000	0.000
Mn	0.078	0.065	0.173	0.177	0.193	0.212	0.187	0.201	0.162	0.161	0.155	0.203	0.205	0.206	0.174	0.168	0.170	0.097	0.090	0.096	0.097	0.095
Mg	0.365	0.392	0.292	0.299	0.297	0.104	0.142	0.095	0.047	0.058	0.070	0.075	0.096	0.076	0.830	0.866	0.867	1.074	1.070	1.062	1.085	1.111
Ca	0.000	0.007	0.000	0.001	0.000	0.001	0.000	0.000	0.003	0.001	0.000	0.003	0.001	0.000	0.000	0.003	0.000	0.007	0.002	0.001	0.001	0.005
Nb	0.007	0.030	0.020	0.017	0.011	0.053	0.045	0.044	0.020	0.027	0.005	0.042	0.041	0.037	0.005	0.004	0.006	0.048	0.020	0.021	0.031	0.026
Sum	3.970	3.990	4.000	4.000	4.000	4.000	4.000	4.000	4.000	4.000	4.000	4.000	4.000	4.000	4.000	4.000	4.000	3.990	3.980	3.980	3.990	

Tabela F – Análises de pirocloro, Ca-betafita e Fe-columbita de rochas foscoríticas (nelsonitos P2 e P3) de Catalão I. Recalculado assumindo sítio B = 2 cátions.

Amostra	056-1	056-2	056-3	056-4	056-4B	056-5	093-1	093-2	093-3	093-4	093-5	099A-1	099A-1C	099A-2	099A-3B	099A-6	099A-7	099A-8	099A-9	099A-10	
Coord	0	6	9	12	12	15	0	9	16	22	27	0	1	4	9	1	2	3	1	2	
Unidade	DC	DC	DC	DC	DC	P3	P3	P3	P3	P3	P3	P3	P3								
Óxidos (%)																					
Nb ₂ O ₅	50.1	59.93	53.25	59.6	59.2	52.57	61.56	65.55	59.99	61	60.77	63.1	45.65	62.73	52.91	64.03	58.75	62.38	51.66	55.4	
Ta ₂ O ₅	0.77	0.07	0.89	0.59	0.44	0.22	0.71	0.74	0.81	0.79	0.8	0.08	0	0.34	0.18	0.62	0.46	0.4	0.48	0.32	
SiO ₂	2.93	0.12	2.14	0.07	0.08	0.08	1.15	0.11	1.2	0.55	0.87	0.16	0.1	0.89	2.03	0.26	0.49	0.27	1.34	1.67	
TiO ₂	5.27	6.15	6.44	6.47	6.21	5.3	3.62	3.39	3.16	3.14	3.57	4.7	3.16	3.64	4.77	3.86	5.15	4.13	3.67	3.75	
ZrO ₂	2.44	2.13	2.67	2.72	2.53	0.77	0.14	0.18	0.06	0.04	0.2	1.87	1.27	0.25	1.61	0.24	1.35	0.46	1	0.44	
UO ₂	1.01	1.02	1.73	1.17	1.02	0	1.06	1.02	0.77	1.03	1	0.23	0.09	1.12	0.62	0.71	1.51	0.76	1	0.94	
ThO ₂	2.15	2.04	2.23	2.13	2.41	1.61	0.35	0.53	0.41	0.6	0.47	1.83	1	0.67	1.32	0.53	1.05	1.21	1.28	1.16	
La ₂ O ₃	0.32	0.62	0.48	0.58	0.79	0.44	1.26	1.3	1.3	1.12	1.47	0.43	0.38	0.85	0.45	0.88	0.68	0.36	0.56	0.49	
Ce ₂ O ₃	2.91	2.37	2.83	2.76	2.49	1.73	3.48	3.39	3.37	3.48	2.78	2.04	1.33	2.25	2.5	1.74	2.32	2.23	2.33	2.41	
Y ₂ O ₃	0.4	0.55	0.41	0.64	0.52	0.35	0.32	0.4	0.26	0.3	0.35	0.55	0.36	0.29	0	0.46	0.28	0.54	0	0.08	
FeO	4.47	0.4	0.8	0.5	0.4	0.88	0.47	0.16	0.69	0.48	0.74	1.44	24.2	0.9	1.72	0.34	0.79	0.37	1.75	1.2	
MnO	0	0	0.037	0	0.034	0.055	0.029	0.021	0.108	0.063	0.019	0.005	0	0.018	0.086	0.038	0	0.062	0.102	0.072	
CaO	2.796	16.137	3.356	16.336	16.006	18.194	5.923	9.877	5.105	7.451	7.331	14.601	9.375	7.966	3.64	12.149	8.825	11.044	3.735	6.067	
BaO	14.611	0	13.136	0	0	0	8.732	1.604	11.034	7.799	7.271	0.798	0.381	7.566	14.94	2.91	7.286	2.476	12.629	9.993	
SrO	2.233	1.17	1.706	1.233	1.321	1.506	2.947	3.084	4.645	3.598	3.704	1.809	1.638	4.627	6.878	2.765	2.241	1.956	6.631	4.607	
Na ₂ O	0.77	4.705	0.221	5.163	5.402	4.878	0.989	3.383	0.341	1.139	0.646	5.98	4.384	1.853	0.558	4.789	1.233	4.192	1.063	1.95	
Cations (p.f.u.)																					
Nb	1.464	1.647	1.477	1.615	1.629	1.682	1.742	1.819	1.753	1.796	1.753	1.721	1.739	1.761	1.576	1.788	1.675	1.768	1.664	1.679	
Ta	0.014	0.001	0.015	0.01	0.007	0.004	0.012	0.012	0.014	0.014	0.014	0.001	0	0.006	0.003	0.01	0.008	0.007	0.009	0.006	
Si	0.189	0.007	0.131	0.004	0.005	0.006	0.072	0.007	0.077	0.035	0.055	0.01	0.008	0.055	0.133	0.016	0.031	0.017	0.095	0.112	
Ti	0.256	0.281	0.297	0.292	0.284	0.282	0.17	0.156	0.153	0.154	0.172	0.213	0.2	0.17	0.236	0.179	0.244	0.195	0.197	0.189	
Zr	0.077	0.063	0.08	0.08	0.075	0.026	0.004	0.006	0.002	0.001	0.006	0.055	0.052	0.008	0.052	0.007	0.041	0.014	0.035	0.014	
U	0.0146	0.0138	0.0236	0.0156	0.0138	0	0.0148	0.014	0.0111	0.015	0.0143	0.003	0.0017	0.0154	0.0091	0.0097	0.0212	0.0107	0.0159	0.0141	
Th	0.0316	0.0282	0.0312	0.029	0.0334	0.0259	0.0049	0.0074	0.0061	0.0088	0.0068	0.0251	0.0192	0.0095	0.0198	0.0074	0.0151	0.0172	0.0208	0.0177	
La	0.0077	0.0138	0.0109	0.0127	0.0177	0.0114	0.0292	0.0294	0.031	0.0269	0.0345	0.0095	0.0117	0.0194	0.0108	0.0201	0.0157	0.0084	0.0146	0.0121	
Ce	0.0689	0.0527	0.0636	0.0606	0.0555	0.0449	0.0797	0.0763	0.0798	0.083	0.065	0.0451	0.0411	0.0511	0.0602	0.0392	0.0536	0.0511	0.0607	0.0591	
Y	0.0137	0.0177	0.0135	0.0204	0.0167	0.013	0.0105	0.0129	0.009	0.0103	0.0119	0.0177	0.016	0.0096	0	0.0151	0.0092	0.0179	0	0.0028	
Fe ²⁺	0.2414	0.0204	0.0411	0.0248	0.0206	0.0518	0.0245	0.0082	0.0371	0.0262	0.0393	0.0725	1.7061	0.0466	0.0948	0.0177	0.0418	0.0196	0.104	0.0671	
Mn	0	0	0.0019	0	0.0018	0.0033	0.0015	0.0011	0.0059	0.0035	0.001	0.0003	0	0.0009	0.0048	0.002	0	0.0033	0.0062	0.0041	
Ca	0.1937	1.0513	0.2206	1.049	1.0436	1.3797	0.3971	0.6495	0.3536	0.5199	0.5013	0.9438	0.8467	0.5301	0.2569	0.8038	0.5965	0.7418	0.2851	0.4358	
Ba	0.3702	0	0.3159	0	0	0	0.2142	0.0386	0.2796	0.1991	0.1819	0.0189	0.0126	0.1842	0.3857	0.0704	0.1801	0.0608	0.3527	0.2626	
Sr	0.0837	0.0413	0.0607	0.0429	0.0466	0.0618	0.107	0.1098	0.1742	0.1359	0.1371	0.0633	0.0801	0.1667	0.2627	0.099	0.082	0.0711	0.274	0.1791	
Na	0.0965	0.5547	0.0263	0.6	0.6374	0.6694	0.12	0.4026	0.0427	0.1438	0.0799	0.6995	0.7165	0.2232	0.0713	0.5734	0.1508	0.5095	0.1468	0.2535	
A	1.122	1.7939	0.8093	1.855	1.8871	2.2612	1.0034	1.3498	1.0301	1.1724	1.073	1.8987	3.4517	1.2567	1.1761	1.6578	1.166	1.5114	1.2808	1.308	

Tabela F – Análises de pirocloro, Ca-betafita e Fe-columbita de rochas foscoríticas (nelsonitos P2 e P3) de Catalão I. Recalculado assumindo sítio B = 2 cátions. (Cont. I)

Amostra	099A-11	116-1B	116-2	116-3	116-1	149-1	149-2	156-2	156-3	156-4	156-5	156-6	157B-1C	157B-2	157B-3	157B-4	157B-5	157B-6	157B-7	157B-8
Coord	3	1	10	18				1	5	9	13		0	5	9	13	19	1	3	7
Unidade	P3	P2	P2	P2	DC	DC	DC	P2	P2	P2	P2	P2	P3	P3	P3	P3	P3	P3	P3	P3
Óxidos (%)																				
Nb ₂ O ₅	62.54	62.05	64.86	67.44	66.99	68.71	84.68	62.97	65.69	65.07	64.24	56.77	66.12	64.87	66.74	65.85	65.62	64.26	64.48	64.24
Ta ₂ O ₅	0.09	0.28	0.53	0.36	0.05	0.28	0.34	0.36	0.03	0.23	0.26	2.28	0	0	0.12	0	0.1	0.02	0	0
SiO ₂	0.04	2.01	0.26	0.16	0	0.05	0.03	0.39	0	0	0.11	0.3	0.02	0	0	0.04	0	0	0.02	0.05
TiO ₂	3.91	3.32	3.58	3.33	4.12	2.04	1.37	3.71	4.84	4.89	5.4	6.94	3.4	3.97	3.43	3.76	3.71	3.91	4.17	4.46
ZrO ₂	1.98	0.23	0.26	0.23	0.28	0.53	0.48	0.46	0.4	0.36	0.24	0	0.27	0.35	0.17	0.32	0.31	1.78	1.34	1.13
UO ₂	0.32	0.37	0.46	0.39	0.02	0.02	0	0.89	0.28	0.31	0.16	3.78	0.33	0.18	0.14	0.07	0.07	0.14	0.12	0.01
ThO ₂	1.27	0.95	0.9	0.6	0.53	0.22	0	2.14	2.45	2.48	2.29	3.35	0.69	1.57	0.96	1.11	1.41	1.12	1.35	1.3
La ₂ O ₃	0.38	1.22	1.5	1.04	0.79	1.63	0.05	0.5	0.55	0.42	0.41	0.51	1.1	0.9	1.08	1.12	0.95	0.95	0.81	0.59
Ce ₂ O ₃	1.85	3.5	3.29	2.78	2.21	3.26	0.07	1.94	1.97	1.92	1.88	2.63	3.01	2.68	2.83	2.64	2.7	2.47	2.13	1.96
Y ₂ O ₃	0.74	0.42	0.43	0.37	0.47	0.57	0.94	0.6	0.63	0.6	0.58	0.52	0.46	0.57	0.47	0.49	0.47	0.45	0.42	0.55
FeO	0.72	0.75	0.27	0.23	0.13	0.18	8.9	3.13	0.21	0.19	0.17	0.23	0.6	0.13	0.05	0.2	0.83	0.86	0.67	0.38
MnO	0.058	0.021	0	0	0	0.002	1.528	0.069	0	0	0.055	0.035	0.044	0.025	0.031	0.052	0	0.011	0	0.043
CaO	14.2	8.476	9.745	10.727	14.001	9.868	0.01	7.673	14.67	14.991	14.924	11.404	10.89	11.772	11.387	11.878	11.719	13.112	13.827	15.447
BaO	0.217	2.623	1.481	1.15	0	0	0.046	1.596	0	0	0.56	2.43	0	0	0	0	0	0	0	0
SrO	1.835	3.136	2.892	3.357	2.793	2.501	0	1.125	1.168	1.218	1.083	0.96	2.163	2.167	2.379	2.345	2.304	2.292	2.197	1.467
Na ₂ O	5.834	4.348	3.989	4.825	6.754	7.311	0	2.007	5.847	5.814	5.485	1.843	6.194	6.307	7.07	5.936	6.33	5.943	6.128	4.647
Cations (p.f.u.)																				
Nb	1.753	1.714	1.802	1.827	1.806	1.884		1.781	1.771	1.765	1.739	1.603	1.833	1.806	1.836	1.816	1.818	1.768	1.769	1.76
Ta	0.002	0.005	0.009	0.006	0.001	0.005		0.006	0	0.004	0.004	0.039	0	0	0.002	0	0.002	0	0	0
Si	0.003	0.123	0.016	0.01	0	0.003		0.024	0	0	0.006	0.018	0.001	0	0	0.003	0	0	0.001	0.003
Ti	0.183	0.152	0.166	0.15	0.185	0.093		0.174	0.217	0.221	0.243	0.326	0.157	0.184	0.157	0.172	0.171	0.179	0.19	0.203
Zr	0.06	0.007	0.008	0.007	0.008	0.016		0.014	0.012	0.01	0.007	0.015	0.008	0.01	0.005	0.009	0.009	0.053	0.04	0.033
U	0.0044	0.005	0.0063	0.0051	0.0002	0.0002		0.0123	0.0037	0.0042	0.0022	0.0526	0.0045	0.0025	0.0019	0.0009	0.001	0.0019	0.0016	0.0002
Th	0.0179	0.0132	0.0126	0.0082	0.0072	0.003		0.0305	0.0332	0.0339	0.0312	0.0476	0.0096	0.022	0.0133	0.0155	0.0196	0.0156	0.0187	0.0179
La	0.0086	0.0275	0.0339	0.023	0.0173	0.0365		0.0115	0.012	0.0093	0.0091	0.0117	0.0248	0.0205	0.0242	0.0252	0.0215	0.0213	0.0182	0.0132
Ce	0.0421	0.0784	0.074	0.0611	0.0482	0.0723		0.0444	0.043	0.0423	0.0413	0.0601	0.0675	0.0603	0.063	0.059	0.0607	0.0551	0.0474	0.0435
Y	0.0244	0.0138	0.014	0.0117	0.0148	0.0184		0.02	0.0199	0.0192	0.0186	0.0172	0.015	0.0187	0.0152	0.016	0.0153	0.0144	0.0136	0.0177
Fe ²⁺	0.0372	0.0384	0.0138	0.0116	0.0062	0.0092		0.1639	0.0106	0.0095	0.0084	0.0117	0.0308	0.0066	0.0023	0.0099	0.0423	0.0435	0.034	0.0194
Mn	0.003	0.0011	0	0	0	0.0001		0.0037	0	0	0.0028	0.0019	0.0023	0.0013	0.0016	0.0027	0	0.0006	0	0.0022
Ca	0.9436	0.5548	0.6417	0.6889	0.8948	0.6411		0.5144	0.9372	0.9638	0.9576	0.763	0.7157	0.7766	0.7424	0.7762	0.7696	0.855	0.899	1.0033
Ba	0.0053	0.0628	0.0357	0.027	0	0		0.0391	0	0	0.0131	0.0595	0	0	0	0	0	0	0	0
Sr	0.066	0.1111	0.1031	0.1167	0.0966	0.088		0.0408	0.0404	0.0424	0.0376	0.0348	0.0769	0.0774	0.084	0.083	0.0819	0.0809	0.0773	0.0516
Na	0.7015	0.5151	0.4753	0.5608	0.7811	0.8595		0.2435	0.6759	0.6764	0.6369	0.2231	0.7366	0.7529	0.8342	0.702	0.7523	0.7013	0.721	0.5462
A	1.854	1.4212	1.4104	1.5141	1.8664	1.7283		1.1241	1.7759	1.801	1.7588	1.2832	1.6837	1.7388	1.7821	1.6904	1.7642	1.7896	1.8308	1.7152

Tabela F – Análises de pirocloro, Ca-betafita e Fe-columbita de rochas foscoríticas (nelsonitos P2 e P3) de Catalão I. Recalculado assumindo sítio B = 2 cátions. (Cont. II)

Amostra	157B-9	157B-10	157B-10B	157B-11	157B-12	170-1	170-2	170-3	170-4	170-5	170-6	170-7	170-8	178-1	178-2C	183-1	183-2	183-3	183-4	183-5
Coord	11	1	1	5	9										0	2	4	6	8	
Unidade	P3	P3	P3	P3	P3	DC	P2	P2	P3	P3	P3	P3	P3							
Óxidos (%)																				
Nb ₂ O ₅	62.51	63	64.34	61.45	63.14	53.4	52.85	69.5	72.56	70.42	63.96	70.29	74.84	61.68	62.66	52.36	55.02	55.58	58.57	62.17
Ta ₂ O ₅	0	0	0	0	0.07	0.88	0.92	0.77	1.61	1.79	0.81	1.85	0.94	0.33	0.15	0.9	0.86	0.7	0.52	0.57
SiO ₂	0.08	0.01	0.03	0.07	0.04	0.16	0	0	0	0.04	1.1	0	0	0.61	0	0.64	0.42	0.57	0.29	0.02
TiO ₂	4.9	4.6	4.54	4.59	4.71	10.59	17.35	1.26	0.78	1.4	1.26	0.63	5.1	3.15	3.52	3.08	3.71	4.16	3.99	4.87
ZrO ₂	1.47	1.45	1.52	1.64	1.65	0.12	0.09	0.19	0.02	0.19	0.75	0	1.41	0.13	0.17	4.39	3.8	3.95	4.49	0.32
UO ₂	0	0.07	0	0.15	0.05	0	0	0	0.02	0	0.12	0	0	0.59	0.36	3.1	2.56	2.35	1.75	1.17
ThO ₂	1.38	1.16	1.13	1.29	1.13	0.03	0.06	0.02	0.19	0.15	0.74	0.03	0	1.09	1.08	2.74	2.69	2.69	3.07	4.66
La ₂ O ₃	0.62	0.84	0.57	0.52	0.68	0.57	0.35	0.6	0.37	0.54	0.92	0.11	0	1.14	1.21	0.51	0.46	0.62	0.58	1.13
Ce ₂ O ₃	2	1.94	1.87	2.22	2	0.55	0.24	0.88	0.73	1.03	3.54	0.42	0.11	3.42	4.2	2.79	2.67	2.92	2.97	4.09
Y ₂ O ₃	0.66	0.41	0.51	0.41	0.46	0.25	0.2	0.37	0.39	0.57	0.68	0.41	0.75	0.32	0.44	0.05	0.22	0.26	0.48	0.48
FeO	0.68	0.79	0.77	0.52	0.46	10.12	4.22	0.5	0.18	0.25	0.77	0.64	10.1	0.94	0.14	2.56	2.2	1.93	1.34	0.4
MnO	0	0	0	0.079	0	0.615	0.899	0.049	0.057	0	0.006	0.078	1.103	0.074	0.002	0.216	0.223	0.361	0.191	0.037
CaO	15.995	15.797	15.957	15.537	15.742	8.492	10.981	11.602	11.317	12.002	0.121	11.75	1.089	7.464	9.017	6.772	7.624	8.528	11.203	8.512
BaO	0	0	0	0	0	0	0	0.179	0	15.203	0.096	0	4.894	0.353	7.411	3.219	3.666	1.706	2.811	
SrO	1.642	1.445	1.762	1.647	1.586	3.019	3.008	3.816	4.614	2.824	0.747	4.259	0.577	3.951	2.776	5.207	3.279	3.48	2.029	2.03
Na ₂ O	5.846	5.832	5.366	4.612	6.089	5.297	7.747	6.875	7.826	6.487	1.287	6.844	0.749	4.09	5.591	1.124	2.136	2.519	2.261	1.162
Cations (p.f.u.)																				
Nb	1.726	1.744	1.749	1.731	1.733	1.483	1.284	1.924	1.939	1.9	1.833	1.94		1.798	1.822	1.632	1.649	1.624	1.65	1.752
Ta	0	0	0	0	0.001	0.015	0.013	0.013	0.026	0.029	0.014	0.031		0.006	0.003	0.017	0.016	0.012	0.009	0.01
Si	0.005	0.001	0.002	0.004	0.003	0.01	0	0	0	0.003	0.07	0		0.039	0	0.044	0.028	0.037	0.018	0.001
Ti	0.225	0.212	0.205	0.215	0.215	0.489	0.701	0.058	0.035	0.063	0.06	0.029		0.153	0.17	0.16	0.185	0.202	0.187	0.228
Zr	0.044	0.043	0.045	0.05	0.049	0.004	0.002	0.006	0.001	0.006	0.023	0		0.004	0.005	0.148	0.123	0.125	0.137	0.01
U	0	0.0009	0	0.002	0.0007	0	0	0	0.0003	0	0.0017	0		0.0085	0.0052	0.0476	0.0377	0.0338	0.0243	0.0162
Th	0.0192	0.0161	0.0155	0.0183	0.0156	0.0004	0.0007	0.0003	0.0025	0.0021	0.0106	0.0004		0.016	0.0157	0.043	0.0405	0.0395	0.0436	0.0661
La	0.0139	0.019	0.0125	0.0119	0.0152	0.013	0.0069	0.0136	0.0082	0.0119	0.0215	0.0025		0.0271	0.0288	0.013	0.0113	0.0147	0.0134	0.026
Ce	0.0448	0.0435	0.0411	0.0507	0.0445	0.0123	0.0047	0.0196	0.0157	0.0224	0.0822	0.0093		0.0808	0.0989	0.0704	0.0648	0.0692	0.0678	0.0934
Y	0.0216	0.0133	0.0164	0.0136	0.0149	0.0082	0.0058	0.0119	0.0123	0.018	0.0229	0.0134		0.0108	0.0151	0.0017	0.0078	0.0091	0.016	0.0158
Fe ²⁺	0.0347	0.0406	0.0385	0.0268	0.0233	0.5199	0.1894	0.0256	0.0087	0.0122	0.041	0.0325		0.0505	0.0074	0.1478	0.1221	0.1044	0.0699	0.0211
Mn	0	0	0	0.0042	0	0.032	0.0409	0.0025	0.0029	0	0.0003	0.004		0.004	0.0001	0.0126	0.0125	0.0198	0.0101	0.002
Ca	1.0467	1.0364	1.0279	1.0373	1.0239	0.5589	0.6321	0.7611	0.7166	0.7674	0.0082	0.7688		0.5158	0.6213	0.5002	0.5414	0.5907	0.7478	0.5684
Ba	0	0	0	0	0	0	0	0	0.0041	0	0.3777	0.0023		0.1237	0.0089	0.2002	0.0836	0.0929	0.0417	0.0687
Sr	0.0582	0.0513	0.0614	0.0595	0.0558	0.1076	0.0937	0.1355	0.1582	0.0977	0.0275	0.1508		0.1478	0.1035	0.2082	0.1261	0.1305	0.0733	0.0734
Na	0.6923	0.6924	0.6255	0.5572	0.7167	0.6308	0.8069	0.8161	0.8968	0.7506	0.1582	0.8104		0.5114	0.6971	0.1502	0.2745	0.3157	0.2731	0.1404
A	1.9314	1.9135	1.8388	1.7815	1.9106	1.8831	1.7811	1.7862	1.8263	1.6823	0.7518	1.7944		1.4964	1.602	1.3949	1.3223	1.4203	1.381	1.0915

Tabela F – Análises de pirocloro, Ca-betafita e Fe-columbita de rochas foscoríticas (nelsonitos P2 e P3) de Catalão I. Recalculado assumindo sítio B = 2 cátions. (Cont. III)

Amostra	183-6	183-7	183-8	183-9	192B-C	192B-2	192B-3	192B-4	192B-5	192B-6	192B-7	192B-8	207-1	207-2B	207-3	230A-1	230A-2	230A-3	230A-4B	230A-5B	230B-1
Coord	10	12	14	16	1	3	6						1	4	7	0	5	11	17	23	0
Unidade	P3	P3	P3	P3	P2	P3	P3	P3	P2	P2	P2	P2	P3								
Óxidos (%)																					
Nb ₂ O ₅	56.92	61.37	54.51	59.53	60.17	59.26	54.14	56.68	57.85	58.77	58.68	55.76	53.18	62.84	64.77	58.61	63.76	64.94	65.3	64.25	59.98
Ta ₂ O ₅	0.49	0.57	0.74	0.45	0.05	0	0.05	0.02	0.08	0.48	0	0.07	0.32	0.43	0.21	0	0.37	0	0.03	0	0.2
SiO ₂	0.51	0	0.5	0.24	0	0	0.23	0.51	0.03	0.16	0	0.16	3.15	0.55	0.03	0.74	0.03	0.02	0	0.03	0.69
TiO ₂	5.68	4.8	4.26	4.35	4.62	4.64	5.34	4.99	5.31	5.16	4.97	5.59	4.45	4.55	3.72	5.47	4.2	4.33	4.01	4.05	4.03
ZrO ₂	1.09	0.99	2.04	3.45	1.97	2.05	1.84	0.43	1.24	0.84	1.22	0.9	0.6	0.39	0.37	0.32	0.94	0.27	0.61	0.22	0.3
UO ₂	0.15	2.16	2.08	1.72	0	0	0	0.08	0.02	0.09	0.08	0.04	0.7	0.75	0.54	0	0.82	0.52	0.29	0.03	0.1
ThO ₂	12.18	3.41	4.09	3.22	3.47	3.39	3.48	2.73	2.31	1.97	2.26	2.13	2.22	2.21	1.93	3.48	1.72	2.06	1.81	2.45	2.77
La ₂ O ₃	0.42	0.57	0.62	0.56	0.61	0.39	0.61	0.82	0.81	0.64	0.46	0.75	0.56	0.86	0.98	0.8	0.96	1.34	0.65	1.1	1.19
Ce ₂ O ₃	2.6	2.72	3.23	2.78	2.87	2.9	3.21	2.79	2.78	3.1	3.08	2.85	2.86	3.04	2.93	3.52	2.68	3.88	2.22	3.52	3.57
Y ₂ O ₃	0.59	0.62	0.2	0.49	0.55	0.57	0.56	0.47	0.5	0.55	0.57	0.49	0.31	0.46	0.54	0.31	0.55	0.52	0.5	0.47	0.15
FeO	1.35	0.47	2	0.94	0.56	0.5	0.47	0.86	0.56	0.48	0.76	0.7	1.82	0.81	1.09	0.98	0.16	0.04	0.13	0.18	1.72
MnO	0.29	0.031	0.214	0.071	0.048	0.052	0.046	0.056	0.071	0.077	0.065	0.037	0.102	0.053	0.022	0.259	0	0	0	0.059	0.155
CaO	8.435	12.976	7.382	10.537	14.169	14.309	14.668	11.87	15.234	13.278	15.233	14.46	1.427	10.054	11.964	6.611	12.054	11.268	12.972	10.178	6.834
BaO	3.391	0	4.731	2.445	0	0	0.783	2.658	0	0.508	0	0.244	17.432	4.097	0.302	9.865	0	0	0	0.652	6.509
SrO	0.82	1.021	3.867	1.151	0.939	0.686	1.186	1.76	0.756	1.432	1.067	1.057	3.376	2.169	1.978	3.265	2.077	2.311	1.76	2.468	5.104
Na ₂ O	0.675	4.227	2.7	0.989	4.491	4.226	4.043	3.736	4.348	4.187	4.962	3.833	0.256	2.737	5.458	2.394	6.462	6.556	5.769	5.538	2.449
Cations (p.f.u.)																					
Nb	1.651	1.734	1.668	1.67	1.719	1.713	1.652	1.702	1.698	1.706	1.719	1.679	1.555	1.738	1.811	1.682	1.77	1.792	1.798	1.802	1.747
Ta	0.008	0.01	0.014	0.008	0.001	0	0.001	0	0.001	0.008	0	0.001	0.006	0.007	0.004	0	0.006	0	0	0	0.003
Si	0.033	0	0.034	0.015	0	0	0.015	0.034	0.002	0.01	0	0.011	0.204	0.033	0.002	0.047	0.002	0.001	0	0.002	0.045
Ti	0.274	0.226	0.217	0.203	0.22	0.223	0.271	0.25	0.259	0.249	0.242	0.28	0.217	0.21	0.173	0.261	0.194	0.199	0.184	0.189	0.195
Zr	0.034	0.03	0.067	0.104	0.061	0.064	0.06	0.014	0.039	0.026	0.039	0.029	0.019	0.012	0.011	0.01	0.028	0.008	0.018	0.007	0.009
U	0.0021	0.03	0.0314	0.0237	0	0	0	0.0012	0.0003	0.0013	0.0012	0.0007	0.0101	0.0101	0.0074	0	0.0112	0.0071	0.0039	0.0004	0.0014
Th	0.1779	0.0485	0.063	0.0454	0.05	0.0493	0.0535	0.0412	0.0342	0.0288	0.0334	0.0322	0.0327	0.0307	0.0272	0.0503	0.024	0.0286	0.0251	0.0346	0.0406
La	0.01	0.0131	0.0154	0.0129	0.0141	0.0091	0.0152	0.02	0.0194	0.0153	0.0109	0.0184	0.0134	0.0195	0.0224	0.0187	0.0218	0.0302	0.0146	0.0251	0.0284
Ce	0.061	0.0623	0.08	0.0632	0.0663	0.0679	0.0793	0.0679	0.0661	0.0728	0.0731	0.0695	0.0676	0.0682	0.0662	0.0818	0.0602	0.0866	0.0494	0.0799	0.0841
Y	0.02	0.0205	0.0072	0.0162	0.0186	0.0193	0.0201	0.0168	0.0172	0.0186	0.0197	0.0174	0.0108	0.0149	0.0178	0.0104	0.018	0.017	0.0163	0.0155	0.0051
Fe ²⁺	0.0722	0.0247	0.1131	0.0488	0.0294	0.0267	0.0263	0.0479	0.0303	0.026	0.0412	0.039	0.0982	0.0416	0.0564	0.052	0.0082	0.0021	0.0068	0.0091	0.0929
Mn	0.0158	0.0016	0.0123	0.0037	0.0026	0.0028	0.0026	0.0032	0.0039	0.0042	0.0036	0.0021	0.0056	0.0027	0.0012	0.0139	0	0	0	0.0031	0.0085
Ca	0.5798	0.8691	0.5354	0.7006	0.9593	0.9804	1.061	0.845	1.0598	0.9135	1.0575	1.032	0.0989	0.6592	0.7927	0.4497	0.793	0.7369	0.8463	0.6766	0.4719
Ba	0.0853	0	0.1255	0.0595	0	0	0.0207	0.0692	0	0.0128	0	0.0064	0.442	0.0983	0.0073	0.2455	0	0	0	0.0159	0.1644
Sr	0.0305	0.037	0.1518	0.0414	0.0344	0.0254	0.0464	0.0678	0.0285	0.0533	0.0401	0.0408	0.1267	0.077	0.0709	0.1202	0.074	0.0818	0.0622	0.0888	0.1908
Na	0.084	0.5123	0.3544	0.119	0.5502	0.524	0.5292	0.4813	0.5474	0.5213	0.6233	0.495	0.0321	0.3247	0.6544	0.2947	0.7693	0.7758	0.6811	0.6662	0.306
A	1.1386	1.6191	1.4895	1.1344	1.7249	1.7049	1.8543	1.6615	1.8071	1.6679	1.904	1.7535	0.9381	1.3469	1.7239	1.3372	1.7797	1.7661	1.7057	1.6152	1.3941

Tabela F – Análises de pirocloro, Ca-betafita e Fe-columbita de rochas foscoríticas (nelsonitos P2 e P3) de Catalão I. Recalculado assumindo sítio B = 2 cátions. (Cont. IV)

	230B- 2B	230B- 3B	304A- 1B	304A- 2B	304A- 4	304A- 5	304A- 6	304A- 7	304A- 8	304A- 9	304A- 10	304A- 11	304A- 12	304A- 13	304A- 14	304B- 1	304B- 2	304B- 3	339- 3C	339- 4	
Amostra																					
Coord	5	10														0	3	5	0	3	
Unidade	P3	P3	P2	P2	P2	P2	P2	P2	P2	P2	P2	P2	P2	P2	P2	P3	P3	P3	P2	P2	
Óxidos (%)																					
Nb ₂ O ₅	63.39	62.3	52.58	64.05	65.83	62.67	59.39	59.6	65.85	57.37	55.98	64.26	57.33	56.64	63.22	56.93	52.26	57.03	62.41	55.26	59.55
Ta ₂ O ₅	0	0.11	0.54	0.1	0.09	0.19	0.12	0.1	0.21	0	0.07	0.36	0.88	0.6	0	0.49	0.8	0.26	0.13	0.16	0.36
SiO ₂	0	0.15	0.69	0.58	0.29	0.31	1.8	0.33	0	0.08	0.26	0.36	0.1	0.16	0.32	0.75	0.61	0.43	0.66	0	1.89
TiO ₂	4.35	4.94	2.9	5.52	5.09	4.19	3.89	1.5	4.05	4.11	5.07	5.5	3	2.78	4.91	2.93	2.37	2.38	4.31	3.67	4.1
ZrO ₂	0.53	0.38	3.31	0.45	0.01	0.86	0.16	1.77	0	0	0.16	0.15	1.57	1.6	0.14	3.21	3.2	3.26	0.47	0.26	0.13
UO ₂	0	0	2.46	0.14	0.01	0.31	0.47	1	0.04	0.12	0.2	0	2.01	1.79	0.05	2.06	3.72	2.25	0.54	0.19	0.85
ThO ₂	2.4	3.14	4.97	0.23	0.19	1.46	0.64	2.11	0.21	0.24	0.09	0.02	3.1	3.3	0.11	5.35	4.94	6.23	1.36	1.44	1.2
La ₂ O ₃	0.71	0.66	0.49	0.69	0.69	0.83	1.04	0.87	0.69	0.73	0.85	1.01	0.59	0.35	0.84	0.53	0.42	0.51	0.88	0.87	0.82
Ce ₂ O ₃	2.72	2.96	3.5	1.72	1.74	2.24	2.49	3.37	2.01	1.48	1.7	1.48	3.02	2.35	1.41	2.78	3.04	2.73	2.92	3.09	2.74
Y ₂ O ₃	0.53	0.46	0.51	0.48	0.36	0.45	0.3	0.57	0.32	0.37	0.32	0.46	0.38	0.51	0.36	0.44	0.2	0.55	0.31	0.34	0.52
FeO	0.2	0.79	1.82	0.33	0.21	0.55	2.81	1.14	0.16	0.14	0.2	0.13	0.99	0.99	0.1	2.02	1.49	2.18	0.85	0.31	0.71
MnO	0.063	0.122	0.13	0.027	0.017	0.042	0	0.015	0	0.052	0.128	0.015	0.091	0.103	0	0.144	0.083	0.093	0	0.002	0.039
CaO	11.86	10.615	2.232	15.525	14.90	10.75	11.07	9.891	13.22	18.21	16.241	16.168	8.49	9.801	15.272	8.906	3.339	7.812	8.378	14.50	5.311
BaO	0	1.881	14.15	0	0	4.376	0.77	2.358	0	0	0	4.106	3.546	0	2.705	12.24	4.613	4.65	0.132	9.663	
SrO	2.353	2.368	1.854	2.411	2.676	1.959	2.717	1.604	4.054	3.305	2.79	2.545	1.441	1.245	2.862	2.031	3.558	1.655	3.68	2.407	2.793
Na ₂ O	5.929	4.881	0.345	4.945	5.867	2.734	4.678	3.167	5.949	5.676	5.942	5.237	0.372	1.51	6.15	2.208	0.384	1.604	3.801	2.958	1.414
Cations (p.f.u.)																					
Nb	1.781	1.747	1.674	1.707	1.755	1.756	1.695	1.839	1.811	1.782	1.717	1.723	1.771	1.778	1.75	1.694	1.7	1.738	1.743	1.79	1.68
Ta	0	0.002	0.01	0.002	0.001	0.003	0.002	0.002	0.003	0	0.001	0.006	0.016	0.011	0	0.009	0.016	0.005	0.002	0.003	0.006
Si	0	0.009	0.048	0.034	0.017	0.019	0.113	0.023	0	0.005	0.017	0.021	0.007	0.011	0.02	0.049	0.044	0.029	0.041	0	0.118
Ti	0.203	0.231	0.154	0.245	0.226	0.195	0.185	0.077	0.185	0.212	0.259	0.245	0.154	0.145	0.226	0.145	0.128	0.121	0.2	0.198	0.192
Zr	0.016	0.012	0.114	0.013	0	0.026	0.005	0.059	0	0	0.005	0.004	0.052	0.054	0.004	0.103	0.112	0.107	0.014	0.009	0.004
U	0	0	0.0386	0.0019	0.000	0.004	0.006	0.015	0.001	0.002	0.003	0	0.0306	0.0276	0.0006	0.030	0.06	0.034	0.007	0.003	0.012
Th	0.0339	0.0443	0.0797	0.0031	0.003	0.020	0.009	0.033	0.003	0.004	0.0014	0.0003	0.0483	0.0521	0.0015	0.080	0.081	0.096	0.019	0.023	0.017
La	0.0162	0.015	0.0127	0.015	0.015	0.019	0.024	0.022	0.015	0.018	0.0214	0.022	0.0147	0.009	0.0189	0.013	0.011	0.013	0.02	0.023	0.019
Ce	0.0618	0.0672	0.0901	0.0372	0.037	0.051	0.057	0.084	0.045	0.037	0.0423	0.0322	0.0754	0.0598	0.0317	0.067	0.080	0.067	0.066	0.081	0.063
Y	0.0176	0.0151	0.019	0.015	0.011	0.015	0.01	0.021	0.010	0.014	0.0115	0.0144	0.0139	0.019	0.0116	0.016	0.007	0.02	0.010	0.013	0.017
Fe ²⁺	0.0106	0.0408	0.107	0.0161	0.010	0.028	0.148	0.065	0.008	0.008	0.0115	0.0065	0.0564	0.0576	0.005	0.111	0.09	0.123	0.044	0.019	0.037
Mn	0.0033	0.0064	0.0078	0.0013	0.001	0.002	0	0.001	0	0.003	0.0074	0.0008	0.0053	0.0061	0	0.008	0.005	0.005	0	0.000	0.002
Ca	0.7895	0.7054	0.1684	0.9803	0.942	0.714	0.749	0.723	0.862	1.340	1.1808	1.0277	0.6214	0.7292	1.0019	0.628	0.257	0.564	0.554	1.113	0.355
Ba	0	0.0457	0.3906	0	0	0.106	0.019	0.063	0	0	0	0	0.1099	0.0965	0	0.07	0.345	0.122	0.113	0.004	0.236
Sr	0.0848	0.0852	0.0757	0.0824	0.092	0.070	0.1	0.064	0.143	0.138	0.1098	0.0876	0.0571	0.0501	0.1016	0.077	0.149	0.065	0.132	0.1	0.101
Na	0.7142	0.587	0.0471	0.5651	0.671	0.329	0.573	0.419	0.702	0.756	0.7818	0.6024	0.0493	0.2033	0.7301	0.282	0.054	0.21	0.455	0.411	0.171
A	1.7319	1.6121	1.0367	1.7174	1.782	1.36	1.696	1.51	1.789	2.314	2.1709	1.7939	1.0823	1.3103	1.9029	1.382	1.138	1.318	1.421	1.79	1.031

Tabela G – Análises de carbonatos em rochas da série foscorítica de Catalão I, recalculados como carbonatos.

Amostra	103-1	103-2	110-1	110-46-2	110-46-3	152-1	152-2	156-3	157A-1	170-1	178-1	178-2	183-1	183-2	183-3	183-4	183-5	183-6	183-7	183-8	183-9
Unidade	P3	P3	P1	P1	P1	P2	P2	P2	P2	DC	P2	P2	DC								
Óxidos (wt%)																					
CaO	29.5	29.7	0.5	0.5	29.3	29.0	27.7	30.4	29.1	29.3	28.3	28.1	30.9	30.1	30.3	30.2	26.4	0.0	0.2	0.3	1.5
SrO	2.39	1.93	0.00	0.00	0.59	2.22	1.99	0.96	1.90	2.43	3.16	0.68	0.47	2.77	2.34	1.78	1.42	0.03	0.32	0.21	0.20
BaO	0.00	0.00	0.13	0.00	0.04	0.05	0.00	0.00	0.64	0.04	0.09	0.13	0.05	0.12	0.18	0.10	0.11	56.72	56.82	55.66	56.70
MgO	23.5	22.2	40.5	40.1	23.1	22.8	24.3	22.3	22.7	23.6	22.6	21.8	23.7	22.8	22.7	22.6	20.0	14.3	14.2	14.1	14.1
FeO	0.67	0.57	7.64	8.34	0.11	0.95	1.21	0.57	0.13	0.69	0.93	1.06	0.40	0.67	0.45	0.56	1.15	0.07	0.09	0.22	0.11
MnO	0.34	0.18	0.00	0.00	0.00	0.36	0.54	0.26	0.35	0.00	0.00	0.00	0.00	0.00	0.00	0.00	0.00	0.00	0.00	0.00	0.00
Carbonatos (wt%)																					
CaCO ₃	50.5	50.9	0.9	0.8	50.2	49.7	47.5	52.1	49.9	50.2	48.5	48.2	52.9	51.5	52.0	51.8	45.2	0.0	0.4	0.6	2.6
SrCO ₃	3.32	2.67	0.00	0.00	0.81	3.08	2.76	1.33	2.63	3.37	4.38	0.94	0.65	3.84	3.24	2.47	1.97	0.05	0.44	0.29	0.27
BaCO ₃	0.00	0.00	0.16	0.00	0.06	0.07	0.00	0.00	0.80	0.05	0.11	0.16	0.07	0.15	0.22	0.13	0.13	71.51	71.65	70.18	71.50
MgCO ₃	46.8	44.3	80.6	79.9	46.0	45.5	48.4	44.5	45.2	47.1	45.1	43.5	47.3	45.4	45.1	45.0	39.8	28.5	28.3	28.1	28.0
FeCO ₃	1.04	0.88	11.89	12.98	0.18	1.47	1.89	0.89	0.19	1.08	1.45	1.65	0.63	1.04	0.70	0.88	1.79	0.11	0.15	0.34	0.17
MnCO ₃	0.53	0.27	0.00	0.00	0.00	0.57	0.84	0.40	0.54	0.00	0.00	0.00	0.00	0.00	0.00	0.00	0.00	0.00	0.00	0.00	0.00
Total	102.2	99.0	93.6	93.7	97.2	100.3	101.4	99.2	99.3	101.8	99.5	94.5	101.5	101.9	101.3	100.3	88.8	100.2	100.9	99.5	102.5

Tabela G – Análises de carbonatos em rochas da série foscorítica de Catalão I, recalculados como carbonatos. (Cont. I)

Amostra	183-10	192A-1	200-1	206-1	207-1	207-2	230A-1	230B-1	304A-1	304A-1	339-1	339-2	339-1	339-2	339-3	339-4	339-5	339-6	339-7	339-8	339-9
Unidade	DC	P2	P3	P3	P3	P2	P3	P2	P2	DC	DC	DC	DC	DC	DC	DC	DC	DC	DC	DC	DC
Óxidos (wt%)																					
CaO	0.5	30.5	28.3	28.9	30.3	29.0	29.5	29.7	27.9	26.4	0.5	0.4	0.2	0.4	0.3	0.4	0.4	0.3	0.3	0.3	0.4
SrO	0.17	0.61	3.86	1.97	2.08	1.93	2.46	3.01	4.13	4.73	0.11	0.23	0.16	0.13	0.14	0.26	0.12	0.06	0.00	0.03	0.20
BaO	56.08	0.00	0.04	0.00	0.00	0.11	0.00	0.00	0.07	0.00	58.32	59.34	58.56	58.49	59.13	59.53	58.73	59.07	59.22	59.67	57.66
MgO	13.4	22.8	22.6	23.1	23.8	22.3	22.8	23.9	22.1	23.7	12.5	12.7	15.0	14.8	14.6	14.4	14.4	14.2	14.2	14.1	13.8
FeO	0.12	1.45	0.68	1.04	0.74	0.93	0.70	0.66	0.64	0.63	0.07	0.11	0.04	0.08	0.06	0.04	0.12	0.00	0.09	0.12	0.06
MnO	0.00	0.97	0.29	0.00	0.36	0.32	0.00	0.00	0.36	0.00	0.00	0.00	0.00	0.00	0.00	0.00	0.00	0.00	0.00	0.00	0.00
Carbonatos (wt%)																					
CaCO ₃	0.9	52.3	48.5	49.4	52.0	49.7	50.6	50.8	47.8	45.2	0.9	0.7	0.4	0.6	0.5	0.6	0.7	0.6	0.6	0.6	0.8
SrCO ₃	0.24	0.84	5.35	2.73	2.88	2.67	3.41	4.18	5.72	6.55	0.15	0.32	0.22	0.18	0.20	0.37	0.16	0.09	0.00	0.05	0.28
BaCO ₃	70.72	0.00	0.05	0.00	0.00	0.13	0.00	0.00	0.08	0.00	73.54	74.82	73.84	73.75	74.56	75.06	74.06	74.48	74.67	75.24	72.71
MgCO ₃	26.7	45.5	45.0	46.0	47.4	44.5	45.5	47.6	44.0	47.3	25.0	25.2	29.9	29.6	29.1	28.7	28.6	28.4	28.2	28.0	27.5
FeCO ₃	0.18	2.26	1.05	1.62	1.16	1.44	1.09	1.03	0.99	0.98	0.11	0.17	0.07	0.12	0.09	0.06	0.19	0.00	0.13	0.19	0.10
MnCO ₃	0.00	1.52	0.45	0.00	0.57	0.49	0.00	0.00	0.56	0.00	0.00	0.00	0.00	0.00	0.00	0.00	0.00	0.00	0.00	0.00	0.00
Total	98.7	102.4	100.4	99.8	103.9	99.0	100.6	103.6	99.2	100.0	99.7	101.2	104.4	104.3	104.5	104.8	103.7	103.6	103.6	104.1	101.4

Tabela G – Análises de carbonatos em rochas da série foscorítica de Catalão I, recalculados como carbonatos. (Cont. II)

Amostra	339-10	339-11	339-1	339-2	339-3	339-4	339-5	339-6	339-8	339-9	339-10	87-1	87-2	87-3	93-1	99A-1	99A-2	99A-3	99B-1
Unidade	DC	DC	DC	DC	DC	DC	DC	DC	DC	DC	DC	P3	P3	P3	P2	P3	P3	P2	
Óxidos (wt%)																			
CaO	0.6	0.3	0.2	0.2	0.3	0.4	0.3	0.4	0.4	0.4	0.4	29.0	29.2	28.6	29.7	29.4	29.5	29.7	30.1
SrO	0.11	0.20	0.18	0.08	0.25	0.08	0.26	0.18	0.17	0.10	0.17	2.28	1.80	2.40	1.43	1.80	1.80	2.09	2.20
BaO	59.62	56.63	59.84	58.20	58.30	57.54	58.01	58.14	58.99	57.85	54.41	0.33	0.76	0.12	0.00	0.07	0.00	0.07	0.23
MgO	13.5	12.3	14.1	14.1	13.8	13.6	13.6	13.6	13.4	12.6	11.6	23.8	22.3	22.8	21.9	22.4	22.4	22.4	23.0
FeO	0.14	0.06	0.06	0.06	0.08	0.00	0.06	0.08	0.08	0.07	0.05	1.03	0.29	0.22	0.50	0.68	0.64	1.10	1.07
MnO	0.00	0.00	0.00	0.00	0.00	0.00	0.00	0.00	0.00	0.00	0.00	0.33	0.08	0.44	0.65	0.26	0.23	0.28	0.53
Carbonatos (wt%)																			
CaCO ₃	1.0	0.6	0.3	0.3	0.5	0.7	0.5	0.6	0.7	0.8	0.8	49.7	50.1	49.0	50.8	50.4	50.6	50.9	51.5
SrCO ₃	0.15	0.28	0.25	0.11	0.35	0.11	0.36	0.25	0.24	0.14	0.23	3.16	2.49	3.33	1.98	2.49	2.49	2.89	3.05
BaCO	75.17	71.41	75.45	73.38	73.51	72.55	73.15	73.31	74.38	72.95	68.61	0.42	0.95	0.15	0.00	0.08	0.00	0.08	0.28
MgCO ₃	27.0	24.6	28.1	28.0	27.6	27.2	27.1	27.0	26.8	25.1	23.1	47.5	44.5	45.4	43.7	44.7	44.6	44.7	45.9
FeCO ₃	0.22	0.10	0.09	0.09	0.12	0.00	0.09	0.13	0.12	0.11	0.08	1.60	0.45	0.35	0.78	1.06	1.00	1.71	1.66
MnCO ₃	0.00	0.00	0.00	0.00	0.00	0.00	0.00	0.00	0.00	0.00	0.00	0.51	0.12	0.69	1.01	0.41	0.35	0.44	0.82
Total	103.5	96.9	104.2	101.9	102.1	100.5	101.3	101.3	102.2	99.1	92.8	102.9	98.6	98.8	98.3	99.2	99.0	100.8	103.3

Tabela H – Análise modal e de rocha total de rochas foscoríticas e glimerito de Catalão I

Sample	F4	056B	91	099a	116	149	156	157b	170	178	183G1	183r
Estrut	rock	dike	rock	rock	rock	glob	rock	rock	glob	rock	glob	rock
Unidade	P1	DC		P3	P2	DC	P2	P3	DC	P2	DC	P2
Carb	22		19	1	6		1	4		15		3
Opacos	27		71	68	32		33	59		23		40
Flogopita	21		10	2	24		5	5		23		44
Apatita	5		0	17	32		58	19		34		4
Pirocloro	0		0	11	6		3	13		5		9
Barita	0		0	1	0		0	0.1		0		0
Olivina	25		0	0	0		0	0		0		0
SiO₂	23.8	3.29	2.72	1.39	9.69	9.07	1.26	1.79	3.98	8.44	2.04	13.12
Al₂O₃	0.2		0.16	0.03	0.08	0.01	0.1			0.2	0.03	0.07
Fe₂O_{3T}	18.25	19.38	70.6	61.24	38.96	27.82	43.31	58.85	20.88	30.62	17.9	53.92
MgO	25.03	15.07	7.98	2.18	9.42	12.86	1.5	2.27	11.7	8.43	16.01	9.91
CaO	12.36	22.24	5.42	13.69	13.85	11.74	27.56	14.93	11.9	18.92	15.9	5.86
Na₂O	0.03	0.22	0.02	0.33	0.29	0.26	0.17	0.63	0.23	0.66	0.06	0.23
K₂O	2.09	0.92	0.68	0.27	1.88	2.36	0.34	0.48	0.87	2.17	0.48	3.4
TiO₂	2.35	1.02	1.76	2.31	7.16	2.62	0.58	2.51	16	0.9	1.73	1.42
P₂O₅	2.03	2.82	0.41	9.25	8.61	5.07	22.58	10.62	1.23	13.7	1.27	3.22
MnO	0.31	0.37	0.4	0.28	0.45	0.28	0.14	0.26	0.86	0.18	0.39	0.22
Cr₂O₃	0.037	0.003	0.002	0.004	0.003	0.003	0.015	0.002	0.002	0.006	0.004	0.008
Nb₂O₅	0.062	1.217	0.23	3.329	1.816	1.82	0.575	3.162	1.577	2.452	0.399	1.981
SrO	0.365	1.462	0.254	1.04	0.933	1.621	0.956	1.117	3.561	1.762	1.761	0.476
BaO	0.082	1.391	0.298	1.099	0.194	9.17	0.087	0.521	8.202	2.656	11.134	0.299
REE₂O₃	0.12	0.437	0.051	0.636	0.635	0.587	0.511	0.772	0.28	1.436	0.16	0.352
ZrO₂	0.056	0.342	0.217	0.889	0.03	0.029	0.025	0.327	0.02	0.03	0.175	1.431
LOI	12.5	29.4	8.5	1.6	5.5	15.4	0.1	1.4	17.4	6.8	30.6	3.6
Total	99.67	99.58	99.7	99.56	99.5	100.72	99.81	99.64	98.69	99.36	100.04	99.52
C	2.76	8.44	2.64	0.73	1.29	3.92	0.22	0.51	4.75	1.41	9.12	0.65
S	0.24	0.98	0.08	0.15	0.04	0.38	0.02	0.14	2.17	1.54	0.85	0.12
Ba	733	12457	2673	9844	1739	82136	776	4668	73462	23788	99722	2678
Rb	99.2	55.6	41.9	17.1	114.6	143.5	22.1	29.1	45.4	135.3	28.9	199.8
Sr	3089	12359	2145	8791	7890	13707	8084	9448	30109	14902	14891	4026
Cs	1.1	0.4	0.2	0.1	0.8	0.8	0.1	0.3	0.2	0.6	0.1	1.2
Ga	3.1	1.2	10.2	0.5	2.8	2.1	3.1	0.5	0.5	3.8	1.3	4
Ta	18	82.2	162.3	131.9	134.8	83.4	77.5	54.5	146.1	113	30.4	186.3
Nb	432	8508	1610	23272	12697	12724	4021	22101	11026	17144	2789	13849
Hf	11.1	61.7	42.9	135.3	10.1	11	5.1	70.9	8.6	11.4	23.2	202.9
Zr	416.1	2534	1606	6578	220.8	214.6	181.6	2420	149.4	222.4	1296	10592
Y	24.4	137	5.1	46.3	60	43.7	52.4	51.1	21.9	86.6	15.6	23.9
Th	64.7	576.1	167.1	738.8	322.9	284.8	250.6	1198	80.5	746.3	100.6	928.9
U	14.3	252.4	55.7	533.6	207.9	333.7	155.4	271.4	62.2	665	75.1	651.9
Cr	253.16	20.53	13.68	27.37	20.53	20.53	102.63	13.68	13.68	41.05	27.37	54.74
Ni	598.6	13.8	10.5	7.3	9	12.9	19.8	5.8	33.3	14.6	7.7	5.8
Co	99.4	59.2	106.3	136.7	102.3	69.1	28.4	104.2	44.9	73.2	77	93.3
Sc	28	20	41	25	12	12	5	17	21	11	17	45
Cu	46.5	95.3	1.9	2.85	88.4	22.3	1.3	16	6.7	109.1	64.9	2.5
Pb	1.8	20.5	0.7	1.5	1.9	4.7	1.3	1.6	6	28.9	3.5	1.6
Zn	111	103	209	240	155	101	87	170	145	218	125	170
La	196.3	707.6	79	1084	1273	1193	883.3	1347	586.2	2820	333.8	580.5
Ce	461.3	1738	232.6	2689	2424	2412	2083	3359	1147	5933	654.5	1565
Pr	59.89	208	24.11	313.9	337.3	288.9	258.1	384.2	127.7	735.6	70.6	179
Nd	217	686.1	75.1	1076	1102	913	892.8	1228	420.4	2305	236.5	558
Sm	28.24	96.7	9.15	116	119.6	92.27	100.2	125.8	45.94	223.1	25.33	59.52
Eu	7.27	28.9	2.13	25.88	30.11	22.02	23.9	28.84	9.91	52.28	5.84	14.04
Gd	11.76	57.63	2.47	50.1	41.14	24.06	39.31	33.01	14.77	56.81	10.81	11.65
Tb	1.89	9.76	0.52	5.38	6.18	4.38	5.27	5.86	2.23	9.67	1.41	2.8
Dy	7.32	40.65	2.13	17.83	20.68	14.61	17.69	20.3	8	31.5	5.74	8.99
Ho	1.03	5.51	0.22	1.61	2.14	1.46	2.04	2	0.78	2.88	0.51	0.98
Er	1.93	8.87	0.37	2.81	2.88	2.14	2.87	2.52	1.02	3.87	0.89	1.49
Tm	0.27	0.85	0.05	0.33	0.38	0.28	0.36	0.32	0.14	0.54	0.11	0.21
Yb	1.3	3.53	0.28	2.08	1.93	1.6	1.63	1.73	0.63	2.87	0.6	1.3
Lu	0.15	0.34	0.04	0.2	0.18	0.16	0.15	0.16	0.07	0.26	0.07	0.17

Tabela H – Análise modal e de rocha total de rochas foscoríticas e glimerito de Catalão I (Cont. I)

Sample	192B	206	207	225	230A	230B	244	304 A	304 BR	304BG	319	339
Estrut	rock	rock	rock	rock	rock	rock	rock	rock	rock	glob	rock	rock
Unidade	P2	P3	P3	GLIM	P2	P3	P1	P2	P3	DC	P1	P3
Carb	27	20	7	0.1	3	5	2	10	13		1	1
Opacos	7	48	59	8	25	69	11	35	61		26	20
Flogopita	12	18	8	84	9	2	25	11	19		0	26
Apatita	43	12	20	8	60	18	37	33	5		26	51
Pirocloro	11	2	5	0	3	6	0	11	2		0	2
Barita	0	0	1	0	0	0	0	0	0		0	0
Olivina	0	0	0	0	0	0	25	0	0		47	0
SiO₂	4.87	4.21	3.91	32.75	5.84	2.64	12.22	5.62	5.92	2.74	12.75	6.89
Al₂O₃	0.06	0.03	0.05	9.46			0.35	0.07			0.26	0.03
Fe₂O_{3T}	15.05	55.17	50.38	12.61	35.79	69.8	15.83	37.05	56.82	19.27	28.12	18.56
MgO	8.22	5.95	5.27	20.46	4.99	4.65	13.16	6.18	6.95	16.17	16.15	9.37
CaO	33.39	14.31	18.59	5.88	22.5	7.21	26.61	21.61	11.59	19.43	18.51	31.01
Na₂O	0.73	0.08	0.1	0.03	0.47	0.25	0.08	0.49	0.14	0.08	0.06	0.14
K₂O	1.25	1.1	0.9	8.89	1.55	0.54	2.66	1.41	1.46	0.71	0.84	1.78
TiO₂	0.69	0.97	0.86	1.69	1.69	2.23	1.75	1.41	1.78	0.51	3.36	0.34
P₂O₅	17.71	9.34	12.6	4.16	16.8	3.53	18.8	13.87	6.07	0.91	11.68	19.12
MnO	0.14	0.23	0.21	0.14	0.21	0.32	0.26	0.21	0.3	0.3	0.37	0.14
Cr₂O₃	0.004	0.002	0.002	0.002	0.004	0.002	0.004	0.007	0.003	0.0025	0.009	0.002
Nb₂O₅	1.98	0.465	0.291	0.059	2.52	1.503	0.065	3.352	1.101	0.596	0.114	0.219
SrO	1.478	0.691	0.739	0.166	1.467	0.526	0.462	1.177	0.852	2.711	0.459	0.937
BaO	0.398	1.191	0.104	0.237	0.77	2.208	0.036	0.783	1.195	3.428	0.125	0.671
REE₂O₃	0.988	0.266	0.299	0.188	0.959	0.352	0.668	0.742	0.312	0.194	0.409	0.453
ZrO₂	0.722	0.791	0.773	0.212	0.735	0.543	0.192	0.367	0.512	0.1	0.208	0.463
LOI	11.1	4.7	4.88	2.5	3.1	2.8	6.8	5	4.3	32.6	6.3	9.7
Total	98.78	99.5	99.96	99.43	99.39	99.1	99.95	99.35	99.31	99.75	99.72	99.82
C	2.73	1.53	1.35	0.26	0.65	1.44	1.56	1.42	1.56	9.43	1.45	2.82
S	0.49	0.47	0.02	0.02	0.02	3.78	0.04	0.02	0.2	0.1	0.19	0.03
Ba	3567	10664	931	2120	6893	19772	320	7013	10707	30705	1120	6013
Rb	80.7	63.4	49.4	439.2	88.1	30.8	121.6	88.9	80.7	40.6	46.1	101.5
Sr	12494	5846	6249	1407	12405	4448	3907	9949	7202	22926	3884	7924
Cs	0.6	0.5	0.28	4	0.6	0.2	0.9	0.6	0.7	0.35	0.8	0.5
Ga	0.5	4.1	4.22	13.3	2.9	0.5	4.8	4.7	1	2.4	2.8	0.5
Ta	15.4	110.1	27	18.5	21.7	11.7	15.9	153.7	91.8	55.6	27.3	18.6
Nb	13842	3253	2033	413	17617	10508	454	23434	7694	4167	794	1528
Hf	89.7	133	115.4	35.7	110.4	78.4	35.2	75.4	89.1	19.5	38.5	63.4
Zr	5345	5853	5725.6	1568	5440	4019	1425	2719	3791	739.3	1539	3427
Y	101.9	39.3	42.4	25.1	85.7	20	124	53.8	26.9	11.1	82.6	65.5
Th	2854	418	116.5	21.8	1761	844.8	162.1	2041	1135	368.2	155	49.9
U	84.2	890.1	41.4	15.5	83	36.3	36.1	789.1	522.8	193.1	16.2	16.2
Cr	27.37	13.68	12.84	13.68	27.37	13.68	27.37	47.9	20.53	17.11	61.58	13.68
Ni	4.6	9.5	4.8	26.9	4.8	62.6	63.5	9.8	18.4	6	28.4	6.4
Co	103.4	256.1	92.3	59.8	111.6	866.2	47.8	40.4	93.2	26.6	48.1	41.1
Sc	34	39	30	50	23	26	37	25	32	20	46	16
Cu	14.8	974.9	0.56	7.3	41.4	2735	167.8	0.7	40.3	4.4	33.1	8.3
Pb	3.3	4.3	1.1	0.5	2	4	14.1	2.3	3.3	2.2	2.3	2.2
Zn	58	140	139	69	160	307	117	128	263	88	102	69
La	1394	448.5	505	374.1	1812	637.7	1202	1246	499.5	408	663.6	774.9
Ce	4329	1079	1184.5	751.8	3752	1543	2477	3226	1350	832.8	1543	1751
Pr	528.4	133.4	147.18	90.29	523.2	173.1	341.2	378.7	155.5	88.79	205.9	227.3
Nd	1729	454.8	537	300.7	1681	535.8	1235	1210	519.7	272.1	775.5	837.9
Sm	200.3	56.42	65.69	34.12	183	55.03	150.6	129.8	58.2	27.21	99.25	100.3
Eu	46.99	13.79	16.45	8.19	45.53	11.94	38.15	29.04	14.43	5.79	25.58	25.81
Gd	49.29	24.87	30.9	12.04	55.1	13.01	66.28	29.11	19.82	3.75	46.54	45.59
Tb	10.12	3.54	4	1.94	9.06	2.47	9.65	6.2	3.1	1.13	6.54	6.15
Dy	34.26	12.92	14.98	6.96	30.28	8.19	37.15	20.03	10.86	3.83	25.57	22.6
Ho	3.89	1.76	1.79	0.8	3.21	0.8	4.74	2	1.02	0.36	3.24	2.5
Er	6.07	2.6	2.46	1.42	5.05	0.81	8.82	3.02	1.71	0.54	6.05	4.22
Tm	0.76	0.36	0.34	0.18	0.58	0.14	1.03	0.38	0.23	0.09	0.69	0.51
Yb	3.73	1.81	1.71	0.95	3.14	0.94	5.41	2.04	1.1	0.45	3.46	2.45
Lu	0.36	0.2	0.16	0.09	0.32	0.1	0.64	0.21	0.13	0.05	0.38	0.29

Tabela I – Análises de isótopos estáveis (C-O) e radiogênicos (Sr-Nd-Sm) em carbonatitos associados com a série-foscorítica de Catalão I (m=medido; i= inicial recalculado para 85 Ma).

Amostra	038G1	040G1	040V1	051V1	056B	056E	91	93	093G1	103G1	116G1	116V1	149	157G1	157G2	170	178G1	178G2	179G1	183G1	191G1
_tipo	bolsão	rocha	veio	dique	dique	rocha	rocha	carb	bolsão	bolsão	veio	bolsão	bolsão	carb	bolsão	bolsão	bolsão	rocha	bolsão	bolsão	
$\delta^{13}\text{C}_{\text{PDB}}$	-5.81	-5.72	-6.17	-6.6	-5.53	-5.86	-5.85	-5.38	-5.53	-5.91	-6.4	-7.01	-5.76	-5.61	-5.48	-6.31	-5.85	-5.16	-5.45	-5.82	-5.74
$\delta^{18}\text{O}_{\text{SMOW}}$	10.35	9.39	17.16	13.23	11.8	20.23	11.38	19.99	10.42	9.8	13.33	21.49	13.04	9.89	23	12.44	15.92	11.06	10.44	11.9	9.06
Sm									17.841	36.161	97.557	17.744	251.668	51.8							
Nd									111.711	288.166	911.238	192.397	2450.459	453.989							
Sr											13707										30109
(147Sm/144Nd)											0.09650	0.07590	0.06470	0.05580	0.06210	0.06900					
(143Nd/144Nd)m											0.51213	0.51202	0.51215	0.51212	0.51214	0.51216					
(143Nd/144Nd)i											0.51208	0.51198	0.51211	0.51209	0.51210	0.51212					
eNd0											-9.890	-12.060	-9.590	-10.080	-9.810	-9.320					
eNd											-8.8100	-10.7468	-8.1674	-8.5580	-8.3536	-7.9409					
(87Sr/86Sr)m											0.70538	0.70541	0.70549	0.70540	0.70540	0.70549					
(87Sr/86Sr)i												0.70545				0.70548					
(147Sm/144Nd)											0.0965		0.0647			0.0690					
T (DM)											1.186	1.132	0.922	0.894	0.917	0.934					

Tabela I – Análises de isótopos estáveis (C-O) e radiogênicos (Sr-Nd-Sm) em carbonatitos associados com a série-foscorítica de Catalão I (m =medido; i = inicial recalculado para 85 Ma).

Amostra	192G1	206	210G1	210G2	210V1	210V2	239	242G1	242G2	247B	250G1	250G2	250G3	252G1	252V1	257G1	257G2	304BG	309V1	334	339G1	
	bolsão	rocha	xeno	rocha	dique	veio	rocha	bolsão	rocha	rocha	rocha	rocha	rocha	bolsão	veio	bolsão	bolsão	bolsão	veio	carb	veio	
$\delta^{13}\text{C}_{\text{PDB}}$	-6.14	-5.66	-7.74	-5.87	-5.69	-6.79	-5.65	-5.77	-5.88	-5.37	-5.14	-3.55	-4.23	-5.86	-5.23	-5.58	-5.53	-5.82	-5.11	3.835	-6.1	
$\delta^{18}\text{O}_{\text{SMOW}}$	8.59	10.62	19.86	10.95	14.94	18.63	14.52	18	14.78	9.53	12.35	23.12	16.41	9.67	14.84	15.83	10.02	10.98	12.47	20	21.43	
Sm			66.359								137.643	197.898	2084.62							42.182		
Nd			491.976								2101.188	3356.648	35940.84							575.627		
Sr																				22926		
(147Sm/144Nd)			0.08150								0.03960	0.03560	0.03510							0.04430		
(143Nd/144Nd)m			0.51216								0.51205	0.51205	0.51215							0.51215		
(143Nd/144Nd)i			0.51212								0.51203	0.51203	0.51213							0.51213		
eNd0			-9.26								-11.50	-11.50	-9.56							-9.44		
eNd			-8.0183								-9.7876	-9.7641	-7.8068							-7.7900		
(87Sr/86Sr)m			0.70540								0.70541	0.70540	0.70537							0.70544		
(87Sr/86Sr)i																				0.70543		
(147Sm/144Nd)																				0.04430		
T (DM)			1.035								0.777	0.856	0.770							0.806		